SUITABILITY OF DYNAMIC IDENTIFICATION FOR DAMAGE DETECTION IN THE LIGHT OF UNCERTAINTIES ON A CABLE STAYED FOOTBRIDGE

Dissertation

submitted to and approved by the

Faculty of Architecture, Civil Engineering and Environmental Sciences
Technische Universität Braunschweig

and the

Department of Civil and Environmental Engineering
University of Florence

in candidacy for the degree of a
Doktor-Ingenieurin (Dr.-Ing.) /
Dottore di Ricerca in Civil and Environmental Engineering[*)]

by
Chiara Pepi
22/12/1985
from Todi, Italy

Submitted on	11 February, 2019
Oral examination on	07 May, 2019
Professorial advisors	Prof. Hermann G. Matthies Prof. Massimiliano Gioffrè

2020

*) Either the German or the Italian form of the title may be used.

DEALING WITH UNCERTAINTIES IN STRUCTURAL DYNAMIC IDENTIFICATION AND DAMAGE DETECTION ON CABLE STAYED FOOTBRIDGES

The theory of probabilities is at bottom nothing but common sense reduced to calculus;
it enables us to appreciate with exactness that which accurate minds feel
with a sort of instinct for which of times they are unable to account.

P.S. Laplace, Introduction to Théorie Analytique des Probabilitiés

---

Acknowledgements

Firstly, I would like to thank my supervisor Prof. Dr. Massimiliano Gioffré for the continuous support, for his motivation, confidence and kind guidance during all these three years. Thank you to my German advisor Prof. Dr. Hermann Matthies for hosting me at the Institute of Scientific Computing of the University of Braunschweig and for his contributions of time and ideas. I could not have imagined having better advisors and mentors!

I would like also to thank Prof. Mircea Grigoriu, whose observations and insightful comments inspired me to greatly improve my work. Thank you to Prof. Dr. Vittorio Gusella, Prof. Dr. Federico Cluni and Prof. Dr. Nicola Cavalagli for all the suggestions and the passionate discussions.

This thesis is dedicated:

To Chiara, an amazing PhD journey companion!

To my soulmate and life partner Daniele. I could have not reached all of this without his huge patient and unconditional confidence!

To Mum and Dad, who have worked hard for my life and future. They taught me that life is not a spectator sport, that the game is in progress and you have to go ahead, change the rules and always play. I owe every goal I have achieved to them!

Abstract

Structural identification is a very important task especially in all those countries characterized by significant historical and architectural patrimony and strongly vulnerable infrastructures, subjected to inherent degradation with time and to natural hazards e.g. seismic loads. Within this context the combined use of experimental tests, monitoring systems and numerical finite element procedures can provide useful information to improve the reliability of the estimated structural parameters.

Structural response of existing constructions is usually estimated using suitable numerical models which are driven by a set of geometrical and/or mechanical parameters that are mainly unknown and/or affected by different levels of uncertainties. Some of these information can be obtained by experimental tests but it is practically impossible to have all the required data to have reliable response estimations. For these reasons it is current practice to calibrate some of the significant unknown and/or uncertain geometrical and mechanical parameters using measurements of the actual response (static and/or dynamic) and solving an inverse structural problem. Model calibration is also affected by uncertainties due to the quality (e.g. signal to noise ratio, random properties) of the measured data and to the algorithms used to estimate structural parameters (e.g. Operational Modal Analysis – OMA).

As an example, the identification of structural dynamic characteristics (e.g. natural frequencies, mode shapes and damping ratios) based on monitoring data provided by Ambient Vibration Tests (AVT) are of long-standing interest especially for seismic protection of existing buildings and for monitoring the safety and serviceability of structures. Ambient vibration sources include wind, seismic micro tremors, pedestrian and traffic, which are not deterministic and can be only described by random processes. In the OMA technique this input excitation is not measured and it is assumed to be a stationary white noise. Nevertheless these ambient vibrations can be very far to be stationary as it happens when seismic induced vibrations are recorded. Tools are therefore needed to take into account

all these sources of uncertainties in order to have quantitative information on the level of accuracy of the estimated structural parameters.
In this thesis a new robust framework to be used in structural identification is proposed in order to have a reliable numerical model that can be used both for random response estimation and for structural health monitoring (SHM). First a parametric numerical model (FEM) of the existing structural system is developed and updated using probabilistic Bayesian framework. Second, virtual samples of the structural response affected by random loads are evaluated. Third, this virtual samples are used as "virtual experimental response" in order to analyze the uncertainties on the main modal parameters varying the number and time length of samples, the identification technique and the target response. Finally, the information given by the measurement uncertainties are used to assess the capability of vibration based damage identification method.
The obtained results will be crucial to follow the structural performance and reliability in - time (SHM) and to develop suitable damage detection procedures to be used in a early warning framework

Contents

List of Figures

List of Tables

List of Abbreviations

$\mathcal{F}$	σ-Field
$\mathcal{P}$	Probability Measure
Ω	Probability Space
AVT	Ambient Vibration Tests
BFT	Basic Frequency Domain
CF	Correlation Matrix
DOF	Degree of Freedom
ED	Experimental Design
EFDD	Enhanced Frequency Domain Decomposition
EMA	Experimental Modal Analysis
FDD	Frequency Domain Decomposition
FEM	Finite Element Model
FFT	Fast Fourier Transform
FRF	Frequency Response Function
gPCE	General Polynomial Chaos Expansion
LH	Lathin Hypercube
MAC	Modal Assurance Criterion
MAC	Modal Assurance Criterion

MC Monte Carlo

MCMC Markov Chain Monte Carlo

MDOF Multiple Degree of Freedom

NeXT Natural Excitation Technique

OMA Operational Modal Analysis

PC Polynomial Chaos

PDF Probability Density Function

PSD Power Spectral Density

QMC Quasi Monte Carlo

QoI Quantity of Interest

RV Random Variable

SDOF Single Degree of Freedom

SFEM Stochastic Finite Elements

SV Singular Value

SVD Singular Value Decomposition

UQ Uncertainty Quantification

Chapter 1

Introduction

1.1 Introduction and motivations

Cable-stayed footbridges and bridges are gaining worldwide interest because of some inherent features that determine the reduction of deck bending moment and deformations under live loads if compared to suspension bridges. These structures are now built in more unusual styles for both structural and aesthetic reasons. Despite their advantages, cable-stayed bridges and footbridges pose serious concerns regarding the high sensitivity to dynamic loads - such as wind or earthquakes - and the structural performance of the structure.

In the past decades several attention has been posed on long - span bridges [1]. Furthermore, recent failures of pedestrian bridges lead to increased care in design and construction of this kind of structures for both practitioner and researchers. Footbridges are subjected to the simultaneous actions of groups of pedestrian and because of their slender structure and particular shape it is expected that a wide range of frequency components can be induced by pedestrians. The careful assessment of pedestrian bridges modal characteristics in operating conditions is crucial to reduce the risk and/or avoid accidents.

Within this context it is of utmost to develop effective tools in order to characterize both

the significant structural parameters and the modal characteristics. The modal characteristics of a structure include its natural frequencies, mode shapes and associated damping ratios. Knowing the natural frequencies of a structure can avoid the occurrence of resonance phenomenon causing serious damage and risk. Mode shapes reflect the distribution of stiffness and mass as well as boundary conditions and, moreover, affect the nature and the spatial distribution of vibrations. Damping is another important quantity related to vibration level and energy dissipation of structures. A reliable dynamic - based assessment is based on the combined use of experimental analysis provided by data during full - scale measurements and Finite Element Analysis (FEA) predictions [2].

A possible way to assess the vibration characteristics of a structural system is by means of different kinds of vibration tests such as: forced and ambient vibration tests.

In the forced vibration tests some known input loads are artificially applied to the structure using a shaker mass or a sledge hammer. The input force and the response output time histories are used together for modal identification. When sufficient excitation power is applied, force vibration tests provide an accurate estimation of the modal properties especially for damping ratio. However, this kind of tests is really expensive and special equipment is required. Furthermore, if the excitation is not controlled properly, unexpected damage can occur.

Ambient vibration tests (AVT) are the most popular and convenient. In this kind of tests, dynamic data (e.g. structural acceleration and/or displacement time histories) are recorded when a structure is subjected to an unknown but statistically random loading having white noise characteristics. The data can be processed using Operational Modal Analysis (OMA) algorithms on frequency and/or time domain. The fundamental idea of OMA techniques is that the structure to be tested is subjected to some type of excitation that have approximately white noise characteristics. Actually, structures are subjected to natural excitations such as wind, traffic, tremors earthquake that are non - white. For this reason loading is modeled as the output of an imaginary loading filter that is loaded by white noise. The reliability of the results obtained from the measurements is related to the validity of this specific assumption. Even though the identified modal characteristics have lower precision than their counterparts from forced vibration tests, AVT have became very popular since they do not interfere with the normal use of structure/infrastructure and have the strong advantage of being very practical and economical.

The main disadvantages and limitations of AVT are due to the lack of information about the input excitation. A number of different kind of loads can occur during each measurement together with changes in temperature, humidity and level of excitation itself,

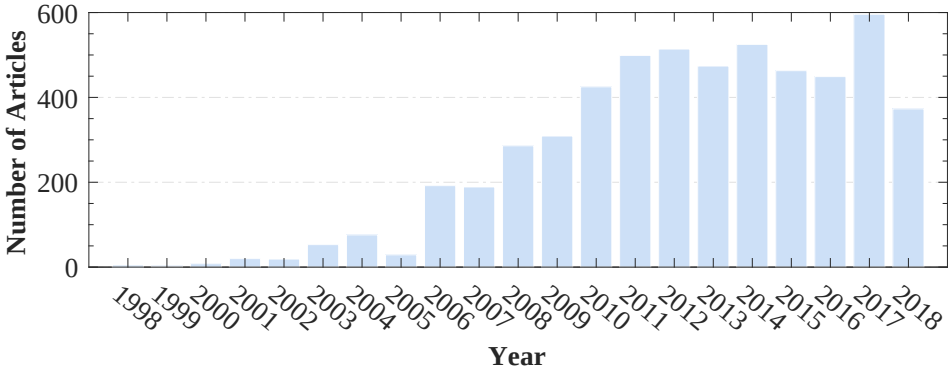

Fig. 1.1: Number of articles about Structural Health Monitoring from 1998 to November 2018.

especially when wind is blowing during the test. All of these uncertain factors lead to different estimations of the modal properties for each data set.
In OMA the obtained modal properties are strongly dependent also on the data used for dynamic identification. Uncertainties due to the limited data can arise. The amount of data is finite in terms of monitored Degree of Freedoms (DOFs). This aspect can be faced using a significant number of sensors or by means of multiple setups combining the time histories recorded in different time and with different time length. Also the sampling rate and the time length of the signals have significant influence on the results especially on damping ratio and finally measurement errors due to noise, transmission system and data processing cannot be neglected. Therefore, one first research question needs to be answered:

- *Is it possible to reduce the uncertainties related to the modal parameter estimates and due to different operating conditions occurring during the tests and signal processing parameters?*

This is an obvious problem when single measurement campaign are requested and carried out for structural identification and/or damage identification and in continuous Structural Health Monitoring (SHM). SHM is the process of equipping a structure with sensors and then extracting features (e.g modal or model parameters) for the main purpose of damage detection and structural performance assessment. The main idea at the base of SHM is that the modal parameters are related to the structural properties and that any change in the structural properties cause changes in modal properties. The vibration based damage assessment represents a powerful instrument since it does not require visual, complicated

and expensive inspections. For this reason dynamic SHM has gained a lot of attention in the last few years with increasing number of articles as shown in Figure 1.1 with a lot of practical applications to historic masonry structure, buildings and bridges or footbridges. One of the most interesting recent application is the single ambient vibration measurement campaign on the "Viadotto Polcevera" - so called "Morandi bridge" - in Genova (Italy) collapsed last August. As shown in the inspection final document (Figure 1.2 [3]) published by "Italian Transport and Infrastructures Minister", the bridge has been the object of a single measurement campaign carried out in 2017 by the researchers and engineerings of the Department of Architecture, Built, Environment and Construction Engineering of Milan University. Results showed that the pre stressed concrete stays were characterized by a non symmetric longitudinal and transversal behavior and further analysis were suggested for better understanding the structural performance of the stays.

In SHM field, the detection of damage presence, localization and severity is still a chal-

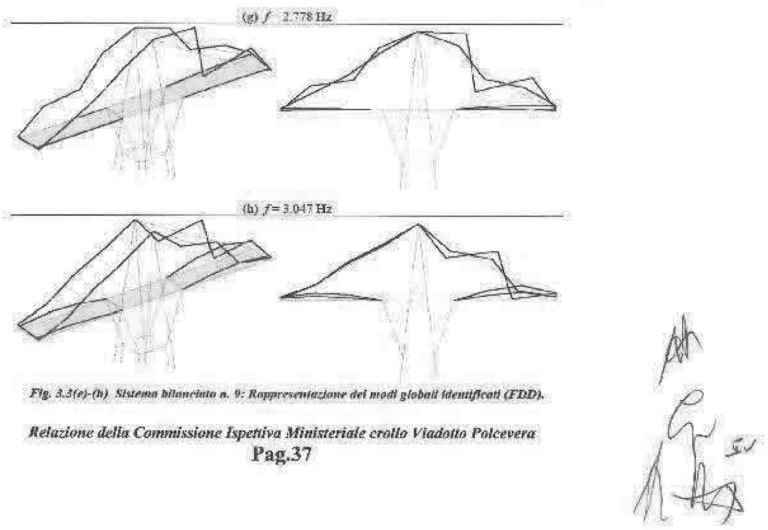

Fig. 1.2: Results of the experimental measurement campaign carried out for the dynamic identification of "Morandi Bridge" as shown in the final inspection document published by "Italian Transport and Infrastructures Minister".

lenge, especially in complex redundant structure such as cable-stayed footbridge. Therefore, a second main research question needs to be answered:

- *Is it possible to identify the existence, the localization and the severity of damage by means of global quantities such as the modal parameters? Which are the most suitable damage indicators to be used?*

The experimental results are of paramount importance to calibrate suitable finite element numerical models that can accurately describe the structural response. Many uncertainties arise also in model calibration because of several factors such as simplifications, idealized connections, internal constraints, uncertain material properties and geometry as well as boundary conditions. These uncertainties can cause large difference between the experimental estimations and the corresponding numerical model computations. These differences can be reduced through calibration using suitable updating procedures in deterministic or stochastic setting.

In the deterministic approach the structural parameters (mainly the stiffnesses of the whole structural members) are estimated using an iterative procedure: the numerical model parameters are tuned minimizing the difference between the modal parameters estimated from the measurements and from the Finite Element Model (FEM). This procedure leads to a constrained optimization problem that is often ill - posed since the consequent minimization function is multimodal and non-differantiable. Moreover this fitting-based approach provides for just a single point solution and uncertainties related to measurements and model are completely neglected. For this reason in the last few years probabilistic model updating procedures gained growing interest in the scientific community. A review of the probabilistic approaches that take into account uncertainties can be found in [4] , [5] and [6]. This kind of techniques can be grouped in two main classes: classical probabilistic approaches and Bayesian methods.

The classical methods are based on the evaluation of the statistics of parameters such that the statistics of the model output response correspond to the statistics of the observed data, while Bayesian methods are founded on the very well known Bayes' theorem [7].

A complete Bayesian framework relies on the knowledge of the prior uncertain parameters probability density functions (PDFs) and takes explicitly into account all the sources of errors involved in the process, including measurement errors and modeling errors to obtain updated probability estimates for the uncertain parameters in terms of joint, or marginal, PDFs and/or confidence intervals.

Beck and Katafygiotis [8] were among the first to introduce the Bayesian approach in structural dynamics in 1998. They defined a comprehensive general statistical framework for system identification through the concept of model identifiability using dynamic test data and providing a quantitative assessment of the accuracy of the model output prediction when a large amount of measurement data points are available. Vanik et Al. [9] and Yuen [10] were among the first to apply the Bayesian statistical system identification framework to SHM. Important reference works were developed by Katafygiotis et Al. [11], Beck [12]

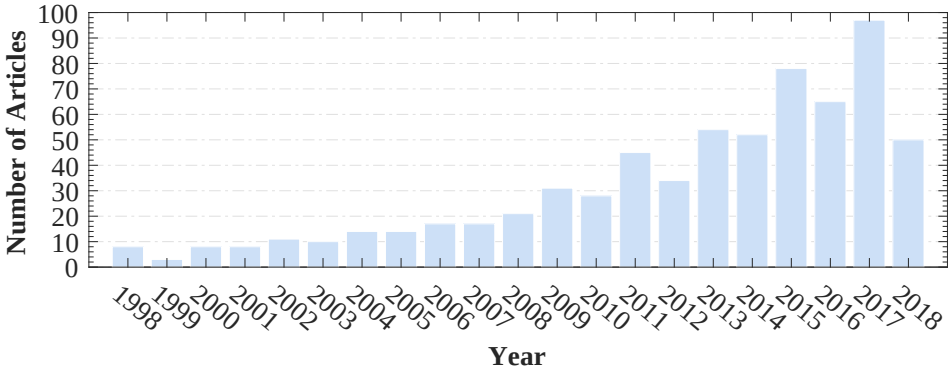

Fig. 1.3: Number of articles about Bayesian inference in structural identification from 1998 to November 2018.

and Box and Tiao [13].

The necessity to improve the accuracy of the system response prediction to different dynamic actions made this approach of particular interest and a vast amount of literature is available: Figure 1.3 shows the increasing number of articles about Bayesian inference in structural identification from 1998 to November 2018.

It is quite popular to use the identified modal characteristics to update the model parameters within the Bayesian approach. However direct mode shape matching is typically required in the most bayesian updating approaches using modal data and when incomplete measurements of mode shapes are only available, direct mode matching is not an easy task. In addition, including the measured mode shape in the reference data is a further challenge since the eigenvectors are very sensitive to measurement operating conditions. Mode matching due to local loss of stiffness from damage may affect some modal frequencies more than others making the case even worse. For all these reasons in most of practical applications the updating is carried out by means of modal parameters extracted from simulated data or using only the system modal frequencies as reference and the modal vectors as constraints for ensuring mode matching.

Another important issue in the Bayesian updating framework is the characterization of the so called posterior distribution since only simple problems can be solved through an analytical solutions. In most of practical case the posterior evaluation is carried out by means of very demanding procedure, especially in civil, mechanical and aerospace engineering practical applications.

The Bayesian updating framework represents one of the most powerful and interesting tool for the estimation of the main structural parameters accounting for measurements/-

modeling uncertainties but its use in continuous monitoring and vibration based damage detection applications is limited for the high time consuming computational costs. Therefore, a final research question needs to be answered:

- *Is it possible to overcome the limitations of the Bayesian updating framework speeding up the posterior evaluation by means of suitable and reliable procedures?*

1.2 Summary of the main contributions

This dissertation deals with uncertainties in structural, dynamic and damage identification. According to the three research questions the obtained results offer an interesting approach for evaluating structural and dynamic response of a very complex structure in presence of multiple uncertainties, over the existing methods.
The first part of the thesis is focused on the Bayesian framework selected as a useful tool for numerical model updating by means of global quantities (elastic moduli) able to consider both model and measurement uncertainties.
The classical Bayesian updating procedure has been improved by means of reliable surrogate model based on Polynomial Chaos Expansion Methods for reducing the high computational costs related to the solution of the inverse problem.
The robustness of the Bayesian analysis with respect to the likelihood function formulation is improved. In this sense two main intermediate contributions can be recognized.
Firstly, the use of real experimental modal parameters as reference (e.g natural frequencies and vibration modes) in the updating framework is a challenge. When output only dynamic identification technique are used for the dynamic characterization of a complex structure, the main hypotheses introduced for modeling the dynamics of a structure are not complied and complex eigenvectors are obtained. Furthermore, when dealing with complex structure measurements of partial mode shapes at a limited number of monitored DoFs are available. For all these reasons in most of practical applications the updating is carried out by means of modal parameters extracted from simulated data or using as reference only the system modal frequencies. In this sense a suitable formulation for the likelihood function able to consider the degree of correlation between two modal vectors is proposed and applied by means of Modal Assurance Criterion. The prediction error is thus defined as "a measure of the distance from perfect correlation" between pairs of experimental and numerical modal vectors.
The second addressed issue is represented by the role of the prediction error parameters. In the most of practical applications the prediction error parameters are treated as constant

values even if uncertain prediction errors play a crucial role in the likelihood function formulation and in the solution of the Bayesian inverse problem. For this reason the proposed procedure treats the prediction error variances as additional uncertain parameters.
The role of uncertainty in dynamic identification is also pointed out in the second part of the thesis. A best experimental setup to be used for data processing in output-only based dynamic identification in frequency domain is assessed through a parametric sensitivity analysis carried out for the evaluation of the effects of different operating conditions (e.g. base excitation amplitude) and signal sampling parameters on the structural system eigenproperties with special reference to the damping estimates.
Finally, the role of uncertainty in damage detection is assessed. Pseudo experimental response data of the parametric numerical model of a cable stayed footbridge with damage in cables are simulated under different operating conditions (different amplitude of excitation and changing temperature) and the effectiveness of the vibration based damage detection method, in terms of damage existence, localization and quantification is assessed. Artificial damage and artificial dynamic measurements are also used for assessing the most suitable modal parameter to be used as damage indicator.

1.3 Structure of the thesis

The thesis is organized as follows: Chapter 1 defines the general framework and the main objectives and contributions of this work. Chapter 2,3 and 4 review the state of the art respectively in the output - only dynamic identification technique, in the uncertainty quantification methods and in the Bayesian approach to the stochastic inverse problem. Chapter 5 and 6 illustrates the main applications and they represent the most original part of this work. In particular:

- In **Chapter 1** a general overview of the research topics is presented and the motivations that make the topics an interesting research area are highlighted. The main contributions of the research activities are briefly introduced.

- In **Chapter 2** the basic concepts on the characterization of the structural dynamic response by means of output - only dynamic identification techniques are reported together with some basic concepts of random vibrations analysis and classical dynamics. A brief literature overview about damage detection using continuous monitoring is provided and the main sources of variability in the modal characteristics of structures are analyzed.

- **Chapter 3** starts with basic introductions and some fundamentals of uncertainty quantification problem for characterizing the dynamic model response given input parameter distributions. A special focus is posed on polynomial chaos expansion method for developing reliable surrogate models to be used in the Bayesian inverse problem and to perform a robust global sensitivity analysis based on Sobol' indices.

- **Chapter 4** reports the main concepts of Bayesian updating framework: the definition of the prior distribution, the formulation of the likelihood function and the computational methods for the evaluation of the posterior distribution. Attention is especially drawn on the formulation of the likelihood function when noisy dynamic data (natural frequencies and modal parameters) are used as well as on the role of prediction error variances. Finally, the advantages of spectral expansion method in Bayesian inference are presented and discussed.

- In **Chapter 5** the results of a single ambient vibration measurement campaign on a cable stayed footbridge are firstly presented together with the development of the

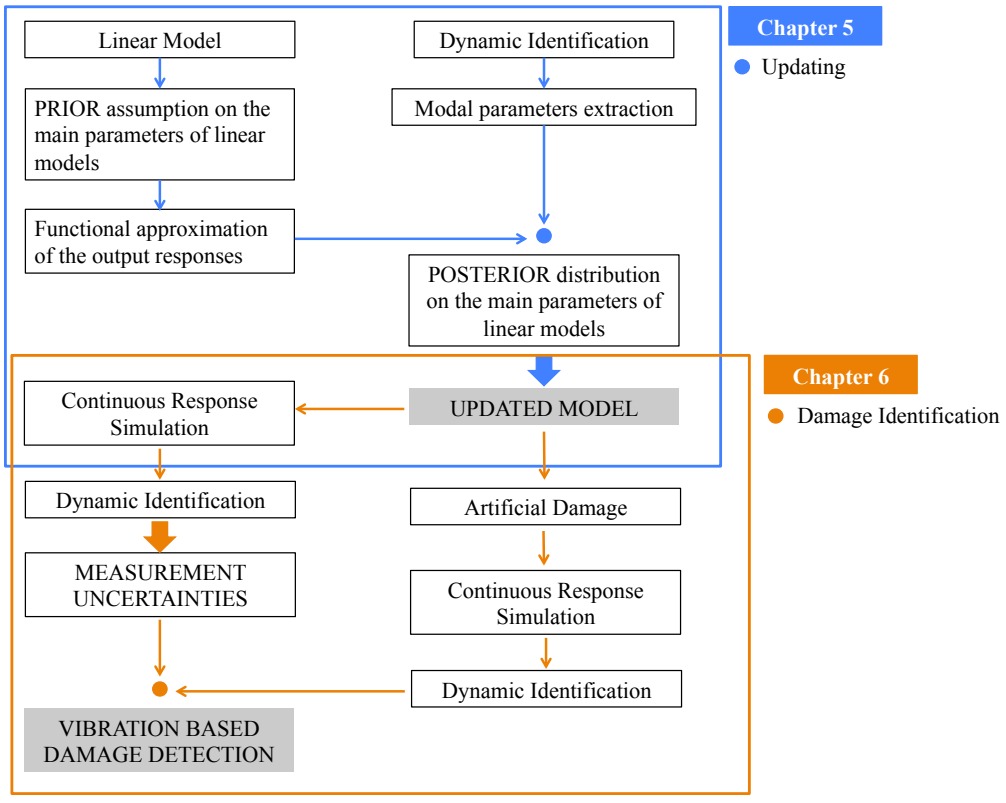

Fig. 1.4: Scheme of the thesis.

finite element numerical model. An in depth sensitivity analysis is performed in order to select the main mechanical parameters affecting natural frequencies and mode shapes to be used for model updating using Bayes' theorem. Finally, the posterior probability distributions of all the selected updating parameters is estimated and the importance of using a proper informative reference data set is addressed by a quantitative assessment of the model uncertainty remaining after the updating.

- The calibrated cable stayed footbridge numerical model is used in **Chapter 6** for the measurement uncertainty analysis when Enhanced Frequency Domain Decomposition system identification is used on virtual data. Under the main hypothesis of base excitation having white noise characteristics and that the structure is lightly damped the effect of different sources of uncertainties has been assessed by numerical simulations. Parametric numerical analyses are carried out for the evaluation of temperature and damage effects on the modal parameters in order to discuss the effectiveness and the capability of vibration based damage detection procedure when uncertainties are taken into account.
  A full - scheme of the proposed procedure is reported in Figure 1.4

- **Chapter 7** collects the main conclusion of the PhD research activities.

Chapter 2

System identification using Operational Modal Analysis

2.1 Introduction

The identification of the structural dynamic characteristics is of great importance in many fields of applications. In structural engineering it concerns the identification of the natural frequencies, the mode shapes and the damping ratios of existing structures using measured dynamic data (e.g. acceleration and/or displacements time histories). There has been a huge research activities on both numerical and experimental techniques aimed to identify the dynamic properties of structures.
Early research in modal testing resulted in an approach called Experimental Modal Analysis (EMA) [14]. In EMA, the tested structure is excited by a known input force - by means of shaking hammer or mechanical shaker - and the modal parameters are extracted from the recorded measurements. This method has been widely used over the years and it is well-established in literature. The main disadvantage is represented by the fact that the execution of the experimental tests is expensive, impracticable and not suitable for large and complex structures that cannot be isolated from their environmental conditions.

These reasons motivate researchers to study effective tools in order to identify the dynamic characteristics of structures considering just the dynamic responses under unknown input loads (output-only procedures). These kind of procedures are gathered under the name of Operational Modal Analysis (OMA) and primary results were obtained at the beginning of 1990. Nowadays OMA represents the most effective tool for modal identification with several applications to bridges and footbridges [15] [16] [17] historical structures [18] [19], platforms [20] and wind turbines [21] [22].
In contrast to EMA, OMA testing does not require any known excitation and the response of the structure is measured in operating conditions under the main hypothesis that the nature of the input load is stochastic, smooth and broadband. OMA testing techniques are so much attractive due to their relatively low cost and simplicity.
The main disadvantages and limitations of AVT are due to the lack of information about the input excitation. A number of different kind of loads can occur during each measurement together with changes in temperature, humidity and level of excitation itself, especially when wind is blowing during the test. All of these uncertain factors lead to different estimations of the modal properties for each data set. In fact the identified modal properties only reflect their values at ambient vibration level and this is particularly true for the vibration modes and the damping ratios that are amplitude dependent. Therefore, regardless the OMA identification procedure used, the modal properties cannot be identified with perfect precision from a given set of data. The source of uncertainties in fact cannot be reduced and the potential model error in the interpretations of the results needs to be considered.
OMA procedures can be divided into two main groups:

- *Time Domain Methods* They are based on the analysis of response time histories and the estimation of correlation functions. Natural Excitation Technique (NexT) is one of the earliest algorithms of OMA in time domain presented in 1995 [23]. Other examples of time domain OMA algorithm are the Auto Regressive Moving Average (ARMA) methods and the most recent Stochastic Subspace Identification (SSI) [24] and [25]. This latter represents a data driven method having the main advantage to use directly the response data, avoiding the computation of the covariances between the outputs and allowing the identification of close natural frequencies.

- *Frequency Domain Methods* In this dissertation the focus of interest is posed on the OMA algorithms in frequency domain that are based on the processing of time-correlated signals through a Discrete Fourier Transform (DFT) procedure, with the

purpose of evaluating the Power Spectral Density (PSD) functions of the structural system responses. The Basic Frequency Domain (BFT) is the first and most simple frequency domain method applied in the modal identification of a single degree of freedom structure [14]. The BFD is based on the fact that the frequencies can be identified directly from the peaks of the PSD matrix computed for the time histories recorded at the measurement points. This method has been widely used for many years together with its implementation basing on the averaged normalized PSD (ANSPSDs). This technique is suitable for low damping structures and very well separated modes. The Frequency Domain Decomposition (FDD) was introduced by Brincker et Al [26] and it represents one of the most popular OMA algorithm removing some of the shortcoming of the BFT. The modal frequencies and the vibration modes are evaluated by means of a singular value decomposition (SVD) of the output PSD matrix. Later Brincker [27] introduced the Enhanced Frequency Domain Decomposition (EFDD) technique allowing to evaluate also the modal damping ratios.

The estimated modal parameters are usually not the final objective of the tests. They are often used for numerical model calibration/updating ensuring a more accurate prediction of the structural model to extreme and complex excitation (e.g. wind and seismic events), for damage detection or Structural Health Monitoring (SHM). The numerical model calibration/updating problem will be deeply discussed in the following chapters.
Vibration based damage detection is one of the most relevant fields of application of the identification of modal parameters. It relies on the changes in dynamic properties of the structure caused by damage. In fact, the integrity of a structure can be assessed by comparing the modal parameters estimates with those obtained in healthy conditions. The vibration based damage assessment has received a lot of attention from the researchers: an extensive literature review can be found in [28]. The main limitation of damage detection technique is represented by the fact that changes in modal properties can be due not only to damage but also to the environmental conditions especially temperature, humidity and level of excitation. In the recent years a number of techniques able to remove the effect of the environmental factors have been developed [29] [30].
In sections 2.2 and 2.3 some basic mathematical concepts in random vibration analysis and classical dynamics are presented. The main concepts, merits and limitations of the output only frequency domain decomposition methods are addressed in sections 2.4 and 2.5 for discussing the accuracy of the experimental modal parameters with special reference to damping estimates. Finally, a general overview concerning vibration-based methods for structural health monitoring and damage detection with particular reference to its appli-

cation on bridge structures is discussed in section 2.6. In section 2.7 a special attention is posed on the main sources of variability in the modal characteristics of the structural system (e.g wind, temperature).

2.2 Mathematical tools in random vibrations analysis

2.2.1 Background definitions of probability theory

Let us a consider a Random Variable (RV) $X : \Omega \to \mathbb{R}$ defined according to some probability space $(\Omega, \mathcal{F}, \mathcal{P})$, where Ω is the probability space, $\mathcal{F}$ is the $\sigma-$field and $\mathcal{P}$ is the probability measure. The PDF $p(x)$ is related to the the probability that X is in the small interval $[x, x + dx]$ as in the following equation:

$$Pr\big[X \in [x, x + dx]\big] = p(x)dx \tag{2.1}$$

Since the probability $Pr\big[X \in [-\infty, +\infty]\big] = 1$, the PDF must fulfill the condition:

$$\int_{\Omega} p(x)dx = 1 \tag{2.2}$$

In a similar way in the presence of two RVs $X : \Omega \to \mathbb{R}$ and $Y : \Omega \to \mathbb{R}$, the joint probability distribution function can be defined as the probability that the RVs are in a small area $dxdy$ in the xy plane and it can be estimated by generalizing Eq. 2.1 :

$$Pr\big[X \in [x, x + dx] \text{and} Y \in [y, y + dy]\big] = p_{xy}(x, y)dxdy \tag{2.3}$$

The marginal density of the RVs X and Y is evaluated by integrating over the other variable:

$$p_x(x) = \int_{\Omega} p_{xy}(x, y)dy \qquad \text{and} \qquad p_y(y) = \int_{\Omega} p_{xy}(x, y)dx \tag{2.4}$$

Two RVs are said statistically independent if:

$$p(x, y) = p(x)p(y) \tag{2.5}$$

When a RV X assumes values in the range $(-\infty, \infty)$ its mean μ_X and variance σ_X^2 can be easily estimated as follow:

$$\mathbb{E}[X] = \int_{-\infty}^{+\infty} xp(x)dx = \mu_X \qquad \mathbb{E}[(X - \mu_X)^2] = \int_{-\infty}^{+\infty} (x - \mu_X)^2 p(x)dx = \sigma_X^2 \tag{2.6}$$

The covariance matrix of two random variables X and Y provides a simple measure of the dependence between two variables and is defined as:

$$\mathbb{E}[(X-\mu_X)(Y-\mu_Y)] = \int_{-\infty}^{+\infty}\int_{-\infty}^{+\infty}(x-\mu_X)(y-\mu_Y)p(x,y)dxdy = C_{XY} \tag{2.7}$$

The correlation coefficient can be thus introduced as a measure of the correlation between two RVs and is defined as:

$$\rho_{XY} = \frac{C_{XY}}{\sigma_X \sigma_Y} \tag{2.8}$$

It is noteworthy that the correlation coefficient assumes value equal to +1 and -1 when X and Y are perfectly correlated; it assumes value equal to zero when the two RVs are uncorrelated.

2.2.2 Correlation functions

A structural system is vibrating if it is shaking or trembling in some way. If this motion is unpredictable then the system is said to be in random vibration and the observed vibration responses $x(t)$ represent data about the quantity X as a function of time. Taking into account that a random process is the collection of all possible physical realizations of a random phenomenon and that a sample function is a single time history representing the random process, the observed vibration time history $x(t)$ is the sample function of the random process $X(t)$.

Recognizing that the exact behavior of the quantity $X(t)$ may be unknown, $X(t)$ can be completely described by its probability density function (PDF), the first and the second statistic moments. It is noteworthy that the focus on the first and second order statistics is justified by the central limit theorem since in output-only identification methods the vibration responses are approximately Gaussian independently from the distribution of the input loads.

In the following, attention is focused on stationary random process and, in particular, on ergodic stationary random process. A random process $X(t)$ is said to be stationary if its probability distribution is not a function of time and consequently its mean and variance also do not change over time. A random process is said to be ergodic if its statistical properties can be deduced from a single, sufficiently long, random sample of the process.

Assuming that a signal is known in the time interval $[0, T]$ and that the time length of the considered sample function $x(t)$ is long enough, the mean μ_x and the variance σ_x of the

sample function can be estimated using time averaging:

$$\mu_x = \mathbb{E}[x(t)] = \frac{1}{T}\int_0^T x(t)dt \qquad \sigma_x^2 = \mathbb{E}[(x(t)-\mu_x)^2] = \frac{1}{T}\int_0^T (x(t)-\mu_x)^2 dt \tag{2.9}$$

In a similar way, the covariance function can be computed directly from the two sample functions $x(t)$ and $y(t)$:

$$C_{xy}(t) = \mathbb{E}[x(t)y(t)] = \frac{1}{T}\int_0^T x(t)y(t)dt \tag{2.10}$$

or, analogously, the correlation function R_{xy}:

$$R_{xy}(t) = \mathbb{E}[(x(t)-\mu_x)(y(t)-\mu_y)] = \frac{1}{T}\int_0^T (x(t)-\mu_x)(y(t)-\mu_y)dt \tag{2.11}$$

The concept of correlation is a key issue in the output-only dynamic identification procedures. It is noteworthy that the correlation is defined in the same way as the covariance but with mean values removed from the signal. Since in random vibration applications the mean is removed from the recorded data at the beginning of signal analysis, the covariance and the correlation represent the same quantitiy.
When dealing with a single time varying ergodic process the autocorrelation function R_{xx} is used in order to assess the relationship between the two adjacent points $x(t)$ and $x(t+\tau)$, with a separation time τ in between them. By taking $y(t)$ as $x(t+\tau)$ Eq 2.11 becomes:

$$R_{xx}(\tau) = \mathbb{E}[(x(t)x(t+\tau)] = \frac{1}{T}\int_0^T x(t)x(t+\tau)dt \tag{2.12}$$

Within the hypothesis of stationary ergodic and zero mean random process, it is possible to explicit some useful properties of autocorrelation functions [31]:

- The autocorrelation function is equal to the variance σ_x^2 when τ is equal to zero;
- For $\tau \to \infty$ the two variables in Eq. 2.12 become independent and $R_{xx}(\tau)$ approaches to zero;
- If the signal $x(\tau)$ is stationary the density function does not depend on time as well as all the expectations. The correlation function does not depend on the time t and for any shift time -specifically for $-\tau$ - it is possible to obtain the symmetry relation: $R_{xx}(\tau) = R_{xx}(-\tau)$.

The crosscorrelation is simply defined by generalizing Eq. 2.12 to two random processes:

$$R_{xy}(\tau) = \mathbb{E}[(x(t)y(t+\tau)] = \frac{1}{T}\int_0^T x(t)y(t+\tau)dt \tag{2.13}$$

$$R_{yx}(\tau) = \mathbb{E}[(y(t)x(t+\tau)] = \frac{1}{T}\int_0^T y(t)x(t+\tau)dt \tag{2.14}$$

Under the same hypothesis of stationary and ergodic signal also the cross correlation function is characterized by symmetry relation for a time shift equal to $-\tau$. In general $R_{xy}(\tau)$ and $R_{yx}(\tau)$ are not the same and, unlike the autocorrelation function, they are not even in τ.

In practical applications of output-only dynamic identification the dynamic response of a structural system is usually recorded at several positions. Normally the N recorded vibration time histories are recorded and gathered in a response vector $\mathbf{y}(t) = \{y_1(t), y_2(t), ..., y_N(t)\}$. The autocorrelation and the crosscorrelation functions can be thus gathered in a correlation matrix $\mathbf{R}(\tau)$ having diagonal elements equal to autocorrelation functions and off-diagonal elements equal to cross-correlation functions as:

$$\mathbf{R}(\tau) = \mathbb{E}[\mathbf{y}(t)\mathbf{y}(t+\tau)^T] = \frac{1}{T}\int_0^T \mathbf{y}(t)\mathbf{y}(t+\tau)^T dt = \mathbf{R}(-\tau) \tag{2.15}$$

2.2.3 Spectral Density Functions

The Power Spectral Density (PSD) function $G_{xx}(\omega)$ for a time series $x(t)$ shows the distribution of the spectral frequencies as a function of frequency and is defined as the Fourier transform of the correlation function $R_{xx}(\tau)$ in Eq. 2.12 [31]:

$$G_{xx}(\omega) = \frac{1}{2\pi}\int_{-\infty}^{\infty} R_{xx}(\tau)e^{-i\omega\tau}d\tau \tag{2.16}$$

Inversely, the autocorrelation function can be derived as the inverse Fourier Transform of the PSD:

$$R_{xx}(\tau) = \int_{-\infty}^{\infty} G_{xx}(\omega)e^{i\omega\tau}d\omega \tag{2.17}$$

Eqs. 2.16 and 2.17 are also known as the Wiener-Khintchine relations [31] [32]. Within the main hypothesis of zero mean sample function $x(t)$ as in practical application of output-only identification methods the autocorrelation function at the initial value $\tau = 0$ becomes:

$$R_{xx}(0) = \mathbb{E}[x(t)^2] = \sigma_x^2 = \int_{-\infty}^{\infty} G_{xx}(\omega)d\omega \tag{2.18}$$

Eq. 2.18 is the mathematical representation of the Parseval theorem meaning that the area under the spectral density equals the second moment of the stochastic process $X(t)$. It is easy to see that if $X(t)$ is bandpass filtered so that only the frequency content of the signal from ω_1 to ω_2 is considered, the variance of the band filtered signal σ_{xbf} is given by:

$$\sigma_{xbf}^2 = 2\int_{\omega_1}^{\omega_2} G_{xx}(\omega)d\omega \tag{2.19}$$

In a similar way the cross spectral density function for two time series $x(t)$ and $y(t)$ is defined as the Fourier transform of the cross correlation $R_{xy}(\tau)$ in Eq. 2.13:

$$G_{xy}(\omega) = \frac{1}{2\pi}\int_{-\infty}^{\infty} R_{xy}(\tau)e^{-i\omega\tau}d\tau \tag{2.20}$$

And, inversely, the cross correlation function can be defined as:

$$R_{xy}(\tau) = \int_{-\infty}^{\infty} G_{xy}(\tau)e^{i\omega\tau}d\tau \tag{2.21}$$

The Parseval theorem in this case provides the relation:

$$R_{xy}(0) = \mathbb{E}[xy] = C_{xy} = \int_{-\infty}^{\infty} G_{xy}(\omega)d\omega \tag{2.22}$$

and the area under the cross density spectrum equals the covariance C_{xy}.
Using the definition of the PSD and the time reversal properties of the Fourier transform, it is easy to observe that the spectral density matrix $G(\omega)$ has similar symmetric properties of the correlation function matrix. Furthermore, it is always Hermitian meaning that is always equal to the complex conjugate transpose:

$$G(\omega)^H = G(\omega) \tag{2.23}$$

In practical applications PSDs can be obtained by computing first the correlation functions and then the Fourier transforming them. This approach is also known as Blackman-Tukey method. A less demanding procedure also known as Welch procedure is instead based on direct computation of the Fast Fourier Transform (FFT) of the records. In fact given a time series $x(t)$ the one sided auto spectral density function can be estimated by dividing the record into n_s continuous segments each of length $T = N_{FL}\Delta T$ and then Fourier transforming each segment. The auto spectral density is thus computed through

an averaging operation over all the segments:

$$\hat{G}_{xx}(\omega) = \frac{2}{n_s N_{FL} \Delta t} \sum_{i=1}^{n_s} |X_i(\omega)| \tag{2.24}$$

where $X_i(\omega)$ is the Fourier transform of the time series:

$$X_i(\omega) = \int_0^T x(t) e^{-i2\pi\omega t} dt \tag{2.25}$$

and N_{FL} is the number of data values in each data segment able to determine the frequency resolution of the resulting estimates. Even if the Welch procedure is advantageous from a computational point of view, specific procedures are required to avoid the occurrence of unpredictable errors arising from the fact the record has a finite length. A time series can be seen as the product between an unlimited record and a rectangular time window assuming value equal to 1 when $0 \leq t \leq T$ ond 0 elsewhere. As a consequence the Fourier transform of the time series is given by the convolution of the Fourier transform of both the unlimited record and the rectangular time window.
The Fourier transform of a rectangular time window is basically a sinc function with side lobes characterized by a fairly large amplitude with respect to the main lobe. This large side lobes allow the energy at a certain frequency to spread to nearby the frequency causing large error. This phenomena is called leakage and it may introduce significant distortions of the estimated spectra. This phenomena is avoided when the analyzed data are periodic with a period equal to the time length meaning that the discrete frequency values are equally spaced at $\Delta\omega = \frac{1}{T}$. In such case the discrete frequency value corresponds to the zero of the spectral window in the frequency domain with the only exception of the frequency line in the main lobe. There are a lot of commonly employed window and the most common one is the Hanning window.

2.3 Basics of classical dynamics

The dynamic behavior of a structure can be represented by a set of differential equations in time domain, or by a set of differential equations in frequency domain. Let us consider a N multiple degree of freedoms system. The governing equations of motion in time domain are given by:

$$\mathbf{M}\ddot{\mathbf{y}}(t) + \mathbf{C}\dot{\mathbf{y}}(t) + \mathbf{K}\mathbf{y}(t) = \mathbf{x}(t) \tag{2.26}$$

where $\mathbf{M}$ is the $[N \times N]$ mass matrix, $\mathbf{C}$ is the $[N \times N]$ damping matrix and $\mathbf{K}$ is the $[N \times N]$ stiffness matrix of the structural system; the responses are gathered in the vector $\mathbf{y}$(t) and $\mathbf{x}$(t) is the input force. This system of equations is based on the main assumptions of linear, time invariant and observable system.
Under the hypothesis of proportional damping any general response can be expressed as a linear combinations of the eigenvectors $\mathbf{\Phi}_n$:

$$\mathbf{y}(t) = \sum_{n=1}^{N} \mathbf{\Phi}_n q_n(t) = [\mathbf{\Phi}_n]\mathbf{q}(t) \tag{2.27}$$

where $[\mathbf{\Phi}_n]$ is the mode shape matrix and $\mathbf{q}$ is the column vector of the modal coordinates as a function of time. Substituting Eq. 2.27 into Eq. 2.26, premultiplying both sides of equation by the transpose of the eigenvectors $\mathbf{\Phi}_n$ and taking into account the orthogonality conditions of the normal modes yields to:

$$m_n\ddot{q}(t) + c_n\dot{q}(t) + k_n q(t) = p_n(t) \tag{2.28}$$

where the term $p_n(t)$ represents the modal load and is given by:

$$p_n(t) = \mathbf{\Phi}_n^T \mathbf{x}(t) \tag{2.29}$$

In this way the system of second order differential equations in Eq 2.26 is decoupled into a set of N independent single degree of freedom (SDOF) differential equations. The general solution can be found by determining the modal loads using Eq. 2.29, solving the SDOF equation of motion given by Eq. 2.28 and then adding the modal solutions together using Eq. 2.27.
As for an SDOF solution the modal coordinates can be found by taking the Laplace transform of both sides of Eq. 2.28 as follow:

$$(m_n s^2 + c_n s + k_n)Q_n(s) = P_n(s) \tag{2.30}$$

where s is the the complex variable $s = \sigma + i\omega$ and $q_n(t) \leftrightarrow Q_n(s)$ and $p_n(t) \leftrightarrow P_n(s)$ are Laplace transform pairs.
The mass scaled modal transfer function $H_n(s)$ of the mode n can be thus found as the ratio between the Laplace transform of the output $Q_n(s)$ and the Laplace transform of the

input $P_n(s)$:

$$\frac{Q_n(s)}{P_n(s)} = H_n(s) = \frac{1}{(m_n s^2 + c_n s + k_n)} \tag{2.31}$$

Using the poles of the system and combining the the mass, stiffness and damping values Eq.2.31 can be further modified. The poles represent the resonant frequencies of the vibrating system or, in other words, the frequency values at which the input is amplified. Let us define respectively ω_{0n} and ζ_n as the undamped angular frequency of vibration ω_n and the damping ratio ζ_n of the nth mode:

$$\omega_{0n} = \sqrt{\frac{k_n}{m_n}} \qquad \text{and} \qquad \zeta_n = \frac{c_n}{2\sqrt{m_n k_n}} \tag{2.32}$$

It is noteworthy that the undamped natural frequency depends only on the mass and the stiffness and it is independent from the damping of the system; the damping ratio depends on all those quantities defining the physical behavior of the whole system. Therefore the poles can be written as:

$$\lambda_n = -\zeta_n \omega_{0n} + i\omega_{0n}\sqrt{1-\zeta_n^2} \qquad \text{and} \qquad \lambda_n^* = -\zeta_n \omega_{0n} - i\omega_{0n}\sqrt{1-\zeta_n^2} \tag{2.33}$$

The quantity in the imaginary term $\omega_{nd} = \omega_{0n}\sqrt{1-\zeta_n^2}$ is called the damped natural frequency. Using this term the poles in Eq.2.33 can be rewritten obtaining:

$$\lambda_n = -\zeta_n \omega_{0n} + i\omega_{dn} \qquad \text{and} \qquad \lambda_n^* = -\zeta_n \omega_{0n} - i\omega_{dn} \tag{2.34}$$

The mass scaled transfer function can be defined as:

$$H_n(s) = \frac{1}{m_n(s-\lambda_n)(s-\lambda_n^*)} \tag{2.35}$$

where * denotes complex conjugate. The mass scaled modal transfer matrix for a N DOFs system can be thus obtained by taking the Laplace transform of Eq. 2.27:

$$\mathbf{y}(s) = \sum_{n=1}^{N} \mathbf{\Phi}_n Q_n(s) = [\mathbf{\Phi}_n]\boldsymbol{q}(s) \tag{2.36}$$

where $\boldsymbol{y}(t) \leftrightarrow \boldsymbol{y}(s)$ and $\boldsymbol{q}(t) \leftrightarrow \boldsymbol{q}(s)$ are Laplace transform pairs. Eq. 2.31 leads to:

$$\mathbf{y}(s) = \sum_{n=1}^{N} \mathbf{\Phi}_n H_n(s) P_n(s) \tag{2.37}$$

where $P_n(s)$ is the Laplace transform of the modal load in Eq. 2.29 . Therefore:

$$\mathbf{y}(s) = \sum_{n=1}^{N} \mathbf{\Phi}_n H_n(s) \mathbf{\Phi}_n^T \boldsymbol{x}(s) \tag{2.38}$$

where $\boldsymbol{x}(t) \leftrightarrow \boldsymbol{x}(s)$ is a Laplace transform pair.
Finally Eq 2.38 leads directly to the input-response relation stating that in the Laplace domain the solution of the differential equations of motion is just the product between the force and the transfer function:

$$\mathbf{y}(s) = \mathbf{H}(s)\mathbf{x}(s) \tag{2.39}$$

Furthermore, using matrix notation the summation in the above equation can be rewritten obtaining:

$$\sum_{n=1}^{N} \mathbf{\Phi}_n H_n(s) \mathbf{\Phi}_n^T = [\mathbf{\Phi}_n][H_n(s)][\mathbf{\Phi}_n^T] \tag{2.40}$$

where $[H_n(s)]$ is a diagonal matrix having elements equal to the modal transfer functions. The transfer function matrix can be thus defined as:

$$\mathbf{H}(s) = \mathbf{\Phi}_n [H_n(s)] \mathbf{\Phi}_n^T \tag{2.41}$$

Realizing the partial factor expansion [14] [33]:

$$\frac{1}{(s-\lambda_n)(s-\lambda_n^*)} = \frac{1}{\lambda_n - \lambda_n^*} \left(\frac{1}{s-\lambda_n} - \frac{1}{s-\lambda_n^*} \right) \tag{2.42}$$

and using Eq. 2.33 getting $\lambda_n - \lambda_n^* = 2i\omega_{dn}$ the modal transfer function can be rewritten obtaining:

$$H_n(s) = \frac{1}{2i\omega_{dn} m_n} \frac{1}{s-\lambda_n} + \frac{1}{2(-i)\omega_{dn} m_n} \frac{1}{s-\lambda_n^*} \tag{2.43}$$

Let us define the residue matrix $\mathbf{R_n}$:

$$\mathbf{R}_n = \frac{\mathbf{\Phi}_n \mathbf{\Phi}_n^T}{2i\omega_{dn} m_n} \tag{2.44}$$

Eq.2.41 can be further rewritten obtaining:

$$\mathbf{H}(s) = \sum_{n=1}^{N} \left(\frac{\mathbf{R}_n}{s-\lambda_n} + \frac{\mathbf{R}_n^*}{s-\lambda_n^*} \right) \tag{2.45}$$

The mass scaled Frequency Response Function FRF can be defined as the mass scaled modal transfer function calculated at the imaginary axis $s = i\omega$ and in physical terms it represents the amplitude and the phase of the steady state response of a viscous damped SDOF system subjected to an harmonic force of unit amplitude and frequency ω. Therefore the corresponding FRF matrix is given by:

$$\mathbf{H}(\omega) = [\mathbf{\Phi}_n][H_n(\omega)][\mathbf{\Phi}_n]^T = \sum_{n=1}^{N} \Big(\frac{\mathbf{R}_n}{i\omega - \lambda_n} + \frac{\mathbf{R}_n^*}{i\omega - \lambda_n^*} \Big) \tag{2.46}$$

Since the mass, stiffness and damping are symmetric matrices both the transfer function and the the FRF matrices are symmetric. Furthermore Eq. 2.46 shows that every element of the FRF matrix has the same denominator and it shows that each mode gives a contribution to the response of the system at any frequency.
The solution of the differential equilibrium equations can be thus expressed in terms of mass scaled FRF. Using the convolution property of the Fourier transform, $\mathbf{y}(\omega)$ can be obtained as the product between the Fourier transform of the input forces $\mathbf{x}(\omega)$ and the FRF matrix, as follow:

$$\mathbf{y}(\omega) = \mathbf{H}(\omega)\boldsymbol{x}(\omega) \tag{2.47}$$

where $\boldsymbol{x}(t) \leftrightarrow \boldsymbol{x}(\omega)$ and $\boldsymbol{y}(t) \leftrightarrow \boldsymbol{y}(\omega)$ are Fourier transform pairs. This result states that in frequency domain the solution of the differential equation of motion is the product between the input force and the FRF. Manipulating Eq. 2.47 and taking into account the definition of the PSD the fundamental equation of OMA is obtained [31]:

$$\mathbf{G_{yy}}(\omega) = \mathbf{H}(\omega)^* \mathbf{G_{xx}}(\omega) \mathbf{H}(\omega)^T \tag{2.48}$$

where $\mathbf{G_{yy}}$ is the matrix of output PSD and $\mathbf{G_{xx}}$ is the matrix of input force PSD and * and ^{T} denotes complex conjugate and transpose respectively.

2.4 Frequency Domain Decomposition

The Frequency Domain Decomposition (FDD) method was firstly derived by Brincker in [26], [34] and later by Brincker and Zhang [35].
Let us consider the recorded response time histories arranged in a vector $\mathbf{y}(t)$ as a function of modal coordinates and normal modes as in Eq. 2.27. Substituting Eq. 2.46 in Eq. 2.48

it is possible to obtain the PSD matrix of the responses $\mathbf{G}_{yy}(\omega)$ in the form:

$$\mathbf{G_{yy}}(\omega) = \Big[\sum_{n=1}^{N}\big(\frac{\mathbf{R}_n}{i\omega-\lambda_n}+\frac{\mathbf{R}_n^*}{i\omega-\lambda_n^*}\big)\Big]^*\mathbf{G_{xx}}(\omega)\Big[\sum_{s=1}^{N}\big(\frac{\mathbf{R}_s}{i\omega-\lambda_s}+\frac{\mathbf{R}_s^*}{i\omega-\lambda_s^*}\big)\Big]^H \tag{2.49}$$

where the superscript ^{H} denotes complex conjugate and transpose. Assuming that the input load is zero mean Gaussian white noise (i.e. the PSD matrix of the input $\mathbf{G_{xx}}(\omega)$ is a constant matrix C) the output PSD can be expressed in the same residue form:

$$\mathbf{G_{yy}}(\omega) = \Big[\sum_{n=1}^{N}\big(\frac{\mathbf{R}_n}{i\omega-\lambda_n}+\frac{\mathbf{R}_n^*}{i\omega-\lambda_n^*}\big)\Big]^*\mathbf{C}\Big[\sum_{n=1}^{N}\big(\frac{\mathbf{R}_s}{i\omega-\lambda_s}+\frac{\mathbf{R}_s^*}{i\omega-\lambda_s^*}\big)\Big]^H \tag{2.50}$$

In Eq. 2.50, the poles contains the information about the natural frequencies and the damping ratios while the residue holds information about the mode shapes. Introducing the modal participation vector γ_n associated to the n-th mode, the residue in Eq. 2.44 assumes the form:

$$\mathbf{R}_n = \mathbf{\Phi}_n\boldsymbol{\gamma}_n^T \tag{2.51}$$

Multiplying the two partial fraction factors in Eq. 2.49, after some mathematical manipulations the output PSD can be reduced to [36]:

$$\mathbf{G_{yy}}(\omega) = \sum_{n=1}^{N}\frac{\mathbf{A}_n}{i\omega-\lambda_n}+\frac{\mathbf{A}_n^*}{i\omega-\lambda_n^*}+\frac{\mathbf{B}_n}{-i\omega-\lambda_n}+\frac{\mathbf{B}_n^*}{-i\omega-\lambda_n^*} \tag{2.52}$$

where $\mathbf{A}_n$ are the n-th residue hermitian matrix of the output PSD corresponding to the n-th pole λ_n given by:

$$\mathbf{A}_n = \mathbf{R}_n\mathbf{C}\big(\sum_{s=1}^{N}\frac{\mathbf{R}_s^{*T}}{i\omega-\lambda_s}+\frac{\mathbf{R}_s^T}{i\omega-\lambda_s^*}\big) \tag{2.53}$$

Eq.2.52 shows that the output PSD matrix provides four poles in complex conjugate pairs $(\lambda_n, \lambda_n^*, -\lambda_n, -\lambda_n^*)$. The contribution to the residue from the n-th mode is given by:

$$\mathbf{A}_n = \frac{\mathbf{R}_n\mathbf{C}\mathbf{R}_n^{*T}}{2\alpha_n} \tag{2.54}$$

where α_n is minus the real part of the pole $\lambda_n = -\alpha_n + i\omega_n$. Under the main hypothesis of lightly damped structure (i.e. $\zeta_n << 1$) and considering that at a certain frequency ω only a limited number of modes will contribute significantly, the residue becomes proportional to the mode shape vector and the response spectral density matrix can be written in the

final following form:

$$\mathbf{G_{yy}}(\omega) = \sum_{n \in Sub(\omega)} \frac{d_n \mathbf{\Phi}_n \mathbf{\Phi}_n^T}{i\omega - \lambda_n} + \frac{d_n^* \mathbf{\Phi}_n^* \mathbf{\Phi}_n^{*T}}{i\omega - \lambda_n^*} \tag{2.55}$$

where d_n is a scalar quantity and $Sub(\omega)$ the set of the modes that contribute at the certain frequency.
The decomposition of the spectral matrix can also be seen as a result of uncorrelated modal coordinates. In fact the correlation matrix of the response $\mathbf{R}_{yy}$ can be estimated by means of Eq. 2.15:

$$\mathbf{R_{yy}}(\tau) = \mathbb{E}[\mathbf{y}(t)\mathbf{y}(t+\tau)^T] = [\mathbf{\Phi}]\mathbf{R}_{qq}(\tau)[\mathbf{\Phi}]^T \tag{2.56}$$

where $\mathbf{R}_{qq}(\tau)$ is the correlation function matrix of the modal coordinates. The PSD matrix of the output response can be thus obtained by taking the Fourier transform of Eq. 2.56 according to Eq. 2.16:

$$\mathbf{G_{yy}}(\omega) = [\mathbf{\Phi}]\mathbf{G}_{qq}(\omega)[\mathbf{\Phi}]^H \tag{2.57}$$

Assuming that the modal coordinates are uncorrelated, that is the off-diagonal elements of the modal coordinates correlation function matrix $\mathbf{R}_{qq}(\tau)$ are equal to zero, the modal coordinates spectral density matrix $\mathbf{G}_{qq}(\omega)$ is diagonal and positive valued.
The Singular Value Decomposition (SVD) of the spectral density matrix of the output response at a certain frequency ω leads to:

$$\mathbf{G_{yy}}(\omega) = \mathbf{U\Sigma V}^H \qquad \mathbf{UV}^H = 1 \tag{2.58}$$

where $\mathbf{\Sigma}$ is the matrix of singular values arranged in a descending order and $\mathbf{U}$ and $\mathbf{V}$ are respectively the unitary matrices of left and right singular vectors. Since the spectral density matrix is positive definite and Hermitian $\mathbf{U} = \mathbf{V}$ and the decomposition can be rewritten obtaining:

$$\mathbf{G_{yy}}(\omega) = \mathbf{U\Sigma U}^H \tag{2.59}$$

Eqs. 2.59 and 2.57 have got the same form and they identify a one-to-one relationship between singular vectors and mode shapes as well as between singular values and modal response. Using the singular value decomposition, the response of the MDOF system under investigation is thus decoupled into the spectra of equivalent SDOF systems. In fact, assuming that only one mode is dominant at the frequency ω and that the selected frequency is associated to the peak of resonance of the k-th mode, the PSD matrix approximates to

a rank one matrix:

$$\mathbf{G_{yy}}(\omega) = \sigma_1 \boldsymbol{u_1} \boldsymbol{u_1}^H \qquad \mathbf{U}\mathbf{U}^H = 1 \tag{2.60}$$

The first singular vector $\boldsymbol{u_1}$ represents an estimate of the mode shape of the k-th mode and the corresponding singular value σ_1 belongs to the auto PSD function of the equivalent SDOF system corresponding to the mode of interest.
It is noteworthy that unlike the BFD, FDD method allows for the identification of closely spaced modes or even coincident modes since the number of non zero elements in $\mathbf{\Sigma}$ equals the rank of the PSD matrix at the considered frequency. However, it is worth pointing out that the mode shape estimates could be biased. In fact, since the SVD forces the singular vectors to be orthogonal, if the experimental mode shapes are also orthogonal, the obtained estimates are unbiased. On the contrary, if the mode shapes are not geometrically orthogonal, the mode shape estimates for the closely spaced modes are biased. The bias depends on the difference between the first and second singular value: the larger this difference, the smaller the error. Thus, the mode shape estimates should be obtained from singular vectors at frequencies characterized by the largest difference between the first and second singular value.

2.5 Enhanced Frequency Domain Decomposition

The EFDD method was firstly derived by Brincker [27] to estimate not only natural frequencies and mode shapes but also modal damping ratios. In this method the equivalent SDOF PSD function is identified as the set of singular values and corresponding singular vectors around a peak on the singular value curves. The comparison of the mode shape $\bar{\mathbf{\Phi}}_\mathbf{k}$ at the peak of the singular values and the singular vectors associated to each frequency line around the selected peak leads to the identification of the singular values whose singular vectors show a correlation higher than a threshold value. This threshold value is defined by the Modal Assurance Criterion (MAC) coefficient [37].
The MAC allows to obtain information about the correlation between two modal vectors assuming values between 0 (no correlation) and 1 (good correlation) and it is defined by Eq. 2.61:

$$MAC = \frac{|\mathbf{\Phi}^T \mathbf{\Psi}|^2}{\mathbf{\Phi}^T \mathbf{\Phi} \mathbf{\Psi}^T \mathbf{\Psi}} \tag{2.61}$$

where $\mathbf{\Phi}$ and $\mathbf{\Psi}$ are two modal vectors. In general, the MAC coefficient is used in order to compare the numerical and experimental vibration modes or to compare the vibration modes obtained from the measurements with themselves for assessing the quality of the

measurement results. In this latter case the MAC coefficient is called the AutoMAC.
In the estimation of natural frequencies and damping ratios using EFDD method, the MAC is used in order to define the set of singular values around the peak and Eq. 2.61 becomes:

$$MAC = \frac{|\bar{\boldsymbol{\Phi}}_{\mathbf{k}}{}^{T}\boldsymbol{u}_j|^2}{\bar{\boldsymbol{\Phi}}_{\mathbf{k}}{}^{T}\bar{\boldsymbol{\Phi}}_{\mathbf{k}}\boldsymbol{u}_j^T\boldsymbol{u}_j} \tag{2.62}$$

where $\boldsymbol{u}_j$ is the generic singular vector in the vicinity of the peak in the singular value plots corresponding to the k-th mode. It is evident that the lower is the MAC the larger is the number of singular values and corresponding singular vectors used for the estimation of both natural frequencies and damping ratios. The equivalent SDOF correlation function is computed by taking back the selected set of singular values to the time domain through an Inverse Discrete Fourier Transform (IDFT). Thus an estimate of the natural frequency independent of the frequency resolution can be obtained through a linear regression on the zero crossing times of the equivalent SDOF system correlation function.
In a similar way damping ratio can be estimated as the logarithmic decrement δ of the free decay time domain function according to::

$$\zeta = \frac{\delta}{\sqrt{\delta^2 + 4\pi^2}} \tag{2.63}$$

where δ is given by:

$$\delta = \frac{2}{k}\ln\frac{r_o}{|r_k|} \tag{2.64}$$

and r_0 is the initial value of the correlation function and r_k is the kth extreme. Unlike the natural frequencies the damping ratios estimates are strictly dependent on the selected spectral bell, on the time window fixed for autocorrelation function and on the frequency resolution that is defined by Eq.2.65:

$$\Delta f = \frac{f_\nu}{N_{FL}/2} \tag{2.65}$$

where f_ν is the Nyquist frequency and N_{FL} is the number of data points in the data segment considered in the PSD. The dependency on frequency resolution was found to be due to the leakage bias introduced with the estimation of PSD using Welch method, as discussed in previous section. The assumption that all individual data segments are periodic is not fulfilled in case of real data and the resulting distortion of the shape of the PSD can cause serious errors in damping ratios estimation. Therefore the bias error on

damping ζ_b can be defined [38] as a function of the dimensionless natural frequency ω_n of the mode n:

$$\zeta_b = \frac{2f_\nu}{\pi\omega_k N_{FL}} \tag{2.66}$$

It is evident that the bias error on damping converges to zero with an high frequency resolution and therefore the number of data segments has to be chosen accurately. It is well known that the bias errors depends on both the natural frequency and damping ratios: the smaller is the natural frequency and the damping ratio the greater is the bias error. Moreover damping ratio estimates can be affected by errors due to signal noise and signal processing since in output-only dynamic identification technique the lack of knowledge about the input results in a lack of knowledge about the spectral distribution of its energy.

2.6 Vibration based damage detection and structural health monitoring

The most relevant field of application of vibration tests and dynamic identification procedures is the damage detection. Damage can be defined as any change introduced in a system intentionally or unintentionally affecting the actual state and the future performance of that system [39]. Most currently used damage identification methods include visual inspection or local experiment such as acoustic, ultrasonic or thermal tests. However all of these methods require the "a priori" knowledge of the presence of damage and the need to develop effective tool for damage identification and detection has gradually gained the attention of the researchers.

The main idea at the base of SHM is that the modal parameters (natural frequencies, mode shapes and modal damping) are related to the structural properties. Variations in the structural properties (stiffness of components) due to a damage can cause change in modal properties. For this reason developments of non-destructive techniques based on changes in the structural vibration parameters have been extensively studied. For several years this approach has been widely criticized for two main reasons. The first one is the misleading idea that global quantities (such as natural frequencies) are not able to catch local phenomena; the second one is that the local nature of damage can be well captured by higher frequency modes that are the most difficulty to identify using vibration tests and output only identification technique.

Many techniques incorporating modal parameters have been proposed for damage detection, developed and expanded upon over the years, several of which are detailed in the

following review papers [39] [40] [41]. Based on the available scientific literature, many different classification can be promoted concerning vibration based SHM techniques. A first common categorization of damage assessment techniques can be fulfilled defining 4 level of damage diagnosis [42]:

1. Determination of the *presence* of damage;
2. Determination of the damage *location* in the structure;
3. Determination of the damage *severity*;
4. Prediction of the remaining *service life* of the structure;

The first two levels can be performed by the so called data driven method since are essentially based on measurements not requiring structural model. On the contrary, the fourth and, partially, the third levels make use of numerical models (model driven methods).
Another common classification is made on the the basis of the effect of damage on the structure and on types of data available in the measurements of vibrations. More specifically:

- *Linear approaches* are used when the structure is modeled as a linear-elastic system before and after damage occurrence allowing the use of linear equations of motion;
- *Non linear approaches* are used to guarantee a more performing damage identification if a structural anomaly occurrence provides non-linear effects on system behavior.

In this dissertation the attention is posed on the first three level of damage diagnosis (presence, location and severity of damages) by means of a linear approach with a special focus on the modal parameter to use as damage indicator. In literature, the natural frequency shifts are usually used to discern damage. However it is important to point out that the global nature of modal frequencies may not allow the damage localization in complex structures [43]. In this sense the use of mode shapes becomes very attractive since they are the only quantities that contain explicitly a spatial description of the resonance. Some literature works presents successful applications in damage detection by means of MAC coefficients quantifying the correlation between damaged and undamaged state [44] on very simple structural system and in laboratory experiments. However mode shapes are dependent on the spatial distribution of sensors and a great number of measurement points is usually required for a proper mode shape definition. Furthermore they are very sensitive to level of excitation and to measurement noise. Modal damping has been investigated

as a possible damage sensitive feature with some interesting results [45]. Actually the identification of modal damping using output-only dynamic identification technique is a challenge and its use as a reliable damage indicator is not recommended.

2.7 Sources of variability in the modal characteristics of structures

The relevance of a proper estimation of the modal characteristics of the structures has received a lot of attention by the researchers since structural dynamic identification has been revealed an effective tool for damage detection. The main problem to face in case of dynamic measurements on structures concerns the reliability of the evaluated modal parameters since they are significantly affected by environmental and operating conditions and, on the contrary, not so much sensitive to damage.
External factors always produce effects on the modal characteristics of structures. Among them the most relevant one is the temperature whose effects is therefore one of the most investigated in literature [46]. Temperature fluctuations can cause daily frequency shifts of 5% and seasonal shifts greater than 10% [47] [48] leading to mistakes in damage identification.
In case of suspension or cable stayed bridges and footbridges temperature increases cause an equivalent reduction of the steel elastic modulus and an elongation of the cables corresponding to a tension loss and to a reduction of the geometric stiffness. Many researchers pointed out the important role of temperature in influencing the dynamic response of this kind of structures [47] [49], observing, in most of cases, an essentially linear correlation among natural frequencies and temperature even if temperature effect are potentially unpredictable. Therefore statistical approaches are used for the extraction of temperature effects on natural frequencies using regression methods, e.g. principal components analysis [30] [50].
In the field of bridge and footbridge vibration based damage identification one of the most significant environmental factor is the wind action. Increasing and decreasing eigenfrequencies can be observed as a function of wind speed and variations are comparable to those produced by other environmental factors. Changes in the eigenproperties can be due to the aerodynamic properties of the considered bridges and footbridges [51], but also to variations in the geometry of the cables and large displacements [52]. Daily eigenfrequency fluctuations are due also to the operational conditions and, in particular, to traffic loads [53], to pedestrian or to any other kind of excitation in operating conditions [54].

Finally, the data collection and the measurement noise effects on modal parameters need to be considered. This is actually an open field in literature since the effect of measurement errors is unpredictable and depends on many factors such as the kind of devices adopted for monitoring, type of digital/analogic converter and system of communication of the recorded data (wireless devices or wiring). In practical applications a significant variability of modal parameters is also observed when data set different for time length and amplitude of input excitations are used. In this sense another important topic is represented by the signal processing, which includes such methods as Fourier analysis, time-frequency analysis and wavelet analysis. Different sampling frequency, frequency resolution and filters can cause variability in the eigenproperties of the same order of magnitude of damage, temperature and excitations.
In general, the modal characteristics variability is also due to the fact that all the OMA procedures in frequency and time domain are based on the main hypothesis of input Gaussian stationary white noise and proportional damping, e.g lightly damping structures. For some applications the hypothesis on the input load distribution is reasonable. However in a vast amount of situations, the analyzed structure is subject to harmonic forces, transient inputs (such as wave on dam or wind on bridges) or to tremors and micro tremors. Numerous methods and research has enabled to develop methods that are robust to such harmonic contributions [55] [56]. The assumption of proportional damping, instead, is not the most realistic representation of how the system dissipates energy when it vibrates and actually the extension of OMA procedures to general damping is another open issue.
The verification of all these limitations and the study of their effects on the modal characteristics is a crucial task in both single measurement campaign and continuous SHM. Single measurement campaigns are usually carried out for finite element correlation analyses, finite element updating and validation or the experimental evaluation of structural effects under different types of dynamic load. Assessing the reliability and the level of accuracy/ confidence in system identification when different signal time length or parameters used in data processing may represents a useful tool for an accurate definition of a baseline set of dynamic properties that may be subsequently used for the application of vibration based damage detection techniques and the automatic integration of output only modal identification technique.

Chapter 3

Uncertainty quantification with stochastic finite elements

3.1 Introduction

Every numerical prediction model is characterized by several kind of model uncertainty. Modeling uncertainty can arise from the concept of model itself, from the input parameters and from modeling assumptions and simplifications due to the inherent lack of knowledge. The investigation and the categorization of different sources and level of uncertainty is a crucial issue.

Uncertainty on the model parameters, for example, can be due to a lack of knowledge about the main input parameters and to their inherent randomness nature. In structural identification this kind of uncertainty may regard the unknown material properties, the geometric characteristics, the load characteristics and the actions from the surrounding environment.

Uncertainty on the model structure arises from modeling assumptions, simplifications and idealizations that can be due to a lack of knowledge about the real behavior or to a wrong interpretation of reality. Furthermore, the numerical model to update is always

a simplification of a real structure and due to the complexity of the latter the induced modeling error often is not negligible. This kind of uncertainty may regard, instead, the main hypothesis on the boundary condition or the governing physical and mathematical equations and the discrete approximation of the continuous system. According to [57] it is possible to distinguish the uncertainty into two groups:

- *Aleatoric uncertainty*: This kind of uncertainty concerns those phenomena whose occurrence is intrinsically stochastic. By their nature these uncertainties cannot be reduced;

- *Epistemic uncertainty*: This kind of uncertainty refers to an incomplete knowledge of parameters and phenomena. Such lack of knowledge can arise from incomplete or inconsistent experimental data or from model approximations and simplifications. Objectively this kind of uncertainty can be reduced even though this may be non practical and not possible.

The different kind of uncertainties are addressed in different ways by the two main schools of probability interpretation: frequentist and Bayesian interpretation. According to the frequency definition, the probability is defined only when dealing with well-defined random experiments (or random samples). The relative frequency of occurrence of an event observed in a number of repetitions of the experiment is a measure of the probability of that event. In the frequentist context no assumptions on the main hypothesis governing the problem are required and the observed data are samples from that distribution. Bayesian inference models the uncertainty by a probability distribution over an hypothesis and updates the initial knowledge about the unknown parameters with information from data even when a random process is not involved. Therefore on one hand probabilities express objective frequencies; on the other hand probabilities represent an individual's degree of belief in a statement or in an hypothesis.
While the fundamental of uncertainty quantification are well - established in principle, the actual challenge is the complexity of the modern engineering system. Uncertainty analysis and sensitivity analysis are essential parts of a proper analysis of complex systems.
The main target of the uncertainty quantification is to construct effective tools in order to study the output responses of a system with uncertain characteristics and with random inputs. The typical framework (Fig. 3.1) for uncertainty quantification analysis can be divided into the *forward problem*, aimed to characterized the model output, and the *inverse problem* aimed to obtain useful information about the model inputs.

In structural engineering applications, uncertainty quantification problems deal with the

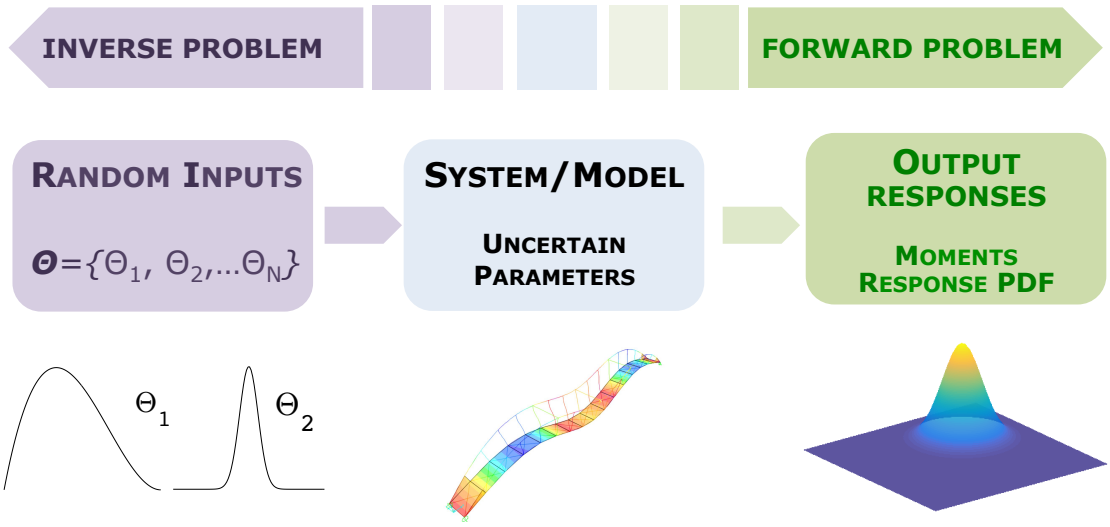

Fig. 3.1: Schematic representation of the uncertainty quantification framework.

characterization of the model/system output response given the uncertain input random variable/random vector with proper probability distribution.
The statistics values like means, variances or moments and the complete probability distribution of the outputs can be assessed using many different probabilistic methods [58]:

- *Sampling based methods*: Methods based on the selection of a subset of observations from a statistical population to estimate the characteristics of the whole population. Monte Carlo and Quasi Monte Carlo simulations or Latin Hypercube sampling belong to this category;

- *Functional expansions - based methods*: Methods based on a functional representation of the input/output of a model/system such as Karhunen - Loeve expansion, polynomial chaos representation and generalized polynomial chaos expansion;

- *Model order reduction* Methods aimed to a simplification of the model maintaining a reasonable accuracy;

- *Surrogate models*: Methods aimed to an approximation of the real model cheaper to evaluate such as response surface methods, meta models or proxy models.

These methods are used for different objectives and they have got limitations. The simulation based methods and the functional expansion based methods allow the evaluation of the statistic moments of the output responses together with the probability density function. The simulation based methods requires an high computational cost since the

uncertainties of the model's outputs are quantified by randomly generating independent realizations of the inputs according to their probability distribution. With this approach the deterministic solution is evaluated through a large amount of simulations. Moreover the convergence is reached slowly requiring a substantial number of individual deterministic realization (typically of the order of 10^4 to 10^5) for an acceptable accuracy of the system performance.

Today, with the important advancements in numerical modeling and with the increase computer powers highly accurate simulations of complex physical phenomena can be obtained, but in the most of cases, prohibitive computational costs are required. Moreover, the computational burden can increase when several solution evaluations with different configurations or different parameters are needed, for example in (stochastic) design optimization, Bayesian inference, uncertainty quantification and propagation or global sensitivity analysis. In order to reduce the computational effort a surrogate (proxy) model of the simulator can be developed in order to represent the original model's behavior. A proxy model can be built starting from a functional representation of the input random variables/random vectors in a mathematical form. Many types of surrogate models exist such as gaussian process models, artificial neural network and polynomial chaos representation based model. In the following just the latter are treated in details.

The use of proxy models and polynomial chaos representation is a topic of continued research for their capability to provide a reliable framework particularly useful for high cost computational simulation.

This chapter is organized as follow: fundamental of uncertainty quantification are reviewed in section 3.2 and 3.3. Global surrogate model based on orthogonal polynomials are deeply discussed in section 3.4 with a brief review on all those methods aimed at the evaluation of the deterministic coefficients. Finally, a suitable and accurate method for a global sensitivity analysis based on Sobol' coefficient is reviewed in section 3.5.

3.2 Engineering model in abstract setting

In the uncertainty quantification (UQ) context, a model of an engineering system/structure is a mathematical representation of the physical system. Consider a computational mechanical model $\mathcal{M}$ characterized by an input random vector $\boldsymbol{\Theta} = \{\Theta_1, ..., \Theta_N\} \in \mathbb{R}^N$ consisting in N independent random parameters defined according to some probability space $\{\Omega, \mathcal{F}, \mathcal{P}\}$ where Ω is the probability space, $\mathcal{F}$ is the $\sigma-$field and $\mathcal{P}$ is the probability measure. Each Θ_i is described by a probability density function (PDF) $\pi(\theta_i)$ so that the

joint PDF is given by the product of the N densities. Let the relation between the vector $\boldsymbol{\Theta}$ and the associated output response quantities $\mathbf{u} = \{u_1, ..., u_M\} \in \mathbb{R}^M$ given by the forward problem $\mathcal{M}$:

$$\mathbf{u} = \mathcal{M}(\boldsymbol{\Theta}) \tag{3.1}$$

and $\mathcal{M} : \mathbb{R}^N \to \mathbb{R}^M$. It is assumed that selecting a given set of parameters $\boldsymbol{\theta} = \{\theta_1, ..., \theta_N\}$, i.e. a realization of $\boldsymbol{\Theta}$, the corresponding deterministic solution is unique and will not change if the model is ran again with the same input. The model is therefore treated as a deterministic uncertain black box and the only requirement is that it is available in an executable form. It is important to observe that the operator $\mathcal{M}$ may be linear or non linear but in both cases since the operator is uncertain even a linear problem becomes non linear.

The input random vector $\boldsymbol{\Theta}$ is uncertain and it can be characterized through its mean vector $\boldsymbol{\mu_\Theta}$ and its covariance matrix $\boldsymbol{\Sigma_\Theta}$:

$$\boldsymbol{\mu_\Theta} = \mathbb{E}[\boldsymbol{\Theta}] = \int_\Omega \boldsymbol{\Theta} \pi_{\boldsymbol{\Theta}} d\boldsymbol{\Theta} \tag{3.2}$$

$$\boldsymbol{\Sigma_\Theta} = \mathbb{E}[\boldsymbol{\Theta} - \boldsymbol{\mu}_u)(\boldsymbol{\Theta} - \boldsymbol{\mu_\Theta})^T] = \int_\Omega (\boldsymbol{\Theta} - \boldsymbol{\mu_\Theta})(\boldsymbol{\Theta} - \boldsymbol{\mu_\Theta})^T \pi_{\boldsymbol{\Theta}} d\boldsymbol{\Theta} \tag{3.3}$$

where $\pi_{\boldsymbol{\Theta}}$ is the density function of the input distribution. The main objective of UQ problems is to quantify the distribution of the model outputs that results from the randomness of the input. Starting from Eq. 3.1 the output can be defined again through its mean vector $\boldsymbol{\mu_u}$and its covariance matrix $\boldsymbol{\Sigma_u}$:

$$\boldsymbol{\mu_u} = \mathbb{E}[\mathcal{M}(\boldsymbol{\Theta})] = \int_\Omega \mathcal{M}(\boldsymbol{\Theta}) \pi_{\boldsymbol{\Theta}} d\boldsymbol{\Theta} \tag{3.4}$$

$$\boldsymbol{\Sigma_u} = \mathbb{E}[(\mathcal{M}(\boldsymbol{\Theta}) - \boldsymbol{\mu_u})(\mathcal{M}(\boldsymbol{\Theta}) - \boldsymbol{\mu_u})^T] = \int_\Omega (\mathcal{M}(\boldsymbol{\Theta}) - \boldsymbol{\mu_u})(\mathcal{M}(\boldsymbol{\Theta}) - \boldsymbol{\mu_u})^T \pi_{\boldsymbol{\Theta}} d\boldsymbol{\Theta} \tag{3.5}$$

For complex problem the full characterization of the input and the output requires also the definition of the higher moments such as Skewness or Kurtosis.

3.3 Direct integration methods

The main goal of a UQ framework is to characterize the statistics of the model output. Different methods can be used. A recent overview on computational approach can be found in [58] and [59].

Let us consider a Lebesgue integrable function $f(x)$. The expectation $\mathbb{E}[f(x)]$ can be computed using different approximation methods:

- **Probability Densities** The probability distribution (mainly the PDF) of $f(x)$ is described by a system of high dimensional equations. The PDF of a random state vector of a random system can be computed directly using the Fokker Planck Equations [60];
- **Direct Integration** The expectation of the function $f(x)$ can be expressed as an integral over the probability space;
- **Galerkin Methods** This kind of methods are based on the transformation of a continuous operator problem into a discrete problem. The integral is computed through an approximation by minimizing the weighted residual [61].

In the following just the direct integration methods are deeply discussed. The key idea is that any statistics or any function of the Quantity of Interest (QoI) can be calculated as an integral over the probability space as in Eqs. 3.4 and 3.5.
The integral can be approximated by taking samples $\boldsymbol{\theta_z} \in \mathbb{R}^Z$ according to the joint probability density $\pi_{\boldsymbol{\Theta}}$ and evaluating the solution of the mathematical model in each set of realizations $\boldsymbol{\theta_z}$. The expected value of the QoI can be then estimating as follow:

$$\boldsymbol{\mu_u} = \int_{\Omega} \mathcal{M}(\boldsymbol{\Theta})\pi_{\boldsymbol{\Theta}} d\boldsymbol{\Theta} \sim \sum_{z=1}^{Z} w_z \mathcal{M}(\boldsymbol{\theta}_z) \tag{3.6}$$

where w_z are the weights. The sampling points can be selected according to different criteria and different methods can be distinguished basing on how the integration points are chosen. Note that when the mathematical model is complex or computationally demanding the computation of the expectation becomes costly since the deterministic solution is required for all the sampling points. As a result, the reduction of the computational costs becomes a crucial issue in UQ problems.

3.3.1 Monte Carlo methods

Monte Carlo (MC) provides a direct robust method for performing simulation and integration. A complete overview of this method can be found in [62] [63]. This method is suitable for integrands with small variances and when low level of accuracy is required.
In MC methods the Z_{MC} integration points are selected by randomly generating independent samples from the input distribution. The weights w_z are taken constant and equal to

$w_z = \frac{1}{Z_{MC}}$. Therefore Eq. 3.6 can be written as:

$$\boldsymbol{\mu_u} = \int_\Omega \mathcal{M}(\boldsymbol{\Theta})\pi_{\boldsymbol{\Theta}} d\boldsymbol{\Theta} \sim \frac{1}{Z_{MC}} \sum_{z=1}^{Z_{MC}} \mathcal{M}(\boldsymbol{\theta}_z) \tag{3.7}$$

The main advantage of the MC method is represented by the fact that both the model response $\boldsymbol{u}$ and the error due to the approximation are random vectors. The law of large number and the central limit theorem ensure that the MC approximation converges for $Z_{MC} \to \infty$. Moreover, for large Z_{MC} the error is approximately Gaussian with variance $\frac{||\boldsymbol{\mu_u}||^2_{L_2}}{Z_{MC}}$ and $L_{2\boldsymbol{\Theta}}$-norm is the standard deviation of the integrand.
The standard deviation of the exact responses represents in practice the deviation from the target mean implying that the convergence rate $\mathcal{O}(\frac{||\boldsymbol{\mu_u}||_{L_2}}{\sqrt{Z_{MC}}})$ is independent from the dimension N of the input random vector. However since the deterministic solution of the mathematical model needs to be evaluated for a great number of independent realizations, the convergence is very slow and often an excessive computational burden is required. As a result different methods such as Quasi Monte Carlo (QMC) [62] and Latin Hypercube (LH) [64] sampling are used for improving the convergence rate.

3.3.2 Gaussian quadrature rule

The quadrature rule can be a useful tool for the evaluation of the integral in Eq. 3.4. The key idea of this method is to interpolate the integrand by a functional approximation whose integral is known analytically.
For sake of simplicity restricting the problem to a one dimensional space, the one dimensional integral $\mathcal{Q}_{Z_Q}$ in the form $\int_\Omega u(\theta)\pi_\Theta(\theta)d\theta$ can be approximated with the evaluation of the deterministic solution in the Z_Q quadrature points, using the form:

$$\mathcal{Q}_{Z_Q} = \sum_{z=1}^{Z_Q} \mathcal{M}(\theta_z) w(\theta_z) \tag{3.8}$$

The sampling points θ_z corresponds to the z-th root of orthogonal polynomials with the weighting function π_Θ. This relation establishes a correspondence between type of probability distribution π_Θ and the Gauss quadrature formula. For example if π_Θ is a Gaussian distribution Gauss Hermite quadrature should be used; instead, if π_Θ is a uniform distribution Gauss - Legendre quadrature should be used. Moreover common weighting functions include $w(\theta) = 1$ for the Gauss Legendre or $w(\theta) = \frac{1}{\sqrt{1-\theta^2}}$ for the Gauss - Chebyshev and

$w(\theta) = e^{-\theta^2}$ for the Gauss Hermite quadrature. Such integration scheme has a degree of polynomial exactness equal to $2Z_Q - 1$.
The extension to the N-dimensional integration can be constructed by the tensorization of the one dimensional quadrature formula according to:

$$\mathcal{Q}^N_{Z_Q} = \otimes^N_{j=1} \mathcal{Q}_{Z_Q} = \sum_{j_1=1}^{Z_Q} \cdots \sum_{j_N=1}^{Z_Q} w_{j_1,z_Q} \cdots w_{j_N,z_Q} u(\theta_{j_1,z_Q}, ..., \theta_{j_N,z_Q}) \tag{3.9}$$

This full tensor grid quadrature evaluates the integrand on a regular mesh of Z^N points. It is evident that the number of sampling points where the solution of the deterministic solver needs to be evaluated exponentially increase with the number of input parameter space. For high dimensional problem a Smolyak quadrature formula [65] can be constructed. The grids of sampling points is then developed combining quadrature formula of high order in only some dimensions with formulas of lower order in other dimensions.

3.4 Surrogate Model

Surrogate models are frequently used tools for the analysis of complex systems behavior. These systems are usually computationally demanding and therefore difficult to explore over the whole domain of input parameters. Ideally, a surrogate model should be able to give a good representation of the QoI reducing as much as possible the error between the approximate and the exact response. The problem of building a cheap proxy model able to give an accurate approximation of the real system is not easy to solve especially for an high number of input random parameters. In typical engineering problems the computational model $\mathcal{M}$ is not known or however uncertain. Using the same notation of Eq. 3.1, a surrogate model $\tilde{\mathcal{M}}$ is a mathematical function defined as follow:

$$\tilde{\mathbf{u}} = \tilde{\mathcal{M}}(\boldsymbol{\Theta}) \tag{3.10}$$

Building a proxy model requires an experimental design (ED) meaning that training data consisting in a set of support points needs to be properly identified and the responses of the original model in these points need to be evaluated. A measure of the accuracy for the surrogate model is the generalized error Err_G [66], which represents the mean square of the relative error $\boldsymbol{\varepsilon} = \mathbf{u} - \tilde{\mathbf{u}}$ computed at a sufficiently large set of points in the input space:

$$Err_G = \mathbb{E}[\boldsymbol{\varepsilon}^2] = \mathbb{E}[(\mathbf{u} - \tilde{\mathbf{u}})^2] \tag{3.11}$$

A suitable proxy model can be built up using several techniques. A common approach allowing for the evaluation of the main statistic moments of the output distribution is to construct a global surrogate model of the mathematical operator in terms of response surface [67] [68]. On the other hand a widespread class of proxy models is based on Polynomial Chaos (PC) expansion [69] [70], Polynomial Decomposition (PD) [71], Artificial Neural (AN) network [72] and Kriging [73] [74]. The latter two methods have their roots in machine learning but today their applications have become of particularly interest especially when a lot of data needs to be managed. In the following just the PC based surrogate models are deeply discussed.

3.4.1 Polynomial chaos expansion

The so called polynomial chaos representation was introduced in 1938 by N. Weiner [75] for turbulence modeling with input Gaussian random variables using Hermite polynomials. Ghanem and Spanos [61] were among the first to apply the PC expansion to the FE method for the uncertainty quantification in solid - mechanics. This Stochastic Finite Elements Method (SFEM) has found a lot of applications including structural mechanics and thermo fluid system. Xiu et Al. [69] extended the Hermite PC based to the Wiener - Askey based PC (or generalized Polynomial Chaos Expansion (gPCE)) for the representation of random processes with inputs of different probability distributions.
In the last decades the literature on the use of PC in SFEM is significantly increased thanks to the recent research developments providing a suitable framework for computational simulation. Complete reviews can be found on Sudret et Al. [76] and Kaintura et Al. [77]. The key idea of PC expansion is to represent the model response into an appropriate basis made of orthonormal multivariate polynomials obtained as the the tensor product of polynomials in each of the input parameter. In this way each RV/random vector is represented in a mathematical series form and both stochastic input and output can be very well approximated as a truncated series of orthogonal random polynomials [78] [79]. Both the PDF and the statistic moments of the model outputs can be directly estimated from the properties of orthogonal polynomials. Moreover a surrogate model can be easily developed facilitating all those procedure such as Bayesian model updating, sensitivity analysis and design and control of structures.
An important feature of the PC expansion method is that the deterministic coefficients of the truncated series needs to be calculated once during the solution process unlike MC or QMC methods. The size of the obtained coupled deterministic system of equations depends on the terms of PC expansions used for the approximation, the type of orthogonal

polynomial used as basis and the number of input RVs.

3.4.1.1 Mathematical Setting

The most general mathematical setting for characterizing all those problems where random uncertainties are defined by a finite number of RVs with arbitrary probability distribution is discussed in the following. A general stochastic system is modeled as a non linear transformation of a finite set of basic RVs defined over a suitable probability space. The finite dimensional character of the basic RVs allows for the extension of the standard Wiener chaos decomposition to the second order RVs with arbitrary probability measure.
Consider the class of non Gaussian $\mathbb{R}^N$- valued RVs, $\boldsymbol{\Theta}$, defined according to some probability space $(\Omega, \mathcal{F}, \mathcal{P})$ having independent components so that the joint distribution is simply the product of the marginal distributions $\{\pi_{\Theta_i}\}_{i=1}^N$ i.e.

$$\boldsymbol{\Theta} = \mathbf{g}(\boldsymbol{\xi}) \tag{3.12}$$

where $\mathbf{g}$ is a deterministic non linear function, $\mathbf{g} : \mathbb{R}^K \to \mathbb{R}^N$, $\boldsymbol{\xi} \sim N(0, \boldsymbol{I})$ is a $\mathbb{R}^K$- valued vector of K independent and identically distributed, zero mean, unit variance Gaussian RVs and $\mathbf{I}$ denotes the identity matrix having dimension $(K \times K)$. Thus without loss in generality the following analysis is carried out for normalized RVs.
The solution of the physical model in Eq. 3.1 can be written as:

$$\mathbf{u} = \mathcal{M}(\boldsymbol{\xi}) \tag{3.13}$$

assuming that $\mathbf{u}$ is a second order random vector such that:

$$\mathbb{E}\{||\mathcal{M}(\xi_1, \cdots, \xi_K)||^2\} < \infty \tag{3.14}$$

and considering first the case of univariate input (ξ_i), i.e. $K = 1$, and a univariate output, i.e. $M = 1$, the series in Eq. 3.15

$$u = \sum_{\alpha \geqslant 0} \hat{u}_\alpha \Psi_\alpha(\xi_i) \tag{3.15}$$

is convergent in L_2 according to Cameron - Martin theorem [80] and constitutes the PC expansion for the model response. Here $\{\hat{u}_\alpha\}_{\alpha=1}^\infty$ are the deterministic coefficients that must be determined and $\{\Psi_\alpha(\xi_i)\}_{\alpha=1}^\infty$ are one dimensional orthogonal polynomials. Eq 3.15 constitutes a spectral representation of the random response u.

Let us consider the Hilbert space $\mathbb{H}_i$ of square integrable real valued functions of ξ_i. For any two elements ϕ_1 and ϕ_2 it is possible to write the following inner product:

$$\langle \phi_1, \phi_2 \rangle_{\mathbb{H}_i} = \int_{\mathbb{R}^k} \phi_1(\xi)\phi_2(\xi)\pi_{\xi_i}(\xi)d\xi_i \tag{3.16}$$

where π_{ξ_i} denotes the marginal PDF of ξ_i.
The r.h.s. of Eq. 3.16 is the expectation $\mathbb{E}[\phi_1(\xi_i)\phi_2(\xi_i)]$ with respect to the marginal distribution π_{ξ_i}. Two such functions are said orthogonal with respect to the probability measure $\mathcal{P}(d\xi) = \pi_{\xi_i}(\xi)d\xi$ if $\mathbb{E}[\phi_1(\xi_i)\phi_2(\xi_i)] = 0$.
The PC representation of the RV u can be obtained by representing the model $\mathcal{M}$ on an Hilbertian basis that is a complete orthonormal family of functions of the Hilbert space of the model solution. Using the classical algebra notation a family of complete orthogonal polynomials $\{\gamma_{k_i}, k \in \mathbb{N}\}$ where k is the degree of polynomial, can be built up as:

$$\langle \gamma_j^{(i)}, \gamma_k^{(i)} \rangle_{\mathbb{H}_i} = \mathbb{E}[\gamma_j^{(i)}(\xi_i)\gamma_k^{(i)}(\xi_i)] = \int \gamma_j^{(i)}(\xi)\gamma_k^{(i)}(\xi)\pi_{\xi_i}(\xi)d\xi = a_j^i\delta_{jk}, \qquad j,k \in N_0 \tag{3.17}$$

where δ_{jk} is the Kronecker symbol equal to 1 when $j = k$ and 0 otherwise and $a_j^{(i)}$ is the normalizing factor defined as the squared norm of γ_j^i i.e:

$$a_j^{(i)} = \mathbb{E}[\gamma_j(\xi_i)^2] = \langle \gamma_j^{(i)}, \gamma_j^{(i)} \rangle_{\mathbb{H}_i} \tag{3.18}$$

The obtained family is usually not orthonormal. By enforcing the normalization an orthonormal family $\{\psi_j^{(i)}\}_{j=1}^{\infty}$can be obtained using Eqs. 3.17 and 3.18:

$$\psi_j^{(i)} = \frac{\gamma_j^i}{\sqrt{a_j^{(i)}}} \tag{3.19}$$

Eq. 3.17 assesses a correspondence between the distributions and the associated family of orthogonal polynomials. In particular, for a standard normal distribution with zero mean value and unit standard deviation the resulting family is that of Hermite polynomials. The families associated to standard distributions are summarized in Table 3.1. Further mathematical details and a complete review of the mathematical formulation can be found in Soize et Al. [81].

Let us extend the formulation to a multivariate input consisting in the random vector $\boldsymbol{\xi}$. The spectral decomposition can be constructed as an Hilbertian basis of the Hilbert space of the model solution $\mathbb{H}$, taking into account the tensorized structure of this vector space.

Table 3.1: Correspondence between the orthogonal polynomials and their underlying random variables [69].

Distribution	Corresponding polynomials	Support
Uniform $U(a,b)$	Legendre (P)	[a,b]
Normal $N(\mu,\sigma^2)$	Hermite (H, He)	$[-\infty,+\infty]$
Gamma	Laguerre ($\mathrm{L}^{(\alpha)}$)	$[0,+\infty]$
Beta (α,β)	Jacobi/hypergeometric ($\mathrm{P}^{(\alpha,\beta)}$)	[a,b]

The Hilbert space $\mathbb{H}$ of the square integrable real valued functions of $\boldsymbol{\xi}$ is equipped with the inner product:

$$\langle \phi_1, \phi_2 \rangle_{\mathbb{H}} = \int_{\mathbb{R}^k} \phi_1(\boldsymbol{\xi}) \phi_2(\boldsymbol{\xi}) \pi_{\boldsymbol{\xi}}(\boldsymbol{\xi}) d\boldsymbol{\xi} \tag{3.20}$$

Under the assumption that the components of the random vector $\boldsymbol{\xi}$ are independent the Hilbert space $\mathbb{H}$ is isomorphic with the Hilbert space $\bar{\mathbb{H}}$ defined by the tensor product $\bar{\mathbb{H}} = \otimes_{i=1}^{K} \mathbb{H}_i$ and equipped with the inner product:

$$\langle \phi_1, \phi_2 \rangle_{\bar{\mathbb{H}}} = \int_{\mathbb{R}^k} \phi_1(\xi_1, \cdots, \xi_K) \phi_2(\xi_1, \cdots, \xi_K) \pi_{\xi_1}(\xi_1), \cdots, \pi_{\xi_K}(\xi_K) d\xi_1 \cdots d\xi_K \tag{3.21}$$

Then the Hilbertian basis in the Hilbert space $\mathbb{H}$ can be obtained as the tensor product of the Hilbertian bases associated with the single basic RVs. Having univariate polynomials $\{\psi_\alpha(\xi_i)\}_{\alpha=1}^{\infty}$ for each RV ξ_i multivariate polynomials in $\boldsymbol{\xi}$ are constructed via tensorization. For this purpose let us define $\boldsymbol{\alpha} = (\alpha_1, ..., \alpha_N) \in \mathbb{N}^K$ as a multi index with $|\boldsymbol{\alpha}| = \alpha_1 + ... + \alpha_K$. Then the multivariate polynomial can be written as the products of the univariate polynomials $\left\{\psi_j^i, j \in \mathbb{N}\right\}$ defined according to the i-th distribution as following :

$$\boldsymbol{\Psi}_{\boldsymbol{\alpha}}(\boldsymbol{\xi}) = \prod_{i=1}^{K} \psi_{\alpha_i}^{(i)}(\xi_i) \tag{3.22}$$

where the univariate polynomials are defined according to the k-th marginal distribution. Following Eqs. 3.17 and 3.21 the multivariate polynomials in the input vector $\boldsymbol{\xi}$ are also orthonormal:

$$\mathbb{E}[\boldsymbol{\Psi_i}(\boldsymbol{\xi})\boldsymbol{\Psi_j}(\boldsymbol{\xi})] = \int \boldsymbol{\Psi_i}(\boldsymbol{\xi})\boldsymbol{\Psi_j}(\boldsymbol{\xi})\pi_{\boldsymbol{\xi}}(\boldsymbol{\xi})d\boldsymbol{\xi} = \delta_{\boldsymbol{\alpha}\boldsymbol{\beta}}, \qquad \boldsymbol{\alpha}, \boldsymbol{\beta} \in \mathbb{N}^K \tag{3.23}$$

where $\delta_{\boldsymbol{\alpha\beta}}$ is the Kronecker symbol which is equal to 1 if $\boldsymbol{\alpha} = \boldsymbol{\beta}$ and zero otherwise. With this notation and consider Eq. 3.15 it is possible to write:

$$u = \mathcal{M}(\boldsymbol{\xi}) = \sum_{\boldsymbol{\alpha} \in \mathbb{N}^K} \hat{\boldsymbol{u}}_{\boldsymbol{\alpha}} \boldsymbol{\Psi}_{\boldsymbol{\alpha}}(\boldsymbol{\xi}) \tag{3.24}$$

Note that the set of the multivariate polynomials in the input random vector $\boldsymbol{\xi}$ forms a basis of the Hilbert space in which u is to be represented. The obtained Eq 3.24 can be interpreted as an intrinsic representation of u in an abstract space through an orthonormal basis and coefficients that are the coordinates of u in this basis.

3.4.1.2 Truncation scheme

The representation of the random response in Eq. 3.24 is exact when an infinite series is considered, but the computation of infinite terms is impossible. In practice, an appropriate truncation scheme needs to be developed.
Let us define the total degree of a multivariate polynomials $\boldsymbol{\Psi}_{\alpha}$ by:

$$|\boldsymbol{\alpha}| = \sum_{i=1}^{K} \alpha_i \tag{3.25}$$

where K is the number of the independent standard normal distributed input RVs ξ_i. Let us define p as the maximum polynomial degree. The response in Eq. 3.24 may be approximated by all the K-dimensional Hermite polynomials of degree not exceeding p (i.e. $\{\boldsymbol{\alpha} \in \mathbb{N}^K : |\boldsymbol{\alpha}| \leq p\}$) as follows:

$$u \sim \tilde{u} = \tilde{\mathcal{M}}(\boldsymbol{\xi}) = \sum_{\boldsymbol{\alpha} \geq 0}^{N_P - 1} \hat{\boldsymbol{u}}_{\boldsymbol{\alpha}} \boldsymbol{\Psi}_{\boldsymbol{\alpha}}(\boldsymbol{\xi}) \tag{3.26}$$

where $\tilde{\mathcal{M}}(\boldsymbol{\xi})$ represents the surrogate model. In this case the number of unknown (vector) coefficients in the summation is given by:

$$N_P = \binom{K+p}{p} = \frac{(K+p)!}{K!p!} \tag{3.27}$$

The polynomial order has to be chosen to guarantee results accuracy. As an example, in SFEM applications it is common to choose p between 3 and 5. A suitable convergence analysis needs to be carried out to determine the optimal PC expansion order.

The PC expansion was initially formulated using standard Gaussian random input parameters and Hermite polynomials [75] but it is in general possible to model input system parameters with any non-Gaussian distribution using suitable mapping with isoprobabilistic transformations. However, it is worth noting some limitations of PC expansion: the rate of convergence of the PC approximation may be slow; accuracy improvements can not be achieved even if adding terms; moments higher than two calculated from PC approximation can be not accurate; PC approximations for stationary non-Gaussian stochastic process might not be stationary [82].

3.4.1.3 Computation of the deterministic coefficient

The computation of the deterministic coefficient $\hat{\boldsymbol{u}}_{\boldsymbol{\alpha}}$ in Eq. 3.26 can be carried out using different approaches: Galerkin projection, orthogonal projection and regression [58]. These three approaches can be distinguished in intrusive or non intrusive methods. In particular, a method is intrusive if the deterministic solver has to be modified in order to obtain the stochastic solution (e.g. Stochastic Galerkin); while a non intrusive method in based on the deterministic solutions of the input realizations (regression and orthogonal projection). A basic overview of these computational approach is given in the following.

Stochastic Galerkin Using a truncated PC expansion means to obtain a residual error equal to the difference between the real model solution $\mathcal{M}(\boldsymbol{\xi})$ and the approximated solution $\tilde{\mathcal{M}}(\boldsymbol{\xi})$.Using Galerkin projection the residual error has to be orthogonal to the space of the basis function used in the expansion [83]. This means that the inner product in Eq. 3.28 is equal to zero.

$$\langle \tilde{\mathcal{M}}(\boldsymbol{\xi}), \Psi_\alpha(\boldsymbol{\xi}) \rangle = 0 \qquad \alpha = 0, ..., N_P - 1 \tag{3.28}$$

The solutions of this linear system of coupled equations can be obtained modifying the numerical code of the mathematical system. For this reason often Stochastic-Galerkin method is not practically useful.

Orthogonal Projection The projection method is based on the orthogonality of PC. Each PC coefficient can be computed orthogonally projecting the random response $\tilde{\mathcal{M}}(\boldsymbol{\xi})$ into the corresponding basis function $\boldsymbol{\Psi}_{\boldsymbol{\alpha}}(\boldsymbol{\xi})$ [84] [85]. Pre multiplying the Eq. 3.26 and

taking the expected value, it comes:

$$\langle \tilde{\mathcal{M}}(\boldsymbol{\xi}), \boldsymbol{\Psi}_{\boldsymbol{\alpha}}(\boldsymbol{\xi}) \rangle = \mathbb{E}[\tilde{\mathcal{M}}(\boldsymbol{\xi}), \boldsymbol{\Psi}_{\boldsymbol{\alpha}}(\boldsymbol{\xi}] = \mathbb{E}\Big[\sum_{\boldsymbol{\beta} \geq 0}^{N_P - 1} \hat{\boldsymbol{u}}_{\boldsymbol{\beta}} \boldsymbol{\Psi}_{\boldsymbol{\beta}}(\boldsymbol{\xi}) \boldsymbol{\Psi}_{\boldsymbol{\alpha}}(\boldsymbol{\xi}) \Big] = \hat{\boldsymbol{u}}_{\boldsymbol{\alpha}} \mathbb{E}[\boldsymbol{\Psi}_{\boldsymbol{\alpha}}(\boldsymbol{\xi})^2] \quad (3.29)$$

where $\hat{\boldsymbol{u}}_{\boldsymbol{\alpha}}$ is the orthogonal projection of the random response $\tilde{u}$ into the corresponding basis function.
Rearranging the equation the coefficients $\hat{\boldsymbol{u}}_{\boldsymbol{\alpha}}$ can be expressed using the form:

$$\hat{\boldsymbol{u}}_{\boldsymbol{\alpha}} = \frac{\mathbb{E}[\tilde{\mathcal{M}}(\boldsymbol{\xi}), \boldsymbol{\Psi}_{\boldsymbol{\alpha}}(\boldsymbol{\xi})]}{\mathbb{E}[\boldsymbol{\Psi}_{\boldsymbol{\alpha}}(\boldsymbol{\xi})^2]} \quad (3.30)$$

In this expression the denominator is known analytically. The numerator can be obtained solving the following the multidimensional integral:

$$\mathbb{E}[\tilde{\mathcal{M}}(\boldsymbol{\xi}), \boldsymbol{\Psi}_{\boldsymbol{\alpha}}(\boldsymbol{\xi})] = \int \boldsymbol{u}(\boldsymbol{\xi}) \boldsymbol{\Psi}_{\boldsymbol{\alpha}} \pi_{\boldsymbol{\xi}}(\boldsymbol{\xi}) d\boldsymbol{\xi} \quad (3.31)$$

Unfortunately the integral cannot be directly estimated as the dependence between $\mathbf{u}$ and $\boldsymbol{\Theta}$ is not known. In fact the realizations of $\boldsymbol{g}(\boldsymbol{\xi})$ are available only in the form of runs of the deterministic solver; therefore the functional form of $\boldsymbol{g}(\boldsymbol{\xi})$ is not known and the integral cannot be solved in a close form.
The estimation of the numerical value of the deterministic coefficient may be computed using MC or LH simulation. However the number of samples required for a sufficient accuracy should be large enough. When the mathematical model is complex and computationally demanding this approach becomes practically not applicable. An alternative approach is the use of Gaussian quadrature rule allowing for the evaluation of the multidimensional integral with a small number of deterministic solver running at selected points.

Least square minimization The least square minimization method originally introduced by Choi et Al. [86] is used in this dissertation and it is based on the minimization of the mean square error in the response approximation. To this aim, the random response of the model is written as:

$$\mathcal{M}(\boldsymbol{\xi}) = \sum_{\boldsymbol{\alpha} \geq 0}^{N_P - 1} \hat{\boldsymbol{u}}_{\boldsymbol{\alpha}} \boldsymbol{\Psi}_{\boldsymbol{\alpha}}(\boldsymbol{\xi}) + \varepsilon \quad (3.32)$$

in which the residual error $\boldsymbol{\varepsilon}$ collects the truncated PC terms. The regression approach consists in finding the set of coefficient $\hat{\boldsymbol{u}} = \{\hat{u}_0, ..., \hat{u}_{N_P - 1}\}^T$ which minimizes the variance

of the residual error giving the best approximation of the mathematical model $\mathcal{M}(\boldsymbol{\xi})$:

$$\hat{\boldsymbol{u}} = arg \quad min\left\{\mathbb{E}\left[\left(\mathcal{M}(\boldsymbol{\xi}) - \sum_{\boldsymbol{\alpha}\geq 0}^{N_P-1} \hat{\boldsymbol{u}}_{\boldsymbol{\alpha}} \boldsymbol{\Psi}_{\boldsymbol{\alpha}}(\boldsymbol{\xi})\right)^2\right]\right\} \tag{3.33}$$

The discretized version of the continuous problem in Eq. 3.33 is based on a set of $N_R > N_P$ regression points gathered in the vector $\mathcal{X} = \{\boldsymbol{\xi^1}, ..., \boldsymbol{\xi^{N_R}}\}$, called ED. For each of these points a set of N_R realizations of the input vector $\boldsymbol{\Theta}$ can be evaluated according to Eq. 3.12.

The least square minimization problem can therefore be solved by minimizing the mean square truncation error:

$$\hat{\boldsymbol{u}} = arg \quad min \frac{1}{N_R} \sum_{i=1}^{N_R} \left\{\mathcal{M}(\boldsymbol{\xi}^i) - \sum_{\boldsymbol{\alpha}\geq 0}^{N_P-1} \hat{\boldsymbol{u}}_{\boldsymbol{\alpha}} \boldsymbol{\Psi}_{\boldsymbol{\alpha}}(\boldsymbol{\xi}^i)\right\}^2 \tag{3.34}$$

Eq. 3.34 is equivalent to the linear system of equations:

$$\begin{bmatrix} \psi_0(\boldsymbol{\xi^1}) & \psi_1(\boldsymbol{\xi^1}) & \cdots & \psi_{N_P-1}(\boldsymbol{\xi^1}) \\ \psi_0(\boldsymbol{\xi^2}) & \psi_1(\boldsymbol{\xi^2}) & \cdots & \psi_{N_P-1}(\boldsymbol{\xi^2}) \\ \vdots & \vdots & \ddots & \vdots \\ \psi_0(\boldsymbol{\xi^{N_R}}) & \psi_1(\boldsymbol{\xi^{N_R}}) & \cdots & \psi_{N_P-1}(\boldsymbol{\xi_{N^R}}) \end{bmatrix} \begin{bmatrix} \hat{u}_0 \\ \hat{u}_1 \\ \vdots \\ \hat{u}_{N_P-1} \end{bmatrix} = \begin{bmatrix} \mathcal{M}(\boldsymbol{\xi^1}) \\ \mathcal{M}(\boldsymbol{\xi^2}) \\ \vdots \\ \mathcal{M}(\boldsymbol{\xi^{N_R}}) \end{bmatrix} \tag{3.35}$$

with the design matrix $\mathcal{A}$ defined as follow:

$$\mathcal{A} = \begin{bmatrix} \psi_0(\boldsymbol{\xi^1}) & \psi_1(\boldsymbol{\xi^1}) & \cdots & \psi_{N_P-1}(\boldsymbol{\xi^1}) \\ \psi_0(\boldsymbol{\xi^2}) & \psi_1(\boldsymbol{\xi^2}) & \cdots & \psi_{N_P-1}(\boldsymbol{\xi^2}) \\ \vdots & \vdots & \ddots & \vdots \\ \psi_0(\boldsymbol{\xi^{N_R}}) & \psi_1(\boldsymbol{\xi^{N_R}}) & \cdots & \psi_{N_P-1}(\boldsymbol{\xi^{N_R}}) \end{bmatrix} \tag{3.36}$$

Is it important observe that the design matrix $\mathcal{A}$ is a Vandermonde like matrix and it is evident that the problem is well defined if $\mathcal{A}$ is not singular, i.e. $\mathcal{A}^T\mathcal{A}$ is positive definite and invertible.

Gathering the numerical model responses $\mathcal{M}(\boldsymbol{\xi^i})$ in the selected regression points into the vector $\mathcal{Y} = \{\mathcal{M}(\boldsymbol{\xi^1}), ..., \mathcal{M}(\boldsymbol{\xi^{N_R}})\}$, the vector $\hat{\boldsymbol{u}}$ can be then estimated through the following expression written in a matrix form:

$$\hat{\boldsymbol{u}} = (\mathcal{A}^T\mathcal{A})^{-1}\mathcal{A}^T\mathcal{Y} \tag{3.37}$$

Regression has become a popular technique to evaluate the PC deterministic coefficients since it allows for accurate results in an easy manner. However the choice of the regression points highly influence the accuracy of the results. From a theoretical point of view the optimal design of sampling points is given by the roots of the Hermite polynomials [87]. Let us consider a random input consists of a single RV and p is the degree of the polynomials. The optimal design point is given by a vector $\{h_1, ..., h_{p+1}\}$. If the input random vector consists in N independent components an optimal design is obtained by the tensor product of the unidimensional design. Therefore the model solution needs to be evaluated in $(p+1)^M$ different points. The choice of the N-uplets of roots are exactly the integration points used in Gauss - Hermite quadrature. This approach is not practically affordable when the number of input RVs and the degree of polynomials increase.
For this reason various criteria have been proposed in literature. The increase in the computational cost was deeply investigated by Sudret et Al. [76] leading to an approach based on the selection of a subset of all the possible combinations of the N-uplets choosing regression points that are closest to the origin. The authors select a number of optimal points equal to $N_R = 2(N_P + 1)$. Efficient optimal approach have been proposed by Zein et Al. [88] using an optimization algorithm of the design matrix able to couple genetic algorithms and the Fedovov exchange algorithm. A comparison between random, LH and Hemmersley sampling methods have been carried out by Hosder et. Al [89] showing that statistics obtained with Hammersley and LH exhibit a much smoother convergence compared to the cases obtained with random sampling and that the optimal number of regression points is twice more than the minimum number required. Other efficient methods have been built upon the assumption that the PC representation is sparse based on the fact that some parameters may contribute less than others to the model output responses. This assumption leads to the recently developed sparse regression method of Blatman and Sudret [90] allowing for an identification of the most relevant basis functions in the PC expansion from only few samples selected using a suitable criterion.
The regression approach is comparable to the so called response surface method used in many fields of science and engineering [87]. In this dissertation the algorithm followed for the evaluation of the deterministic coefficients is summarized in Algorithm 1:

3.4.2 Validation of the PCE based surrogate model

The surrogate model obtained in Eq. 3.26 needs to be validated in order to assess if the maximal degree in the selected truncation scheme is suitable for minimizing the error between the real model solution and the approximated ones. An error estimator is represented

Data: Specify the basis ψ_α which forms an orthogonal basis with the distribution of the set of input parameters
Determine: The norms of the ψ_α basis function
Get: Integration points and corresponding weights
Solve: Deterministic Eq. 3.35 at the regression points
Evaluate: Basis function ψ_α at all the integration points
Evaluate: PC coefficients
Result: Statistic moments of the output

Algorithm 1: Algorithm for the estimation of the deterministic coefficients using regression.

by the global error in Eq. 3.11 requiring the computation of the deterministic solution in a large number of sampling points. Usually the computation of the global error is carried out through MC simulations, but when PC is used the main objective becomes to reduce the computational cost and the number of real model evaluations. As a result the points used in the experimental design $\mathcal{X}$ can be directly used in the convergence analysis leading to the estimation of the empirical error defined as [76]:

$$ERR_E = \frac{1}{N_R}\sum_{i=1}^{N_R}\left\{\mathcal{M}(\boldsymbol{\xi}^i) - \sum_{\boldsymbol{\alpha}\geq 0}^{N_P-1}\hat{\boldsymbol{u}}_{\boldsymbol{\alpha}}\boldsymbol{\Psi}_{\boldsymbol{\alpha}}(\boldsymbol{\xi}^i)\right\}^2 \tag{3.38}$$

The accuracy of the PC surrogate model can be assessed using the quantity:

$$ERR_{PC} = \frac{\mathcal{M}(\boldsymbol{\xi^i}) - \tilde{\mathcal{M}(\boldsymbol{\xi^i})}}{\mathcal{M}(\boldsymbol{\xi^i})} \tag{3.39}$$

The first two statistical moments estimated using the PC expansion can be used as a sort of error indicator. The relative error on mean ERR^M_{PC} and the relative error on variance ERR^V_{PC}can be assessed using respectively:

$$ERR^M_{PC} = \frac{\mathbb{E}[\mathcal{M}(\boldsymbol{\xi^i})] - \mathbb{E}[\tilde{\mathcal{M}(\boldsymbol{\xi^i})}]}{\mathbb{E}[\mathcal{M}(\boldsymbol{\xi^i})]} \qquad ERR^{var}_{PC} = \frac{var[\mathcal{M}(\boldsymbol{\xi^i})] - var[\tilde{\mathcal{M}(\boldsymbol{\xi^i})}]}{var[\mathcal{M}(\boldsymbol{\xi^i})]} \tag{3.40}$$

3.4.3 Moment analysis

Given the orthogonality conditions of the PC expansion basis the output response statistics can be estimated from the deterministic coefficients. In particular, the mean value $\mu_{\tilde{u}}$ and the variance $\sigma^2_{\tilde{u}}$ of the surrogate model response $\tilde{u}$ can be obtained by

$$\mu_{\tilde{u}} = \mathbb{E}[\tilde{\mathcal{M}}(\boldsymbol{\xi})] = \mathbb{E}\Big[\sum_{\boldsymbol{\alpha}\geq 0}^{N_P-1} \hat{\boldsymbol{u}}_{\boldsymbol{\alpha}} \boldsymbol{\Psi}_{\boldsymbol{\alpha}}(\boldsymbol{\xi})\Big] = \hat{u}_0 \tag{3.41}$$

$$\sigma^2_{\tilde{u}} = \mathbb{E}[(\tilde{\mathcal{M}}(\boldsymbol{\xi}) - \hat{u}_0)^2] = \sum_{\boldsymbol{\alpha}\neq 0} \hat{\boldsymbol{u}}^2_{\boldsymbol{\alpha}} \tag{3.42}$$

where $\boldsymbol{\Psi_0} = 1$ and $\mathbb{E}[\boldsymbol{\Psi}_{\boldsymbol{\alpha}}(\boldsymbol{\xi})] = 0, \forall \boldsymbol{\alpha} \neq 0$.

3.4.4 Extension to a multivariate output

The multivariate output in Eq. 3.13 consists in the random vector $\boldsymbol{u} = \{u_1, ..., u_M\}$. The operator $\mathcal{M}$ maps inputs $\boldsymbol{\Theta}$ - or referring to the germ distribution $\boldsymbol{\xi}$ - to multiple outputs such that each component u_i can be predicted as $u_i = \mathcal{M}_i(\boldsymbol{\xi})$ where $\mathcal{M}_i : \mathbb{R}^N \to \mathbb{R}$. Accordingly for $i = 1, ..., M$ one can represent and approximate each $\tilde{\mathcal{M}}_i(\boldsymbol{\xi})$ separately with the theory discussed above.

3.5 Sensitivity Analysis

The sensitivity analysis is a method for quantifying the impact of input parameters into the output QoI. In practice, input factors are considered unessential when they have no effect on the output variability. The identification of unessential input parameters can lead to a significant reduction of the problem dimension. This aspect is crucial especially when dealing with probabilistic design problem or Bayesian updating for the estimation of input parameters. Methods of sensitivity analysis are usually divided into two categories:

- **Local Sensitivity Analysis (LSA)** This method is aimed to determine the local effect of input parameters on the model basing on the computation of the gradient of the response;
- **Global Sensitivity Analysis (GSA)** This method tries to quantify the output uncertainty due to the uncertainty on the main input parameters taken alone or in combination with the others.

Various methods have been developed for an accurate analysis of the latter topic. A deep review can be found in [91].
The most common GSA method is based on the variance decomposition of the output as a sum of contributions of each input RVs. It was originally investigated by Sobol[92] [93].

3.5.1 Variance based method and Sobol' decomposition

Let us consider a mathematical model defined as in Eq. 3.1. The Sobol' decomposition states that any square integrable function $\mathcal{M}$ with respect to a probability measure associated with a joint PDF $\pi_{\boldsymbol{\Theta}}(\boldsymbol{\theta}) = \prod_{i=1}^{N} \pi_{\Theta_i(\theta_i)}$ may be expressed using the following summation of constant $\mathcal{M}_0$, univariate $\{\mathcal{M}_i(\Theta_i)\}$ and bivariate functions $\{\mathcal{M}_{ij}(\Theta_i, \Theta_j)\}$:

$$\mathcal{M}_{\boldsymbol{\Theta}} = \mathcal{M}_0 + \sum_{i=1}^{N} \mathcal{M}_i(\Theta_i) + \sum_{i<j}^{N} \mathcal{M}_{ij}(\Theta_i, \Theta_j) + \cdots + \mathcal{M}_{1,2,\cdots,M}(\Theta_1, \Theta_2, \cdots, \Theta_N) \quad (3.43)$$

in which, the term $\mathcal{M}_0$ is the mean value of the output:

$$\mathcal{M}_0 = \mathbb{E}[\mathcal{M}(\boldsymbol{\Theta})] \quad (3.44)$$

The other summands are given by:

$$\mathcal{M}_i(\Theta_i) = \mathbb{E}[\mathcal{M}(\boldsymbol{\Theta})|\Theta_i] - \mathcal{M}_0 \quad (3.45)$$

$$\mathcal{M}_{ij}(\Theta_i, \Theta_j) = \mathbb{E}[\mathcal{M}(\boldsymbol{\Theta})|\Theta_i, \Theta_j] - \mathcal{M}_i(\Theta_i) - \mathcal{M}_j(\Theta_j) - \mathcal{M}_0 \quad (3.46)$$

where $\mathbb{E}[\mathcal{M}(\boldsymbol{\Theta})|\Theta_i]$ is the conditional expectation of $\mathcal{M}(\boldsymbol{\Theta})$ when Θ_i is set and $\mathbb{E}[\mathcal{M}(\boldsymbol{\Theta})|\Theta_i, \Theta_j]$ is the conditional expectation of $\mathcal{M}(\boldsymbol{\Theta})$ when Θ_i, Θ_i are set.
The decomposition in Eq. 3.43 exists and is unique when the integral of each summand over any of its independent RVs is zero, i.e.:

$$\int_{\mathbb{R}^N} \mathcal{M}_{i1,\cdots,is}(\Theta_{i1}, \cdots, \Theta_{is}) d\Theta_{ik} = 0 \quad \text{for} \quad 1 < k < s \quad s < N \quad (3.47)$$

Eq. 3.47 represents the orthogonality condition between each summands for any function $\mathcal{M}$ square integrable in $\mathbb{R}^M$. Accordingly the functional decomposition in Eq. 3.43 may be squared and integrated obtaining:

$$\int_{\mathbb{R}^N} \mathcal{M}(\boldsymbol{\Theta})^2 - \mathcal{M}_0^2 d\boldsymbol{\Theta} = \sum_{s=1}^{N} \sum_{i_1<\cdots<i_s}^{N} \int_{\mathbb{R}^N} \mathcal{M}^2_{i_1<\cdots<i_s} d\Theta_{i_1} \cdots d\Theta_{i_s} \quad (3.48)$$

The l.h.s of this equation is equal to the total variance of the response u while the r.h.s are defined as partial variances terms.

This leads to the decomposition of the total variance:

$$\mathrm{Var}[\mathcal{M}(\boldsymbol{\Theta})] = \sum_{i=1}^{N} V_i + \sum_{i<j}^{N} V_{i,j} + \cdots + V_{1,2,\cdots,N} \tag{3.49}$$

where:

$$V_i = \mathrm{Var}_{\Theta_i}(\mathbb{E}_{\Theta\text{-}_i}[\mathcal{M}(\boldsymbol{\Theta})|\Theta_i]) \tag{3.50}$$

$$V_{ij} = \mathrm{Var}_{\Theta_{ij}}(\mathbb{E}_{\Theta\text{-}_{ij}}[\mathcal{M}(\boldsymbol{\Theta})|\Theta_i,\Theta_j]) - V_i - V_j \tag{3.51}$$

The notation $\Theta\text{-}_i$indicates the set of all variables except Θ_i. It is evident that the total variance of the model output can be decomposed into a summation of terms depending on each input RV taken alone and on the interactions between them.

3.5.2 Sobol' indices

Starting from Eq. 3.49 and dividing all terms for $\mathrm{Var}[\mathcal{M}(\boldsymbol{\Theta})]$ it is possible to obtain the following relation:

$$1 = \sum_{i=1}^{N} S_i + \sum_{i<j}^{N} S_{i,j} + \cdots + S_{1,2,\cdots,N} \tag{3.52}$$

Where S_i is used to indicate the so-called Sobol' indices. Thus, each index is a sensitivity measure describing which amount of total variance is due to the uncertainties related to the input. The first order indices $S_i = \frac{Var[V_i]}{Var[\mathcal{M}(\boldsymbol{\Theta})]}$ corresponding to the i-th RV are used to quantify the influence of each input parameter taken alone; while the higher order indices $S_i = \frac{Var[V_{ij}]}{Var[\mathcal{M}(\boldsymbol{\Theta})]}$are used to account for the influence of all possible combination of input RVs.

The computation of the Sobol' indices is usually carried out through MC simulation estimating the mean value, the total and partial variance of the output. In order to obtain a significant level of accuracy for the computation of the 2^M integrals, MC requires a lot of simulations making the problem not practically affordable when high dimension and complex systems are object of study.

In order to bypass the problem Sudret [76] has proposed a sensitivity analysis based on PC expansion. Starting from the two equations 3.41 and 3.42 it is evident that any functional of the output of a model can be expressed by combinations of the deterministic coefficients. Let us define $\mathcal{G}_{i_1,\cdots,i_s}$ the set of $\boldsymbol{\alpha}$ tuples such that only the indices $i_1,\cdots,i_s$ are non zero. In this way each $\mathcal{G}_i$ corresponds to the polynomials depending only on parameter Θ_i and

the $N_P - 1$ terms in Eq. 3.26 can be gathered according to the parameters they depend on.

The Sobol' sensitivity indices can be easily obtained as:

$$S_{i_1,\ldots,i_s} = \frac{\sum_{\boldsymbol{\alpha}\in\mathcal{G}_{i_1,\cdots,i_s}} \hat{u}^2_{\boldsymbol{\alpha}}\mathbb{E}[\boldsymbol{\Psi}_{\boldsymbol{\alpha}}]}{\sum_{\boldsymbol{\alpha}\neq 0} \hat{u}^2_{\boldsymbol{\alpha}}} \tag{3.53}$$

Although the mathematical settings is quite burden, the computation of the Sobol' indices using the PC expansion can be carried out as simply a combination of the expansion coefficients gathered according to the dependency of each basis polynomial, square summed and normalized.

Chapter 4

Bayesian inference for parameter estimation using incomplete noisy modal data

4.1 Introduction

Model updating problems are inverse problems aiming to invert the standard forward relation between the unknown/uncertain parameters and the predicted response of a model. A physical model may be described by a *forward problem*, which predicts some quantities of interest of the system given a set of unknown/uncertain input set of parameters. The corresponding *inverse problem* consists in estimating the set of these parameters from a set of measured/observed data, taking into account that in realistic applications the data are noisy, incomplete and characterized by a significant level of uncertainty. Classical inverse problem are studied in many fields including social, medicine, physics and structural and mechanical engineering. In particular, a classical inverse problem in structural engineering is finite element model updating.
Usually the inverse problem is solved through a deterministic approach such that the best

correspondence between the model output and the observed data is obtained. The problem can be formulated using a constrained optimization minimization problem that, in many case, is ill posed since the existence and the uniqueness of the solution can be not fulfilled. Moreover using the deterministic method uncertainty related to measurement and to model are completely neglected.

The role of uncertainty in model updating is crucial and suitable procedures needs to be considered for both assessing the effect of the uncertainty on the model input/output and for evaluating uncertainties on the model response prediction. Uncertainty can be treated using two different methods: probabilistic and non-probabilistic fuzzy approach [94] [95] [96]. Among the probability method the two main school of frequentist and Bayesian interpretation of probabilities needs to be separately treated.

In this dissertation a Bayesian framework is proposed as an effective robust tool for using incomplete noisy modal data to update the initial knowledge of the structural model allowing for treating simultaneously measurement and modeling uncertainty. The popularity of the Bayesian approach is due to its power to quantify and reduce the uncertainty related to complex problem. In the Bayesian setting the inverse problem becomes well posed since the solution is not a single point/value but a probability distribution able to summarize all the information about the adjustable parameters. Generally speaking the unknown parameters are taken to be uncertain and modeled as random variables with a proper probabilistic distribution. The *prior probability density function* which reflects the uncertainty on the prior information is transformed into the *posterior probability density function* which reflects the uncertainty on the prior information and on both model and measurements. The transformation is carried out through the so-called *likelihood function* which reflects how well the model can explain the measurements. The likelihood function can be computed using proper probabilistic model for the prediction error. A schematic representation of the Bayesian approach for the stochastic inverse problem is resumed in Figure 4.1. Contrary to the forward uncertainty quantification problem the epistemic uncertainty of the unknown/uncertain parameters are reduced including the measurement uncertainty in the whole framework.

The computation of the posterior distribution requires the solution of a multidimensional integral which may be computed using asymptotic or sampling methods. Besides classical approximations methods (Monte Carlo, quadrature and cubature) attention is drawn on the use of Markov Chain Monte Carlo (MCMC) methods, the most feasible ones especially for high dimensional distributions. All of these methods requires the solution of the deterministic forward problem at many values of the input parameters taking the posterior

from the asymptotic one. For MCMC simulations - requiring 10^5 or 10^6 samples - and for complex forward problem the total cost of all the simulations is quite prohibitive.
In the proposed Bayesian method the stochastic spectral expansion is introduced for speeding up the evaluation of the posterior distribution. Expanding the dynamic responses of the mathematical model loaded by uncertain/unknown input parameters into the polynomial chaos representation/approximation allows for both quantifying the uncertainty of the output of a system given uncertain input parameters and to facilitate the identification procedure when measurement of the model prediction are available.
The foundations of a full Bayesian framework for the estimation of the parameters of a finite element numerical model is presented in section 4.2 and 4.3 with special attention to the formulation of the prior distribution, the likelihood function and the probabilistic model on the prediction error. In section 4.4 the application of polynomial chaos expansion method for speeding up the evaluation of the posterior distribution is deeply discussed together with the concept of surrogate model.

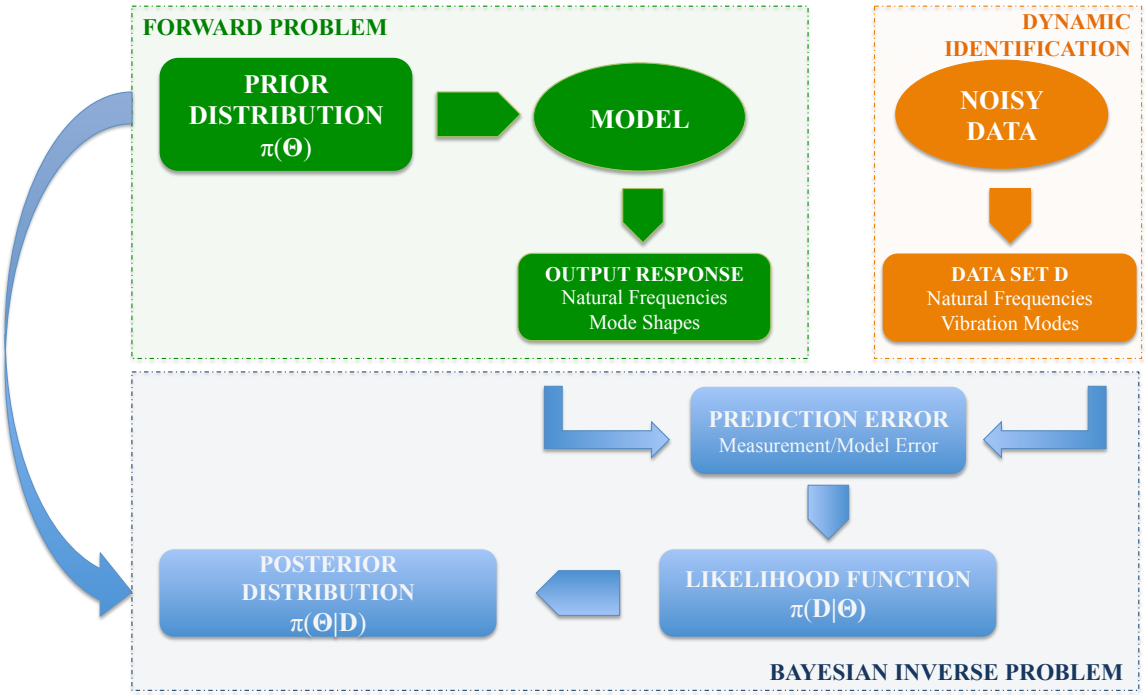

Fig. 4.1: Schematic representation of the Bayesian approach to the stochastic inverse problem.

4.2 The Bayes' Theorem

The Bayes' theorem follows the axiom of conditional probability. Let us consider a sequence of events $\{A_i\}$ with $i = 1, .., n$ - mutually exclusive and mutually exhaustive - partition of the sample space Ω. Suppose an event B occurs with $P(B) > 0$ and $P(B|A_i)$ is known for each A_i. Using the theorem of total probability and for any event B:

$$P(A_i|B) = \frac{P(B|A_i)P(A_i)}{\sum_{i=1}^{n} P(B|A_i)P(Ai)} \tag{4.1}$$

The general form of Bayes' theorem was presented by Laplace in [97] by late 18th century introducing for the first time the concept of inverse problem.
Specifying the prior distribution $f(\theta)$ of the random parameter Θ the posterior distribution should be proportional to what we now call likelihood of the data $(x_1, x_2, ..., x_n)$:

$$f(\theta|x_1, x_2, ..., x_n) \propto f(x_1, x_2, ..., x_n|\theta) \tag{4.2}$$

The Bayes' theorem incorporates the information or prior beliefs for the parameter and takes into account the observed data and makes inference. For the case where the parameter Θ is continuous the posterior distribution can be obtained according to Eq. 4.3:

$$f(\theta|x_1, x_2, ..., x_n) = \frac{f(x_1, x_2, ..., x_n|\theta)f(\theta)}{\int f(x_1, x_2, ..., x_n|\theta)f(\theta)d\theta} \tag{4.3}$$

The integral at the denominator is called marginal likelihood or evidence and it is the distribution of the observed data marginalized over the parameters.
By parameterizing the space of parameters the initial belief in the parameters can be updated using single step when new data becomes available. It is evident that this represents the main advance in Bayesian inference with respect to the frequentist approach which provide for a fixed point prediction finding an optimum point estimate of the parameters underestimating the variance of the predictive distribution. In Bayesian inference the model and the measurement uncertainty can be taken into account explicitly using a proper probabilistic model on the prediction errors which represent the differences between the observed data and the prediction system/model response.
Within this context Bayesian updating becomes a useful tool for the analysis of a sequence of dynamic data and for this reason has found a lot of applications in a wide range of activities including structural identification using dynamic/static noisy data.

4.3 Bayesian Inference for parameter estimation using noisy incomplete modal data

In recent years Bayesian model updating techniques based on measured dynamic data have been applied to structural [98] and modal identification [99]. In this section the specifics of the application of Bayesian inference for uncertainty quantification in FEM updating are presented.

For the complexity of the real systems and the modeling hypotheses on mechanical and physical properties as well as on boundary conditions, a numerical model cannot predict the exact reality. Modal measurements (eigenvalues and eigenvectors) may be used in order to update the structural parameters by minimizing a measure of the distance between the modal frequencies and modal vectors measured in dynamic tests and those estimated from analytical model of structure.

This procedure has to be carried out taking into account that the model updating problem is ill posed and there may be more than one optimal model. Moreover only some of DOFs of the model are used and so the solution is estimated using incomplete modal data.

In Bayesian inference there are no "true models" and both the measured data and the uncertain model parameters are considered as RVs. In the Bayesian approach the updated probabilities of the unknown/uncertain parameters gathered in a real valued random vector $\mathbf{\Theta} = \{\Theta_1, \Theta_2, ..., \Theta_N\} \in \mathbb{R}^N$ and characterizing a model class M when data $\overline{\mathbf{D}}$ becomes available is quantified by a joint PDF which is known as *posterior distribution* and it is expressed through Eq. 4.4:

$$p(\mathbf{\Theta}|\overline{\mathbf{D}}, M) = c^{-1} p(\overline{\mathbf{D}}|\mathbf{\Theta}, M) p(\mathbf{\Theta}|M) \tag{4.4}$$

The term $p(\overline{\mathbf{D}}|\mathbf{\Theta}, M)$ - called *likelihood function* - expresses the probability of the data conditional to the unknown/adjustable vector $\mathbf{\Theta}$. The term $p(\mathbf{\Theta}|M)$ is the *prior distribution*, which quantifies the initial plausibility of vector of parameters $\mathbf{\Theta}$ associated with the model class M. The normalizing constant c is actually the $p(\overline{\mathbf{D}}|M)$ and is called the *evidence of model class M*. The evidence is used for the integration of a posterior PDF over the parameter space become unitary. This normalization makes the integration over the parameter space of the posterior PDF in Eq. 4.4 equal to one. The c constant is given by the multidimensional integration over the parameter space:

$$c = p(\overline{\mathbf{D}}|M) = \int p(\overline{\mathbf{D}}|\mathbf{\Theta}, \mathbf{M}) p(\mathbf{\Theta}|M) d\mathbf{\Theta} \tag{4.5}$$

The evidence for model class M plays a determinant role in Bayesian model class selection [100], [101].
The Bayesian approach is herein used in order to update the parameter values for better representing the structural behavior, but the updating process is directed from the prior information and from the information about the measurements. Two different kind of uncertainties, that affect both experimental and numerical predictions, have to be properly taken into account.
The most obvious source of uncertainty comes from the recorded data. In FEM updating the experimental data are the system modal characteristics extracted from recorded acceleration/displacements time histories using different kind of dynamic identification technique. In all these methods the excited true system is approximated by a mathematical model. Uncertainty can arise from both measurements noise, the finite number of data sampling used, the data filtering and on the source of excitation.
The experimental data $\overline{\mathbf{D}}$ may consists of N_s different tests $\overline{\mathbf{D}} = \{\hat{\omega}_{1,j}...\hat{\omega}_{m,j}, \hat{\mathbf{\Phi}}_{1,j}...\hat{\mathbf{\Phi}}_{m,j}\}_{j=1}^{N_s}$, composed of N_m modal frequencies $\hat{\omega}_{r,j}$ and N_m incomplete mode shape vectors $\hat{\mathbf{\Phi}}_{r,j}$.
Measurements errors determine a difference between the observed structural behavior $\overline{\mathbf{D}}$ and the actual response $\mathbf{D}$. For this reason measurements uncertainties are taken into account defining the modal prediction error as:

$$\overline{\mathbf{e}} = \overline{\mathbf{D}} - \mathbf{D} \tag{4.6}$$

Model uncertainties are due to lack of knowledge on the mechanical and geometrical properties, materials, boundary conditions, construction process and type of coupling between the structural components. An inevitable systematic error may arise also from the difficulty of modeling damping in all structural dynamics models. Hence the prediction error $\mathbf{e}$ is used to provide information about the differences between the numerical model prediction vector $\mathcal{M}(\mathbf{\Theta})$ and the actual structural behavior $\mathbf{D}$:

$$\mathbf{e} = \mathbf{D} - \mathcal{M}(\mathbf{\Theta}) \quad \text{or} \quad \mathbf{D} = \mathcal{M}(\mathbf{\Theta}) + \mathbf{e} \tag{4.7}$$

Both model and modal errors need to be considered in order to improve the matching between the numerical model and the data estimations. The sum of the measurement and the modeling errors can be obtained by Eqs. 4.6 and (4.7)

$$\overline{\mathbf{e}} + \mathbf{e} = \overline{\mathbf{D}} - \mathcal{M}(\mathbf{\Theta}) \tag{4.8}$$

which represents the main equation for the whole UQ problem, avoiding to explicitly consider the unknown structural response $\mathbf{D}$.
Without loss of generality, the explicit dependency to the model class M can be omitted and the likelihood function can be obtained from the convolution of the measurement and modeling errors PDFs [102]:

$$p(\overline{\mathbf{D}}|\mathbf{\Theta}) = \int p_{\overline{\mathbf{D}}}(\overline{\mathbf{D}}|\mathbf{\Theta},\overline{\mathbf{D}})p_{\mathbf{D}}(\mathbf{D}|\mathbf{\Theta})d\mathbf{D} \tag{4.9}$$

$$= \int p_{\overline{\mathbf{e}}}(\overline{\mathbf{D}}-\mathbf{D}|\mathbf{\Theta},\overline{\mathbf{D}})p_{\mathbf{e}}(\mathbf{D}-\mathcal{M}(\mathbf{\Theta})|\mathbf{\Theta})d\mathbf{D} \tag{4.10}$$

where $p_{\overline{\mathbf{e}}}(\overline{\mathbf{D}}-\mathbf{D}|\mathbf{\Theta},\overline{\mathbf{D}})$ is the probability of obtaining a measurement error $\overline{\mathbf{e}}$ when the model is driven by a set of parameters $\mathbf{\Theta}$ and the selected data set $\overline{\mathbf{D}}$, while $p_{\mathbf{e}}(\mathbf{D}-\mathcal{M}(\mathbf{\Theta})|\mathbf{\Theta})$ is the probability of obtaining the modeling error $\mathbf{e}$ given the same set of parameters $\mathbf{\Theta}$.
Using the notation in Eq. 4.10 the Bayes' theorem in Eq 4.4 can be expressed as follow:

$$p(\mathbf{\Theta}|\overline{\mathbf{D}}) = \frac{\int p_{\overline{\mathbf{e}}}(\overline{\mathbf{D}}-\mathbf{D}|\mathbf{\Theta},\overline{\mathbf{D}})p_{\mathbf{e}}(\mathbf{D}-\mathcal{M}(\mathbf{\Theta})|\mathbf{\Theta})d\mathbf{D} \quad p(\mathbf{\Theta})}{\int p(\overline{\mathbf{D}}|\mathbf{\Theta})p(\mathbf{\Theta})d\mathbf{\Theta}} \tag{4.11}$$

4.3.1 The prior distribution

The prior density reflects the probability of the model parameters when no evidence/information are taken into account and its definition is of utmost importance in Bayesian inference. When dealing with parameter estimation from noisy data the prior PDF expresses the degree of belief that a certain value of the input parameters can be representative for the numerical model. It is important to note that the prior PDF is used in order to model the epistemic uncertainty related to the values of the parameters.
When a large amount of observations such as previous experiments or measurements are available the prior PDF can be obtained as a density from the series of observations by constructing an histogram. The role of the "population of the parameters" becomes crucial since samples of the collected data can be non representative of the complete density distribution and sampling errors can occur.
A very general a classification of the Bayesian priors can be carried out according to the way they are selected and/or the contained information and/or the function they perform. Firstly one may distinguish between subjective and objective priors. The subjective priors are chosen based on expert judgment, i.e. on the basis of personal belief. Within this approach the problem of a subjective choice is relevant since different results of the Bayesian

updating framework may be obtained when the data set used is small or not proper informative. For this reason the Bayesian approach has been often criticized as a fragile approach and a lot of literature works are dedicated to the definition of suitable prior distributions able to reflect situation when little a priori information are known. Objective priors instead can be constructed according to some formal rules. In this sense the most useful and widely used method for definition of prior distributions is based on the principle of maximum entropy, introduced in the Bayesian method by Jaynes in [103] [104]. Entropy measures the amount of uncertainty related to a probability distribution and it has a direct relationship to information theory. The principle of maximum entropy states that the probability distribution which best represents the current state of knowledge is the one which results in the largest information entropy. This method determines the PDF that maximizes the Shannon information entropy with respect to the restrictions imposed by the known information in the form of known moments of the distribution and its support. Another distinction can be carried out in terms of informative and non informative priors. These terms are used in order to characterize the priors with respect to their information contents. In the last decades a lot of methods aimed to define theoretically non informative robust prior PDF has been developed. The main idea behind this kind of approach is that an ideal situation occurs when the choice of the prior had minimal influence on the results of the Bayesian updating. The non informative family of prior distributions includes the Jeffreys' prior [105], defined as the square root of the determinant of the Fisher information matrix, and the reference prior distributions introduced by Bernardo [106] and developed by Berger [107]. The latter method consists in maximizing the Kullback − Leibler distance between the prior distribution and the posterior with respect to the prior.

Another kind of priors can be chosen for mathematical convenience and regularization properties. One of the most widely used approach is that of conjugate priors introduced by Raiffa and Schlaifer [108]. A family of prior distributions is conditionally conjugate (for the likelihood function) if the conditional posterior distribution is also in that class [109] [110]. For example, choosing a Gaussian prior over the mean will ensure that the posterior distribution is also Gaussian. The main advantage of the conjugate priors is that it facilitates the computation of the posterior. In fact by choosing a particular functional form for the prior distribution, given the form of the likelihood, the posterior distribution has the same form and parameters are updated by sampling the information without the estimation of the normalizing factor (or evidence of the model class).

In structural engineering practice uniform distributions may be chosen for parameters that are bounded from above and below; Gaussian and Lognormal distributions are often used

for parameters that are strictly positive or however unbounded.

4.3.2 The likelihood function

The likelihood function represents the contribution of the measured data in the definition of the posterior distribution and practically reflects how likely the measurements can be explained from the model when a particular set of parameters is defined. According to Eqs. 4.4 and 4.11 the formulation of the likelihood function has to be carried out taking into account all the uncertainties involved in the estimation of both modal parameters (measurement errors) and discrepancies between the model output and the dynamic identification results (modeling errors). Formulation of the likelihood function depends on the type of available data/observations.

Contrary to the prior PDF the construction of the likelihood function has not received a lot of attention from the researchers even though it has a significant influence on the main results of the Bayesian framework. This is mainly due to the fact that often not so much information are available on the measurement and/or on the model error and different assumptions for the probabilistic model has to be set up. When a lot of data are available - such as acceleration time histories recorded in continuous and for a long period - a realistic estimate of the measurement error can be made considering the statistic series of the observed data evaluating a density. Same procedure can be used for the modeling errors when a lot of measurements are available such as results of experimental investigations on the elastic modulus of the material used or the effect of boundary conditions with proper experimental campaign carried out in order to determine the main characteristics on the soil for the characterization of soil-structure interaction behavior. Often this kind of information are not available and suitable assumptions and hypotheses need to be set up basing on subjective expert judgment and taking into account that the probabilistic model on the prediction error plays a crucial role the Bayesian updating framework.

Considering the general formulation of Eq. 4.4 and dropping the dependency on the model class M, the likelihood function $p(\overline{\mathbf{D}}|\boldsymbol{\Theta})$ can be derived according to [9] within the hypothesis that the user's uncertainties in the n-th modal Data Set when a structural model is specified by the parameters $\boldsymbol{\Theta}$ are not influenced by the previous modal Data Set:

$$p(\overline{\mathbf{D}}|\boldsymbol{\Theta}) = p(\overline{\mathbf{D}}_1|\boldsymbol{\Theta})p(\overline{\mathbf{D}}_2|\boldsymbol{\Theta})\cdots p(\overline{\mathbf{D}}_{N_s}|\boldsymbol{\Theta}) = \prod_{n=1}^{N_s} p(\overline{\mathbf{D}}_n|\boldsymbol{\Theta}) \tag{4.12}$$

where $\overline{\mathbf{D}}_n \in \mathbb{R}^{N_m}$ is the nth data test. The PDF of $p(\overline{\mathbf{D}}_n|\mathbf{\Theta})$ in Eq. 4.12 represents the distribution of a single modal data set given the model parameters.
The modal parameters are then assumed to be independently distributed from mode to mode and from frequency to mode shape obtaining:

$$p(\overline{\mathbf{D}}_n|\mathbf{\Theta}) = \prod_{r=1}^{N_m} p(\hat{\omega}_r|\mathbf{\Theta}) p(\hat{\mathbf{\Phi}}_r|\mathbf{\Theta}) \tag{4.13}$$

where $\hat{\omega}_r$ and $\hat{\mathbf{\Phi}}_r$ are the identified eigenvalues and eigenvectors respectively; $p(\hat{\omega}_r|\mathbf{\Theta})$ and $p(\hat{\mathbf{\Phi}}_r|\mathbf{\Theta})$ are the distribution of the rth natural frequency and the rth mode shape, given the unknown parameters $\mathbf{\Theta}$.
The PDF of the natural frequencies prediction error is derived basing on the difference r_f between the natural frequencies identified from the measurements and those computed with the FE numerical model with respect to the rth dynamic mode and defined as:

$$r_f^r(\mathbf{\Theta}, \overline{\mathbf{D}}_n) = \omega_r(\mathbf{\Theta}) - \hat{\omega}_r^n, \qquad r = 1, \cdots, N_m \qquad n = 1, \cdots, N_s \tag{4.14}$$

where $\hat{\omega}_r^n$ is used for the measured natural frequency in the n-th Data Set and $\omega_r(\mathbf{\Theta})$ is the corresponding model predicted natural frequency. A Gaussian model with zero mean and variance equal to k_f^2 is set up for the description of the prediction error on natural frequencies as suggested by the principle of of maximum entropy. The likelihood function can be written as:

$$p(r_f^r|\mathbf{\Theta}) = \frac{1}{\sqrt{2\pi k_f^{r^2}}} exp\left[-\frac{1}{2k_f^{r^2}} r_f^r(\mathbf{\Theta})\right] \tag{4.15}$$

The same procedure is carried out for the formulation of the likelihood function using mode shapes. Each mode shape vector is composed by a number of modal displacements equal to the number of monitored DOFs N_0. Therefore the error between the measured mode shape $\hat{\mathbf{\Phi}}_r^n$ and the numerically computed one $\mathbf{\Phi}_r(\mathbf{\Theta})$ needs to be estimated with respect to the rth dynamic mode in the nth dataset as:

$$\mathbf{r_{ms}}^r(\mathbf{\Theta}, \overline{\mathbf{D}}_n) = MSSF\left(\frac{\hat{\mathbf{\Phi}}_r^n}{\hat{\Phi}_{r,d}^n}, \mathbf{\Phi}_r(\mathbf{\Theta})\right)\mathbf{\Phi}_r(\mathbf{\Theta}) - \frac{\hat{\mathbf{\Phi}}_r^n}{\hat{\Phi}_{r,d}^n}, \qquad r = 1, \cdots, N_m \qquad n = 1, \cdots, N_s \tag{4.16}$$

where $\hat{\Phi}_{r,d}^n$ denotes a particular reference DOF of mode shape $\hat{\mathbf{\Phi}}_r^n$ and $MSSF\left(\frac{\hat{\mathbf{\Phi}}_r^n}{\hat{\Phi}_{r,d}^n}, \mathbf{\Phi}_r(\mathbf{\Theta})\right)$ is a mode shape scaling factor to be used in order to compare the model predicted and the observed mode shapes. Since the mode shapes are defined up to a constant, a scaling

factor is used in order to change the scale of the computed mode shapes $\mathbf{\Phi}_r(\mathbf{\Theta})$ minimizing the difference between both vectors with respect to the least square perspective [111] [112]. The MSSF can be defined as $\frac{\mathbf{\Phi}_r(\mathbf{\Theta})^T \hat{\mathbf{\Phi}}_r^n}{|\mathbf{\Phi}_r(\mathbf{\Theta})|^2}$, where $|\cdot|$ is used for the Euclidean norm.
In $\mathbf{r_{ms}}^r$ the experimental mode shapes are scaled to 1 in a reference component $\hat{\Phi}_{r,d}^n$ – which is the component with larger amplitude – and the numerical mode shapes are fitted to the experimental ones in a least-squares sense.
When dealing with real data and complex structures the eigenvectors derived from the measurements are not real and neglecting the imaginary part in the estimation of the residual vector means to obtain not reliable results. Usually complex eigenvectors are associated to a significant level of noise in the measurements and to non proportional distribution of damping within the structure. Complex eigenvectors can arise when the damping system matrix is not symmetric occurring typically when vibration of the structure involves rotation about two axes simultaneously. The complexity can be due also to a significant level of excitation (e.g. wind component): an additional damping is provided by the aerodynamic forces and the effect is to split a real mode shape into a double complex mode shape.
For this reason a different formulation needs to be developed in order to define the residual of mode shapes. The percentage error between the measured and the calculated mode shapes can be expressed using MAC coefficient defined in Eq. 2.61 denoting the degree of consistency between the measured $\hat{\mathbf{\Phi}}_\mathbf{r}$ and the computed $\mathbf{\Phi}_r(\mathbf{\Theta})$ mode shapes. Taking into account that MAC coefficient assumes values between 1 and 0 respectively for perfect match and no correlation between mode shapes, its complement 1-MAC can be considered as the residual error for mode shapes as follow:

$$r_{ms}^r = \left[1 - \frac{|\hat{\mathbf{\Phi}}_\mathbf{r}^T \mathbf{\Phi}_r(\mathbf{\Theta})|^2}{(\hat{\mathbf{\Phi}}_r^T \hat{\mathbf{\Phi}}_\mathbf{r})(\mathbf{\Phi}_r^T(\mathbf{\Theta})\mathbf{\Phi}_r(\mathbf{\Theta}))}\right] \tag{4.17}$$

Assuming again that the variances k_{ms} are equal for all the N_m mode shapes and that the percentage error follows a zero mean Gaussian distribution, the likelihood function for mode shapes can be expressed using:

$$p(r_{ms}^r|\mathbf{\Theta}) = \frac{1}{\sqrt{2\pi k_{ms}^{r^2}}} exp\left[-\frac{1}{2k_{ms}^{r^2}} r_{ms}^r(\mathbf{\Theta})\right] \tag{4.18}$$

where $k_{ms}^{r^2}$ is the variance of the mode shape with respect to the rth dynamic mode.
The error standard deviations k_f^r and k_{ms}^r can be assumed on the basis of statistical measurements of the identified natural frequencies and mode shapes. As pointed out by Au in a recent work [113], a proper error standard deviation can be also selected considering

the posterior variance of the natural frequencies and the posterior covariances of the mode shapes estimated by means of the Bayesian Operational Modal Analysis (BayOMA) for the recorded data.

Usually it is assumed that the errors in natural frequencies and mode shapes for all the dynamic modes have the same variances k^2 providing:

$$p(\overline{\mathbf{D}}|\mathbf{\Theta}) = \frac{1}{\sqrt{2\pi k^2}} exp\left[-\frac{1}{2k^2}(r_f^r(\mathbf{\Theta}))\right] exp\left[-\frac{1}{2k^2}(r_{ms}^r\mathbf{\Theta}))\right] \tag{4.19}$$

The formulation of the likelihood function in Eq. 4.19 can be further modified within the main hypothesis that both modal frequencies and mode shapes are independent and then the PDF for all modal parameters of all the dynamic modes can be estimated multiplying the PDFs of each mode:

$$p(\overline{\mathbf{D}}|\mathbf{\Theta}) = \prod_{r=1}^{N_m}\prod_{n=1}^{N_s} p(r_f^r)p(r_{ms}^r) = exp\left(-\frac{1}{2}\mathcal{J}(\mathbf{\Theta})\right)\prod_{r=1}^{N_m}\prod_{n=1}^{N_s}\frac{1}{2\pi k^2} \tag{4.20}$$

where $\mathcal{J}(\mathbf{\Theta})$ is the objective (measure-of-fit) function defined as the difference between the measured and the model predicted natural frequencies and mode shapes. Obviously when real experimental modal data are considered in the reference Data Set $\overline{\mathbf{D}}$ a proper mode shape pairing needs to be considered in the whole framework, meaning that the differences between the modal properties obtained from the measurements and from the numerical model are considered only if they correspond to the same dynamic mode. In most of practical applications the mode shape matching is ensuring by considering the MAC as a soft constraint.

The assumption of uncorrelated zero mean Gaussian model for the prediction error is supported by the principle of maximum entropy maximizing the entropy with respect to the sum of measurement and model errors even though the magnitude of the errors remains unknown. The hypothesis of uncorrelated errors may have a significant influence on the results of Bayesian updating solution since data and prediction errors can be spatial and/or temporal correlated. Simoen at Al. [114] demonstrate that the assumption of uncorrelated prediction error does not guarantee the highest posterior uncertainty on the parameter estimates and that, if a suspected correlation between data is present, it has to be taken properly into account.

Different approaches can be used for avoiding incorrect or unsuitable assumptions. One of the most widely used approach is deeply discussed in [115] and [116] and it consists in a hierarchical formulation of the Bayesian updating scheme by including the variance

parameters of uncorrelated zero - mean Gaussian models σ^2 in the updating scheme. In fact the observed noisy data depend strictly from the environmental conditions (e.g. temperature, humidity), from the loading excitation characteristics (e.g. presence of wind) or change in stiffness of the structure itself due to damage or to a significant modification of the boundary conditions. The hierarchical Bayesian approach allows to evaluate the total uncertainty of the updating model parameters and their variability and the Bayes' theorem in Eq. 4.4 is modified:

$$p(\boldsymbol{\Theta}, \sigma^2|\overline{\mathbf{D}}) \propto p(\overline{\mathbf{D}}|\boldsymbol{\Theta}, \sigma^2)p(\boldsymbol{\Theta}, \sigma^2) \tag{4.21}$$

where $p(\overline{\mathbf{D}}|\boldsymbol{\Theta}, \sigma^2)$ is the likelihood function and $p(\boldsymbol{\Theta}, \sigma^2)$ is the prior probability. The hierarchical formulation is particularly useful when system reliability analysis is under investigations since it allows an increase confidence in results reducing the influence of the assumptions regarding the statistical structure of the prior information.

Other similar approaches try to estimate the random error identifying additive terms to fit the model to the observed data by means of auxiliary functions [117]. Let us consider the set of N unknown/uncertain parameters gathered in the random vector $\boldsymbol{\Theta}$ and one single set of data ($N_s = 1$) consisting in N_m modal frequencies and N_m vibration modes. The mathematical formulation can be easily extended to $N_s \neq 1$. According to Eq. 4.17 and considering $1 - MAC$ as a measure of the distance between the analytical model and the experimental results, the set of measures used in Bayesian framework consists in a vector of $2N_m$ elements and the $2N_m$-variate probabilistic model can be written as follow:

$$\mathcal{M}_k(\boldsymbol{\Theta}, \boldsymbol{c}_k, \boldsymbol{\Sigma}) = \hat{m}_k(\boldsymbol{\Theta}) + \gamma_k(\boldsymbol{\Theta}, \boldsymbol{c}_k) + \sigma_k \varepsilon_k \quad k = 1, ..., 2N_m \tag{4.22}$$

where $\mathcal{M}_k(\boldsymbol{\Theta}, \boldsymbol{c}_k, \boldsymbol{\Sigma})$ is a $2N_{m\times 1}$ vector of independent observations and $\hat{m}_k(\boldsymbol{\Theta})$ is a $2N_{m\times 1}$ vector of the selected deterministic model output response; the function $\gamma_k(\boldsymbol{\Theta}, \boldsymbol{c}_k)$ is a correction term for the bias inherent in the deterministic model that can be expressed as a function of the input random parameters $\boldsymbol{\Theta}$ and parameters $\boldsymbol{c}_k$. The term ε_k is a $2N_{m\times 1}$ vector of normal RVs having zero mean and unit variance; σ_k represents the standard deviation of the model errors. When dealing with a multivariate probabilistic model, $\boldsymbol{\Sigma}$ denotes the covariance matrix of the variables $\sigma_k \epsilon_k$ and it includes $2N_m$ unknown variances and $\frac{2N_m(2N_m-1)}{2}$ unknown correlation coefficients.

Particular attention is required for the correcting function $\gamma_k(\boldsymbol{\Theta}, \boldsymbol{c}_k)$ that is unknown since the deterministic model usually involves approximations and idealizations. In order to estimate the bias a suitable set of p explanatory functions $h_{k,j}$ and combination coefficients

collected in the vector $\boldsymbol{c}_{k,j}$ are used as follow :

$$\gamma_k(\boldsymbol{\Theta}, \boldsymbol{c}_k) = \sum_{j=1}^{p} c_{k,j} h_{k,j}(\boldsymbol{\Theta}) \tag{4.23}$$

By examining the posterior statistics of the unknown parameters it is possible to identify these explanatory functions that are significant in describing the bias in the deterministic model.
In assessing the model the different kind of uncertainty may be explicitly treated. The aleatoric uncertainties are present in the variables $\boldsymbol{c}_k$ and partly in the error term ε_k; the epistemic uncertainties are instead present in the set of the unknown parameters and partly in the error term. Therefore the model uncertainties gathered in the term $\gamma_k(\boldsymbol{\Theta}, \boldsymbol{c}_k)$ provide a correction for the deterministic model able to consider model inexactness.
The corrected probabilistic model is valid when the following assumptions are satisfied:

- *Homoskedasticity assumption*: the model standard deviation is independent in $\boldsymbol{\Theta}$;
- *Normality Assumption*: the model error is normally distributed;

The uncertain parameters can be then gathered in the vector $\{\boldsymbol{\Theta}, \boldsymbol{X}\}^T$ with $\boldsymbol{X} = \{\boldsymbol{c}, \boldsymbol{\Sigma}\}^T$. Therefore the Bayesian framework is applied in order to update the prior distribution $p(\boldsymbol{\Theta}, \boldsymbol{X})$.
The prior distribution of the main unknown parameters $\boldsymbol{\Theta}$ can be selected on the basis of expert judgment or considering the results of investigation campaigns and past observations. When no information are available such as in the case of the combination coefficients and the global error covariance matrix the main objective becomes to choose non informative priors able to minimize the effect of the priors choice on the posterior distributions. For this reason it is generally assumed that $\boldsymbol{c}$ and $\boldsymbol{\Sigma}$ are independent so that $p(\mathbf{X}) \simeq p(\boldsymbol{c})p(\boldsymbol{\Sigma})$. As shown in Box and Tiao [13] the non informative priors for the unknown/uncertain parameters is locally uniform so that $p(\boldsymbol{X}) \simeq p(\boldsymbol{\Sigma})$ leading to the non informative Jeffrey's priors. Furthermore since the uncertain parameters are the standard deviation σ_i and the correlation coefficients ρ_{ij} of the global model error, the non informative priors for the elements $\Sigma_{i,j}$ takes the following form defined in [118] and [119]:

$$p(\boldsymbol{\Sigma}) \propto |\mathbf{R}|^{-\frac{(2N_m)+1}{2}} \prod_{i=1}^{2N_m} \frac{1}{\sigma_i} \tag{4.24}$$

where $|\cdot|$ denotes the determinant and $\mathbf{R}$ is the correlation matrix.
The problem of formulating the likelihood function for a set of $2N_m$-variate observations can be easily solved maximizing the bias and gathering all the residuals term in the vector $\mathbf{r}$ having components r_k in the form:

$$r_k(\boldsymbol{\Theta}) = \sigma_k \varepsilon_k = \mathcal{M}_k - \hat{m}_k(\boldsymbol{\Theta}) \tag{4.25}$$

Substituiting Eqs. 4.14 and 4.17 in Eq. 4.25, the residual vector takes the form:

$$\mathbf{r}(\boldsymbol{\Theta}) = \begin{bmatrix} \mathbf{r}_f \\ \mathbf{r}_{ms} \end{bmatrix} \tag{4.26}$$

and the likelihood function can be expressed as:

$$P(\overline{\mathbf{D}}|\boldsymbol{\Theta}, \boldsymbol{\Sigma}) = (2\pi)^{\frac{2N_m}{2}} |\boldsymbol{\Sigma}| exp(-\frac{1}{2}\mathbf{r}^T \boldsymbol{\Sigma}^{-1} \mathbf{r}) \tag{4.27}$$

When a N_s set of data is considered Eq. 4.27 is modified considering the joint distribution of the N_s sets of data:

$$P(\overline{\mathbf{D}}|\boldsymbol{\Theta}, \boldsymbol{\Sigma}) = (2\pi)^{\frac{2N_m}{2}} |\boldsymbol{\Sigma}| exp(\sum_{n=1}^{N_s} -\frac{1}{2}\mathbf{r}_n^T \boldsymbol{\Sigma}^{-1} \mathbf{r}_n) \tag{4.28}$$

A practical issue in this approach is to guarantee the respect of homoskedastic model. Considering the non negative nature of the QoIs in Bayesian inference based on dynamic data (natural frequencies and vibration modes to be take in the form of distance between perfect correlation) a logarithmic transformation can be used. The residual vector $\mathbf{r}_n$ can be therefore estimated by taking the logarithmic transform of Eqs. 4.14 and 4.17.
This method is not widespread in practical applications even though it allows to consider the prediction errors as further noisy parameter. In this dissertation it is used and implemented for the estimation of the uncertain/unknown structural parameters (in terms of elasticity moduli) using real experimental dynamic data.
It is important to point out that the use of real data in Bayesian structural dynamic identification field represents an important newly element. In fact in most of literature works the use of artificial data is often preferred since the use of modal parameters, especially modal vectors, in the reference Data Set $\overline{\mathbf{D}}$ poses further challenges. As already pointed out in Chapter 2, the frequency domain dynamic identification technique is based on the fundamental hypotheses: (i) the structure to be tested is subjected to some kind of excita-

tion having white noise characteristics; (ii) the structure to be tested is lightly damped and that the mass, stiffness, damping matrices are positive, symmetric and diagonalizable in some basis. When these hypotheses are not complied each pole of the system is associated to a complex eigenvector. Neglecting the imaginary part of the eigenvector components as it is usually done in practice can cause significant errors. Furthermore if the prediction error modal vector is expressed in terms of distance from the perfect correlation by means of MAC matrix, the multivariate problem can be reduced to a sum of univariate problems making the whole procedure fast, easy and computationally advantageous.

4.3.3 The posterior distribution

Once the prior PDF and the likelihood function are defined, experimental observations and Eq. 4.11 allows for the parameter estimation with Bayesian framework from noisy experimental data. Multidimensional integration are involved in the computation of the marginal posterior PDF of the parameters to update. If the number of parameters and the data space dimension becomes large, the multidimensional integrations in Eq. 4.11 cannot be solved with analytical approaches.

One solution is the Laplace's method for asymptotic approximation of a general integral [97]. The main goal is to find a Gaussian approximation of the marginal posterior PDF that is centered on a moment of the target distribution. This procedure requires only the computation of global maximum of the posterior density in a logarithmic form and the local second order partial derivatives. It yields to a good approximation of the posterior distributions when they are unimodal and symmetric but this assumption might be not proper correct and reasonable in most of cases. One can say that Laplace's method can be applied to a restricted simple distribution only and/or as a first posterior approximation that can be refined via importance sampling.

Standard Monte Carlo (MC) can be applied to evaluate the integration in Eq. 4.11. Generating independent and identically distributed samples of the prior PDF, the posterior PDF can be evaluating using asymptotic approximation according to the law of large number and the central limit theory. Obviously this method requires the solution of the deterministic problem for each sample and for this reason it is not so attractive in Bayesian inference especially when a lot of parameters need to be updated using a large amount of observations.

The most recent and used procedure for posterior sampling is the Markov Chain Monte Carlo (MCMC) [120]. The term MCMC refers to all procedures that are based on random sequences of samples (so called Markov Chain) which are in equilibrium with the target

posterior PDF. Each step of the procedure depends on the previous steps. It follows that the PDF can be estimated by targeting a posterior PDF without knowing the scaling factor c in Eq. 4.5. Examples of MCMC algorithms are the Metropolis Hastings (MH) [121] and the Gibbs Sampling (GS)[122] [123].
The first application of MCMC MH in Bayesian inference is in [124]. The MH algorithm is introduced in order to face the problem of unidentifiable case occurring when asymptotic approximation is used to solve the Bayesian framework. When a large number of model parameters is updated and a small number of observations are used as effective constraints, the bayesian optimization problem is non convex. The MH method is based on the simulation of samples that are special Markov Chain. A random walk in the space of probability is performed and using a proper rejection mechanism the PDF corresponding to the generic Markov Chain sample tends to the target PDF.
Assuming that $P(\boldsymbol{\Theta})$ is the prior PDF and $P(\overline{\mathbf{D}}|\boldsymbol{\Theta})$ is the likelihood function, the solution of the Bayesian updating problem up to a normalizing constant can be obtain by sampling directly the posterior PDF $P(\boldsymbol{\Theta}|\overline{\mathbf{D}})$ through the definition of a proposal distribution used in order to generate a random vector $\boldsymbol{\Theta}$, given the value at the previous step of the chain. The MH procedure can be summarized as in Algorithm 2. In practice, the value of the new samples $\boldsymbol{\Theta^t}$ is generated with the help of the proposal distribution, also known as transition kernel. The proposal p is in general a normal distribution centered at the previous state for respecting the symmetric construction such that $p(\boldsymbol{\Theta}^*|\boldsymbol{\Theta^t}) = p(\boldsymbol{\Theta^t}|(\boldsymbol{\Theta}^*)$. Once new candidate sample $\boldsymbol{\Theta}^*$ is drawn, it has a probability $min\{1, \rho(\boldsymbol{\Theta}^*, \boldsymbol{\Theta}^t)\}$ to be accepted and a probability $1 - min\{1, \rho(\boldsymbol{\Theta}^*, \boldsymbol{\Theta}^t)\}$ to be rejected. If accepted the sample $\boldsymbol{\Theta}^*$ will be taken as the next state of the chain $\boldsymbol{\Theta}^{t+1} = \boldsymbol{\Theta}^*$, otherwise the current state is taken as the next step of the chain $\boldsymbol{\Theta}^{t+1} = \boldsymbol{\Theta}^t$. The process is repeated until N Markov chain samples have been simulated and the specification of the acceptance probability $\rho(\boldsymbol{\Theta}^*, \boldsymbol{\Theta}^t)$ allows generating a Markov chain with desired target density.
The convergences to the target distribution is obtained only when Markov chain is aperiodic and positive recurrent. Factors that mainly affect the efficiency of the algorithm are the choice of the initial values and the spread of the proposal distribution. The tuning of the proposal distribution is a crucial issue often involving errors and a lot of trials. Moreover MCMC MH is characterized by a serial correlation of the obtained posterior samples associated to a low efficiency when compared to independent sampling. Finally, the convergence rate plays an important role and needs to be properly fixed in order to speed up the convergency avoiding wrong results.
Computationally the MH MCMC is a very demanding procedure because the deterministic

Data: Initiate the algorithm with a value $\boldsymbol{\Theta}^0$
for *Each* $t = 1 \rightarrow N$ **do**
  Draw $\boldsymbol{\Theta}^*$ from the proposal probability distribution density $p(\boldsymbol{\Theta}^*|\boldsymbol{\Theta}^t)$
  Compute the acceptance rate $\rho(\boldsymbol{\Theta}^*, \boldsymbol{\Theta}^t)$
  Draw u from a uniform distribution $u \sim \mathcal{U}(0,1)$
  if $u < \rho(\boldsymbol{\Theta}^*, \boldsymbol{\Theta}^t)$ **then**
    Accept the state $\boldsymbol{\Theta}^{t+1} = \boldsymbol{\Theta}^*$
  else
    Reject the state $\boldsymbol{\Theta}^{t+1} = \boldsymbol{\Theta}^t$
  end
end

Algorithm 2: Metropolis Hastings (MH) MCMC.

solution of numerical needs to be evaluated for each new proposed sample and this is the major limitation of this kind of approach, efficient only for low dimension problems.
For this reason Beck proposed a new approach based on GS [125]. The basic idea is to decompose the model parameters into different groups so that exact sampling of one group of parameters is possible when conditional on the other groups. Markov chain needs to be constructed but the target PDF is obtained with no need of assumptions on the acceptance rate, since no rejection sampling is required.
In recent years a vast amount of methods have been developed in order to improve the convergence speed of the classical MH MCMC. The most commonly used is the adaptive MH MCMC [126](AMH MCMC) where the Gaussian proposal distribution is updated using the information obtained in the covariance at the previous steps fulfilling the ergodic properties of the algorithm. The acceptance rate of each step is then defined basing on what happens at the previous state of the chain and not fixed by the user.
Other methods are introduced for dealing with high-dimensional problem such as the Hamiltonian (or hybrid) MCMC (HMC) [127]. Within the HMC the correlation between successive sampled states is reduced by using a Hamiltonian dynamic evolution between states improving the speed of convergency. Another kind of algorithm is the transitional MCMC (TMCMC) [128] introduced in order to avoid the problem of sampling from difficult target probability density functions (PDFs). It is based on the construction of intermediate PDFs that converge to the posterior (target) PDF but easier to sample. The parallelized TMCMC is introduced in order to overcome the issue of high computational cost. Also algorithm involving a sequential sampling strategy belongs to the most popular methods such as the enhanced MCMC developed by Au et Al. in [129]. The sampling process, in this case, is divided into multiple levels using auxiliary bridge PDFs at each level of the

chain. The samples move smoothly and the target PDF can be evaluated.

4.4 Spectral expansion for Bayesian inference using an improved version of MCMC MH method

In order to obtain a significant reduction of the computational burden for the evaluation of the Bayesian integral in Eq. 4.11 described in the previous Section, an effective method is presented in this Section. In particular a newly approach proposed by Matthies et Al. [130] [131] [119] is presented, modified and discussed in order to speed up the computation of Bayesian integrals reducing the cost related to the computation of the numerical model solution required at each step of the chain in MCMC-MH.
The main idea is to decompose the forward model response into polynomial terms that are orthogonal with respect to a weight function identified as a probability density. In this way the likelihood function can be computed using an indirect method based on a surrogate solution of the forward model.
To this end a non intrusive spectral methods is used to replace the governing equations and the output responses of the numerical model. The PC expansion in Eq. 3.26 is constructed for each QoI according to the prior probability distributions of the unknown parameters $\boldsymbol{\Theta}$. The deterministic coefficients gathered in the vector $\hat{\boldsymbol{u}}$ are evaluated using least square minimization method as in Eq. 3.34. At each step of the MCMC MH the solution of the forward problem is estimated using the PC approximation. The use of the least square minimization is often criticized since it does not guarantee accuracy of the results with respect to other methods e.g. stochastic Galerkin or orthogonal projection. In the analyzed case study it is demonstrated that the least square minimization methods together with the Gaussian quadrature direct integration methods is a reliable mean in the Bayesian updating framework.
The Bayesian framework for the estimation of parameters using noisy data is easily reformulated. Knowing the prior density of the parameters contained in the random vector $\boldsymbol{\Theta}$ and mapping the prior PDFs to the germ distribution $\boldsymbol{\xi}$ it is possible to construct the corresponding PCE for each considered univariate output:

$$\tilde{\mathcal{M}}(\boldsymbol{\xi}) = \sum_{\boldsymbol{\alpha}=0}^{N_P-1} \hat{u}_{\boldsymbol{\alpha}} \boldsymbol{\Psi}_{\boldsymbol{\alpha}}(\boldsymbol{\xi}) \tag{4.29}$$

where $\boldsymbol{\xi} \sim N(0, \boldsymbol{I})$ is defined as a $\mathbb{R}^K$- valued vector of independent and identically distributed, zero mean, unit variance Gaussian RVs and $\mathbf{I}$ denotes the identity matrix having dimension $(K \times K)$ and introduced in Eq. 3.12. The extension to a multivariate output has been already discussed in the previous chapter. Eq. 4.11 is modified obtaining:

$$p(\boldsymbol{\xi}|\overline{\mathbf{D}}) = \frac{\int p_{\overline{\mathbf{e}}}(\mathbf{D} - \overline{\mathbf{D}}|\boldsymbol{\xi}, \overline{\mathbf{D}}) p_{\mathbf{e}}(\overline{\mathbf{D}} - \tilde{\mathcal{M}}(\boldsymbol{\xi})|\boldsymbol{\xi}) d\mathbf{D} \quad p(\boldsymbol{\xi})}{\int p(\overline{\mathbf{D}}|\boldsymbol{\xi}) p(\boldsymbol{\xi}) d\boldsymbol{\xi}} \tag{4.30}$$

The essence of this approach is that the likelihood function becomes a function of $\boldsymbol{\xi}$ instead of $\boldsymbol{\Theta}$ and the posterior distributions are evaluated by replacing direct evaluation of the likelihood $P(\boldsymbol{D}|\boldsymbol{\Theta})$ with a likelihood written in terms of $\tilde{\mathcal{M}}(\boldsymbol{\xi})$ by sampling directly from the $\boldsymbol{\xi}$ space.

A suitable choice for the operator $\mathbf{g}$ in Eq. 3.12 becomes crucial depending on the chosen PC basis and the polynomial order. Indeed, errors due to functional approximation of the surrogate model responses may cause fallacious results of the Bayesian updating framework caused by further significant errors not captured in the model and measurement prediction errors. The errors due to the use of PC based surrogate models can be defined according to Eq. 3.11 as the difference between the PC expansion of the forward surrogate model solution and the exact solution of the deterministic numerical model. The error may become negligible when a sufficient polynomial order is used or when a suitable number of ED points is chosen. The validation of the surrogate model is therefore an important step of the whole procedure that needs to be carefully carried out.

When dealing with dynamic data a surrogate model for each QoIs is developed. As just discussed, the likelihood function can be written in terms of MAC matrix in order to include the experimental modal vectors in the reference Data Set $\overline{\mathbf{D}}$. However the MAC coefficients are global quantities particularly sensitive to large eigenvector components. For this reason it is useful to develop a PC based surrogate model for each component of each eigenvector in the Data Set $\overline{\mathbf{D}}$.

The updating process can cause misleading results when experimental modal data are used as reference because of possible frequency matching associated to different mode shapes. To overcome this problem the main idea is to use the MAC coefficient in order to measure the correlation rate between the experimental and numerical mode shapes. MAC coefficient assumes values ranging from 0 to 1, when the two modes have zero or perfect correlation, respectively. The classical MCMC MH algorithm is thus modified using the MAC coefficients as soft constraint so that the total error in Eq. 4.26 at each step of the chain is computed as the difference between the model predicted and the observed natural

Data: Initiate the algorithm with a value $\boldsymbol{\Theta}^0$
for *Each* $t = 1 \rightarrow N$ **do**
  Draw $\boldsymbol{\Theta}^*$ from the proposal probability distribution density $p(\boldsymbol{\Theta}^*|\boldsymbol{\Theta}^t)$
  Estimate the surrogate model solution for $\tilde{\mathcal{M}}(\mathbf{x}, \boldsymbol{\theta}^*)$
  Compute the MAC matrix
  Reorder the natural frequencies
  Compute the residual vector $\boldsymbol{r}_t$ in Eq. (4.26)
  Compute the acceptance rate $\rho(\boldsymbol{\Theta}^*, \boldsymbol{\Theta}^t)$
  Draw u from a uniform distribution $u \sim \mathcal{U}(0, 1)$
  if $u < \rho(\boldsymbol{\Theta}^*, \boldsymbol{\Theta}^t)$ **then**
    Accept the state $\boldsymbol{\Theta}^{t+1} = \boldsymbol{\Theta}^*$
  else
    Reject the state $\boldsymbol{\Theta}^{t+1} = \boldsymbol{\Theta}^t$
  end
end

Algorithm 3: Surrogate model based improved Metropolis Hastings (MH) MCMC algorithm.

frequencies only when they correspond to the same mode shape.
Starting from the results of the previous chapter, this procedure allows also a robust GSA for assessing which are the most sensitive modal vectors to variations in the uncertain parameters needed to update.
Therefore, the main advantage of the surrogate model based MCMC MH method is that, if an accurate approximation $\tilde{\mathcal{M}}(\boldsymbol{\Theta})$ is obtained, the posterior density $p(\boldsymbol{\Theta}|\overline{\mathbf{D}})$ can be evaluated for a large number of samples, without computationally demanding simulations of the forward problem. This is the answer to one of the main research question at the the basis of this dissertation. Moreover, accounting for the constraint used in the random walk to ensure that the residual vector is estimated as the difference between the model predicted and the observed natural frequencies only when they correspond to the same mode shape, an improved version of the classical MCMC MH algorithm based on the surrogate model is obtained and reported in Algorithm 3.

Chapter 5

The role of uncertainties on structural identification of a cable stayed footbridge

5.1 Introduction

In this chapter a probabilistic robust framework for the calibration of a finite element model of a complex structure is presented. The method is discussed with special reference to a relevant case study: a cable-stayed footbridge in Umbria Region (Central Italy). The proposed methodology is based on surrogate models and dynamic measurements of the global system response integrated with Bayesian inference.

The aim of the model updating based on Bayesian approach is to reduce the uncertainties related to the physical and the mechanical characteristics of the main parameters and to provide an alternative use of the dynamic identification results allowing to introduce all the uncertainties related to the measurements in the updating framework. After an investigation on technical information about the footbridge (e.g. technical drawings and photograph) an initial numerical model is set up. Different modal analysis are carried out

by varying the mechanical properties and the boundary conditions of the numerical model in order to identify the main parameters influencing the dynamic response in terms of natural frequencies and associated mode shapes. On the other side a full-scale measurement campaign is carried out in order to measure the structural response in terms of modal parameters. Natural frequencies and associated vibration modes have been estimated using acceleration time histories in operating conditions by means of operational modal analysis algorithm in frequency domain.
Having developed the preliminary phase the first step of the Bayesian inverse problem is to appoint the PDFs for all the uncertain parameters reflecting the degree of belief of the operator judgment about the input parameters. The prior PDFs of the uncertain parameters are transformed into the posterior marginal PDFs through the likelihood function using suitable probabilistic model on the prediction error reflecting the discrepancy between the results of numerical model and the measurements.
First the stochastic forward problem is solved by means of procedures based on functional approximation of the system response in terms of natural frequencies and associated mode shapes with polynomial chaos representation. The response surface of each quantity of interest is then developed providing a collection of input/output pairs.
The Bayesian inverse problem is then solved by Markov Chain Monte Carlo Metropolis Hastings algorithm replacing at each step the solution of the deterministic numerical model with the solution of the surrogate model reducing significantly the computational costs. The complete framework can be summarized as follow:

1. Define and validate the polynomial surrogate models;
2. Assess a robust global sensitivity analysis;
3. Compute the posterior distribution of the unknown parameters.

In particular, three cases are herein considered in Bayesian inverse problem in order to assess the importance of use an informative Data Set in the reliability of the results. The first, reported as *Case1* considers a Data Set used for the updating consisting in just the first natural frequency of the structure identified from the measurements. The second, *Case 2* considers a Data Set consisting in the first six natural frequencies and finally a complete Data Set consisting in the first six natural frequencies and corresponding vibration modes is considered in *Case 3*.

5.2 Cable-stayed footbridge description

The footbridge "Umbria Gateway" is located in Terni - Umbria Region - 100 Km away from Rome. The footbridge has a total length of 180 m consisting of two main parts: a curved shape main part with a total length of 120 m sustained by an asymmetric array of cables attached to a pair of rings and to a 60 m tall inverted tripod tower. The remaining 60 m section is supported by a structural system having the form of two bowstring arches with a 3.89 m height. Figure 5.1 shows a schematic representation of the bridge with plan and elevation.

The cable-stayed deck spans (Figure 5.2) are made of 3.50 m length and composite

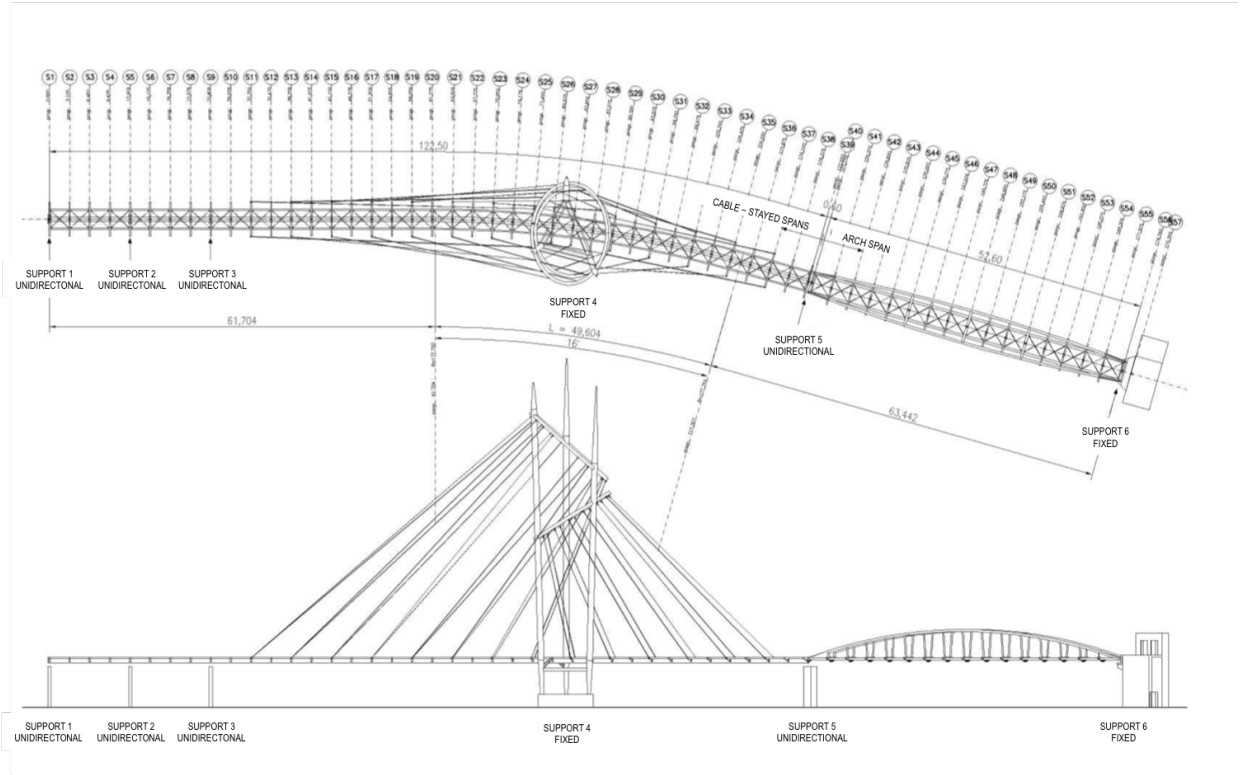

Fig. 5.1: Schematic representation of the footbridge. Plan and elevation [132].

modules with three steel girders: the central one has a circular hollow section with 800 mm external diameter and 30 mm thickness; the two lateral girders are circular hollow sections with 219 mm external diameter and 12.5 mm thickness. The stringers are non - prismatic elements with variable H-type cross section having a maximum 670 mm height

in the deck center. Double-T beams are welded to the stringers in order to sustain the wooden boards of the floor surface. X-bracings consisting of circular cross - section with 40 mm diameter are used in order to increase the horizontal stiffness.
The main tower has the form of tripod erected on a concrete triangular basement. The lower part of the pylons, up to just below the level of the deck, is made of variable diameter steel circular hollow section, which are filled with concrete. The middle part of the pylons, up to the connection with the higher ring, is made of steel circular hollow section with constant diameter while the upper part is realized with steel perforated conical section with 10 mm thickness. The pylons are connected to the deck with tubular elements K-bracings shaped used in order to limit the box girder deformation.
The vertical vertical deck support is made of a double order of full locked coil strands with 30 mm diameter that are connected to the deck stringers using welded plates forming a box shape.

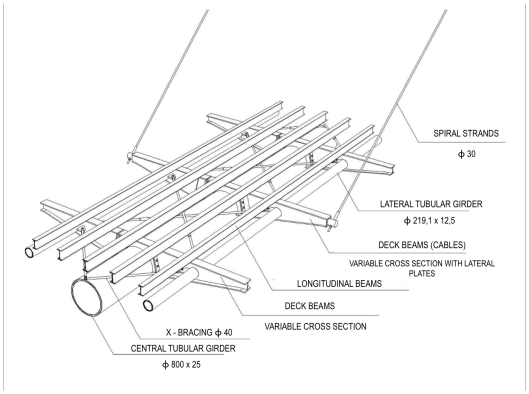

Fig. 5.2: Schematic representation of the typical cross section of composite deck [132].

5.3 FE model of the structure

A detailed initial three-dimensional FEM to be used for the numerical modal analysis of the cable-stayed footbridge has been developed using SAP 2000 ([133]). The numerical model geometry is carefully defined on the basis of available technical drawings and photographs.
The FE model has 395 frame elements, 28 cable elements, 112 shell elements and 429 nodes. The three steel girders, the stringers and the bracings are described by beam elements having three translational DOFs and three rotational DOFs at each node. The deck is modeled by quadrilateral shell elements neglecting the shear deformation and the stress

Table 5.1: Properties of structural members.

Material	E(GPa)	Mass density (KN/m^3)
Steel S355	210	78
Cables	160	77
Concrete C32/40	33.345	25

in the thickness direction. Thirty eight elements of this type are used in the current model. Each stay is modeled with a nonlinear element describing both tension-stiffening and large deflection so that an iterative procedure is required to compute the solution. Different mechanical characteristics are selected for the structural components (Table 5.1).

The tower is modeled considering the variable cross section by means of three different elements: one for the lower level, one for the upper level and one for the end part.
The modeling of footbridge boundary conditions is an important issue in the modal analysis. The connection at the piers and at the base of the tripod needs to be analyzed taking into account the soil-pier interaction. In the initial FE model, the soil–structure interaction is not included in the analysis.
The tower base consists in a basement of diaphragms over a deep foundation made up by 10 piles,. Indeed, the tower bases are considered fixed in all the DOFs. The connections of the deck to the piers at the support 1,2, 3 and 5 - referring to the Figure 5.1 - are realized with a concrete reinforced diaphragm. The longitudinal translation is considered to be free at the pier connections, while vertical translation is considered to be fixed. Different kind of bearings are used. The constructed three - dimensional FE model of the cable - stayed footbridge is shown in Figure 5.3.

Several authors [134] [135] have investigated the significance of the nonlinear behavior of this class of bridge mainly due to cable sag and large deflection. Cable sag is usually the most significant feature since the cable stiffness increases with cable tension. For this reason the dynamic characteristics have been estimated performing two types of modal analysis:

- *Ordinary modal analysis* The initial configuration is the unloaded one;
- *Pre-stress modal analysis* The initial configuration is the deformed equilibrium configuration under dead load and cable pre-tension. Large displacements non linear static analysis is performed and the stiffness matrix updated by means of 200 incremental steps. The equilibrium is reached at each step using the Newton-Raphson method.

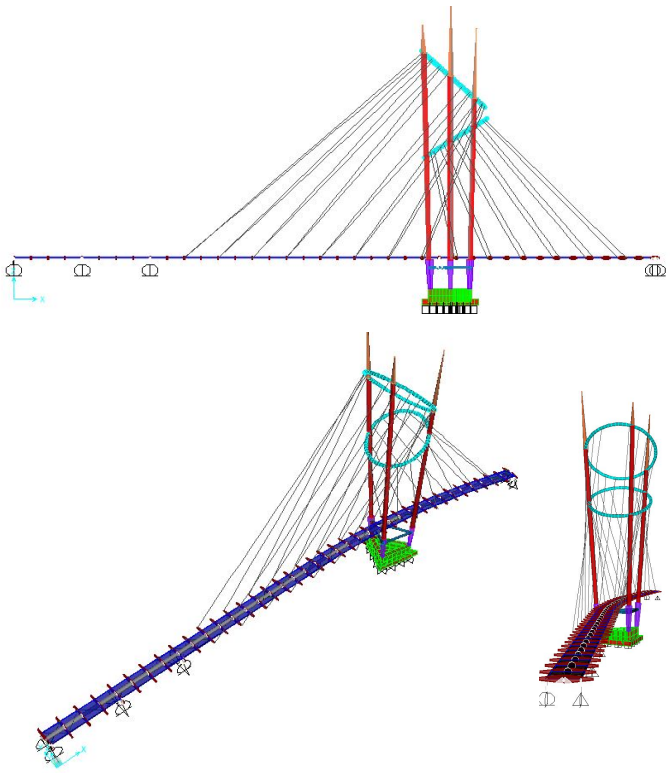

Fig. 5.3: Three-dimensional FEM of the cable-stayed footbridge.

To see the effect of the cable pre-tension and the dead load, the natural frequencies obtained from the deformed position are compared to those obtained from the non-deformed position in Table 5.2. As expected, the cable pretension cause increased footbridge natural frequencies. Although the differences are very small, the reference deformed configuration is crucial to estimate the dynamic response to wind and/or earthquake loads.

Depending on the amplitudes of the mode shapes, modes can be classified into different groups: longitudinal modes are those dominated by a shift of the deck in longitudinal direction; vertical modes are those dominated by the vertical bending of the deck; lateral modes are those dominated by the lateral sliding of the deck while the torsional modes are those dominated by the rotation of the deck along the longitudinal axis. Figure 5.5 shows the typical vertical, horizontal and torsional mode shapes obtained from the pre - stressed modal analysis in the considered range of frequency of interest *0-3.5* Hz. The first mode shape is the out of plane mode shape of the pylon (Figure 5.4a) while the second mode shape is a longitudinal mode (Figure 5.4b). These first two mode shapes cannot be used for the comparison with the results of the dynamic identification since the setup used in

Table 5.2: Comparison of natural frequencies (Hz) without and with pre - stress effect.

Mode	Ordinary Modal Analysis	Pre Stress Modal Analysis	Difference %
1	1.025	1.030	0.49
2	1.491	1.514	1.52
3	1.766	1.774	0.45
4	2.180	2.184	0.18
5	2.306	2.365	2.49
6	2.977	2.982	0.17
7	3.151	3.153	0.06
8	3.419	3.423	0.12

the measurement campaign regards just the deck monitoring.
Then, fourth vertical mode shapes (in Figures 5.5a, 5.5f, 5.5g and 5.5h), one lateral (in Figure 5.5b), one torsional (in Figure 5.5c) and two mixed mode shapes (in Figures 5.5e and 5.5d) are identified. It is worth noting that some dominant modes have frequencies really close to each other.

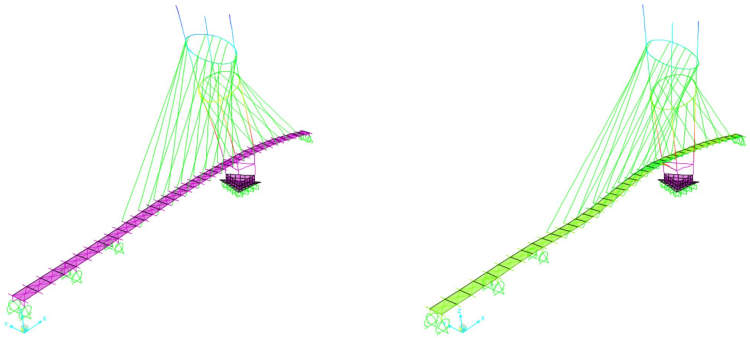

(a) OOP Pylon $f = 0.588$ Hz **(b)** LM $f = 0.746$ Hz

Fig. 5.4: Out of plane mode shape of the pylon (a) and longitudinal mode shape of the deck (b) obtained from the numerical analysis.

5.4 Dynamic Identification using EFDD

The footbridge dynamic characterization in terms of natural frequencies, corresponding modal shapes and damping was obtained by means of full - scale measurements in operating conditions using classical contact measurements in order to provide useful information to properly design tuned mass dampers to mitigate pedestrian - induced vibration. Accel-

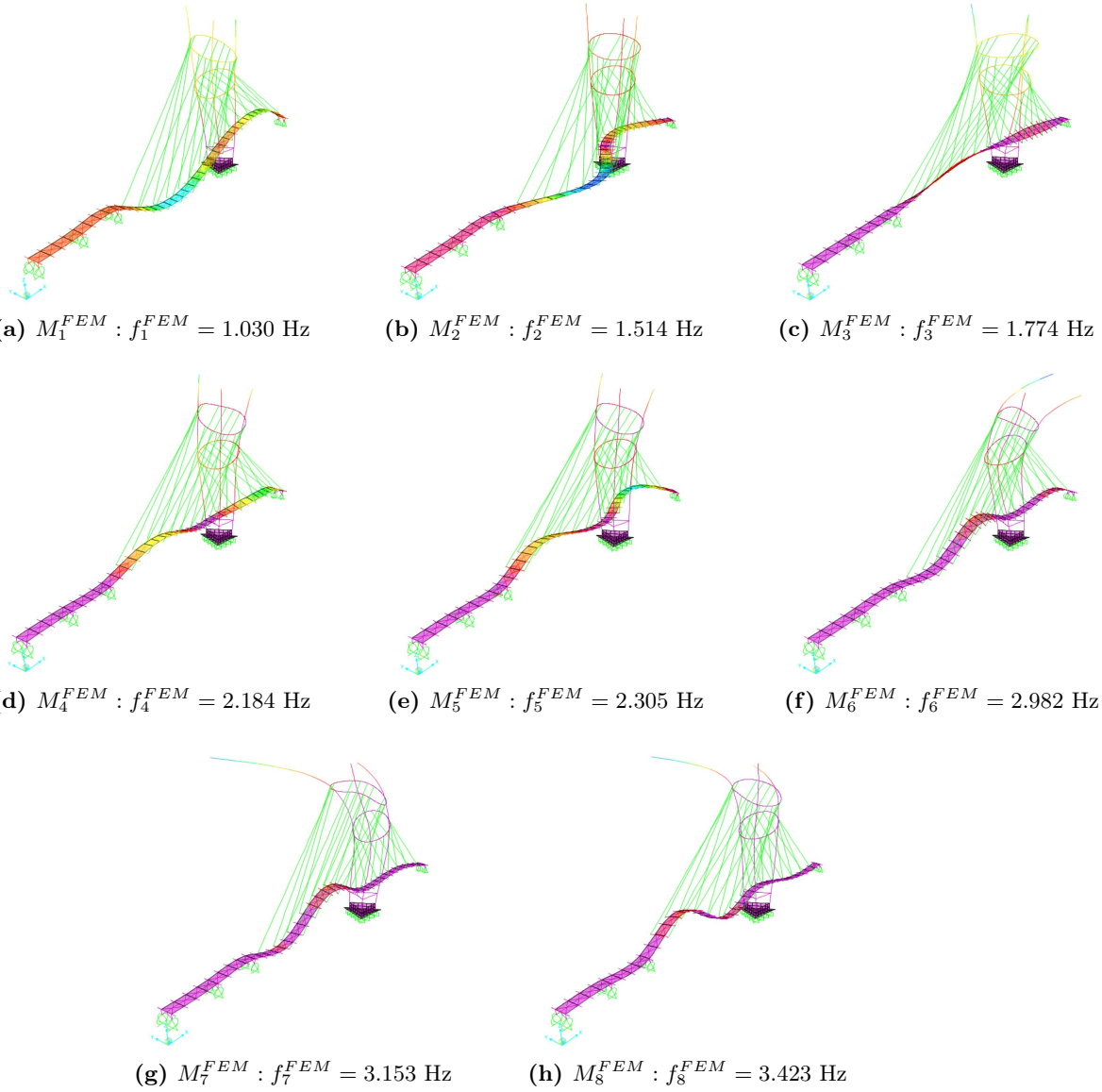

(a) $M_1^{FEM} : f_1^{FEM} = 1.030$ Hz **(b)** $M_2^{FEM} : f_2^{FEM} = 1.514$ Hz **(c)** $M_3^{FEM} : f_3^{FEM} = 1.774$ Hz

(d) $M_4^{FEM} : f_4^{FEM} = 2.184$ Hz **(e)** $M_5^{FEM} : f_5^{FEM} = 2.305$ Hz **(f)** $M_6^{FEM} : f_6^{FEM} = 2.982$ Hz

(g) $M_7^{FEM} : f_7^{FEM} = 3.153$ Hz **(h)** $M_8^{FEM} : f_8^{FEM} = 3.423$ Hz

Fig. 5.5: Mode shapes obtained from the numerical analysis.

eration time histories in operating conditions were recorded and used in order to estimate modal characteristics of the footbridge using Enhanced Frequency Domain Decomposition method.

The dynamic response of the cable stayed spans was measured using fourteen uni-axial accelerometers (10V/g sensitivity) located in the five cross - sections A, B, C, D and E of the bridge deck (Figure 5.6). The obtained acceleration time histories were used to identify

vertical, horizontal and torsional vibration modes. Pairs of accelerometers were installed using specific metallic supports attached to the steel frame of the barriers, which were inclined of about 15 ° from the vertical direction in the cross - section plane. Two sensors used as references were located at section C (Figure 5.6) on both sides of the footbridge. The testing methodology consisted in two different measurements lasting 710 s (Data Set-1) and 926 s (Data Set -2) respectively with a sampling rate of 400 Hz. The two considered measurements started at 11 a.m. and 3.30 p.m on November 15^{th} and 16^{th} 2016.
Before selecting the most suitable signal processing parameters a visual inspection of the acceleration time histories and corresponding PDF was performed. The mean value and any possible linear trends were removed. Figures 5.7a and 5.7b show the plots of acceleration time histories and the corresponding PDFs in a decimal and a logarithmic scale for a vertical and an horizontal recording channel respectively. Same procedure was carried out for all the recording channels showing that the estimated PDFs are not properly Gaussian since the values on the tails are widespread and the Kurtosis coefficient assumes values lower than 3.
Since the frequency range of interest is very low, different parameters have been chosen for signal processing. Data were downsampled with order of decimation 30 and high - pass filtered in order to remove offsets and drifts. After decimation, the data had a sampling frequency of 13,33 Hz and a Nyquist frequency of 6.67 Hz. Furthermore, different values of the frequency resolution are considered changing the number of frequency lines in the spectral density spectrum. Reliability of results is checked using different order of decimation and different type of filters. The obtained singular value curves are presented in

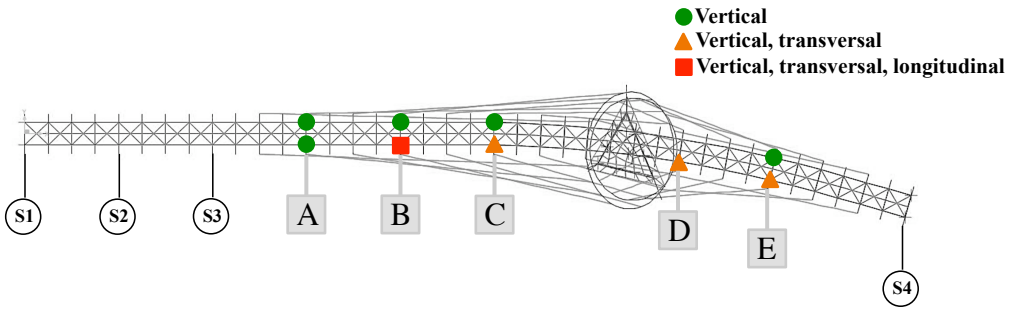

Fig. 5.6: Measurement locations on the cable - stayed spans.

Figure 5.8 for the two recorded data sets. Natural frequencies are estimated from the local maxima of the singular value curves.
A singular value plot is dependent on the estimated output PSDs. In particular, the PSD is

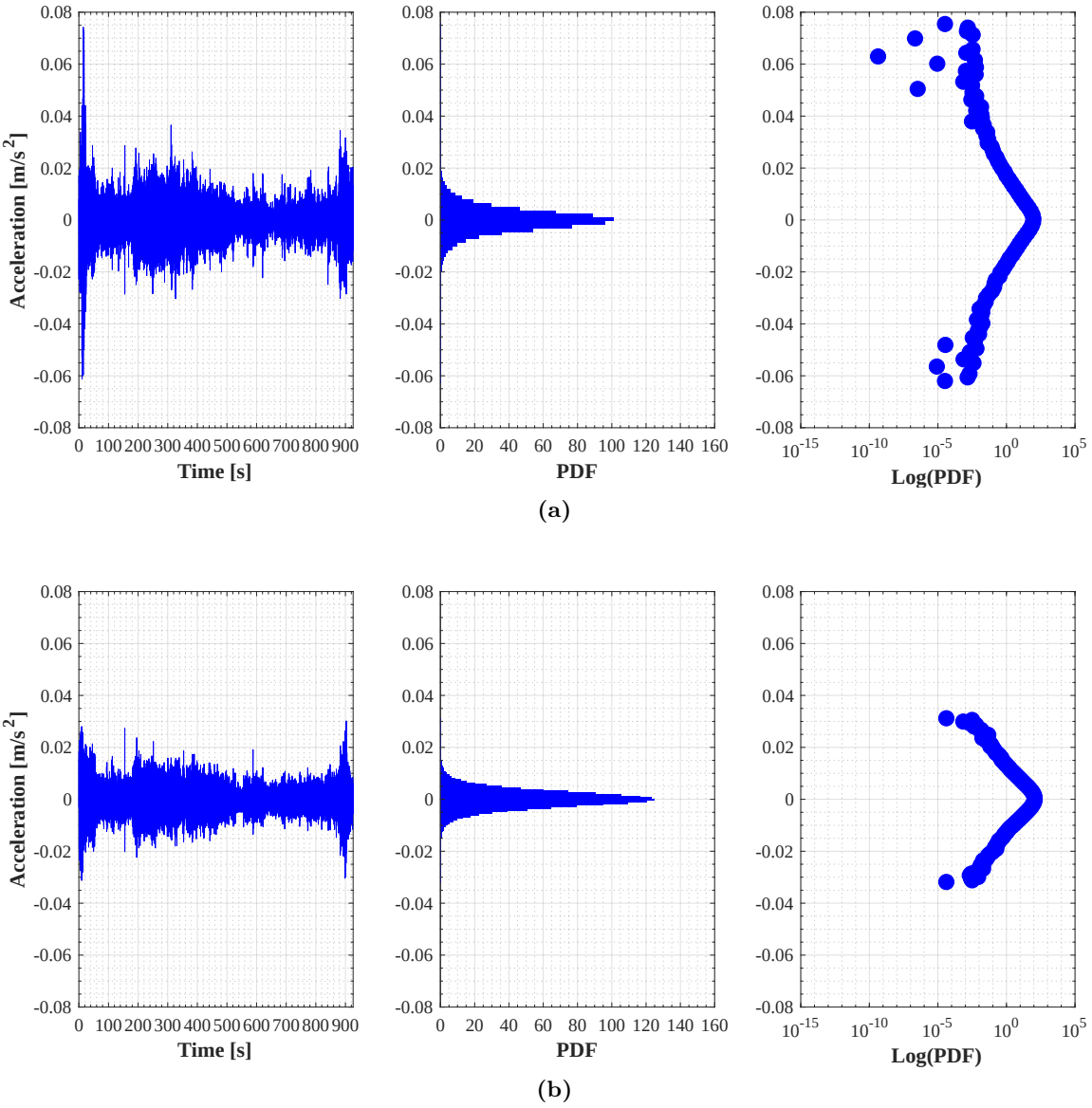

Fig. 5.7: Plots of vertical (a) and horizontal (b) acceleration and estimated PDFs in a decimal and a logarithmic scale .

estimated using Welch method. It can be seen that 8 modes are clearly identified with the Data Set-2, whose frequencies are highlighted with the vertical dash-dotted lines. Seven modes are clearly identified from the Data Set-1 (i.e. the fourth natural frequency f_4^{EXP} cannot be identified). Table 5.3 summarizes the minimum and the the maximum value of the identified natural frequencies considering both data sets, different frequency resolution

and order of decimatio: 20 and 40.

The associated identified mode shapes are presented in polar plots in the two Figures

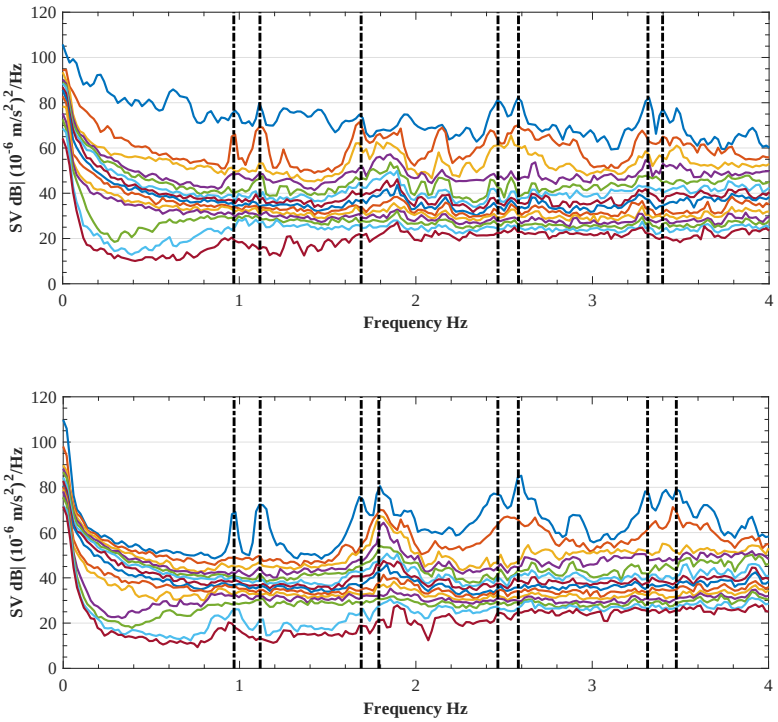

Fig. 5.8: Non zero singular value plots for Data Set-1 (a) and Data Set-2 (b) .

Table 5.3: Maximum and minimum value of natural frequencies (Hz) identified using different signal processing parameters for the two considered Data Sets.

Mode	Minimum Frequency	Maximum Frequency	Nature of Vibration Mode
1	0.97	0.97	Vertical Mode
2	1.11	1.13	Vertical Mode
3	1.67	1.69	Lateral Mode
4	1.79	1.80	Torsional Mode
5	2.40	2.47	Mixed Mode
6	2.58	2.59	Mixed Mode
7	3.30	3.31	Vertical Mode
8	3.35	3.40	Vertical Mode

5.9 and 5.10: cyan lines are used for vertical components, while magenta and green lines are used for transversal and longitudinal components respectively. The representation of

the complex mode shape in the complex plane provides useful information in order to verify the degree of non-classical damping characteristics of the considered mode. The more scattered the mode shape components are in the polar plot, the more the system is not classically damped in that mode.
In both data set results, the identified mode shapes are mainly along the real axis, albeit some components for each mode are rotated in the complex plane. This is particularly true for high frequency vibration modes where the noise increases. The longitudinal component is rotated with a significant phase angle also for the low frequency mode shapes suggesting that low level of excitation and high level of noise could be present.

Figures 5.11a and 5.11b show the AutoMAC matrices of the identified mode shapes re-

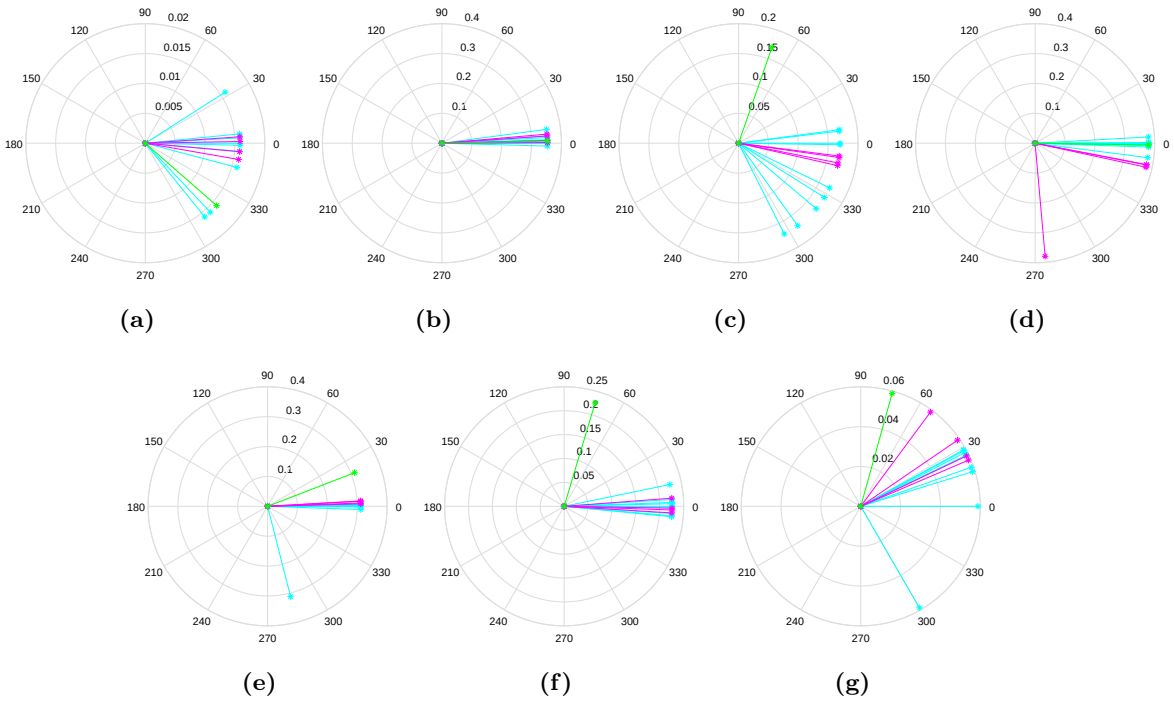

Fig. 5.9: Polar plots of the identified mode shapes: Data Set - 1.

spectively for Data Set-1 and Data Set-2. The AutoMAC compares a set of modal vectors with themselves in order to assess if the number and the location of the monitored DOFs chosen for the measurement campaign allow to distinguish the modes from each other. Therefore the AutoMAC is able to provide useful information about the modal vector consistency representing a useful mean for assessing the quality of the measurement based dynamic identification results. It is worth to note that for both Data Sets the AutoMAC

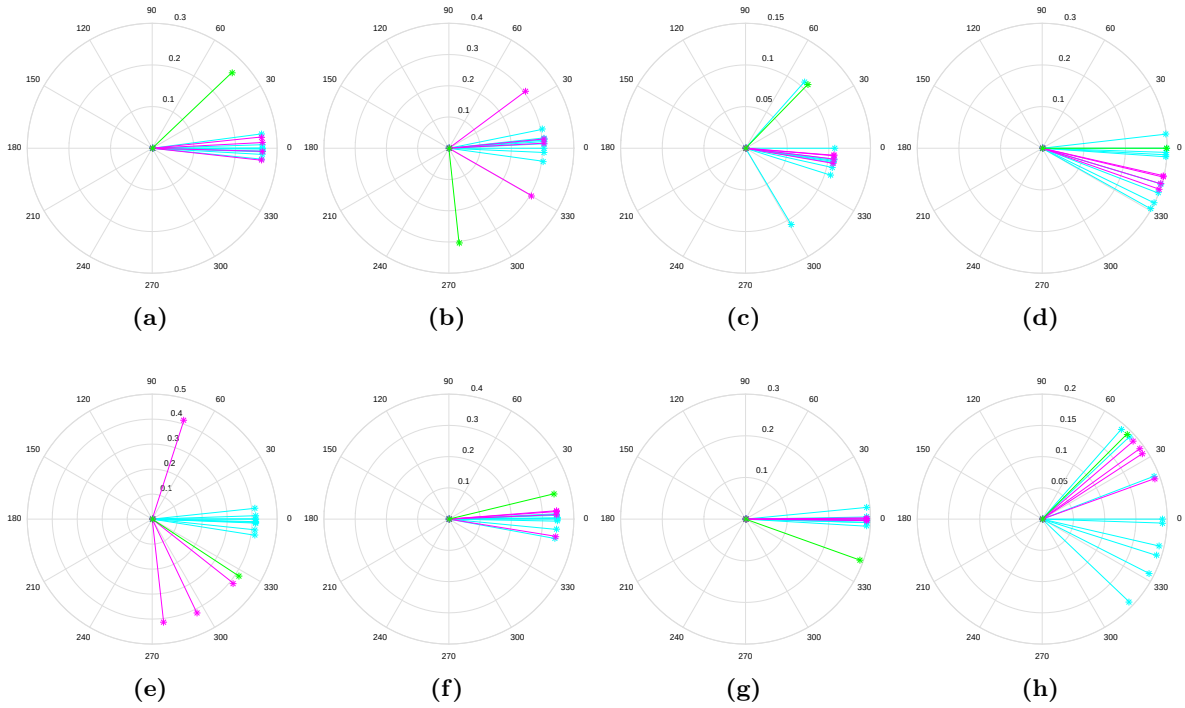

Fig. 5.10: Polar plots of the identified mode shapes: Data Set - 2.

assumes values identical to 1 on the diagonal (each modal vector is paired with itself) and values really close to zero otherwise.

The AutoMAC value of the pair given by M_1^{EXP} and M_2^{EXP} (bending mode shapes with frequencies below 1.2 Hz) is grater than 0.95. This would indicate high chances to deal with the same mode shape but the two corresponding peaks on the singular value curves are clearly separated, being evidence of a sort of mode shape splitting phenomenon. Furthermore, the numerical model presents a single bending mode shape with associated frequency at 1.03 Hz. Further experimental investigation such as a second experimental measurement campaign or a continuous monitoring needed to be developed in order to assess the nature of the these first two modes identified experimentally. This mode shape splitting could be due to temperature effects and/or to an high amplitude of excitation occurs for example in presence of significant wind excitation and its typical of all those structure characterized by non-proportional damping.

Figures 5.11c shows the MAC matrix estimated from the vibration modes identified from the two Data Sets in order to further validate the obtained results. Obviously, the fourth mode shape M_4^{EXP} identified by means of the Data Set-2 is not included in this compar-

ison procedure. In general, a MAC value greater than 0.80 is considered a good match, while a MAC value lower than 0.40 is considered not a good match. It is evident that the level of consistency between the obtained modal vectors is significant: the diagonal MAC presents values really close to one - or however higher than 0.80 - while the MAC values off the diagonal are really close to zero. Therefore Data Set-2 is used for the succeeding analysis ensuring a better level of accuracy.
The tridimensional representation of the identified mode shapes is plotted in Figure 5.12. The magnitudes of the mode shapes at the sensor locations are identified based on the real measured data, while the other magnitudes are interpolated using the boundary conditions and the identified mode shapes at the sensor locations by means of cinematic equations.

5.5 Comparison between analytical and experimental modal parameters

The comparison between the numerical model and the results of the dynamic identification is carried out using just the Data Set-2 that is the most representative one. The selection of the most representative and accurate values of experimental natural frequencies and mode shapes is a crucial issue in model updating procedure since such results represents the starting point for all the updating problem.
The natural frequencies identified from the numerical model and from the measurements are summarized respectively in Tables 5.2 and 5.3. The natural frequencies of the initial FE model are mostly lower than the identified natural frequencies. This is due to the modeling errors such as the omission of non structural components, the idealizations of the connections and to the main hypotheses on the boundary conditions and on the mechanical properties.
The MAC compares the experimental modal vectors and the numerical modal vectors. The obtained MAC matrix is shown in Figure 5.11d. The first two modes identified experimentally M_1^{EXP} and M_2^{EXP} have a MAC value greater than 0.90 when compared to the first mode obtained from the numerical analysis M_1^{FEM}: that is why the diagonal MAC is translated. The terms in the translated diagonal MAC matrix are greater than 0.80 with the exception of the fourth experimental mode shape M_4^{EXP} characterized by a MAC equal to 0.73 indicating a good correlation between the experimental and the initial FEM model.
The mode shapes correlation is generally displayed by plotting the MAC matrix while the natural frequency correspondence is usually checked with a separate plot representing the

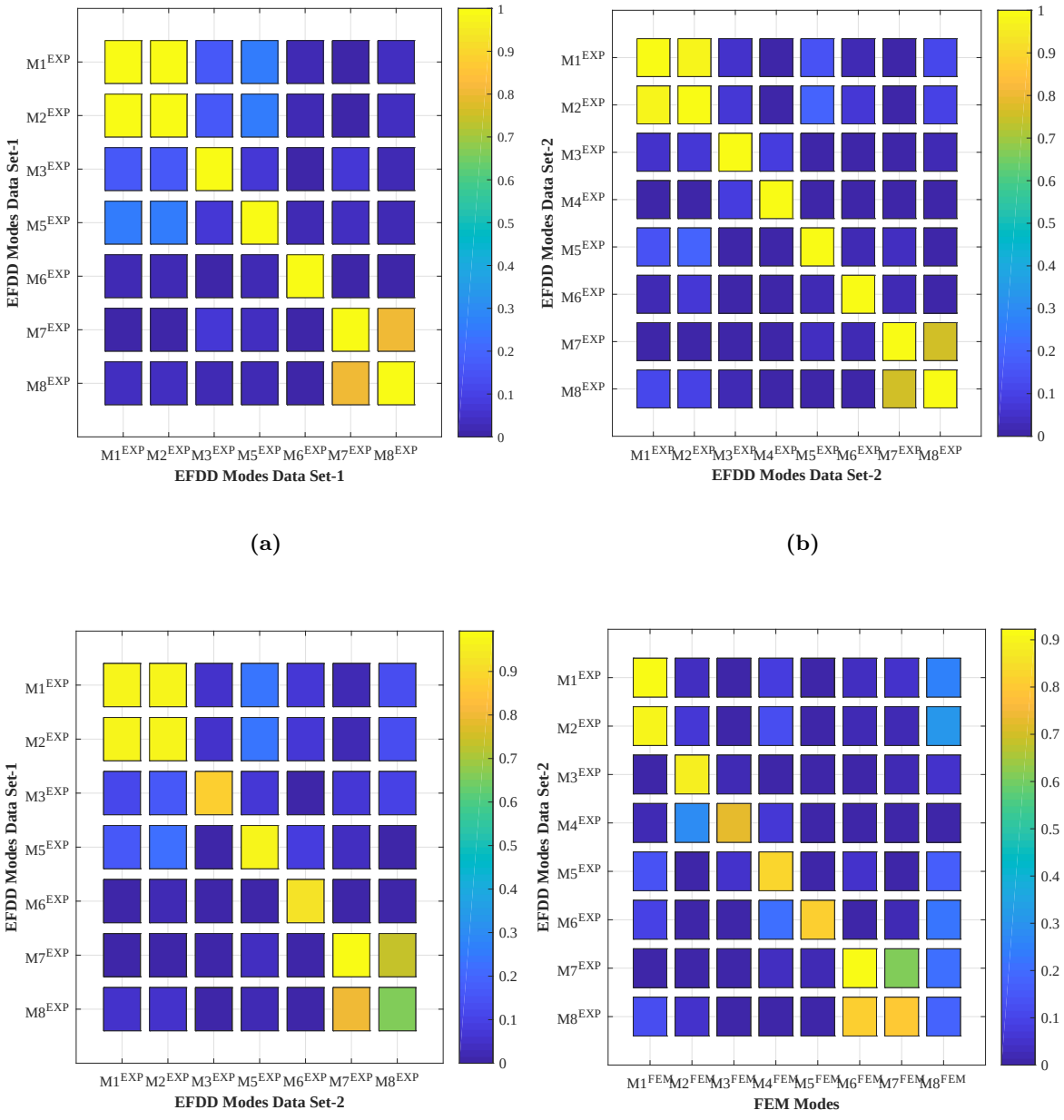

(a) **(b)**

(c) **(d)**

Fig. 5.11: AutoMAC matrix for Data Set-1 (a) and Data Set -2 (b). MAC matrix estimated for Data Set-1 and Data Set-2(c). MAC matrix estimated for Data Set-2 and Numerical Model (d).

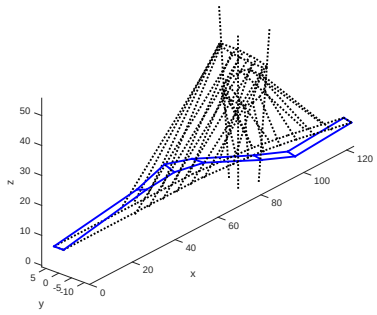

(a) $M_1^{EXP} : f_1^{EXP} = 0.964$ Hz

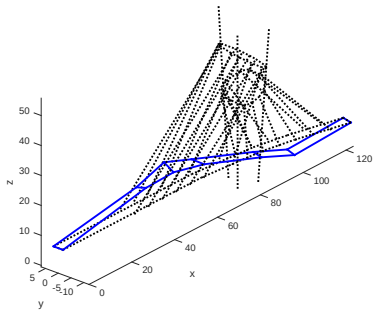

(b) $M_2^{EXP} : f_2^{EXP} = 1.107$ Hz

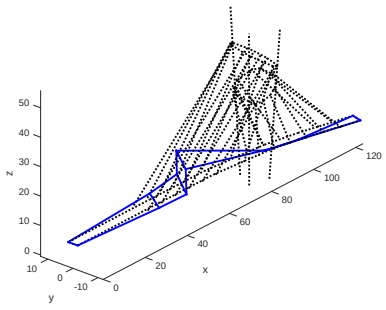

(c) $M_3^{EXP} : f_3^{EXP} = 1.693$ Hz

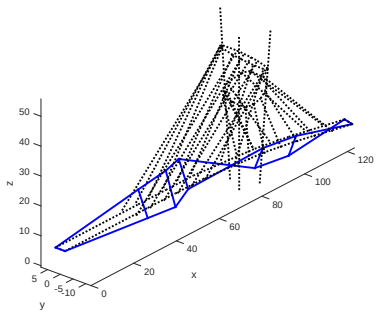

(d) $M_4^{EXP} : f_4^{EXP} = 1.797$ Hz

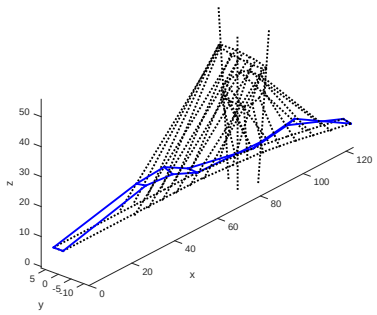

(e) $M_5^{EXP} : f_5^{EXP} = 2.474$ Hz

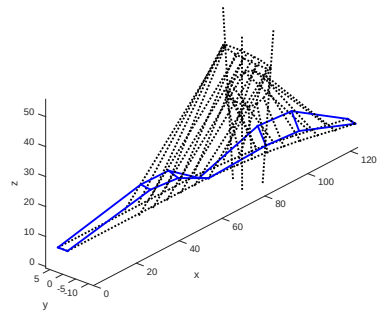

(f) $M_6^{EXP} : f_6^{EXP} = 2.591$ Hz

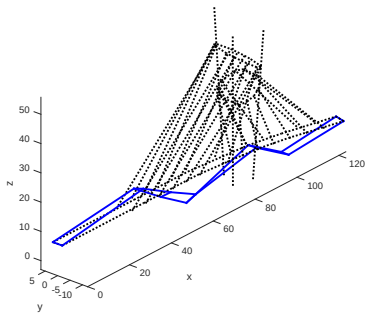

(g) $M_7^{EXP} : f_7^{EXP} = 3.307$ Hz

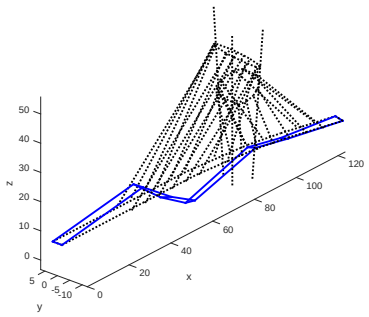

(h) $M_8^{EXP} : f_8^{EXP} = 3.398$ Hz

Fig. 5.12: Vibration modes obtained from the measurements using EFDD.

OMA natural frequency versus the numerical natural frequency. F-MAC plot is a useful type of plot proposed in [136] in order to view simultaneously the natural frequency comparison, the mode shape correlation and the spatial aliasing. A circle with a radius proportional to the value of the MAC is drawn at the coordinates of each frequency pair. This is also done for the AutoMAC. Frequency separation lines are used in order to give a visual scale for the amount of frequency shifting between the OMA and the FEA results. In Figure 5.13a the MAC is represented by the red filled circles, while the AutoMAC is represented by the blue circle. The frequency separation is shown by the horizontal shift from the blue to the red circles. The two dashed lines indicate a ±10% variation of frequency. It is possible to observe a good agreement between the output of the initial numerical model and the experimental analysis for each identified mode shape in terms of both natural frequencies and mode shapes. Natural frequency differences are smaller than 10 % for each identified mode shapes with the exception of the 4th and the 5th experimental mode shape (M_4^{EXP} and M_5^{EXP}).

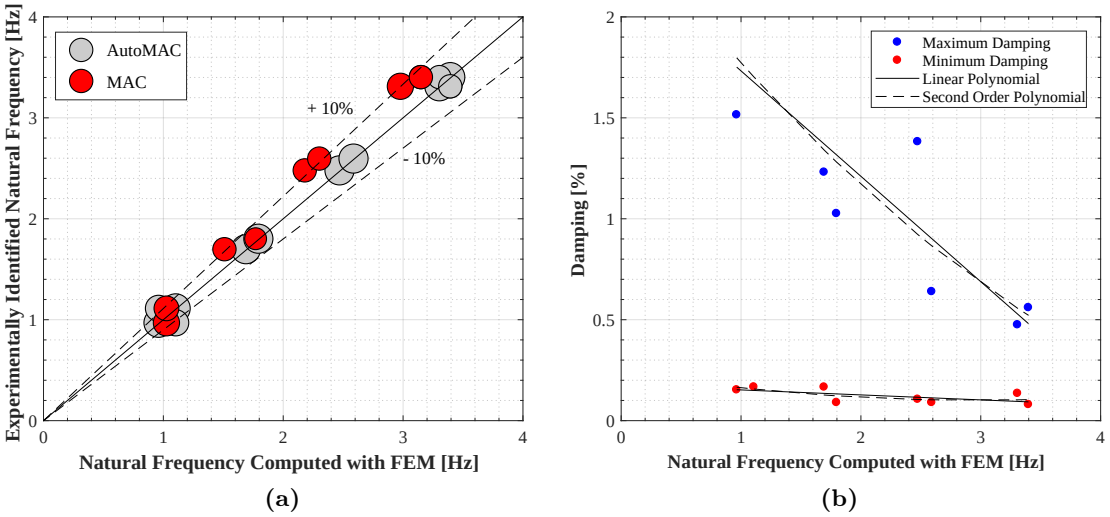

Fig. 5.13: F-MAC plot (a). Variation of maximum and minimum damping ratio with natural frequencies (b).

5.6 Damping estimation using operational modal analysis

The damping ratios are determined from equivalent SDOF correlation function around a resonance peak using Eqs. 2.63 and 2.64. Regression on the logarithmic decrements de-

termines the damping ratio. Therefore the validation of the damping ratio can be carried out by controlling the output PSD function, the frequency resolution and the correlation function.

To investigate the influence of signal processing parameters on the damping ratio the dynamic identification procedure has been repeated a lot of time by changing the frequency resolution and the order of decimation. In particular two different order of decimation are selected: 40 and 30 while the number of frequency lines in the output PSD spectrum are set equal to 256, 512, 1024 and 2048. The maximum and minimum values of damping ratio obtained are summarized in Table 5.4 for each identified mode shape. Figure 5.13b gives a good representation of the damping ratio estimates versus the corresponding experimental natural frequencies.

Minimum values of damping are in a range of variation between 0.2 % and 0.4 % and

Table 5.4: Maximum and minimum value of damping ratio (%) identified using different signal processing parameters for the two considered Data Sets.

Mode	Minimum Damping [%]	Maximum Damping [%]
1	0.159	1.515
2	0.167	2.160
3	0.167	1.231
4	0.090	1.026
5	0.194	1.382
6	0.090	0.639
7	0.135	0.475
8	0.080	0.560

they can be very well interpolated by a linear polynomial with almost constant gradient. Maximum values of damping ratio decrease rapidly with the increase of the natural frequencies.They are scattered and they can be interpolated by a second order polynomial. Figure 5.14a shows that the damping estimation is linearly dependent on frequency resolution Δf in Eq. 2.65 with the exception of the 5-th mode shape M_5^{EXP} presenting scattered values. The varying gradient of the first order curves obtained for each mode confirms that the damping estimation depend also on the natural frequency of each mode shape. Same result is confirmed by the bias error on damping ζ_b in eq. 2.66, shown in Figure 5.14b for each mode shape and for each frequency resolution considered for data analysis. Bias error on damping decreases with the increase of frequency resolution and the gradient of each single first order curve decreases with the the increase of natural frequency. Leakage bias can carry to an estimation of damping values away from the physically present damp-

ing and frequency resolution has to be chosen such that the influence of leakage can be minimized.

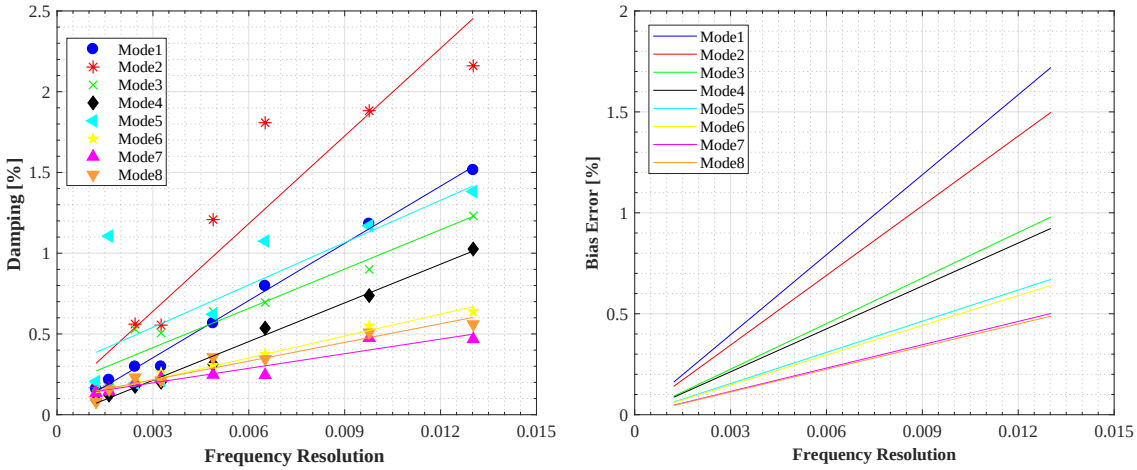

Fig. 5.14: Variation of damping (a) and variation of bias error on damping as a function of frequency resolution (b).

5.7 Selection of updating parameters

The selection of updating parameters is a key issue in the model updating procedure since they have to be directly related to the measurement results used as reference data. Usually this selection depends on expert judgment. A preliminary sensitivity analysis is carried out in order to have information for an efficient selection. In particular, the sensitivity of the natural frequencies to variation of model mass density, structural steel and cable Young's moduli, cable tension stiffening, stiffness of rotational and translational springs used for describing soil-structure interaction is evaluated.

The modulus of elasticity of the deck used in the initial model is typical of S355 structural steel. The sensitivity of the natural frequencies to variations in the model stiffness is investigated for maximum variations in the Young's modulus of the structural steel equal to ±30%. Results are shown in Figure 5.15a. Red continuous line with pentagon markers shows the experimentally identified natural frequencies, while the magenta dashed line with triangular markers shows the numerically identified natural frequencies using the mechanical properties of the initial model. The other two continuous lines are used for the

numerically identified natural frequencies for the considered maximum variations of the modulus of elasticity of ±30%. As expected, the natural frequencies increases when the stiffness increases.
It is evident that the model is improved by means of a higher steel modulus. The mean value of the percentage difference Δf between the FE and measured natural frequencies decreases from -20.1% to 3.07% with the increase of the elastic moduli. Negative values of Δf indicate that the global stiffness of the model is underestimated.
The sensitivity of the eigenvectors to the same variations of the elastic modulus of structural steel is investigated by means of diagonal MAC values estimated using numerical and experimental results. Diagonal MAC values obtained are shown in Figure 5.15b. It is evident that the mode shapes most influenced by the change in stiffness are the torsional and the mixed ones, corresponding to the natural frequency values in the range of *1.7 - 2.4* Hz.
The sensitivity of the initial model to an increase in structural steel mass density of ±10% is investigated and results are shown in Figure 5.16a.The mean values of the percentage difference Δf between the FE and measured natural frequencies decreases from $-10,51\%$ to $-3,68\%$ when the model mass density decreases. The use of lower values of mass density improves the model.
Figure 5.16b shows the results obtained in terms of diagonal MAC values comparing the numerical and experimental eigenvectors. While the use of lower values of mass density improves the model in terms of obtained natural frequency comparison, the use of higher values of mass density improves the model in terms of mode shapes comparison. Moreover, also in this case variations of model mass density mainly influence the torsional and lateral mode shapes in the range of frequency *1.7 - 2.4* Hz.

Having established the initial model also the sensitivity of the natural frequencies and mode shapes is investigated for variations in the elastic moduli and the mean tension of the cables. A basic elastic modulus of 160 GPa has been used for each cable. The pre stressed modal analysis allows to take into account for the cable sag. The effect of maximum variations of ±20% in the cables elastic moduli is investigated and Figure 5.17a shows the obtained results. The differences between the FE and measured natural frequencies are slight with a mean difference Δf decreasing from -6,06 to -5.93 increasing the cables stiffness.
Also the differences between the FE and the measured natural frequencies obtained changing the mean tension in each cable are slight. This can be explained by studying the relation between the equivalent modulus of cables able to account for both the sag effect

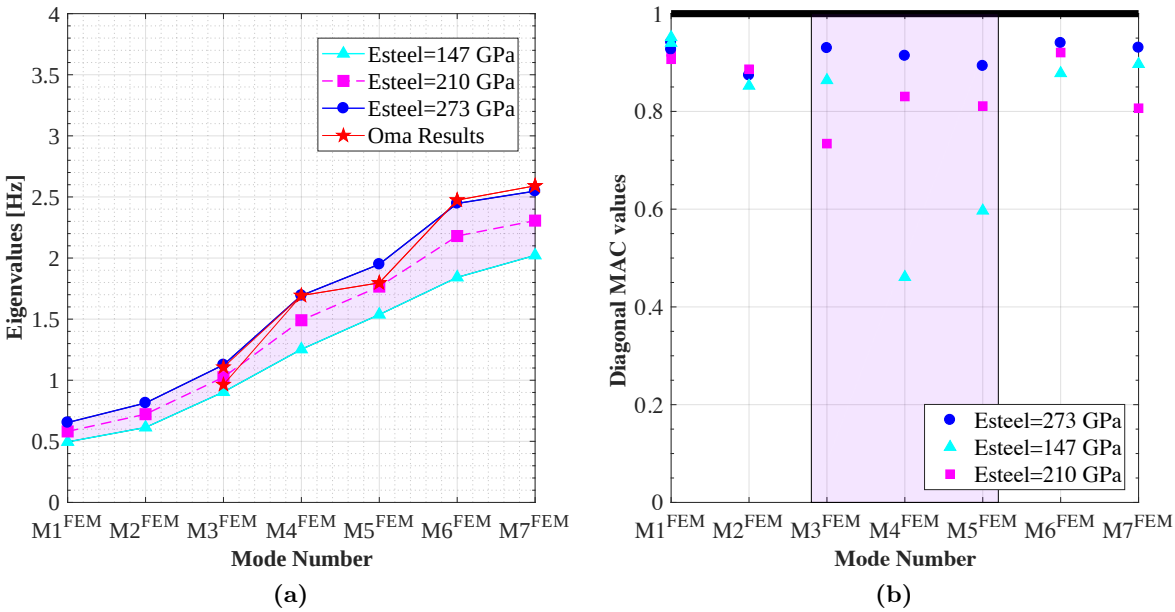

Fig. 5.15: Variation of the natural frequencies (a) and diagonal MAC coefficients (b) using results of the different numerical models obtained by changing the modulus of elasticity of the structural steel.

and the tension [137] that can be expressed as:

$$E_{equivalent} = \frac{E}{1 + \frac{(mgh)^2 A_e E}{12T^3}} \tag{5.1}$$

where E is the basic elastic modulus of cable, m is the cable mass per unit length, g is the acceleration due to gravity, h is the horizontal projected length of cable, A_e is the effective cross-sectional area of cable and T is the mean cable tension. In order to have significant change in equivalent modulus of elasticity of cables accounting for sag and non linear effect, the tensile force has to be increased of an unrealistic quantity.
Figure 5.17b shows the comparison in terms of mode shapes for same variations of the stiffness of the cables. If natural frequencies of the model are not particularly influenced by the cables stiffness, MAC values obtained using numerical and experimental results are subjected to significant changes in values and the most influenced mode shapes are the torsional and the mixed ones.

Soil structure interaction problem has been considered in order to investigate the effect of soil deformability on modal characteristics of structure. The system soil - structure

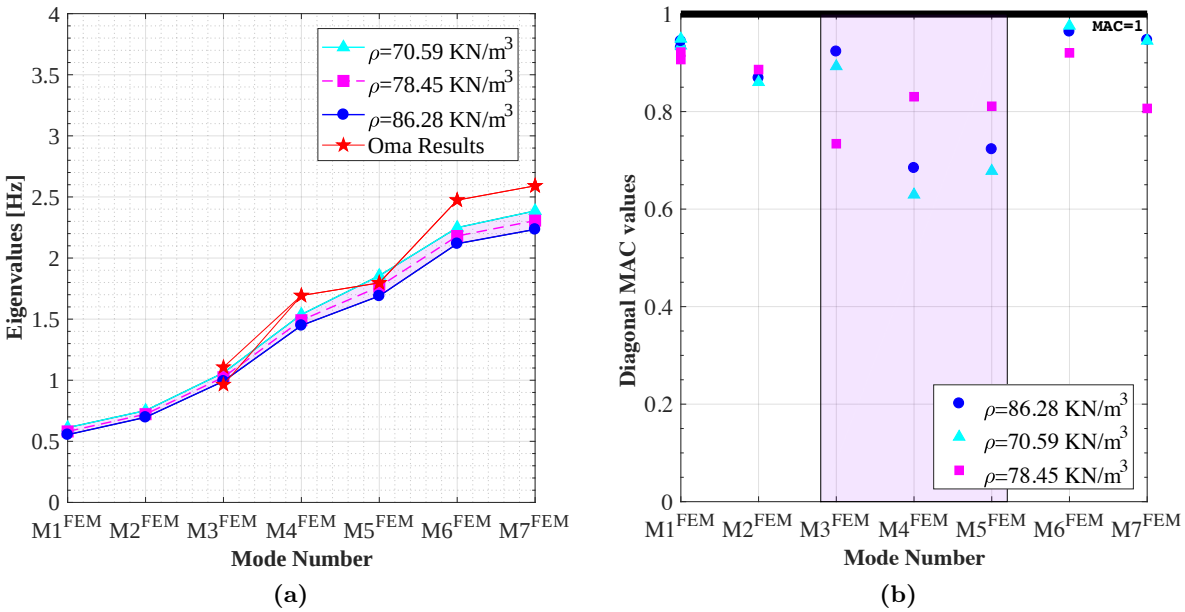

Fig. 5.16: Variation of the natural frequencies (a) and diagonal MAC coefficients (b) using results of the different numerical models obtained by changing the mass density of the structural steel.

has been modeled using elastic equivalent elements for each DoF at the base of the tower. Translational and rotational springs in all the three directions have been used. A parametric analysis changing the stiffness of the springs has been carried out and results are shown in Figure 5.18a and 5.18b. In particular natural frequencies of the first eight mode shapes identified numerically are compared to the corresponding mode shapes identified by means of the FE equipped with the elastic springs highlighting negligible differences for all the considered values of stiffness. Moreover significant changes in diagonal MAC coefficients such as those plotted in Figure 5.18b occur for values of the spring stiffnesses not typically used for soils behavior. The results of the sensitivity analysis show clearly that the most influencing parameters on the model dynamic response are the steel and cables elastic moduli and the model mass density. In the succeeding analysis it is reasonable to assume that the mass density of the model does not varying a lot along the deck. Moreover the mass density and the Young's modulus of the steel are two correlated quantities as a function of the Poisson and the isothermal compressibility.

For this reason the vector of the unknown/adjustable parameters $\boldsymbol{\Theta} = \{\Theta_1, \Theta_2\}^T$ in the Bayesian updating procedure consists only in two surrogate quantities able to consider the

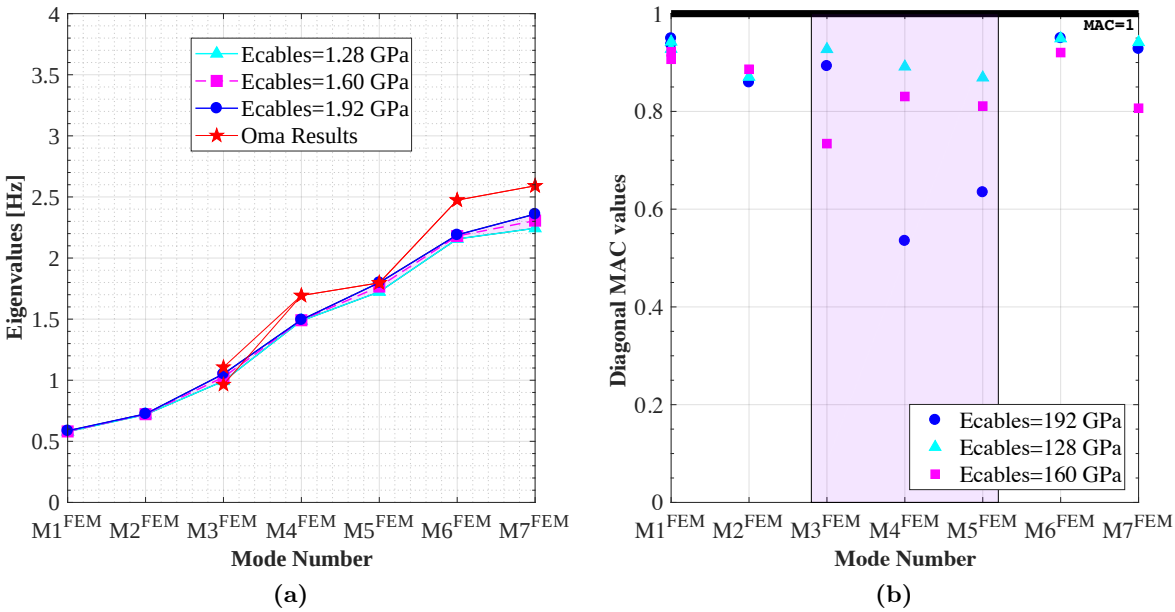

Fig. 5.17: Variation of the natural frequencies (a) and diagonal MAC coefficients (b) using results of the different numerical models obtained by changing the modulus of elasticity of cables.

uncertainty due to the idealization, simplification, the connections and all the main hypothesis used in the numerical model that are the stiffness of the deck Θ_1 and the stiffness of the cables Θ_2. It is noted that these random parameters are assumed as statistically independent of each other.

5.8 Solution of the forward problem

In this case study, the experimental natural frequencies $\{f_i^{EXP}\}$ and the modal vectors in terms of MAC are used as reference Data Set $\bar{\mathbf{D}}$ in the Bayesian updating framework while the first six numerical frequencies $\{f_i^{FEM}\}$ and each component of the first six modal vectors $\{M_i^{FEM}\}$ are set as QoIs. The PC expansion method in Eq. 3.26 is used in order to quantify the uncertainty in the FEM dynamic responses of tested structure and to build a surrogate model, for each of the selected QoI.

According to the results of the deterministic sensitivity analysis two relevant parameters are considered as affected by uncertainties: the deck stiffness of the deck $\Theta_1$and the cables stiffness Θ_2. No direct data (e.g. information about the mechanical characteristics, the

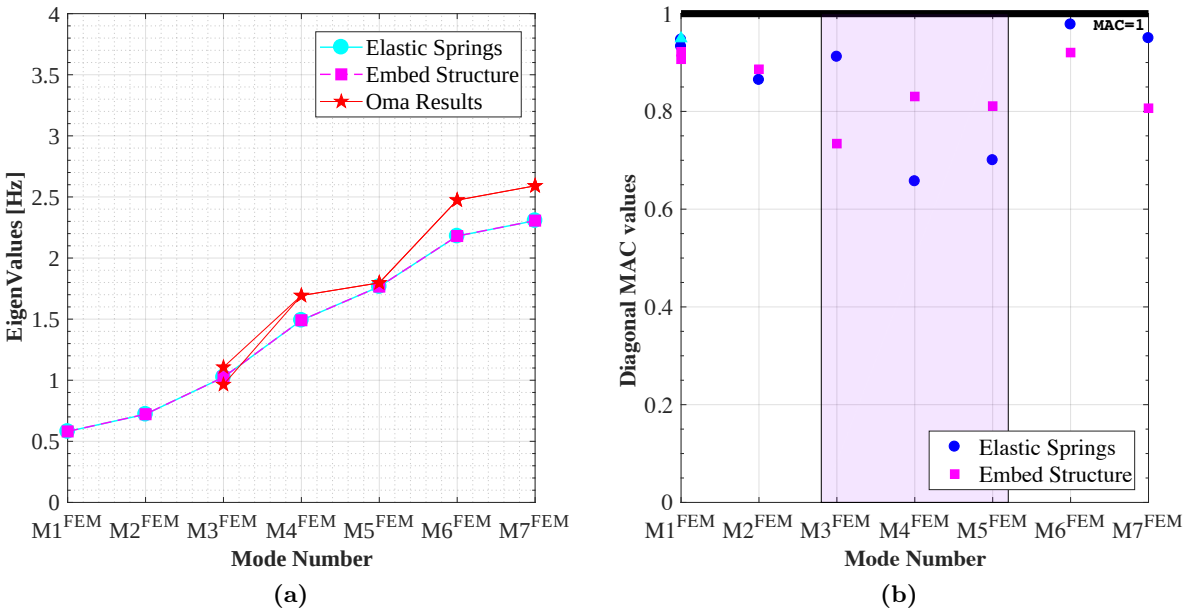

Fig. 5.18: Variation of the natural frequencies (a) and diagonal MAC coefficients (b) using results of the different numerical models obtained by changing the stiffness of the elastic springs for soil structure interaction problem.

effective mean tension in the cables) are available for the random vector $\boldsymbol{\Theta}$. For this reason two normal distributions have been selected for the two input RVs since the probability of the occurrence of very high or very low values is negligible. The nominal value of the two different materials used for deck and cables in Table 5.1 are used as PDF mean value to avoid unfeasible samples in the simulation procedure, i.e. the existence of the deformed equilibrium configuration with dead load and cable pre tension always guaranteed after the non linear static analysis under dead load and cable pre tension.
Therefore a mean value $\mu_{\Theta_1} = 210$ GPa and a coefficient of variation (c.o.v) equal to 0.15 are selected for the normal distributions of the stiffness of the deck Θ_1; and a mean value $\mu_{\Theta_2} = 160$ GPa and a c.o.v equal to 0.20 are selected for the normal distribution of the stiffness of the cables Θ_2. The resulting PDFs are shown in Figures 5.19a and 5.19b.

The distribution of the input random vector $\boldsymbol{\Theta}$ is firstly mapped to germ distributions according to Eq. 3.12 where $\boldsymbol{\xi} = \{\xi_1, \xi_2\}$ is a two dimensional random vector. It is worth noting that in this case $\mathbf{g}$ is a linear function. For normally distributed variables the germ distribution is represented by a standard normal distribution to which Hermite polynomials are associated.

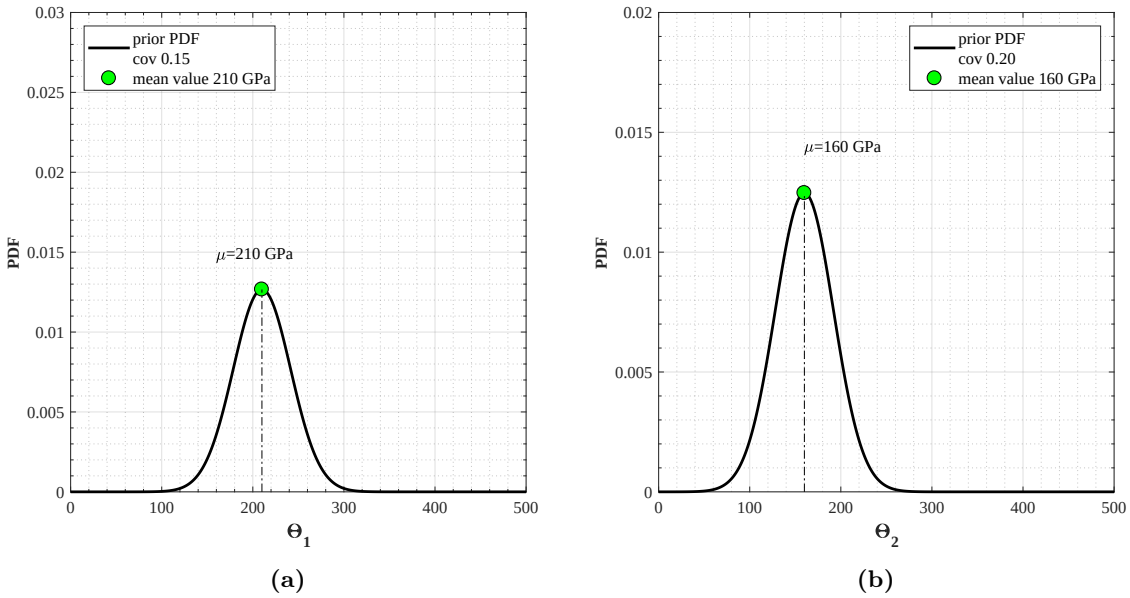

Fig. 5.19: Prior PDF of the stiffness of the deck Θ_1 (a) and the stiffness of the cables Θ_2(b).

The deterministic coefficients of the spectral expansion $\hat{\boldsymbol{u}}_{\boldsymbol{\alpha}}$ in Eq. 3.26 are estimated using least square method according to Algorithm 1, minimizing the error due to the missing terms in the definition of the truncated PC representation: the FE model is considered as a sort of deterministic black box that computes each QoI as a function of the two input random parameters ξ_1 and ξ_2 at the regression points. The accuracy of the stochastic spectral solution of the forward problem depends on the order of the PC basis used and on a suitable choice of the regression points. Usually in SFEM applications the typical polynomials order p is a value between 3 and 5 and the optimal design of sampling points is given by the roots of the Hermite polynomials. Since two independent RVs are considered as the input of the numerical model, the solution of the FEM model needs to be evaluated in just $(p+1)^2$ pairs of sample $\{\xi_1, \xi_2\}$ using a full tensor grid scheme. Figure 5.20 represents the full tensor product grid built for considered two-dimensional problem with polynomials order equal to 3,4 and 5. Note that for the highest considered order of polynomials just 36 simulations are required with a significant reduction of computational costs compared to the most common used simulation methods (e.g. Monte Carlo, Lathyn Hypercube).

Once that the candidate surrogate models are defined their validation is required in order to determine the maximum order degree of polynomials p and the associated level of

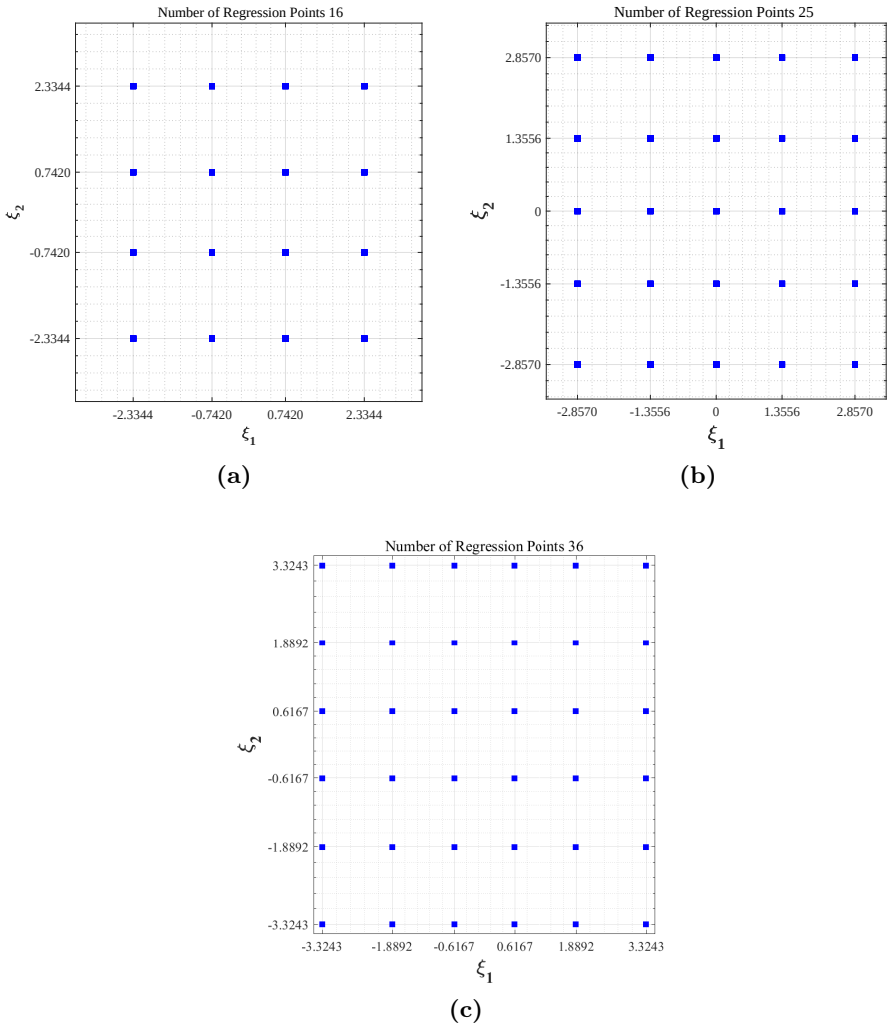

Fig. 5.20: Full tensor product grid for polynomials order 3 (a), 4 (b) and 5 (c) .

accuracy.

The first two statistic moments of each truncated PC representation are estimated using Eqs. 3.41, 3.42 and compared to the first two statistic moments of the exact solution provided directly by the numerical model according to Eq. 3.40. The error on mean and on variance up to fifth order are evaluated and shown in Figures 5.21a and 5.21b for the first six considered natural frequencies. It can be observed that the relative error on mean is negligible and the error on variance decreases increasing the polynomials order p. Furthermore no overfitting phenomena occur increasing the number of sampling points. Figures

5.21c an 5.21d show the relative error on mean and on variance of the second modal vector components. Same plots are obtained for each of the first six modal vectors with similar results.

The selection of the best polynomial order is also pursued by estimating the error vector (i.e. difference between surrogate model and the numerical model response) outside the grid used to calibrate the proxy model, driving the simulation of the parameters $\{\theta_1, \theta_2\}$ in the tail values of the vector $\boldsymbol{\Theta}$ joint probability density function. Figure 5.22 shows the errors, for each of the first six natural frequencies, between the natural frequencies obtained with the numerical model $\{f_i^{FEM}\}$ and the surrogate model $\{\tilde{f}_i^{FEM}\}$ at two of the tail samples $\{\theta_1, \theta_2\}$ varying the polynomial order. Order $p = 4$ seems to give an accurate solution for all the six proxy models with this selection of the input parameters. Similar plots can be obtained for different selection of the tail values. Polynomial order $p = 5$ was found to be the best selection for all the tested pairs of input parameters. Figure 5.23 shows the six surrogate models obtained with polynomial order $p = 5$ in the $\boldsymbol{\xi}$ space, one for each numerical eigenfrequency $\{\tilde{f}_i^{FEM}\}, i = 1, \cdots 6$, together with the corresponding $\{f_i^{EXP}\}$ estimated from data (horizontal surface), and the error absolute value, i.e. $|\tilde{f}_i^{FEM} - f_i^{EXP}|$(blue surface). As it was expected from the sensitivity analyses, the response surfaces show that the natural frequencies are almost constant varying the cables stiffness ξ_2; on the contrary the dependency of the natural frequencies is strongly non linear on the stiffness of the deck ξ_1.

As an example figures 5.24a and 5.24b show the response surfaces obtained for the maximum vertical and the maximum horizontal eigenvector components in the first and second numerical mode shape M_1^{FEM} and M_2^{FEM} respectively. The eigenvector components are significantly non linear on both random input parameters. The results of the dynamic identification procedure are not reported in the two plots since the experimental eigenvector components are characterized by an imaginary part that cannot be plotted.

5.9 Surrogate model based sensitivity analysis

In order to confirm the results obtained by means of the deterministic sensitivity analysis carried out in the preliminary phase of the updating framework a robust global sensitivity analysis based on Sobol' indices is performed. Probabilistic sensitivity analysis represents a crucial tool in the uncertainty analysis of systems allowing to understand how the uncertainty (that can be due to the different sources of uncertainty in the input parameters) affect the output response. Once the surrogate models are build, it is possible to estimate

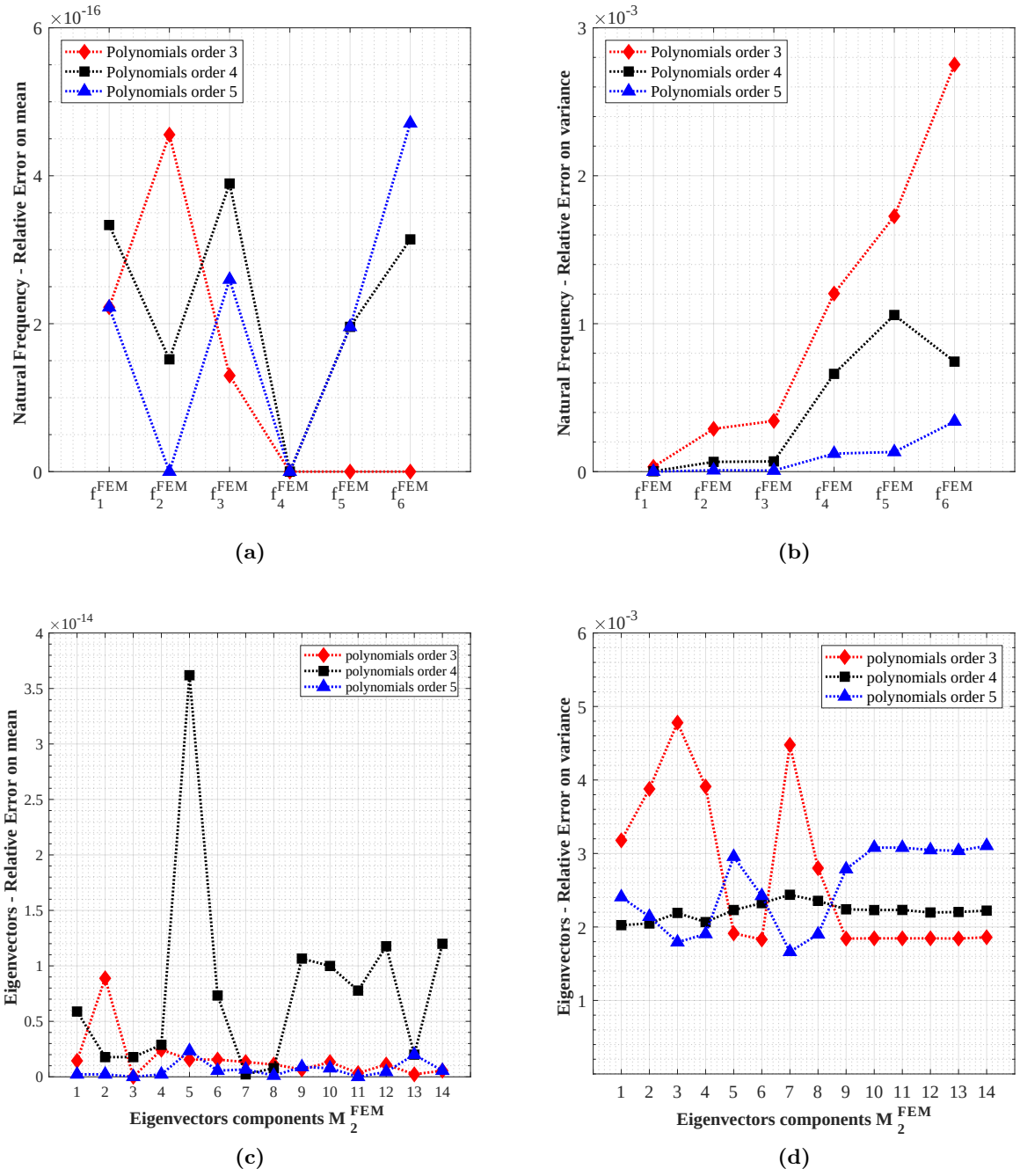

Fig. 5.21: Error in the mean and error in the variance for polynomials order 3, 4 and 5 for the first six natural frequency (a) and for the components of the second mode shape (b) .

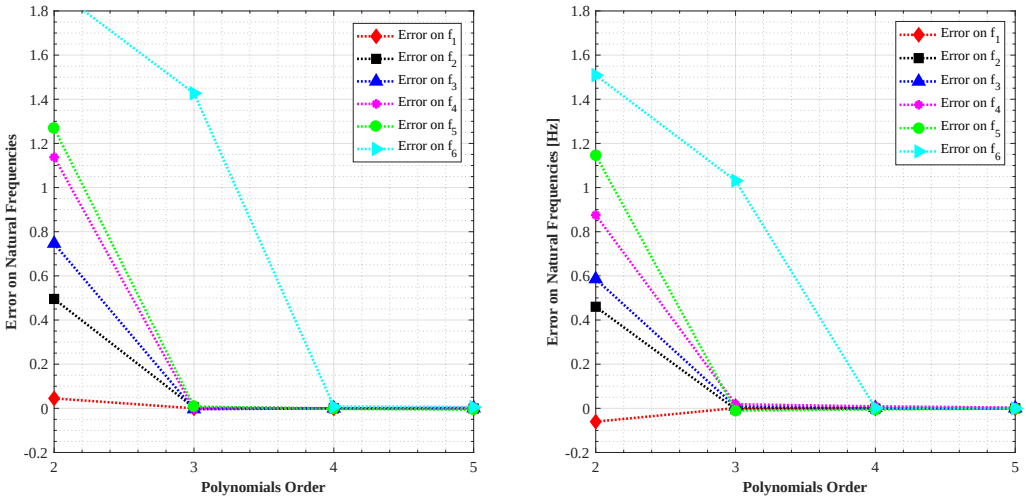

(a) **(b)**

Fig. 5.22: Difference between numerical and surrogate response for tail samples $\boldsymbol{\Theta}$.

the variance of the N_P polynomial coefficients $\hat{\boldsymbol{u}}_{\boldsymbol{\alpha}}$ for each QoI. These variances can be used to estimate for each of the 90 surrogate models the first and the second order Sobol indices in Eq. 3.53. The first order indices represent the influence of each parameter taken alone (Θ_1 and Θ_2); the higher order indices express the sensitivity measures of variance of the responses due to interaction between the input parameters (Θ_1, Θ_2).
Figure 5.25 shows that the natural frequencies are mainly influenced by the stiffness of the deck with Sobol' first order indices greater than 0.8. The combination of the stiffness of the deck and the stiffness of the cable does not play a crucial role in the analysis of the uncertainty related to the natural frequencies.

Same procedure is carried out for each eigenvector components of the 6 numerical mode shapes and results are shown in Figure 5.26. The eigenvector components are significantly influenced by the cables stiffness and by the combination of the cables and the deck stiffness. This is particularly true for the torsional and the mixed mode shapes $M_3^{FEM}, M_4^{FEM}, M_5^{FEM}$ in the range of frequency *1.7-2.4* Hz, confirming the results obtained with the preliminary deterministic sensitivity analysis.

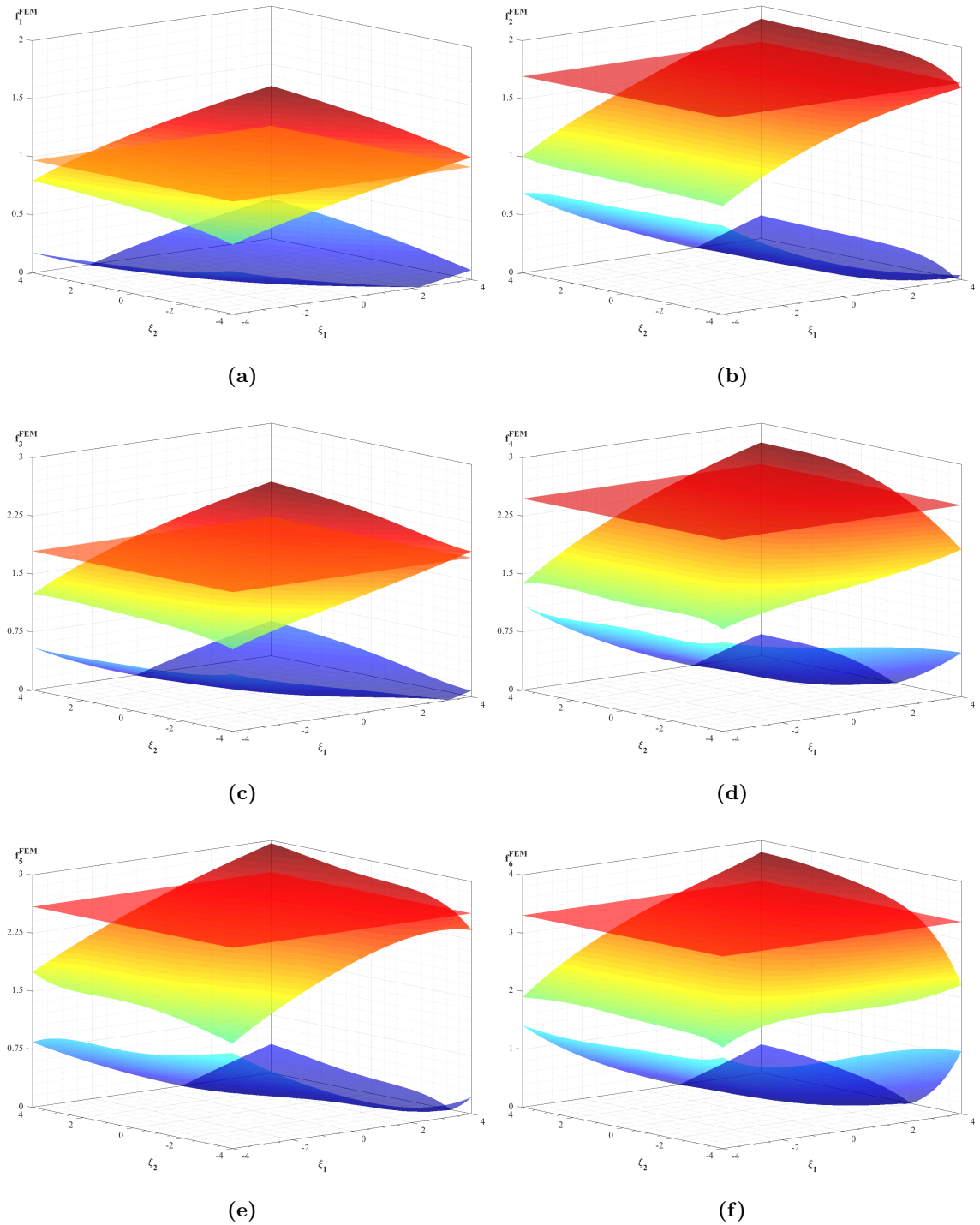

Fig. 5.23: Response surfaces for the first six natural frequencies as a function of the stiffness of the deck and the stiffness of the cables.

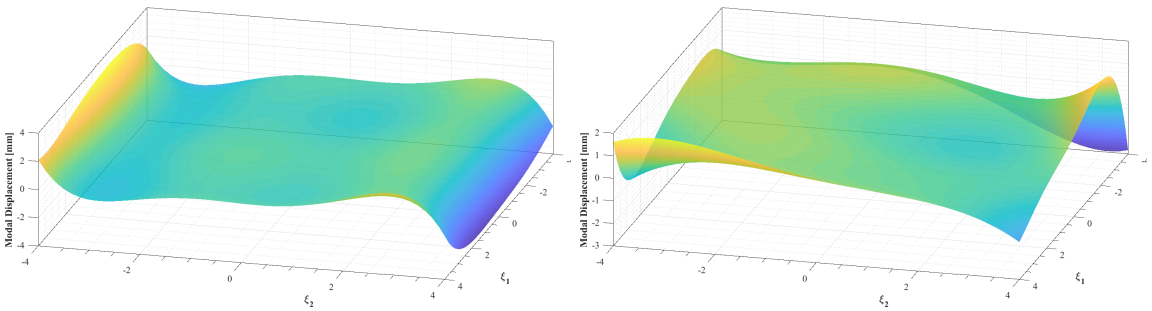

(a) **(b)**

Fig. 5.24: Response surfaces for the maximum vertical (a) and the maximum horizontal (b) eigenvector component.

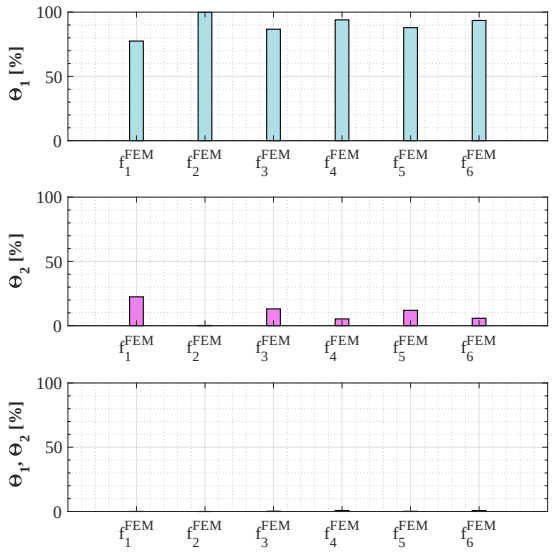

Fig. 5.25: First and second order Sobol' indices for natural frequencies.

5.10 Bayesian Inverse Problem

The MCMC-based Bayesian updating method has been adopted for the evaluation of the posterior marginal distributions of the two dimensional random vector $\boldsymbol{\Theta}$. The Metropolis Hastings algorithm is applied. The procedure is described in detail in Section 4.4.
The prior PDFs of the two independent updating parameters Θ_1 and Θ_2 are reported in Figures 5.19a and 5.19b and their joint probability distribution is plotted in Figure

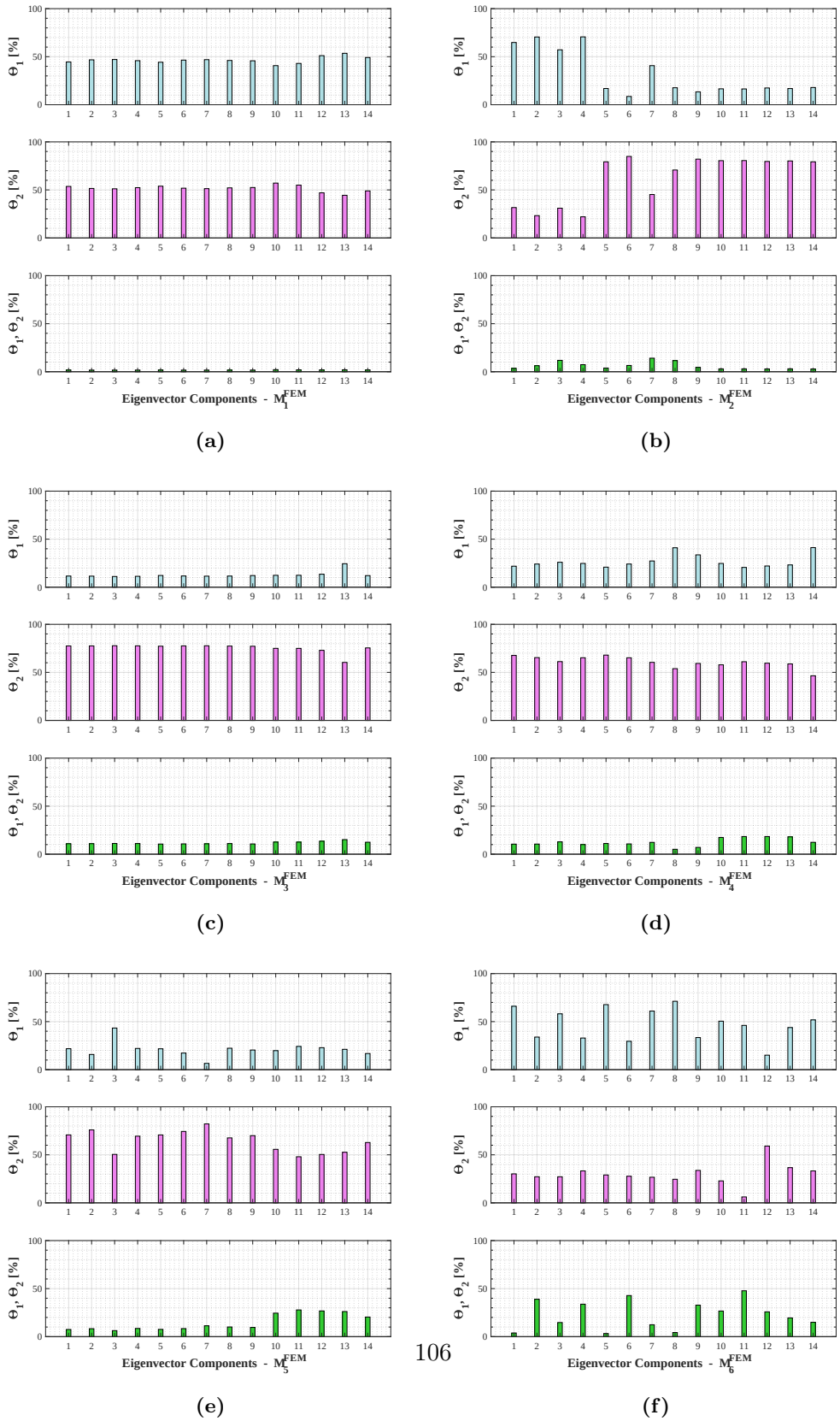

Fig. 5.26: First and second order Sobol' indices for eigenvector components of each mode shape.

5.27. The prior PDFs are then transformed into the posterior PDFs through the likelihood function accounting for both modeling and measurement uncertainties using Eqs. 4.24 and 4.27. Since just the results of one measurement campaign are available the initial uncertainties are represented by zero mean Gaussian distributions with diagonal covariance matrix.
Three cases of model updating are performed in the following which differ by the type of Data Set $\bar{\mathbf{D}}$ used as target:

- *Case 1* Two different modal data sets are considered each having a single system frequency, i.e. the first and the second experimental natural frequencies, in order to assess the effect of the experimental mode shape splitting phenomena already discussed in Section 5.4:
  1. *Case 1A*: $\bar{\mathbf{D}}_{1A} = \{f_1^{EXP}\}$
  2. *Case 1B*: $\bar{\mathbf{D}}_{1B} = \{f_2^{EXP}\}$
- *Case 2* The results obtained in Case 1 are used to select a single modal data set consisting in the first six natural frequencies identified from the measurements:
  $\bar{\mathbf{D}}_2 = \{f_i^{EXP}\} \qquad i = 2, ..., 7$
- *Case 3* The results obtained in Case 1 and Case 2 are used to select a single modal data set consisting in the first six natural frequencies and corresponding vibration modes identified from the measurements:
  $\bar{\mathbf{D}}_3 = \{f_i^{EXP}, M_i^{EXP}\} \qquad i = 2, ..., 7$

5.10.1 Case 1

In this case, the first experimental natural frequency is used in order to update the two main uncertain parameters. It was observed that Figure 5.8b shows two well defined peaks in the range of frequencies 0.97-1.15 Hz corresponding to two high correlated vertical bending vibration modes. In the same range of frequency the numerical analysis is able to catch just one single vertical bending mode shape. As just discussed, this mode shape splitting phenomena could be due to a significant load excitation or to the interaction between the cables and the deck. Since the Bayesian updating framework requires mode shapes and natural frequencies matching, one of the two experimentally identified natural frequencies needs to be properly selected. Indeed, the Bayesian updating framework is herein used to have information on the most representative experimental natural frequency to be used in

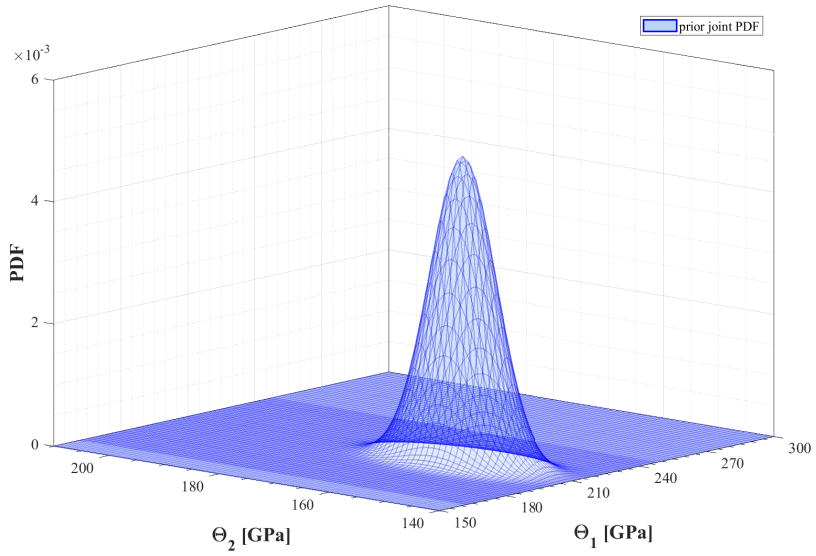

Fig. 5.27: Prior joint probability distribution of the random vector $\boldsymbol{\Theta}$.

the Case 2 and Case 3 modal updating.

Two different updating procedures are thus carried out using first the data set $\bar{\mathbf{D}}_{1A}$, consisting in the natural frequency $f_1^{EXP} = 0.964$ Hz (Case 1A), and then the data set $\bar{\mathbf{D}}_{1B}$, consisting in the second natural frequency $f_2^{EXP} = 1.107$ Hz (Case 1B). The obtained posterior marginal distributions are plotted in Figures 5.28a and 5.28b. The black lines indicate the prior PDFs, while the blue and the green lines indicate the posterior marginal PDFs obtained in Case 1A and Case 1B, respectively.

The Θ_1 posterior distribution has mean values equal to 191 and 270 GPa, about 0.90 and 1.25 times the mean value of the prior PDF, when data sets $\bar{\mathbf{D}}_{1A}$ and $\bar{\mathbf{D}}_{1B}$ are used as target, respectively. Table 5.5 reports the 25th, 50th and 75th percentiles of the prior and posterior distributions.

The Θ_2 posterior marginal distribution is very similar to the prior PDF in both cases. This result was expected since the sensitivity analyses showed that the first natural frequency is mainly influenced by Θ_1.

The posterior mean values of the random vector $\boldsymbol{\Theta}$ are used as the input of the surrogate models in order to compare the accuracy of the obtained results in terms of natural frequencies and MAC values. Figure 5.29a compares the natural frequencies estimated from the experimental data to those obtained with the initial numerical model and the updated

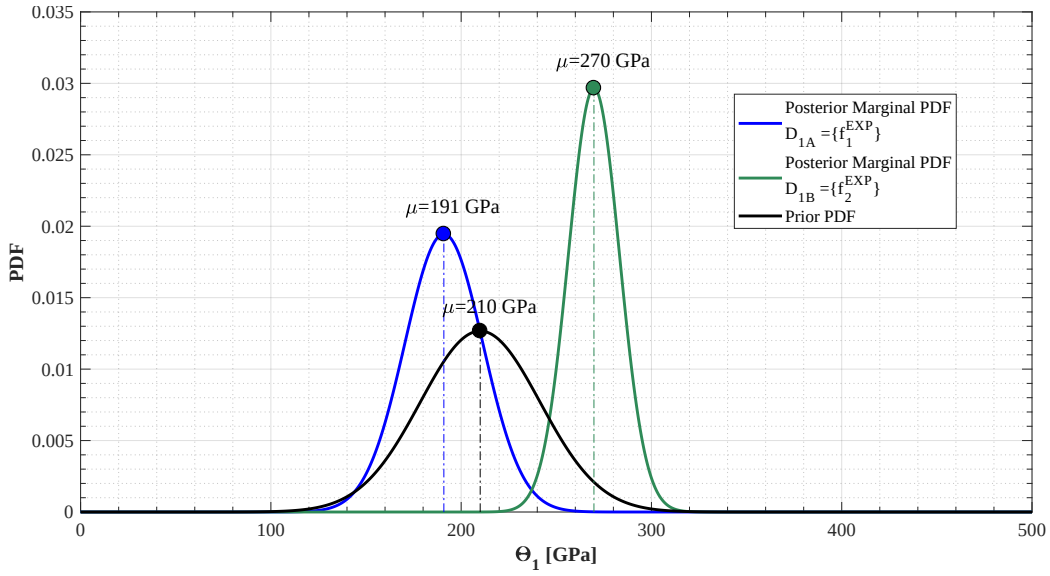

(a)

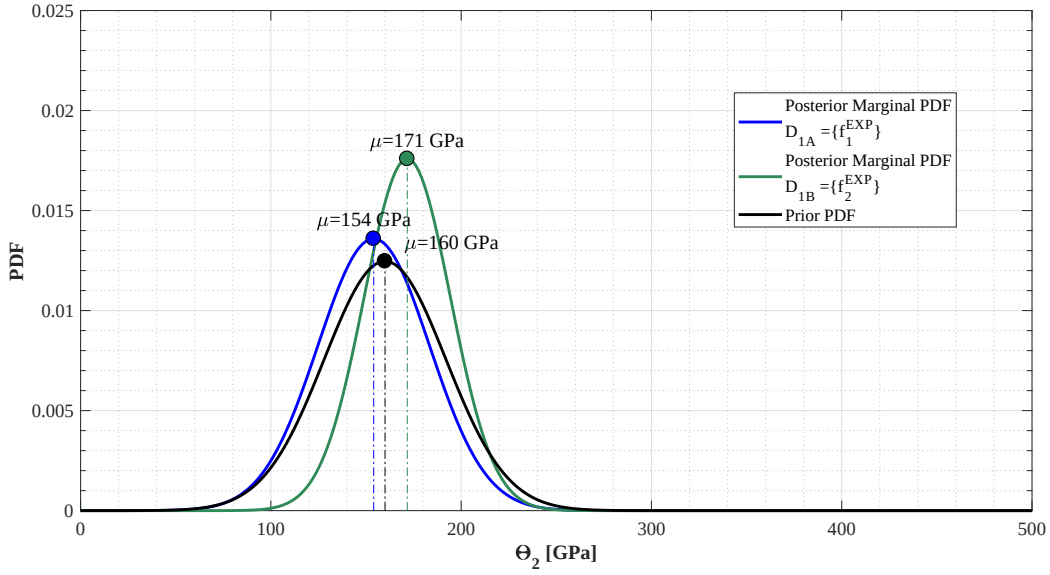

(b)

Fig. 5.28: Marginal posteriorPDFs of the stiffness of the deck (a) and the stiffness of the cables (b) considering two different Data Sets $\bar{\mathbf{D}}_{1A}$ and $\bar{\mathbf{D}}_{1B}$ consisting in the first two experimentally identified natural frequencies taken alone.

model using the posterior mean values of $\boldsymbol{\Theta}$ in Case 1A and 1B. It is rather clear that unsatisfactory results are obtained with the Bayesian updating procedure in Case 1A. The obtained numerical natural frequencies are very similar to those of the initial FEM. The

Table 5.5: Percentiles of the posterior distribution (GPa) of the stiffness of the deck related to the considered Data Set.

Percentiles	Prior	Case 1A	Case 1B
25th	189	177	261
50th	210	191	270
75th	231	270	279

relative error mean is equal to 13 % with the maximum relative error occurring for the mode shapes with higher frequencies. On the contrary, accurate results are obtained in Case 1B. The relative error mean is about 1.5 % with the maximum relative error occurring for the 3rd mode shape. Figure 5.29b compares the diagonal MAC values (numerical vs experimental mode shapes) before and after the two Bayesian updating procedures when using $\bar{\mathbf{D}}_{1A}$ and $\bar{\mathbf{D}}_{1B}$ reference data sets. It is worth noting that the diagonal MAC values obtained after the updating are all lower, with the exception of the 1st, 3rd and 6th modes, than those obtained with the initial FE in both cases.

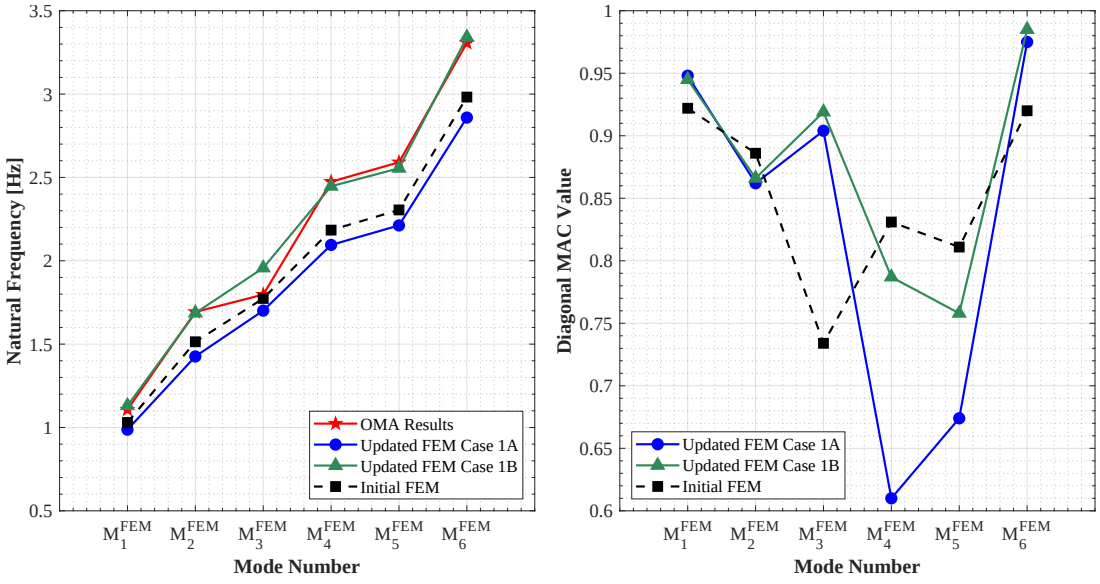

Fig. 5.29: Comparison between the natural frequencies (a) and the diagonal MAC values (b) obtained from the initial FEM and the updated FEM related to the considered Data Sets $\bar{\mathbf{D}}_{1A}$ and $\bar{\mathbf{D}}_{1B}$.

5.10.2 Case 2

The data set $\bar{\mathbf{D}}_\mathbf{2}$ used in this case consists in the first six natural frequencies estimated from the measurements. Since natural frequency and mode shape matching is required by the algorithm, the choice of using one of the two natural frequencies f_1^{EXP} and f_2^{EXP} as first natural frequency of the data set used as reference for the updating needs to be properly investigated. The results obtained in Case 1 clearly indicate that the second experimental natural frequency can be considered the best choice for a reference data set. Therefore, in the following, the results obtained using a data set $\bar{\mathbf{D}}_\mathbf{2} = \{f_2^{EXP}, f_3^{EXP}, f_4^{EXP}, f_5^{EXP}, f_6^{EXP}, f_7^{EXP}\}^T$ are shown.

It is important to point out that the updating framework is improved using the MAC coefficients as constraints in order to guarantee the natural frequency/mode shape matching at each step of the MCMC procedure. Variation in the deck and cables stiffness can cause an exchange of natural frequencies and mode shapes. Each component of the residual vector in the likelihood function is computed as the difference between the experimental natural frequency and the numerical natural frequency corresponding to the same mode shape (i.e. having the highest MAC coefficient).

The posterior marginal PDF of the two dimensional random vector $\boldsymbol{\Theta} = \{\Theta_1, \Theta_2\}$ is herein computed accounting for the correlation of the total model error at each step of evaluation according to Algorithm 3. In particular, the MCMC MH algorithm is used in order to obtain the target posterior PDFs replacing the evaluation of the numerical solution at each step of the chain with the surrogate solution sampling directly from the $\boldsymbol{\xi}$ space. The initial covariance matrix of the total error is assumed to be diagonal with component equal to 0.01 Hz^2 and the model error matrix components are treated ad additive updating parameters with non informative prior distributions according to Eq. 4.24 .

The improved MCMC MH algorithm is applied generating 40,000 posterior samples that are consistent with the unscaled posterior PDF that is proportional to the product between the likelihood function and the prior PDF. In this simulation the initial state enables Markov chains to start around high probability region of the prior PDF. These posterior 40,000 samples are the accepted ones, according to the fixed acceptance rate. In this case, the whole algorithm requires the evaluation of the deterministic solution 150,000 times in order to ensure the convergency. Since the numerical model takes between 1 and 2 minutes for a single analysis the updating framework would have required more than 5 months making the procedure unfeasible. The use of the surrogate models for such complex cases makes the solution possible reducing the computing time to about 60 minutes.

Figure 5.30a shows pairs of the accepted posterior samples. No significant linear or non lin-

ear relationships between the updated parameters are evident meaning that no apparently correlation between the chains is present. Moving means of the samples are calculated to verify the convergence of the Markov chain stationarity. The moving means associated to the deck stiffness and the cables stiffness are shown in Figure 5.30b . The y axes correspond to the two updating random parameters in a logarithmic scale. The convergency is reached after 150,000 steps with a burn-in period of 40,000 steps. The autocorrelation of both of the chains is investigated too, showing a rapid decrease from 1 to 0 after the burn-in period.

The results of the updating procedure are shown in Figures 5.31a and 5.31b. The poste-

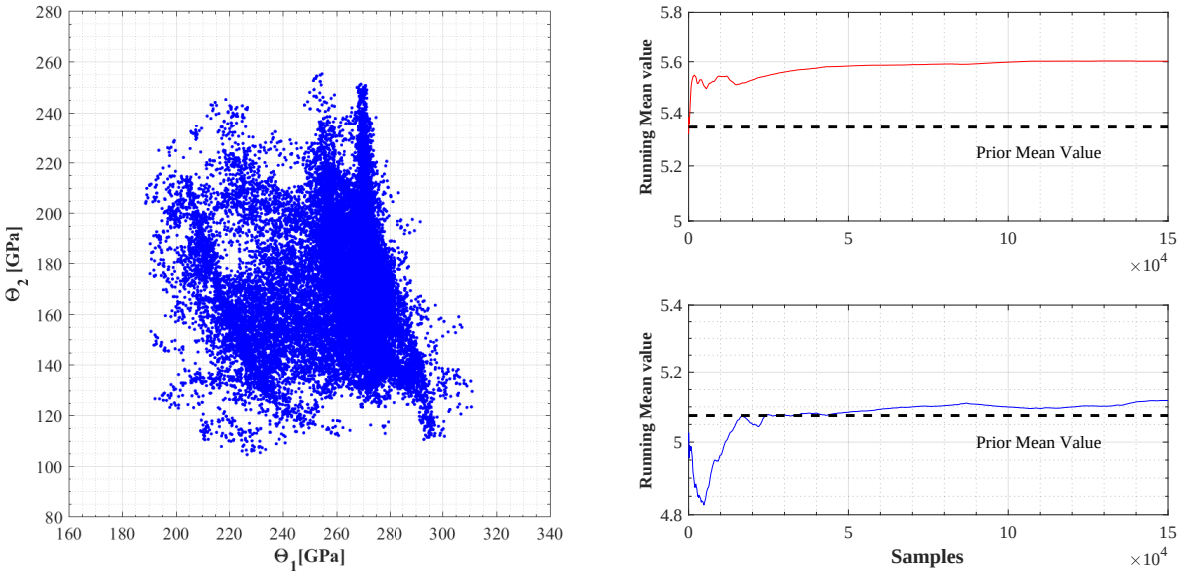

(a) **(b)**

Fig. 5.30: Sample points of the posterior target PDF as obtained from MCMC MH (a). Convergence to stationarity (b): moving averages of the stiffness of the deck (upper panel) and the stiffness of the cables (lower panel) related to the considered Data Set $\bar{\mathbf{D}}_\mathbf{2}$.

rior distribution of Θ_1 has a mean value equal to 266 GPa, 1.25 times the mean value of the prior PDF. In terms of percentile results show a significant reduction of the variability with values very similar to those reported in Table 5.5 for the Case 1B.

The posterior distribution of Θ_2 is very similar to the prior PDF indicating that the data set $\bar{\mathbf{D}}_\mathbf{2}$ is non informative with respect to this random parameter. This result was expected since the natural frequencies are mainly influenced by the deck stiffness as shown by the

first order Sobol indices in previous section.

The posterior samples generated with the MCMC MH are also used for studying how

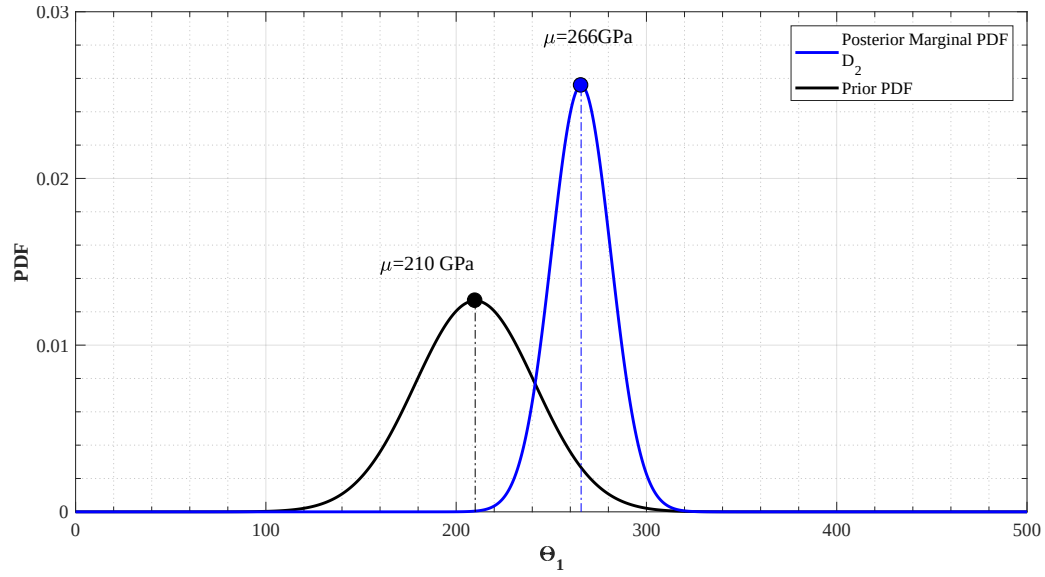

(a)

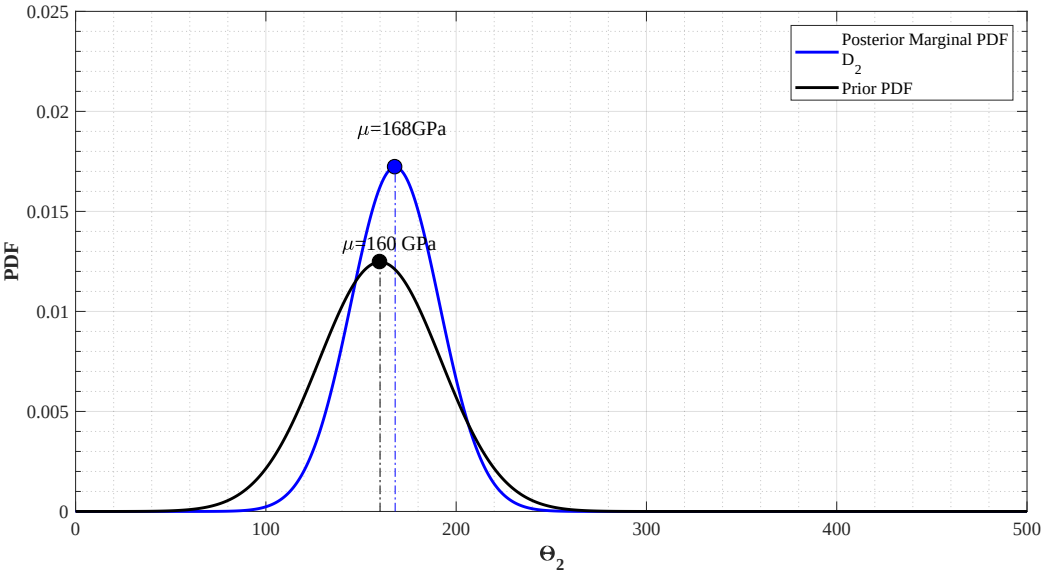

(b)

Fig. 5.31: Marginal posterior PDFs of the stiffness of the deck (a) and the stiffness of the cables (b) considering a Data Set consisting in the first six experimentally identified natural frequencies $\bar{\mathbf{D}}_2$.

the uncertainties of the updated parameters are propagated into the uncertainties of the

natural frequencies. The surrogate model allows to solve the forward problem related to the estimation of the first six natural frequencies given each pair of posterior accepted samples. Figure 5.32 shows the posterior histograms of the natural frequencies and the corresponding marginal PDFs obtained by the kernel density estimation. Also prior histograms obtained by means of Monte Carlo simulation starting from the prior PDFs of the random vector $\boldsymbol{\Theta}$, the initial FEM and the measured eigenfrequencies are included in the figure. It can be seen that due to the incorporation of the information contained in the modal Data Set $\bar{\mathbf{D}}_{\mathbf{2}}$, the prior distributions are shifted towards the measured value leading to a considerably better matching, with the exception of the third mode shape M_3^{FEM}. Moreover c.o.v. of each posterior marginal probability density is calculated and values between 0.012 and 0.015 are observed. This means that each natural frequency is sensitive to the perturbation of the updating parameters in a same way.
Also the effects of the model uncertainties on the agreement of the eigenvectors is investigated and Figure 5.33 shows the posterior histograms and the corresponding marginal PDFs of the diagonal MAC values used in order to measure the correlation between the numerical and the experimental modal vectors obtained from the posterior samples. The prior histograms and the initial FEM result are included in the Figure. A shift of the posterior marginal PDFs towards the perfect correlation can be observed, as well as a strongly non Gaussian behavior. Just the results related to the numerical mode shape M_3^{FEM}, M_4^{FEM} and M_5^{FEM} are shown since the other reference mode shapes are not characterized by a significant uncertainties reduction meaning that they are not sensitive to the perturbation of the considered updating parameters.

Finally, Tables 5.6 and 5.7 compares the natural frequencies and the mode shapes obtained from the measurement to those obtained from the initial FEM and the updated numerical model using the deck and cables stiffness posterior mean values as input parameters of the surrogate models. The second column of the table shows the value of the natural frequencies identified experimentally; the third and the fifth columns report the natural frequencies obtained from the initial FEM and the updated one. The other two columns gather the relative errors. Before the updating the differences between the experimental and the numerical natural frequencies were greater than 7% with the only exception of the 3rd numerical mode shape for which the percentage error was lower than 1%. After the updating these errors are reduced to 1%, with the exception of the 3rd mode shape for which the percentage error is equal to 8%.
The comparison between the experimental and numerical mode shapes before and after the updating is carried out also in terms of diagonal MAC values. The initial numerical

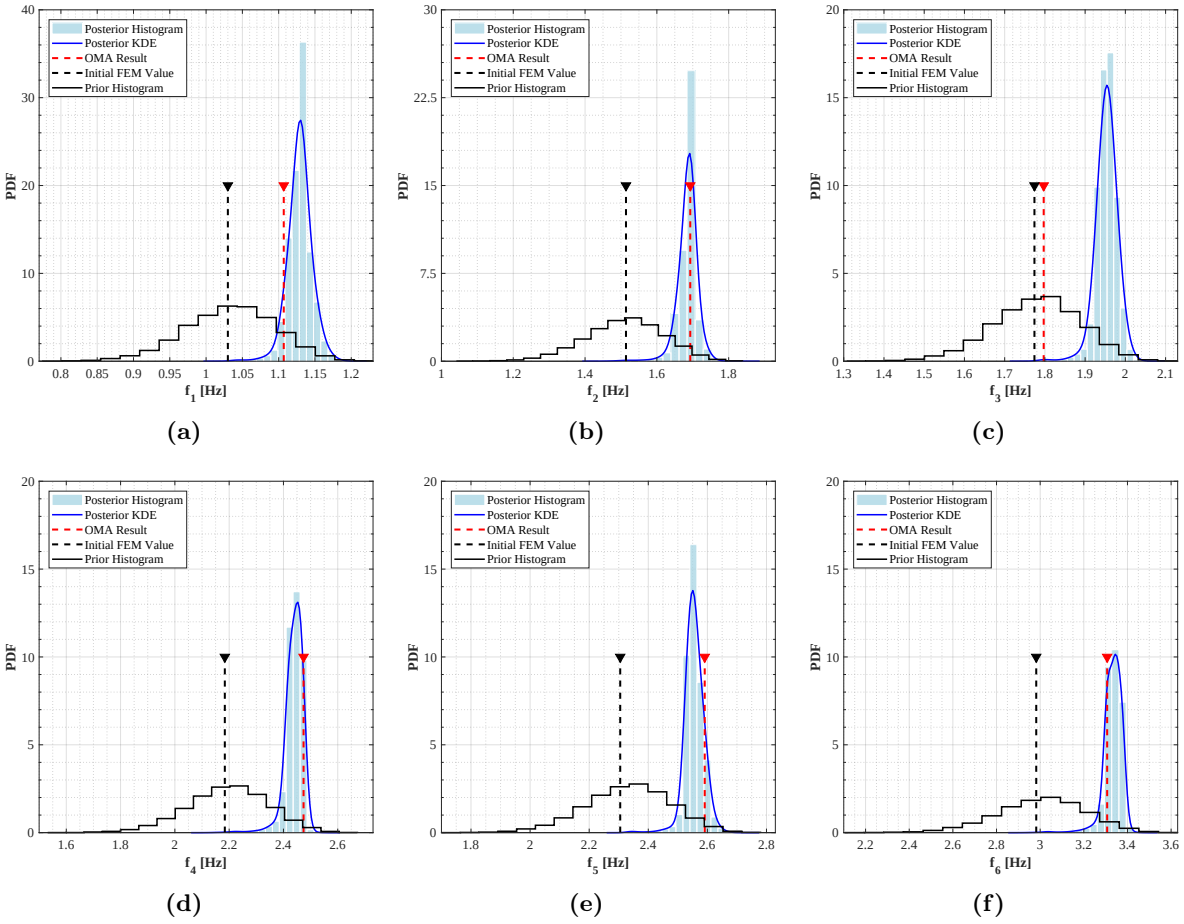

Fig. 5.32: Variation of the natural frequencies of the FEM: histograms and PDFs estimated by Kernel Density Function related to the considered Data Set $\bar{\mathbf{D}}_\mathbf{2}$.

mode shapes and the experimental ones are characterized by high values of the MAC number (i.e. correlated vectors). After the update, the most significant increase of the MAC values, from 73% to 92%, occurs for the 3rd mode shape (torsional), . On the contrary, the diagonal MAC value decrease for the 2nd, the 4th and the 5th mode shapes.

5.10.3 Case 3

In this case a data set $\bar{\mathbf{D}}_\mathbf{3}$ consisting in the first six natural frequencies of the *Case 2* and the corresponding first six vibration modes is considered: $\bar{\mathbf{D}}_\mathbf{3} = \{f_2, ..., f_7^{EXP}, M_2^{EXP}, ..., M_7^{EXP}\}^T$. The Bayesian updating framework is implemented using the theoretical meaning of the

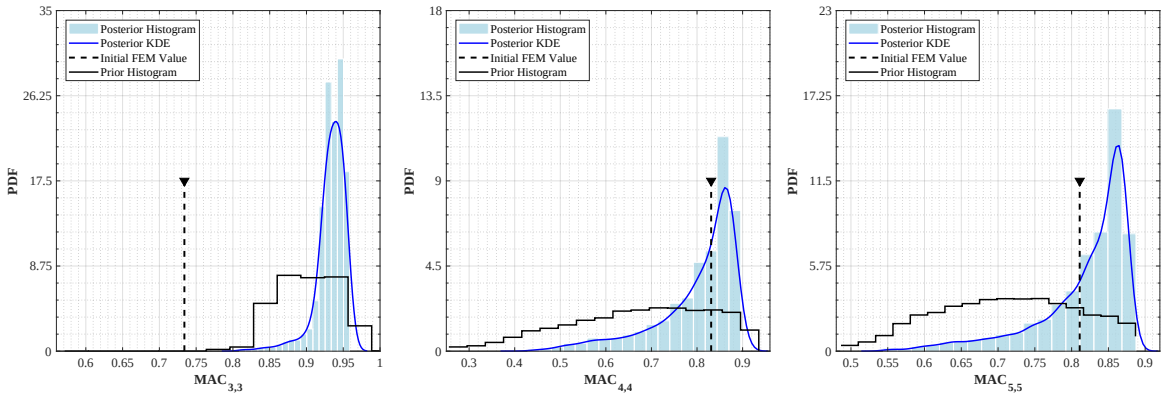

(a) **(b)** **(c)**

Fig. 5.33: Variation of the diagonal MAC coefficients: histograms and PDFs estimated by Kernel Density Function related to the considered Data Set $\bar{\mathbf{D}}_{\mathbf{2}}$.

Table 5.6: Natural frequency values of the FEM before and after Bayesian updating related to the considered Data Set $\bar{\mathbf{D}}_{\mathbf{2}}$.

		Natural	Frequencies[Hz]		
FEM Mode	Experimental	Initial FE	Relative Error	Updated FEM	Relative Error
1	1.107	1.030	0.070	1.129	0.019
2	1.693	1.514	0.106	1.685	0.004
3	1.797	1.774	0.011	1.954	0.087
4	2.474	2.184	0.117	2.445	0.011
5	2.591	2.305	0.110	2.552	0.015
6	3.307	2.982	0.098	3.338	0.009

Table 5.7: Diagonal MAC values of the FEM before and after Bayesian updating related to the considered Data Set $\bar{\mathbf{D}}_{\mathbf{2}}$.

	MAC	Values
FEM Mode	Initial FEM	Updated FEM
1	0.922	0.945
2	0.886	0.865
3	0.734	0.917
4	0.831	0.785
5	0.811	0.778
6	0.920	0.998

MAC matrix. A value of the MAC equal to 1 means perfect correlation between the analytical mode shapes and the experimental ones. Therefore the residual vector at each step of the Markov chains in Eq. 4.26 is estimated as the difference between the measured and the model predicted natural frequencies and the difference between 1 and the effective MAC coefficients. This kind of formulation allows to overcome the problem related to the complex part of the experimental eigenvector being appropriate to complex modes and to all those situations with few measurements.

The posterior marginal PDF of the random vector $\boldsymbol{\Theta} = \{\Theta_1, \Theta_2\}$ is computed using the same approach of Case 2, i.e. treating all the elements of the total error covariance matrix $\boldsymbol{\Sigma}$ in Eq. 4.24 as additive parameters. The initial PDFs of the total error is set equal to $\sigma_f = 0.01$ Hz^2 for the natural frequencies and to $\sigma_{MAC} = 0.01$ for the MAC value related to each mode shape.

The MCMC MH algorithm is applied in order to obtain the target posterior PDFs. The algorithm generates 44,000 posterior samples that are consistent with the unscaled posterior PDF that is proportional to the product between the likelihood function and the prior PDF. The whole algorithm requires the evaluation of the deterministic solution over 150,000 times in order to ensure the convergency.

Figure 5.34a shows pairs of the accepted posterior samples. No significant linear or non linear relationships between the updated parameters are evident indicating that no apparently correlation between chain is present. Figure 5.34b shows the moving mean associated to the stiffness of the deck and the stiffness of the cables in a semilogarithmic scale. The convergency is reached after 150,000 steps with a burn-in period of 30,000 steps. The autocorrelation of both of the chains is investigated showing a rapid decrease from 1 to 0 after the burn-in period.

The results of the Bayesian updating are shown in Figures 5.35a and 5.35b and Table 5.8 shows the comparison in terms of percentiles highlighting a significant reduction in the uncertainties related to both the updated parameters.

The Θ_1 posterior distribution has a mean value equal to 273 GPa, about 1.30 times the

Table 5.8: Percentiles of the posterior distribution (GPa) of the stiffness of the deck and the stiffness of the cables related to the considered Data Set $\bar{\mathbf{D}}_\mathbf{3}$.

Percentiles	Prior	Stiffness of the deck [GPa]	Prior	Stiffness of the cables [GPa]
25th	189	268	138	175
50th	210	273	160	184
75th	231	277	181	193

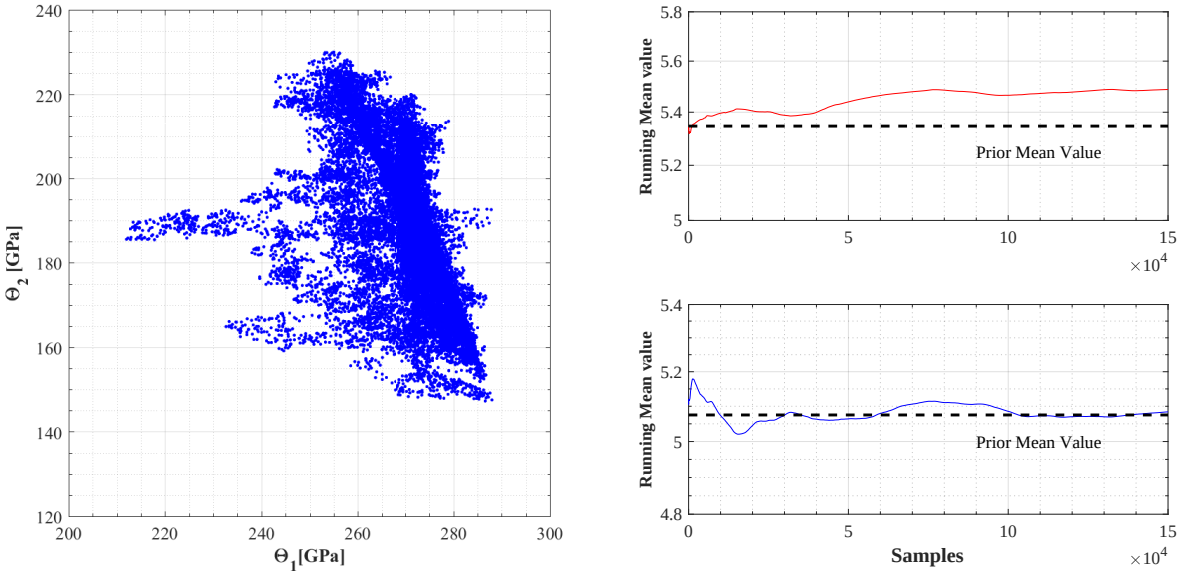

(a) **(b)**

Fig. 5.34: Sample points of the posterior target PDF as obtained from MCMC MH (a). Convergence to stationarity (b): moving averages of the stiffness of the deck (upper panel) and the stiffness of the cables (lower panel) related to the considered Data Set $\bar{\mathbf{D}}_3$.

prior mean value.

The $\Theta_2$posterior distribution is characterized by a very well evident maximum point at the posterior mean. Compared to the prior uncertainties, the posterior uncertainties related to this parameter are reduced because, in this case, the data set $\bar{\mathbf{D}}_3$ is informative with respect to the cables stiffness Θ_2. These result was expected since the eigenvectors are mainly influenced by the cables stiffness Θ_2 as shown from the results of the global sensitivity analysis. The posterior sample generated with MCMC are also used to study how the uncertainties of the updated parameters are propagated into the uncertainties of the modal parameters.

The forward problem is solved for each pair of posterior sampling by means of the surrogate models. Figure 5.36 shows the posterior histograms of the natural frequencies and the corresponding posterior marginal PDFs obtained by the kernel density estimation. Also the prior histograms, the initial FE model and the measured eigenfrequencies are included in the same figure. It can be observed that due to the information included in the modal data set $\bar{\mathbf{D}}_3$, the natural frequency posterior PDFs are characterized by a well defined

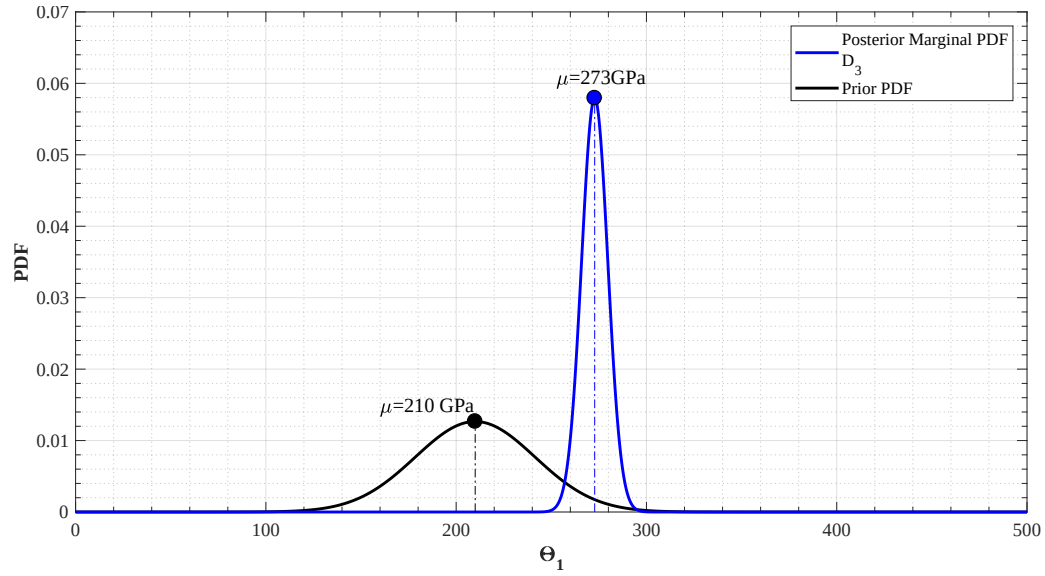

(a)

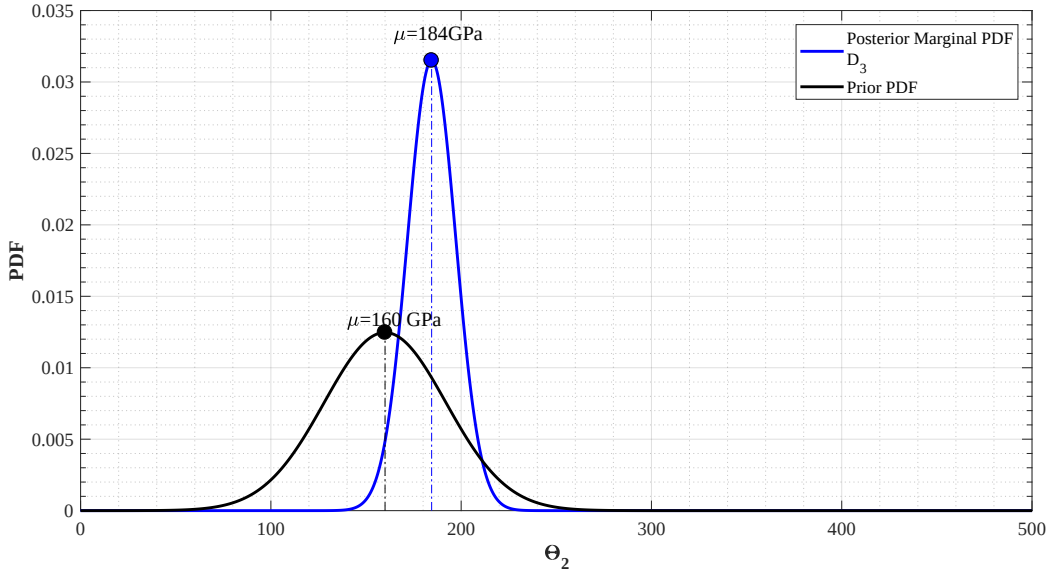

(b)

Fig. 5.35: Marginal posterior PDFs of the stiffness of the deck (a) and the stiffness of the cables (b) considering a Data Set consisting in the first six experimentally identified natural frequencies and the first six vibration modes $\bar{\mathbf{D}}_{\mathbf{3}}$.

maximum at the value of the measured natural frequency with the exception of the 1st and the 3rd mode shape. C.o.v. of each estimated posterior PDF is calculated and values in a range 0.006 - 0.009 are observed, highlighting a significant uncertainty reduction

with respect to both: the prior PDFs and the the posterior marginal PDFs in Case 2. Also the effects of the model uncertainty related to the correlation of the numerical and experimental modal vectors is investigated. Figure 5.37 shows the posterior histograms, the corresponding PDFs and the prior histograms of the diagonal MAC values. A global shift of the posterior PDFs towards the perfect correlation is observed. Just the results related to M_3^{FEM}, M_4^{FEM} and M_5^{FEM} mode shape are shown since the other reference mode shapes are not characterized by a significant uncertainty reduction.

The discrepancies between the experimental and the model predicted natural frequencies

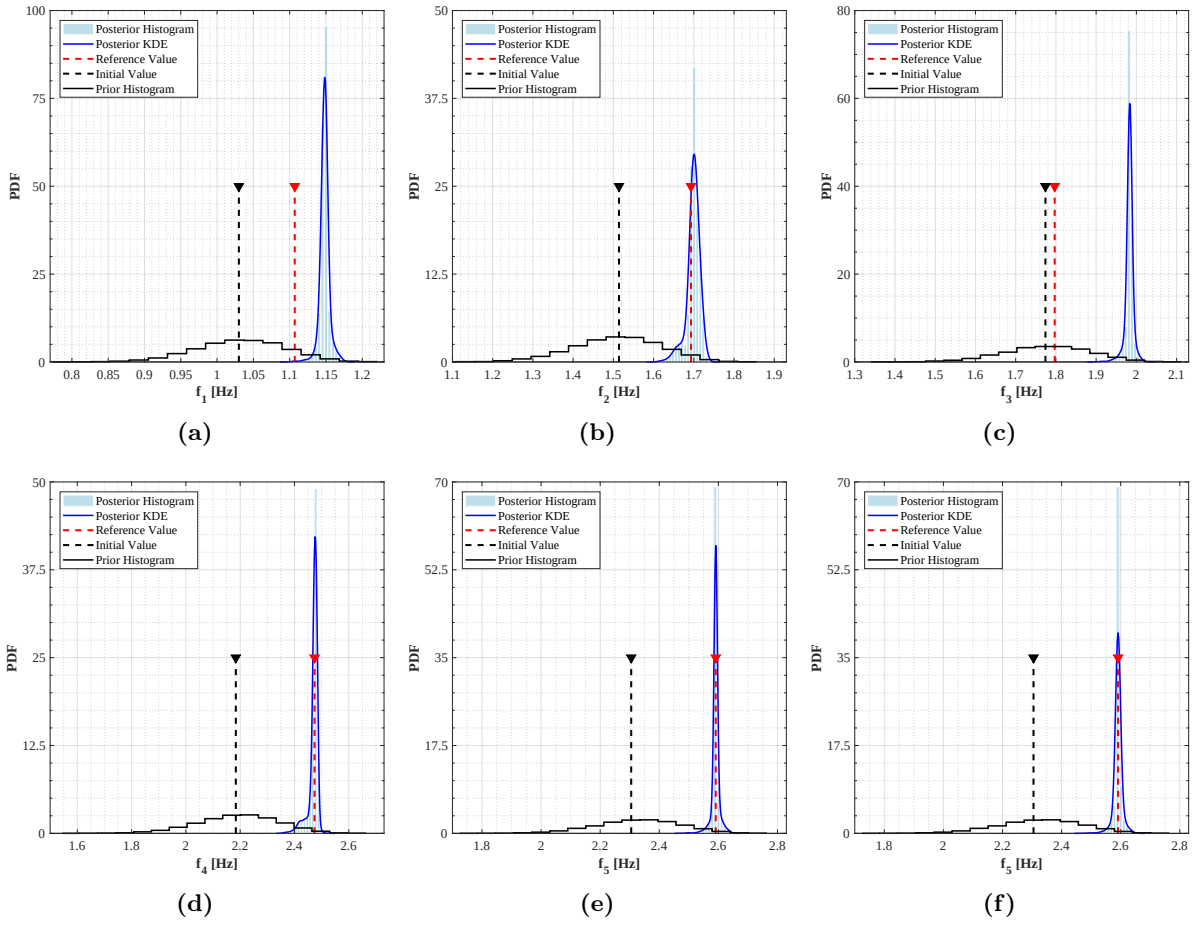

Fig. 5.36: Variation of the natural frequencies of the FEM: histograms and PDFs estimated by Kernel Density Function related to the considered Data Set $\bar{\mathbf{D}}_3$.

(in terms of relative errors) before and after model updating are summarized in Table 5.9. The natural frequencies of the updated numerical model are obtained using the posterior

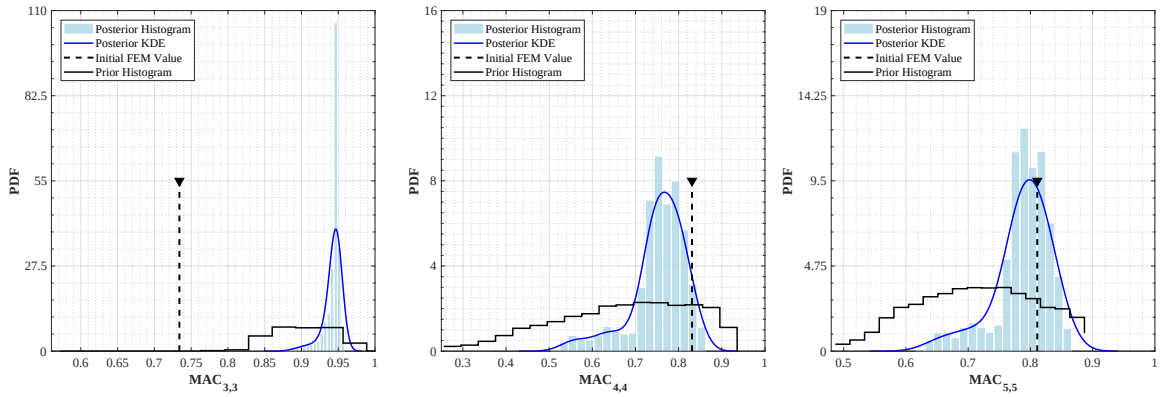

Fig. 5.37: Variation of the diagonal MAC coefficients: histograms and PDFs estimated by Kernel Density Function related to the considered Data Set $\bar{\mathbf{D}}_3$.

mean value of the stiffness of the deck and the stiffness of the cables as input parameters for the surrogate models. It is evident that the initial relative errors are reduced after the updating process with the exception of the 3rd torsional mode shape, for which the percentage error increases of about 8.7%. The calculated discrepancies between the experimental and model predicted mode shapes in terms of diagonal MAC before and after model updating procedure are also summarized in Table 5.10. It can be observed that the initial MAC values were greater than 0.8 also before the model updating. However, model updating fulfills a significant improvement in the diagonal MAC values especially for the 3rd mode shape (from 73% to 93%).

A final comparison between the results of Case 2 and Case 3 is carried out in order to

Table 5.9: Natural frequency values of the FEM before and after Bayesian updating related to the considered Data Set $\bar{\mathbf{D}}_3$.

		Natural	Frequencies[Hz]		
FEM Mode	Experimental	Initial FEM	Relative Error	Updated FEM	Relative Error
1	1.107	1.030	0.070	1.143	0.032
2	1.693	1.514	0.106	1.690	0.002
3	1.797	1.774	0.011	1.974	0.098
4	2.474	2.184	0.117	2.460	0.006
5	2.591	2.305	0.110	2.576	0.006
6	3.307	2.982	0.098	3.366	0.018

Table 5.10: Diagonal MAC values of the FEM before and after Bayesian updating related to the considered Data Set $\bar{\mathbf{D}}_3$.

	MAC Values	
FEM Mode	Initial FEM	Updated FEM
1	0.922	0.943
2	0.886	0.871
3	0.734	0.928
4	0.831	0.853
5	0.811	0.833
6	0.920	0.958

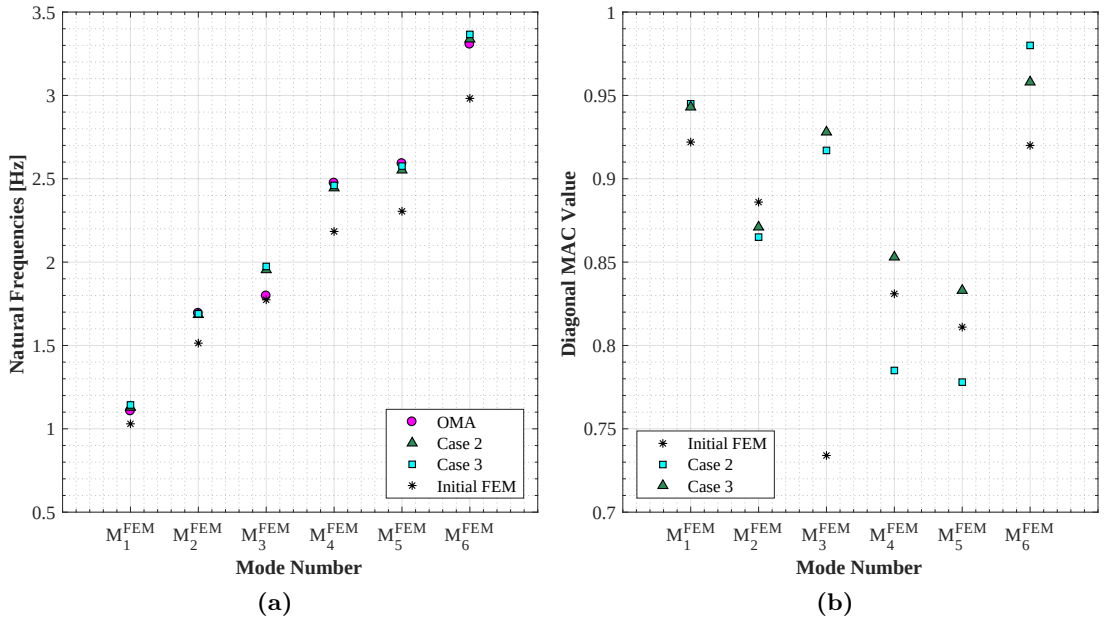

Fig. 5.38: Natural frequencies (a) and MAC values (b) obtained from the updated numerical model related to the considered Data Sets.

assess the importance of choosing a proper informative data set $\bar{\mathbf{D}}$ in the Bayesian updating procedure.

Figure 5.38a compares the natural frequencies obtained from the measurements to those obtained with the initial FEM and the updated numerical model using the posterior mean value of $\boldsymbol{\Theta}$ in Case 2 and Case 3 as input parameters. The natural frequencies obtained at the end of the updating procedure are very similar to the measured ones with relative errors lower than 3 %, with the exception of the 3rd mode shape. Figure 5.38b compares

the diagonal MAC values (numerical vs experimental mode shapes) before and after the two Bayesian updating procedures when using $\bar{\mathbf{D}}_{\mathbf{2}}$ and $\bar{\mathbf{D}}_{\mathbf{3}}$ reference data sets. It is worth noting that the diagonal MAC values are all higher, with the exception of the 2nd mode, than those obtained with the initial FE model after the updating in both cases. Moreover, the diagonal MAC values obtained in Case 3 are all higher, with the exception of the 1st and the 6th modes, than those obtained in Case 2. The most significant diagonal MAC improvement occur for the 3rd mode shape, in both, Case 2 and Case 3.

The importance of using a proper data set is also highlighted from by the 95 % centered

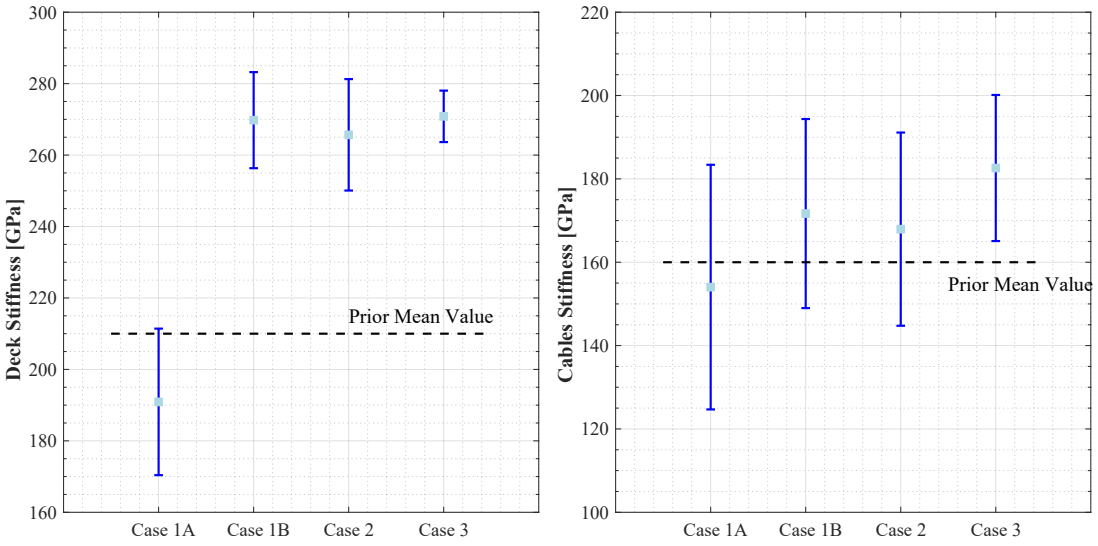

(a) **(b)**

Fig. 5.39: 95 % confidence intervals for the updated parameters related to the considered Data Set.

confidence intervals estimated for the two updated parameters and plotted in Figure 5.39 for the Case 1A, Case 1B and Case 2 and Case 3.

After the updating procedure, a global reduction in the uncertainties associated to the deck stiffness Θ_1 is observed. Instead, the uncertainties related to the cables stiffness Θ_2 are significant when $\bar{\mathbf{D}}_{1A}$, $\bar{\mathbf{D}}_{2A}$ and $\bar{\mathbf{D}}_{\mathbf{2}}$ are used as reference, decreasing when the updating is carried out using $\bar{\mathbf{D}}_{\mathbf{3}}$ as target. Moreover, using the data set $\bar{\mathbf{D}}_{\mathbf{1A}}$ the Θ_1 posterior mean value is very different from the posterior mean value obtained at the end of the other updating cases.

The uncertainty propagation problem allows to define and analyze also the uncertainty

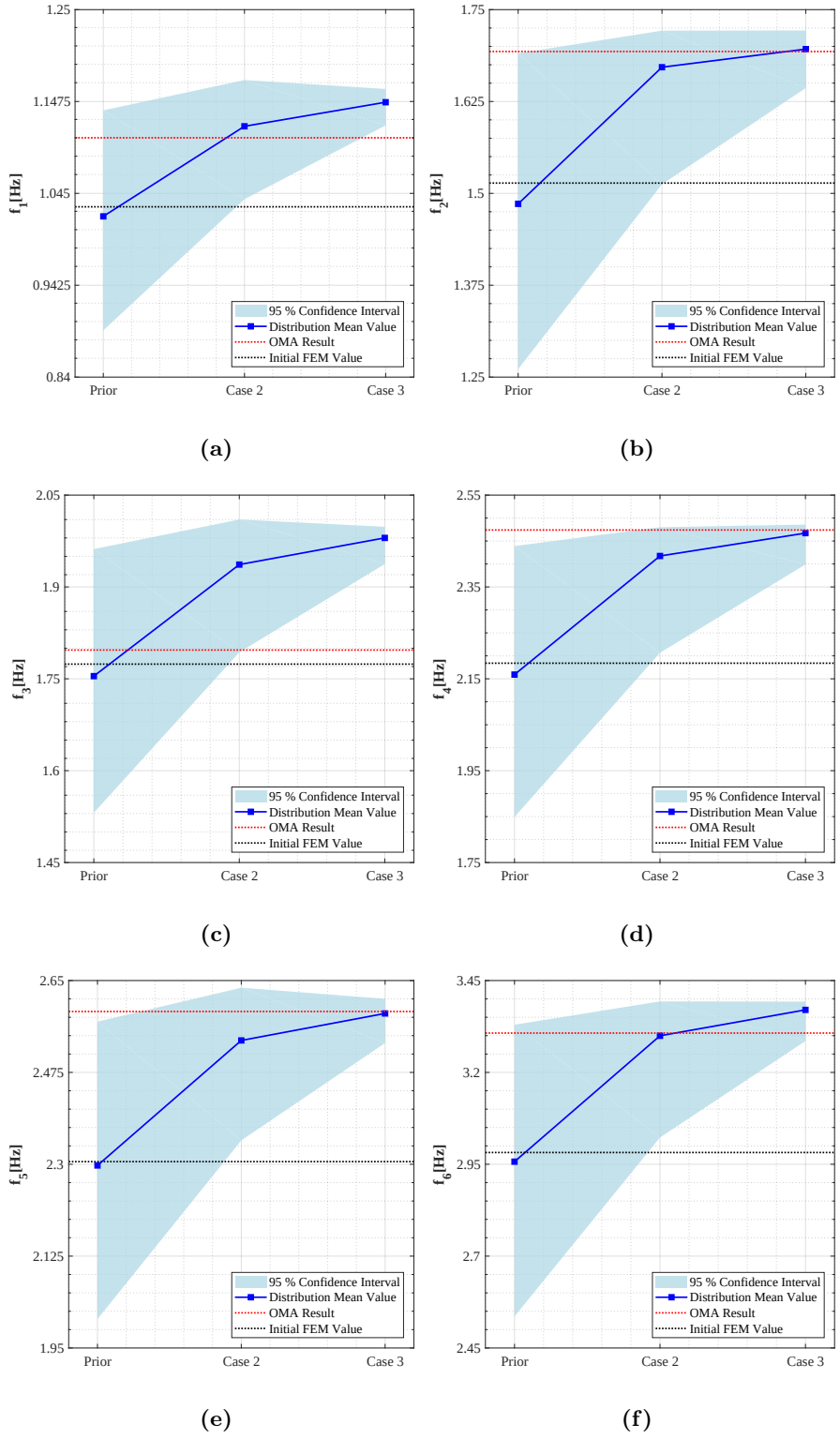

Fig. 5.40: 95 % confidence intervals for the natural frequencies related to the considered Data Set.

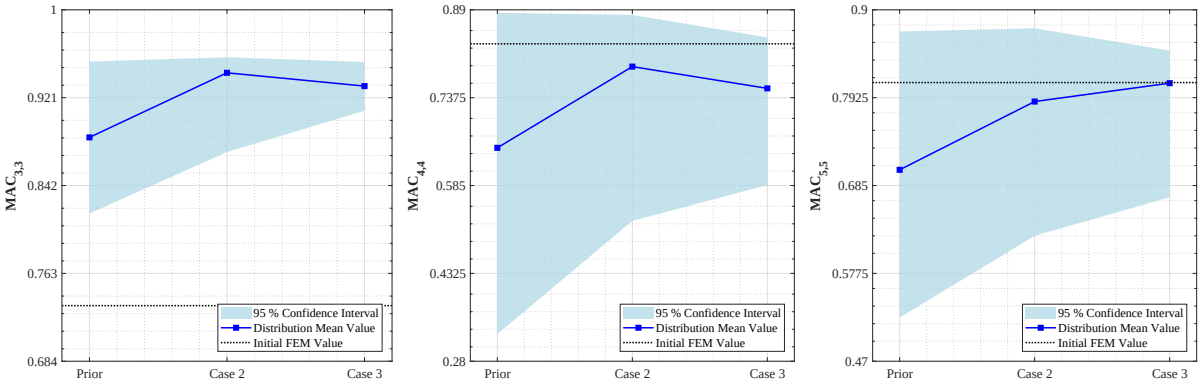

(a) **(b)** **(c)**

Fig. 5.41: 95 % confidence intervals for the diagonal MAC values related to the considered Data Set.

related to the natural frequencies and the mode shapes before and after the updating framework. 95% confidence intervals of the first six natural frequencies are calculated and shown in Figure 5.40. Blue line shows the mean value of the probability distribution before and after the updating procedures. At the end of Case 3 a significant reduction of the uncertainties can be observed. The posterior mean value is shifted towards the measured eigenfrequencies with the exception of the 3rd mode shape. Same procedure is carried out for the diagonal MAC starting from the results already shown in Figures 5.33 and 5.37 and results very similar to those obtained for the natural frequencies are observed.

It is rather evident that this framework allows for an improvement of the numerical model by incorporating all the information contained in the available modal data. A quantitative assessment of all the uncertainties that cannot be captured by the model parameters when different data sets are used as reference is carried out showing how these uncertainties play a crucial role in the updating Bayesian framework.

These results point out that an improvement of the prior model - that is conditional to the data set - can be achieved and that the prediction error variance provides a mean for bridging the gap between the reference data and the computed output.

Chapter 6

The role of uncertainties on dynamic modal parameters in damage detection

6.1 Introduction

In recent years, structural health monitoring has gained increasing interest and attention from the civil engineering researchers as a useful tool to identify damage or, in other words, the "health state" of the tested structures. Vibration-based damage identification procedures may involve continuous monitoring or repeated vibration single measurement campaign aimed to identify changes in the dynamic characteristics of structures without the need for more expensive and complicated inspections.
Operational modal analysis is the most suitable dynamic identification technique for estimating modal parameters of structures using output-only data, i.e., without the knowledge of input excitation. It should be remarked that this technique is based on the strong main hypothesis that the structure to be test is subjected to an unknown excitation having locally white noise characteristics. Therefore the accuracy of the identified modal properties

may strictly depends on the operational condition providing a not consistent dynamic and damage identification. On the other hand the signal processing sampling parameters (e.g. decimation and resampling, filtering and frequency resolution) selected in the preliminary phase of signal analysis play a crucial role in the modal identification procedure. In most of the cases a distortion of the real signal occur causing variations of the modal parameters with respect to the real behavior of the tested structure, compared to those obtained in presence of damage.

This chapter is firstly aimed to investigate systematically the variability of the modal parameters identified using the Enhanced Frequency Domain Decomposition method due to the variability of several input factors. The input sources of variability include: the level of excitation, the data collection in terms of recorded signal time length and the data processing/analysis. The three dimensional updated numerical model of the tested cable stayed footbridge - already deeply described in previous chapter - is used as a sort of black box for simulating dynamic synthetic response time histories to different Gaussian white noise base excitation. The simulated dynamic data are thus used to estimate the modal parameters of the structure in its undamaged state by varying the signal processing parameters in order to assess an optimal time length of the signals and the most suitable signal processing sampling parameters. These information are of particularly interest in both single measurement campaign and continuous structural health monitoring.

Using this procedure the ability to use the Enhanced Frequency Domain Decomposition method for vibration based damage detection is discussed. In fact, in SHM practical applications the time domain operational modal analysis methods are often preferred to the frequency domain methods, since they are easier to be automated. On the other side the Enhanced Frequency Domain Decomposition method is very intuitive and user friendly and for this reason it could be particularly suitable to be used by different kind of users (e.g. members of public administration, researchers and professionals) and for different kind of purposes.

Having addressed the effect of measurement uncertainties, the suitability of vibration based damage identification is finally assessed. First, a deterministic parametric sensitivity analysis is carried out in order to separately evaluate the effects induced on modal frequencies and mode shapes by temperature and different kinds of artificial damage in terms of position and severity. Then, starting from the obtained results, the continuous response of the cable stayed footbridge in its damage state is simulated and the possibility to identify the existence, the localization and the severity of damage by means of global quantities (natural frequencies and mode shapes) in a complex redundant structure is deeply discussed.

6.2 Effects of excitation amplitude and sampling parameters on the dynamic modal response

The objective of this section is to investigate the variability of the modal parameters obtained using the EFDD system identification method due to the uncertainty/variability of the following input factors:

1. excitation amplitude (A);
2. length of structural response records used for system identification (L);
3. number of frequency lines in the output PSD spectrum (NF);

These factors are selected basing on previous works carried out during the PhD practical experience in system identification of civil structures and structural components [138] [139].
In particular, the continuous response of the updated FE model is simulated at different levels of white noise base input excitation. During each dynamic analysis the gravity and the pretension loads are first applied to the model statically, followed by the base excitation which is applied dynamically. As base excitation three acceleration time histories A1, A2 and A3 are generated as Gaussian white noises having a standard deviation equal to (1) 0.03 g, (2) 0.06 g and (3) 0.09 g respectively, where g is the acceleration of gravity. The levels of excitation have been selected in order to assess the accuracy of the system identification procedure also in case of moderate tremors and, in general, of high level of excitation due to wind or to any other extreme operational conditions. It is important to point out that the OMA methods are based on the main hypothesis that the input excitation is unknown and however broadband. If this assumption is not respected additional errors in modal parameters may arise. A direct linear modal time history with a step of 1/400 second is used as time scheme and modal damping ratios of 0.01 are assumed in all the considered first 8 modes obtained from the numerical model in the range of frequency 0-3.5 Hz (i.e. the out of plane mode of the pylon and the longitudinal mode in Figure 5.4 and the modes M_i, i=1,...,6 in Figure 5.5).
Six different lengths of simulated structural dynamic response data are considered in each of the three cases, namely: (L1) 2 min, (L2) 5 min, (L3) 10 min, (L4) 15 min, (L5) 30 min and (L6) 1 hour. It should be noted that in many practical applications of OMA, long durations of structural ambient vibration response are used in the identification process to ensure a suitable level of accuracy. However this part of the dissertation focuses also on

the possibility to identify dynamically the system even in case of short data.
Finally, for each level of excitation and for each time length three different frequency resolution have been considered resulting from three numbers of frequency lines: (NF1) 1024, (NF2) 2048 and (NF3) 4096 use in the output PSD estimation. Obviously, for the 2 minutes simulated acceleration time histories just 1024 number of frequency lines are considered since a smaller frequency resolution is not admittable.
The position and the number of virtual sensors is selected in order to obtain the same configuration of the real experimental data (Figure 5.6) allowing for a complete comparison between virtual and real experimental results discussed Section 5.4.
Table 6.1 summarizes the considered input factors and their different levels. A total num-

Table 6.1: Description of input factors and their considered levels.

Factor	Description	Levels
A	Level of excitation	A1=0.03 g, A2=0.06 g, A3=0.09 g
L	Length of the virtual data	L1=2 min, L2=5 min, L3=10 min L4=15 min, L5=30 min, L6=60 min
NF	Number of frequency line in PSDs	NF1=1024, NF2=2048, NF3=4096

ber of identification runs equal to 48 is performed and used in order to assess the variability of the modal parameters (i.e. natural frequencies, damping ratios and vibration modes in terms of diagonal MAC coefficients) providing a quantification of the measurement uncertainty particularly useful in future applications (i.e structural continuous monitoring).
Figure 6.1 shows the virtual acceleration response time histories and their PSDs at three virtually monitored DOFs of the deck in vertical, horizontal and lateral directions for all the three base excitations. It is observed that the peaks of PSD decreases as the excitation amplitude increases, meaning that the modal parameters may be strictly depend on the excitation amplitude.

The simulated data are decimated 20 times obtaining a Nyquist frequency much higher than the modal frequencies of interest in the range 0 - 3.5 Hz. No digital filters are applied in signal pre processing and no spike removal is required. The EFDD is then used for the dynamic identification, as shown in Chapter 2: the auto/cross PSD functions are estimated using the Welch's method with Hanning windows of different sizes depending on the considered number of frequency lines and measurement length, and 60 % of window overlap. The output PSDs responses matrices are then decomposed by means of SVD.
Figure 6.2 shows the spread of the ratio between the virtually identified modal properties (natural frequencies, damping ratios and vibration modes in terms of diagonal MAC) and

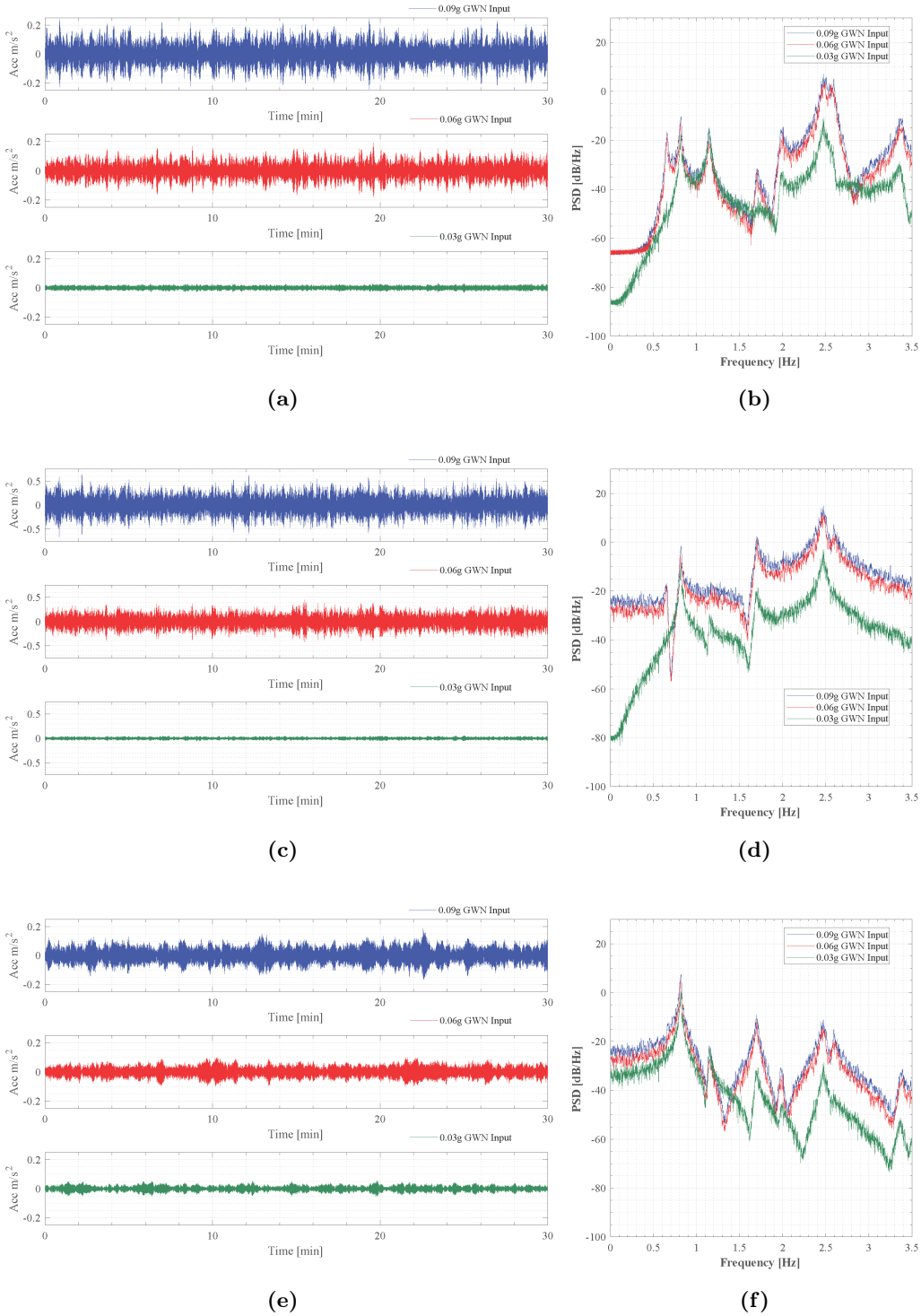

Fig. 6.1: Vertical (a), horizontal (c) and longitudinal (e) time history acceleration responses and their power spectral densities (b,d and f) for 0.03 g, 0.05g and 0.09g white noise base excitations.

those obtained from the updated numerical model. In this way it is possible to immediately evaluate the percentage errors between the numerical value and the virtual ones. It is important to point out that the diagonal MAC is used in order to measure the degree of correlation between the vibration modes obtained from each of the virtual experimental response and those obtained from the updated numerical model.
First, it is important to point out that the out of plane mode of the pylon (OOP in Figure 5.4a) is never identified, as occur using the real experimental data. Further, the longitudinal mode (LM in Figure 5.4b) can be easily identified in all the 48 virtual experimental data sets; the same mode shape cannot be identified using the real data even though the sensors location is the same.
The mixed mode M5 can be not identified in all the virtual data sets. This is mainly due the fact that the two mixed modes M4 and M5 identified from the updated numerical model are very similar (MAC coefficient of about 0.85) and they correspond to very close natural frequencies respectively equal to 2.460 Hz and 2.576 Hz. In particular, the mode shape M5 is identified using the shorter data sets when the system is excited by the low level of excitation A1. It can be identified only from the time histories lasting more than half an hour when the system is excited by the level of excitation A2 and, finally, it is always identified in all the virtual data sets obtained with the level of excitation A3, with the exception of virtual response time histories lasting 2 minutes.
It is rather evident that the modal parameter that is most sensitive to the considered input factor variations is the modal damping ratio, confirming that the damping estimation using EFDD method is characterized by a significant level of uncertainty. The natural frequencies are well estimated in all the virtual data sets; on the contrary, the diagonal MAC coefficients seem to be particularly affected by the variations of all the three considered input factors, with the exception of the lateral mode M2 and the second vertical mode M6.
An in depth analysis is carried out in order to properly investigate which are the input factors that affect mostly the modal response of the cable-stayed footbridge: the contribution of one input factor is assessed taking the observed single input factor as fixed or known, while the other two remaining input factors are assumed to be variable or however unknown.

The distributions of the identified modal parameters as a function of the different amplitudes of excitation are reported in Figure 6.3 for a number of frequency lines equal to 1024, and for three time length of the signals: 2 minutes (left panels), 15 minutes (center panels) and one hour (right panels) in order to show what happens for both short and long data and for the same time length used in the experimental campaign.

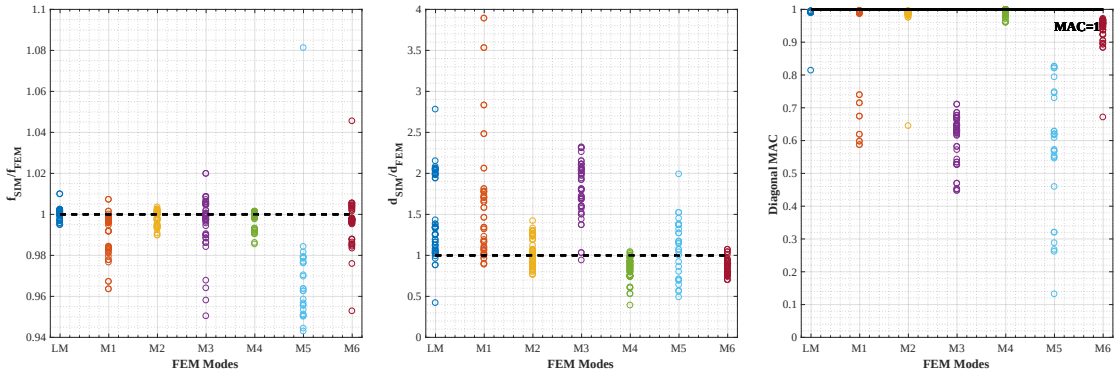

(a) **(b)** **(c)**

Fig. 6.2: Comparison between numerical and virtual eigenproperties: natural frequencies (a), damping ratios (b) and diagonal MAC coefficients for varying the considering input factors.

Figures 6.3a, 6.3b and 6.3c show the significant influence of the excitation amplitude on the distributions of the identified natural frequencies with values very different from one - that means perfect correlation with the updated numerical model - for the highest level of excitation (A3) in all the considered virtual data sets. Such differences are comparatively more significant in the natural frequencies associated to the first, the second vertical (M1 and M6) and the torsional (M3) mode shapes. However, the errors remain lower than 0.5 %.

The dependance of the vibration modes from the excitation level - shown in Figures 6.3g, 6.3h and 6.3i - is not as evident as in the case of natural frequencies. The diagonal MAC coefficients are almost aligned in the horizontal direction in all the virtual data sets with the exception of the first vertical (M1) and the torsional vibration modes (M3) estimated from 1 hour virtual acceleration time histories: the diagonal MAC related to M1 decreases from 0.99 to 0.60 when the level of excitation increases from A1 to A3; same behavior is observed for M3 but, in this case, the MAC coefficients are always lower than 0.7. On the contrary, the other mode shapes are always characterized by a MAC coefficient greater than 0.9 meaning almost perfect correlation with the corresponding numerical results.

The ratios between the modal damping ratio obtained from the virtual measurements and the modal damping ratio assumed in the numerical model are far from the target unit value, even though they are almost aligned on the horizontal direction as shown in Figures 6.3d 6.3e and 6.3f varying the virtual signal time length. This means that the level of accuracy that can be reached in the damping ratio estimates using OMA methods in

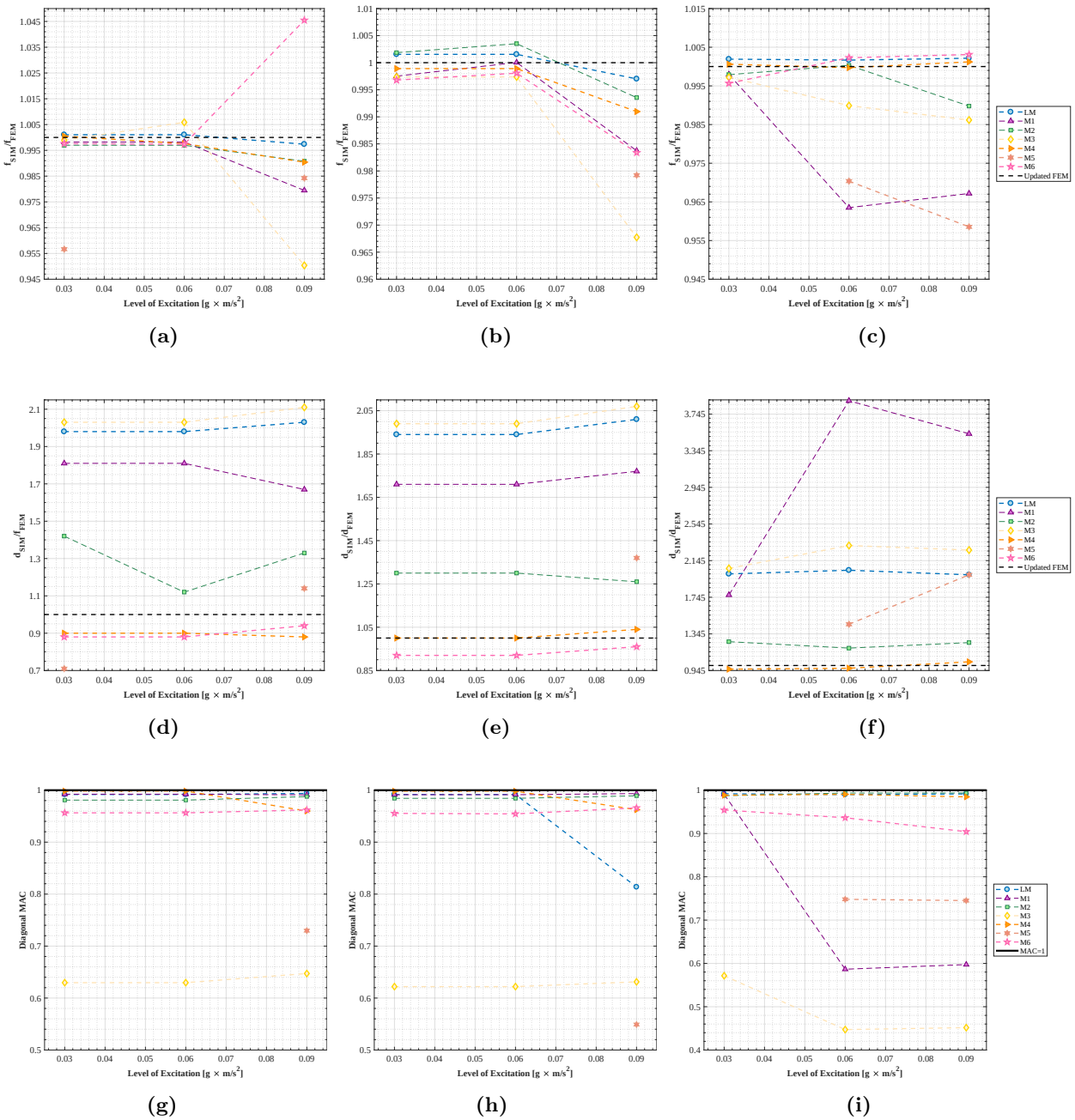

Fig. 6.3: Identified natural frequencies ratios (a, b, and c), damping ratios (d,e and f) and diagonal MAC coefficients (g,h and i) as a function of the level of excitation for time length equal to 2 minutes (left panels), 15 minutes (center panels),1 hour (right panels) and 1024 number of frequency lines.

frequency domain is not related to the level of excitation.
The distributions of the identified modal parameters as a function of the time length of the virtual acceleration time histories is thus discussed. Figure 6.4 shows the ratio between the modal properties identified from the virtual data sets and those identified from the updated numerical model only for the mode shapes that are most sensitive to variations of this input factor: the first vertical mode shape (M1 in left panels), the lateral mode shape (M2 in center panels) and the torsional mode shape (M3 in right panels). Having observed that the level of excitation plays a crucial role, the dependency of all the modal parameters with the signal time length is studied fixing 1024 number of frequency lines for each level of excitation taken alone. All the modal parameters assume almost the same values when virtual acceleration time histories longer than half an hour are used. For this reason, further analysis have been carried out considering also virtual time histories lasting 40 minutes and 50 minutes. Results have confirmed that data sets lasting more than half an hour provide almost the same results.
The natural frequencies of all the first seven mode shapes under investigation are characterized by values following an irregular trend with up and down when time length lower than 15 minutes is used. These variations depend strictly from the level of excitation. As shown in Figures 6.4a 6.4b 6.4c the natural frequency ratio variations as a function of the virtual signal time length increase when the level of base excitation increases.
Similar results are obtained for the diagonal MAC coefficients. MAC values level off for short data lining up on the horizontal direction for data lasting more than half an hour and, as shown in Figures 6.4g, 6.4h and 6.4i, the variability of the MAC with time length of the virtual signals increase with the level of base excitation. The variations in the MAC are significant also when the system is excited by a low base input excitation and this is due to the fact that MAC number is sensitive to large eigenvector components.
Different results are obtained for the damping ratios. On one hand it is evident that the dependency of damping ratios with the virtual signal time length is the same of the natural frequencies and the diagonal MAC numbers, with values fluctuating when shorter data set are used and almost constant when longer data set are used. On the other hand the values identified from the virtual acceleration time histories remains very far from those hypothesized in the updated numerical model, with significant differences greater than 200% occurring for the first vertical (M1 in Figure 6.4d) and the torsional (M3 in Figure 6.4f) mode shapes.

Having assessed the crucial role of the level of excitation and and having observed that the identified modal parameters assume constant values when virtual data set lasting more

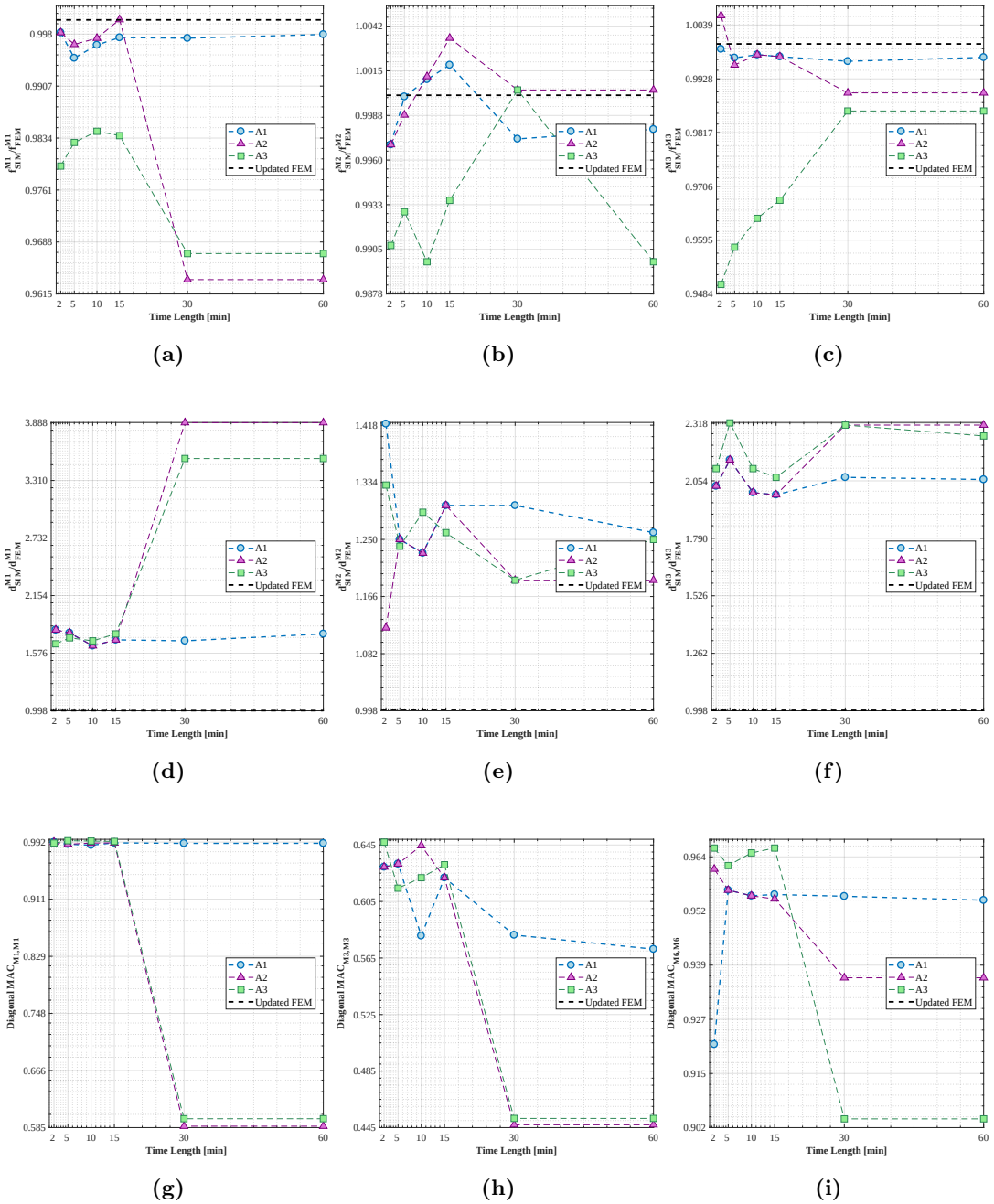

Fig. 6.4: Identified natural frequencies ratios (a, b, and c), damping ratios (d,e and f) and diagonal MAC coefficients (g,h and i) as a function of the time length using 1024 number of frequency lines.

than 30 minutes are used, the distributions of the identified modal parameters as a function of the number of frequency lines is reported for a signal time length equal to one hour and for all the three level of excitation taken alone. Figure 6.5 shows the obtained results. In particular, the effect of the number of frequency lines in the output PSDs on the natural frequencies is almost negligible for lower level of excitation (Figure 6.5a) with maximum percentage errors lower than 0.1%; it is significant for the highest levels of excitation (Figures 6.5b and 6.5c) with maximum percentage variations with respect to the numerical results used as reference state of about 0.5 % for all the mode shapes with significant vertical components.

Figures 6.5d, 6.5e and 6.5f show the variations of diagonal MAC coefficients for each considered mode shape for each of the three excitation levels A1, A2 and A3 in left, central and right panel, respectively. On one side it is rather evident that for low level of excitation the lines are almost horizontal, indicating that the effect of the frequency resolution is negligible; on the other side, for the highest level of excitation significant variations of the diagonal MAC occur with values higher than 12 %, with the exception of the first longitudinal vibration mode (LM) and the vibration modes M1, M2 and M4 for which the single lines are almost horizontal.

The damping ratio is particularly influenced by the frequency resolution as just discussed in Chapter 2. In order to compare the results obtained by virtual data sets and those obtained from the real experimental data (Section 5.6), the dependency of the damping ratio with the number of frequency lines in output PSDs is studied in terms of frequency resolution (Eq 2.65).

Figure 6.6 shows that the damping estimation is almost linearly dependent from the frequency resolution, with the exception of the first and the second vertical vibration modes (M1 and M6) for the highest level of excitation. The varying gradient of the first order curves obtained for each mode confirms that the damping estimates depend also on the natural frequencies of each corresponding mode shapes: maximum gradients are observed for the lowest frequencies. This result is confirmed by the bias error on damping (Eq. 2.66) that is shown in Figures 6.6d, 6.6e and 6.6f for the level of excitation A1, A2 and A3 respectively. Bias error on damping decreases in all the data sets when the frequency resolution increases and the gradient of each single first order curves decreases when the associated natural frequencies increase. The results obtained with the real experimental data are therefore confirmed using virtual Gaussian white noise data: the frequency resolution needs to be chosen such that the influence of the leakage bias is minimized. However it is important to observe that the maximum values of the damping ratio remain very far

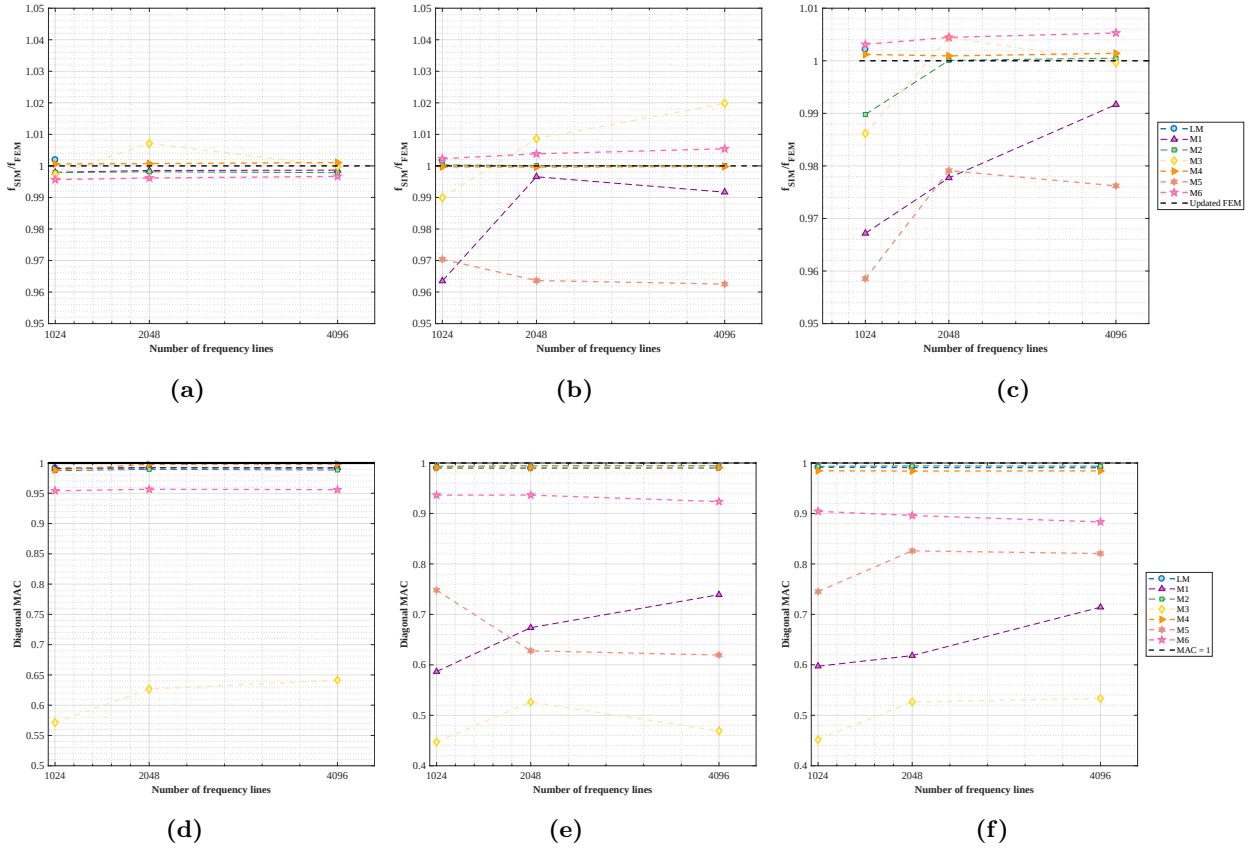

Fig. 6.5: Identified natural frequencies ratios (a, b, and c), and diagonal MAC coefficients (d,e and f) as a function of the number of frequency lines and for level of excitation A1 (left panels), A2 (middle panels) and A3 (right panels).

from those assigned in the updated numerical model, even when a frequency resolution corresponding to the highest number of frequency lines is used.

In order to have a quantitative complete idea of the effect of all the input factors, the coefficients of variation of the modal parameters are estimated following the same procedure of the previous result. The contribution of one input factor is assessed taking the observed single input factor as fixed or known, while the other two remaining input factors are assumed to be variable. Figure 6.7 shows that the variation of the identified modal properties among the different used virtual data sets used is different. Before discussing the results, it is important to point out that all the statistics (mean and variance) related to the mode shape M5 cannot be considered, since just a limited number of samples are available.

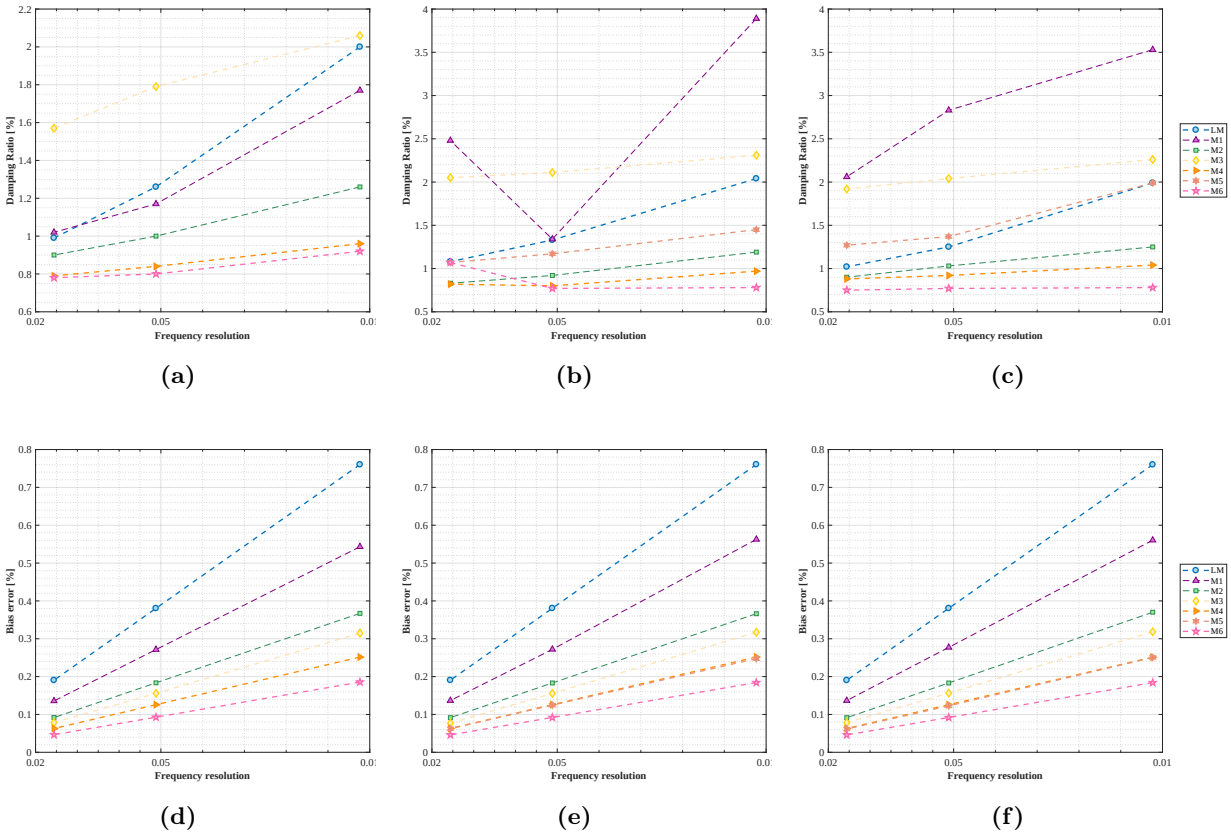

Fig. 6.6: Identified damping ratios (a, b, and c), and bias errors on damping (d,e and f) as a function of the number of frequency lines and for level of excitation A1 (left panels), A2 (middle panels) and A3 (right panels).

The cov of the natural frequencies are estimated for the first seven mode shapes under investigation and plotted in Figures 6.7a 6.7b and 6.7c as a function of the level of excitation, the time length of the virtual responses and the number of frequency lines, respectively. The maximum dispersion of the data points is obtained for the excitation levels with cov reaching values close to 2%. This confirms the fact that the base excitation amplitude has a significant influence on the distributions of the eigenfrequencies, especially for the higher modes. It is noteworthy that the dispersion of the identified natural frequencies increases significantly when the level of excitation amplitude increases. Cov of the same order of magnitude are obtained varying the frequency resolution and the time length of the virtual acceleration time histories. In particular, the dispersion of the natural frequencies seems to increase when data sets lasting more than half an hour are used. This can due to the

fact that the level of excitation continues to play a crucial role.
Similar results are obtained for the cov of the diagonal MAC coefficients when the effect of the excitation level is considered, as shown in Figure 6.7d. The dispersion of the data is maximum for the highest level of excitation. However, the cov assume values significantly different than those obtained for the eigenfrequencies: close to 20% and to 15% for the vertical (M1) and torsional (M3) mode shapes. Also the effect of the frequency resolution is evident with cov lower than 2% only for the mixed mode shape M4 (Figure 6.7e). Finally, the effect of the signal time length is the same of the natural frequencies albeit the order of magnitude of the cov is completely different (Figure 6.7f).
The dispersion of the data related to the damping estimates confirms what already discussed. All the data sets are characterized by a significant dispersion with cov assuming values always greater than 15% for all the considered input factor, as shown in Figures 6.7g, 6.7h and 6.7i.
Therefore it is possible to summarize the obtained results:

- The natural frequencies identified using all the virtual data sets are in excellent agreement with the results of the updated numerical model and their inherent variation is principally related to the higher level of excitation and to the frequency resolution: the better results are obtained for low level of excitation and higher number of frequency lines.

- The uncertainty related to the damping ratio estimates is inherently higher the uncertainty in the corresponding natural frequencies confirming the results already discussed in some literature works (as discussed in Chapter 2). However, in this case study an important result is obtained: the variability/uncertainty in modal damping estimates by means of EFDD is in general attributed to the nature of the input excitation that does not satisfy the input broadband assumption. In this case three different Gaussian white noises are used as base input in order to not violate the main hypothesis of the output-only dynamic identification and even in case of low excitation level the results are not acceptable, with damping ratios assuming values very different from those hypothesized in the updated numerical model. Obviously, the classical damping assumed in the numerical model may not characterize well the actual energy dissipation mechanism of the structure and, in this sense, deeper analysis would be needed to be performed in order to quantify this source of uncertainty. However, having studied the dispersion of the results and the bias errors due to leakage, it is possible to assess that the level of excitation, the time length of the signals

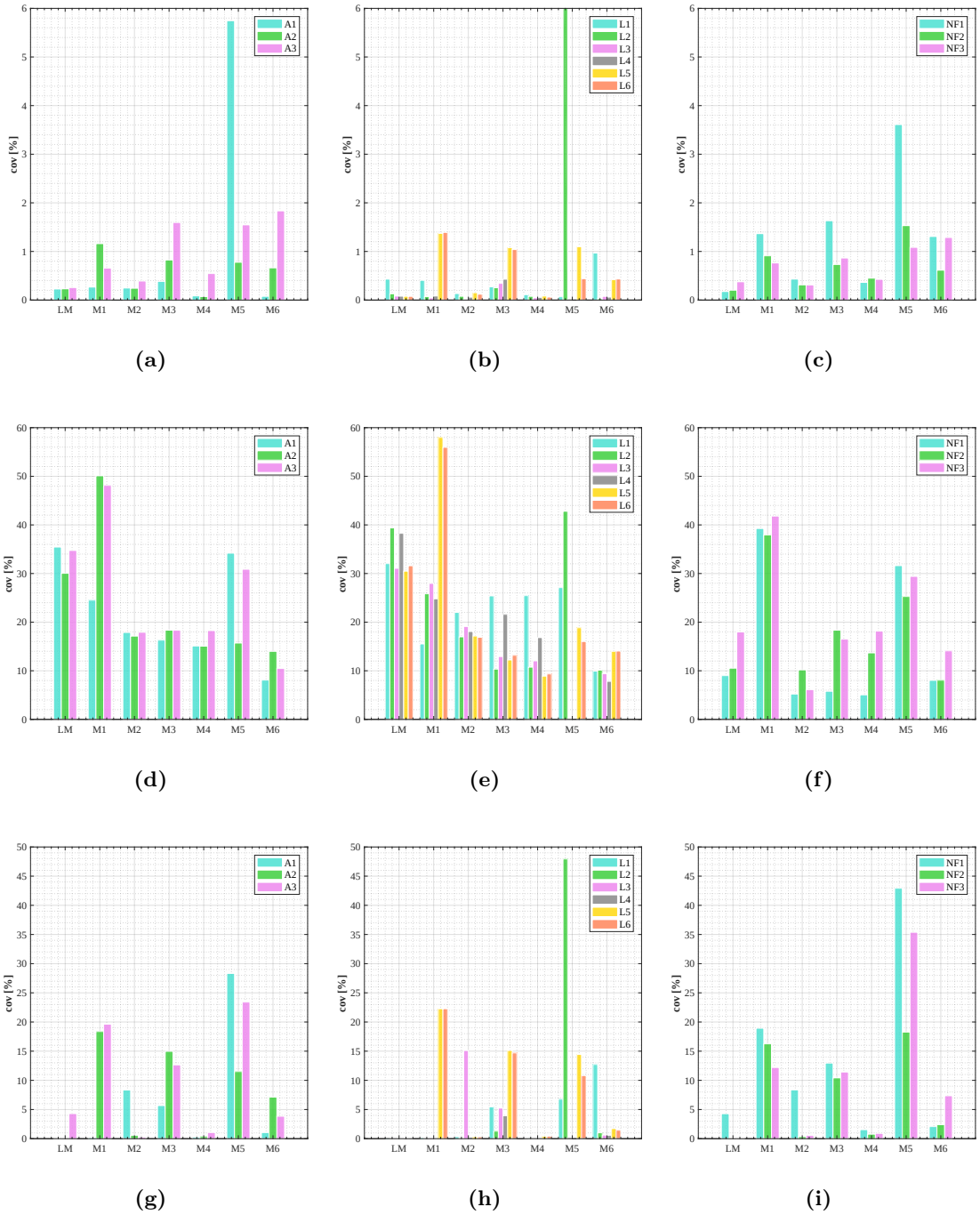

Fig. 6.7: Coefficients of variation of the identified natural frequencies (a,b and c), damping ratios (d,e and f) and diagonal MAC coefficients (g,h and i) related to the singular input factors: level of excitation (left panels), signals time length (middle panels) and number of frequency lines (right panels).

and frequency resolution have got a significant influence on the results related to modal damping and that selecting a proper frequency resolution the bias errors can be minimized.

- The diagonal MAC coefficients presents very scattered values in relation to the single input factor. Moreover, for low level of excitation and long data the diagonal MAC assumes values higher than 0.85 that means a good correlation within the corresponding numerical results with the exception of the torsional mode shape having value of about 0.7 in all the data sets.

For all these reasons the EFDD method can be considered a useful tool for the evaluation of the modal properties with the exception of the damping ratio, especially if a single measurement campaign is carried out. These results are of utmost importance in the field of SHM. In fact, both the parametric and the uncertainty analysis show clearly that when low level of excitation occur and when signal time length lasting more than half an hour are used, the reliability of natural frequency and the mode shape estimates is high and that both of them can be used as indicator for damage detection. In contrast, the use of damping as a dynamic property to represent the structural damage is not recommended.

6.3 Effects of temperature on structural frequencies

The effects of temperature variability on the measured modal properties of structures have been addressed in several studies, as discussed in Chapter 2. Temperature variation may not change only the modal properties of structure but also the boundary conditions of the whole structural system. The main aim of this section is to discuss the effect of the temperature variations on the natural frequencies and the mode shapes of the cable stayed footbridge object of study.
The effects induced by temperature variations on modal properties are evaluated through a deterministic analysis solving the eigenvalues problem of the structural system increasing the value of the temperature between - 10° and + 50° C. In particular, the temperature effects are simulated by means of a pre-stressed modal analysis starting from the deformed equilibrium configuration under dead load, cable pre-tension and temperature effects. The non linear static analysis solution is achieved by means of 200 incremental steps. The equilibrium is reached at each step using the Newton - Raphson method.

Since the variations in the natural frequencies induced by temperature effects are at least comparable with those obtained with the different level of excitation and since the main aim of the following procedure is to assess the possibility to identify damage occurrence in the cables, the thermal effects are applied just on the main cables neglecting any kind of local effects in the deck. Also the effects of temperature variations on the vibration modes is analyzed but results are not herein shown since no significant effects are evaluated.
Figure 6.8 shows the trend of frequency ratios between the natural frequencies obtained for $\Delta T \neq 0$ and those obtained for $\Delta T = 0$ for the most sensitive modes. Although the eigenfrequency variations are very small the linear trends can be easily recognized. The natural frequencies decrease with the increase of temperature for the out of plane mode of the pylon, the torsional and the second vertical mode (M3 and M6, respectively); on the contrary, the natural frequencies decrease with the increase of temperature in all the other observed vibration modes. The variation of the longitudinal mode modal frequency is around 0.01% under a variation of 1°C. It is interesting to observe that the two vertical mode shapes (M1 and M6) have an opposite qualitative trend while, as it was reasonable to expect, a very similar trend is identified for the two close mixed modes M4 and M5.
A different view of the dependencies of the natural frequencies from temperature variations

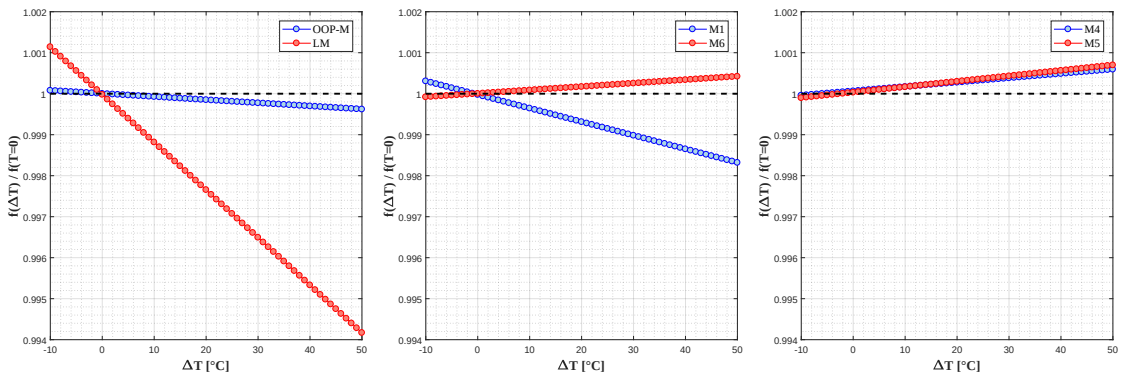

Fig. 6.8: Frequency ratios of the most sensitive vibration modes increasing the temperature variation ΔT: the out of plane mode of the pylon, the longitudinal mode (a), the two vertical modes (b) and the mixed modes(c).

is highlighted in Figure 6.9, where a continuous response analysis is simulated for better analyze the daily fluctuations of the eigenfrequencies due to different real temperature variations. The temperature time histories taken as reference are recorded in a nearly

weather station. Figures 6.9a and 6.9b shows the natural frequency time histories as a function of the temperature time histories in winter and summer season respectively for the most sensitive mode, (i.e. the longitudinal model). The relation between the two considered quantities it is evident. Figures 6.9d and 6.9d shows the natural frequency variations of the first and second vertical vibration mode (M1 and M6, respectively) for the same temperature time histories. In this case it is evident the natural frequency time histories of the two mode shapes are anticorrelated.

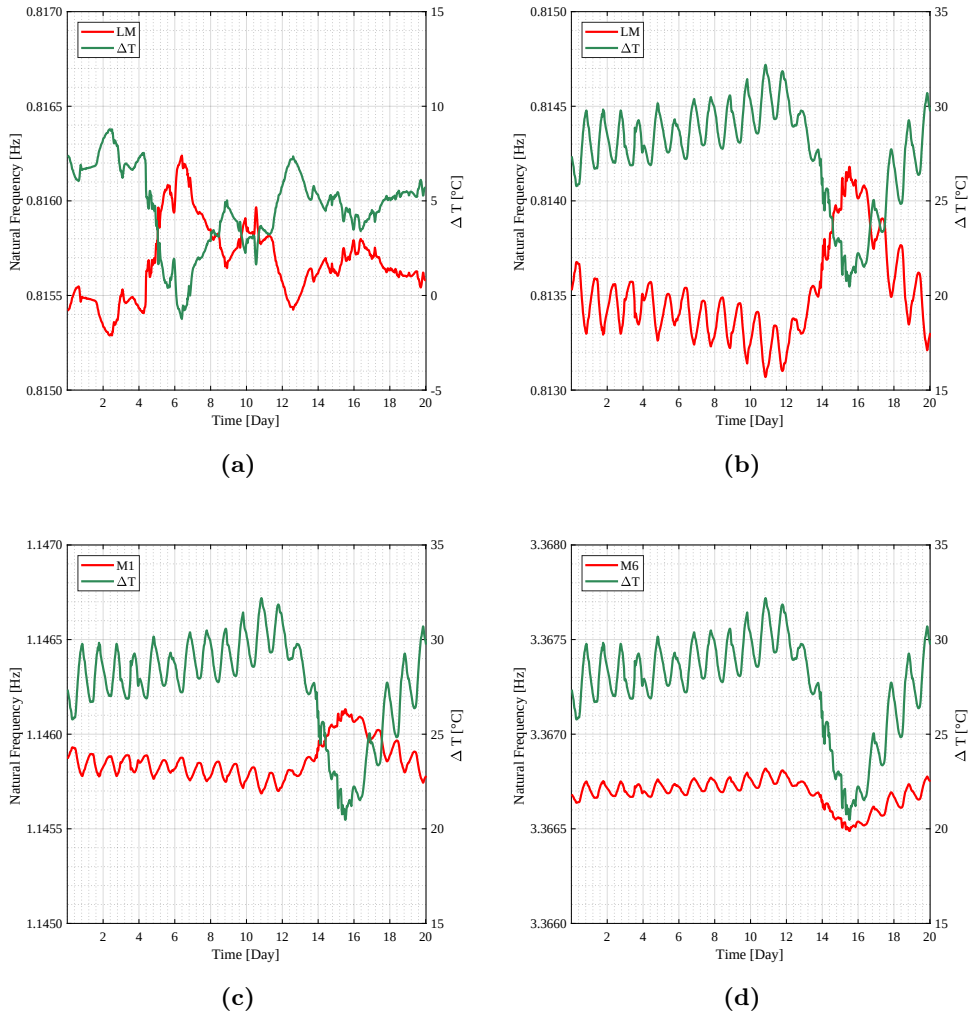

Fig. 6.9: Variations of the natural frequencies in twenty days of temperature fluctuations: (a) winter and (b, c and d) summer for the longitudinal mode LM (upper panels), and for the first (M1) and second vertical (M6) mode shape (lower panels).

6.4 Sensitivity of structural modal parameters to damage scenarios

The main aim of this section is to evaluate the efficacy of permanent vibration based structural health monitoring systems for assessing the health state of the main cables without direct and expensive investigations. Therefore a parametric analysis similar to that presented in previous section is carried out in order to evaluate numerically the main damage effects on the modal properties. In this way a direct comparison with the measurement uncertainties/variability and with the thermal effects is possible.
Cable - stayed footbridge are highly redundant structures that are particularly vulnerable to different kind of events related to tension loss or to a cross section reduction due to cyclic loads or natural corrosion. For these reasons, the cable damage is herein modeled as a reduction of the cables stiffness under different damage scenario. Following [140], a damage scenario is completely described by the damage level, DL, the damage extension, DE, and the damage position, DP. Assuming the occurrence of diffused damage in a single cable or in consecutive cables, six different DL are considered corresponding to a stiffness reduction of about 10 % (DL1) , 20% (DL2), 30% (DL3), 40% (DL4), 50%(DL5) and 60% (DL6) in order to assess the possibility to detect different class of damage severity. The damage extension is a quantity able to consider that the damage may affect more cables consecutively and it can be thus defined as the differences between the horizontal abscissa of the damaged region: $DE = \frac{x_2 - x_1}{L}$, where x_1 and x_2 are the quantities summarized in Figure 6.10 and L is total length of cable span. It is important to point out that the damage is assumed to be diffused in all the length if the cables and that x_1 and x_2 refers to the abscissa of the connection between the damaged cable and the deck. Then the position factor is defined as $DP = \frac{x_1 + x_2}{2L}$.

Variations of natural frequencies and vibration modes are investigated through a parametric analysis focusing firstly on the effect of damage position. The six level of damage extension are thus considered on all the cables taken alone in order to highlight the aspects related to different level of damages induced by local failure or to impulsive high tensile stress in the cable due to some extreme events. Thus the effect of damage position is evaluated for all the first eight numerical eigenfrequencies and plotted in Figures 6.11 and 6.12 in terms of ratio between the damaged f_{DAM} and the undamaged f_{UND} eigenfrequencies. The pylon position is highlighted by the black dashed line. It is observed that the first vertical (M1) and the lateral (M2) vibration modes present a similar behavior: maximum variations of natural frequencies between damaged and undamaged state occur when the

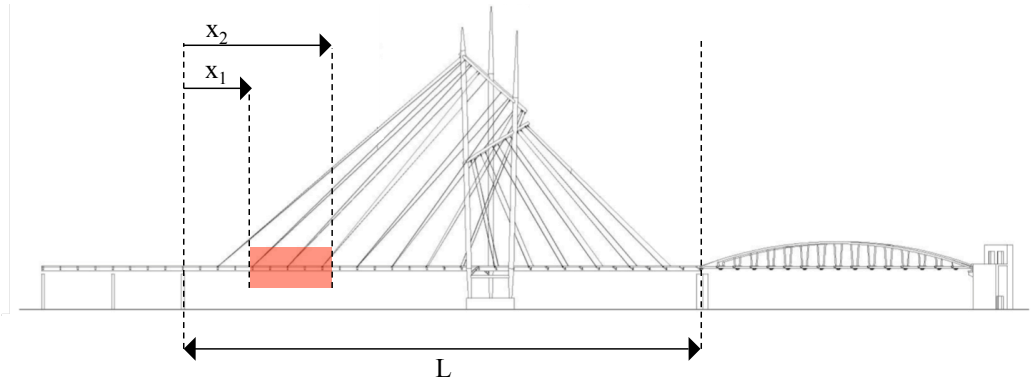

Fig. 6.10: Geometry overview of the cable-stayed footbridge with damaged region.

damaged cables are the most distant from the pylon and zero at the pylon position; on the contrary, the second vertical (M8), the torsional (M3) and the two mixed mode shapes (M4 and M5) are characterized by maximum variations in the eigenfrequencies when damage affects one of the central cables of the two different arrays of cables attached to the two rings. The out of plane (OOP) mode of the pylon is characterized by maximum variation in the frequency ratios when damage affect the cables attached to the lowest ring. The longitudinal mode shape (LM) presents a singular behavior with maximum variations for damage affecting the most external cable on the longest side of the deck. Therefore the most sensitive modes to damage induced frequency variations are the two vertical ones.

The diagonal MAC coefficients are used again in order to measure the correlation between the eigenvectors corresponding to the damaged and the undamaged state. In the present case the obtained MAC values of the out of plane mode of the pylon, the longitudinal mode and the first vertical and lateral ones are very close to one meaning that these modes are characterized by negligible variations with different level and different damage position. On the contrary, the other mode shapes are characterized by variations in MAC values in a range between 2% and 3% when the damage level DL6 occur, as shown in Figure 6.13. Maximum variations in the diagonal MAC coefficients and therefore in the eigenvectors can be observed in the torsional mode (M3) when damage affects a single cable between the most external ones, while all the other modes (M4, M5, M6) are characterized by significant variation when damage occurs in one of the central cable of the two array of cables at the two opposite sides of the pylon. It is clear that the effect of the local damage in the diagonal MAC coefficients is significantly smaller than the effect of the level of excitation

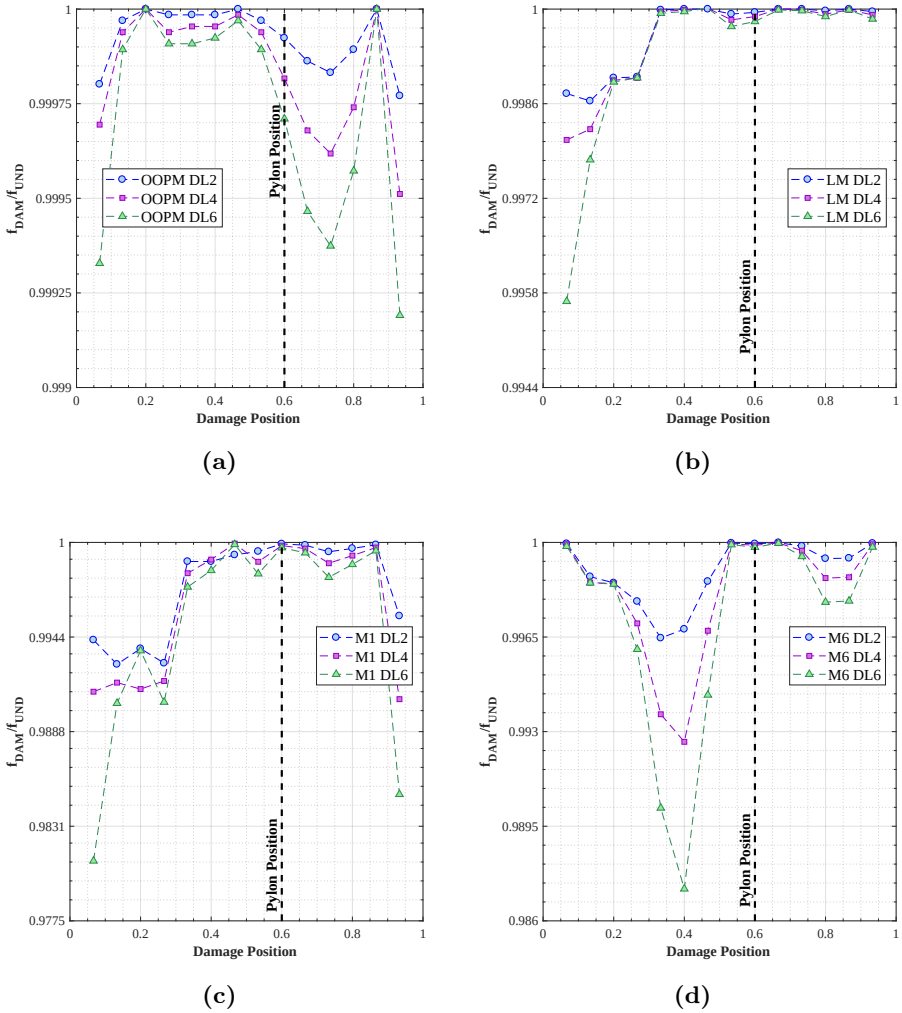

Fig. 6.11: Damage effects on the natural frequencies of the cable-stayed footbridge: frequency ratios of the first out of plane mode of the pylon (a), longitudinal mode (b) and the first and second vertical vibration modes (c and d, respectively) as a function of the damage position for damage level DL2, DL4 and DL6 .

and the signal process parameters, even when severe damage corresponding to a reduction in stiffness of about 60% in one cable occur.

Since the position of the local damage has significant influence on the damage induced natural frequency variations, the results of the parametric analysis carried out in order to evaluate the effect of the different levels of damage are shown only for the damage positions at which the maximum variations of the frequency ratio occur. In particular the maximum

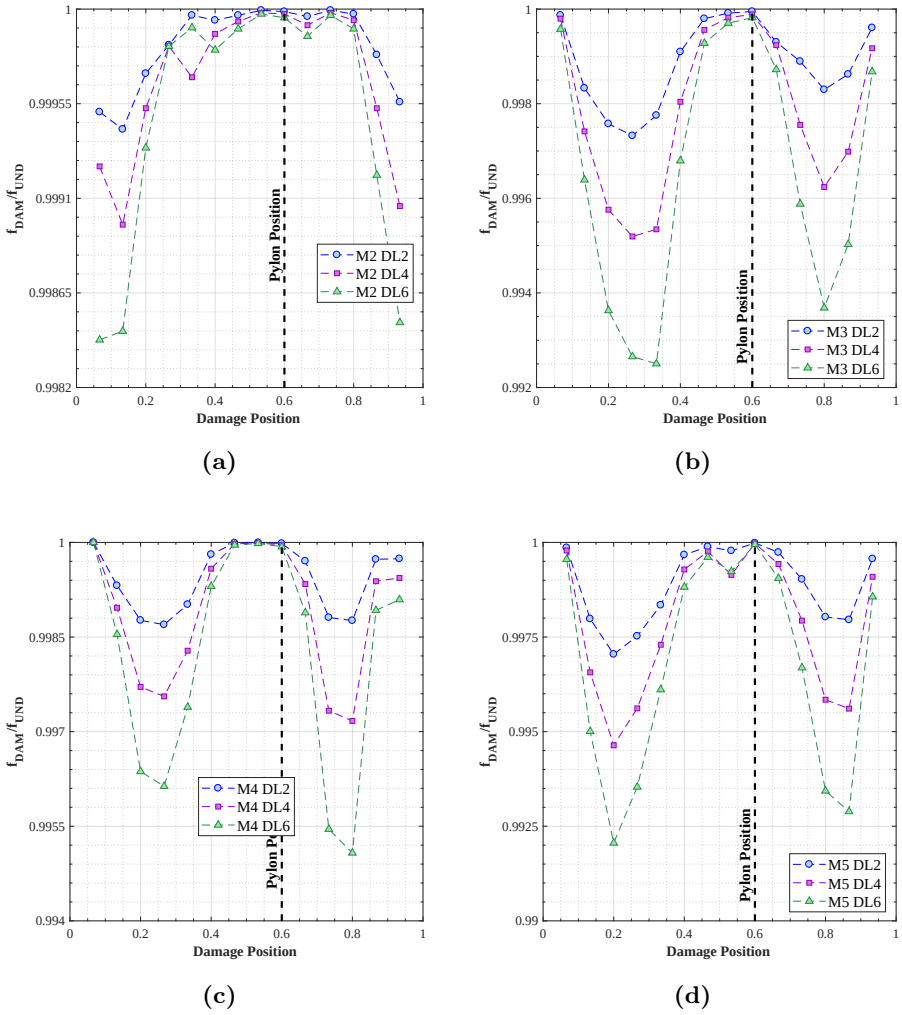

Fig. 6.12: Damage effects on the natural frequencies of the cable-stayed footbridge: frequency ratios of the lateral (a), torsional (b) and the two mixed vibration modes (c and d, respectively) as a function of the damage position for damage level DL2, DL4 and DL6 .

eigenfrequencies variations are equal to 2.0% and 1.8% respectively for the first vertical mode shape (M1) when the maximum level of damage DL6 affects the first cable (with reference to the fixed reference system in Figure 6.10) and for the second vertical mode shape (M6) when the maximum level of damage DL6 affects the first 6^th cable (again, with reference to the fixed reference system in Figure 6.10). Figure 6.14 shows the obtained results. The trend of frequency ratios varying the damage level is almost linear for all the vibration modes. Damage always produces a reduction in the eigenfrequencies and this

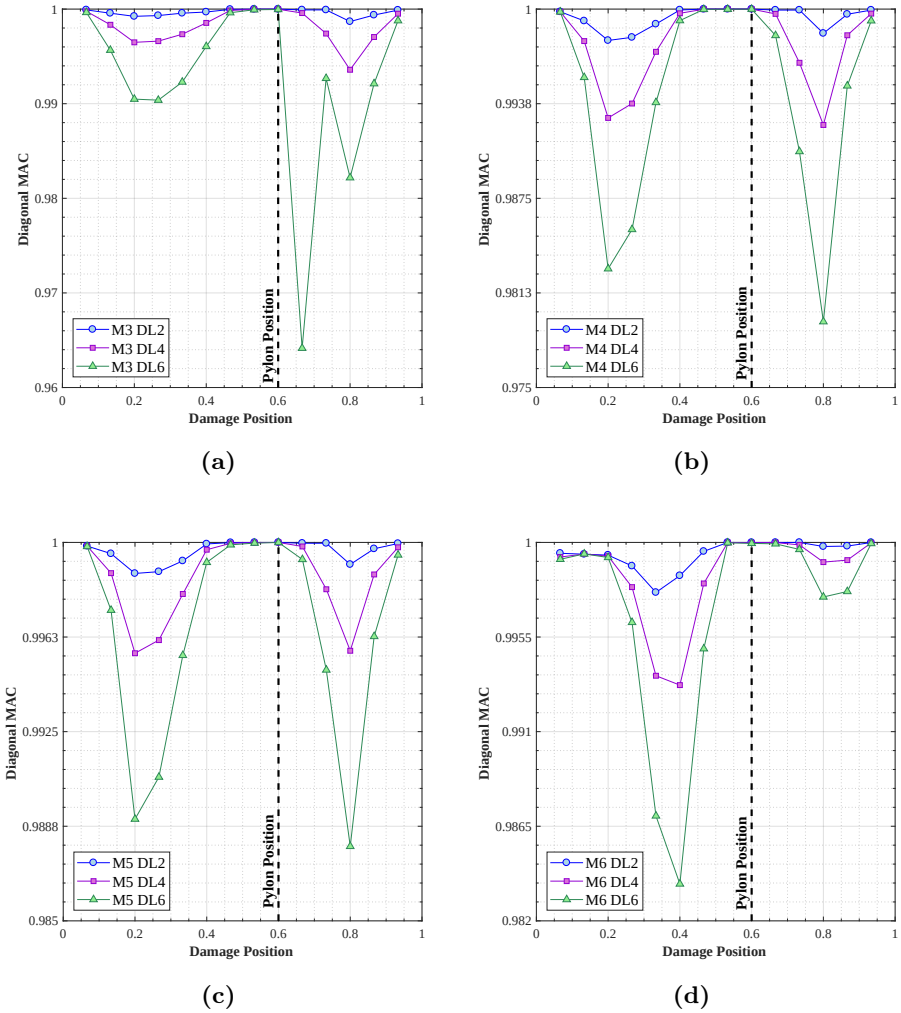

Fig. 6.13: Damage effects on the vibration modes of the cable-stayed footbridge: diagonal MAC coefficients of the torsional (a), the two mixed (b and c, respectively) and the second vertical vibration modes as a function of the damage position for damage level DL2, DL4 and DL6 .

reduction increases with the increase of damage severity. It can be further observed that the local damage induced eigenfrequencies variations for the two mixed modes (in Figure 6.14d) are so small that they lose essentially any practical interests.

The comparison between temperature and damage effects highlights that temperature produces apparent changes in frequencies of the same order of magnitude than those produced by a significant level of local damage, with the exception of the two vertical mode

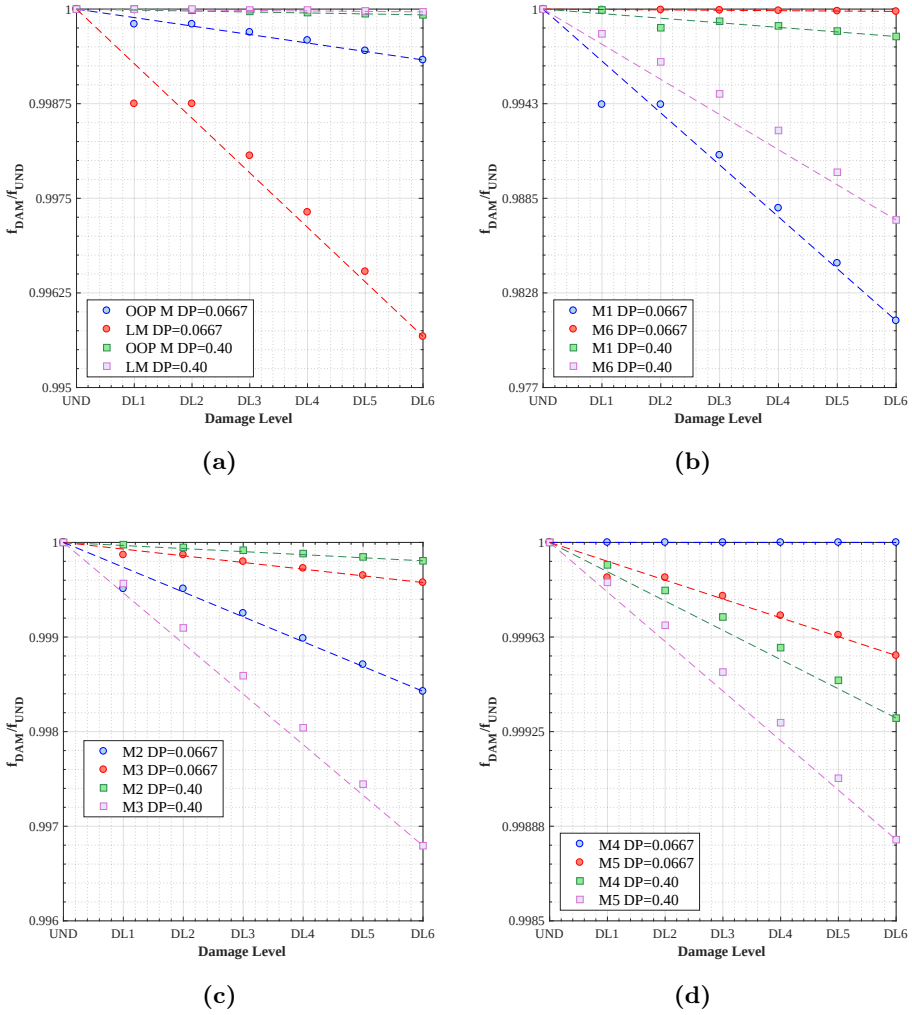

Fig. 6.14: Damage effects on the natural frequencies of the cable-stayed footbridge: frequency ratios of the out of plane mode of the pylon and the longitudinal modes (a), the first and the second vertical modes (b), the lateral and the torsional modes (c) and the two mixed vibration modes (d) as a function of the damage levels for two fixed positions DP=0.0667 and DP=0.40 (corresponding to the first and the sixth cable respectively).

shapes. It is important also to observe that all the variations produced by the excitation level and the signal processing parameters continue to play a crucial role providing variations in the eigenfrequencies comparatively most significant than those produced by this damage scenario. These results imply that in redundant structure like cable stayed footbridge the damage quantification and localization is not possible using eigenfrequencies

and mode shapes as control parameters.
The effect of damage extension in both natural frequencies and mode shapes is thus considered assuming that same level of damage affects more cables consecutively. This kind of simulation is used to reproduce the effect of a severe damage diffused into a region and due for example to a diffused corrosion process or to a local phenomena affecting the deck. Therefore the damage induced variations in the considered numerical eigenfrequencies - as a function of the damage position - are firstly studied and shown in Figures 6.15 and 6.16 for the different damage level affecting 4 cables consecutively in order to identify the worst damage position. The maximum percentage variation equal to 4.5 % occur for DP=0.4 (diffused damage in the 4^{th},5^{th},6^{th},7^{th} cable with reference to Figure 6.10) and maximum damage level DL6 in the second vertical vibration mode (M6 in Figure 6.15d). Significant variations higher than 2.5% occur for DP=0.80 (diffused damage in the 10^{th},11^{th},12^{th},13^{th} cable with reference to Figure 6.10) and for DL6 in the two mixed vibration modes (M4 and M5 in Figures 6.16c and 6.16d). It is noteworthy that, from a qualitative point of view, the trend of the induced eigenfrequency variations is the same of that obtained in case of damage affecting just a single cable, even though the order of magnitude is completely different.

Therefore in the following results, two fixed damage positions are considered corresponding to DP=0.40 and DP=0.80 in order to assess the relationship between the damage levels and the damage induced natural frequency variations. Figure 6.17 shows clearly than the trend of the frequency ratios for varying DL is almost quadratic and the most sensitive modes are the second vertical modes (M6 in Figure 6.17b) and the torsional mode (M3 in Figure 6.17c). Changes in frequency of the other modes especially the out of plane mode of the pylon (OOPM) and the longitudinal mode (LM) are comparatively small with variations lower than 0.1% for the considered damage levels (Figure 6.17a).

The same procedure is carried out in order to evaluate the effect of the same kind of damage on the diagonal MAC coefficients. First, the effect of damage position is investigated showing that the most sensitive modes are the torsional mode (M3 in Figure 6.18a), the two mixed modes (M4 and M5 in Figures 6.18b and 6.18c) and the second vertical mode (M6 in Figure 6.18d) where maximum variations are in the range of 12-25%. The other mode shapes are characterized by diffused damage induced diagonal MAC variations so small that they lose any practical interest especially in comparison with the corresponding variations due to measurement uncertainty/variability and thermal effects. It is noteworthy that the trend of the variations as a function of the damage position is almost symmetric with respect to the pylon position, reaching maximum variations when the damage affects

the central group of the 2 arrays of cables.
The variations in the most sensitive mode shapes as a function of the damage level are therefore discussed and showed in Figure 6.19 with reference to the position at which maximum variations of MAC occur: DP=0.2667 (a) and DP=0.80 (b). The diagonal MAC decreases rapidly with the increase of the damage level following almost a quadratic trend. The lower variations are obtained for the second vertical mode shape (M6) while the other

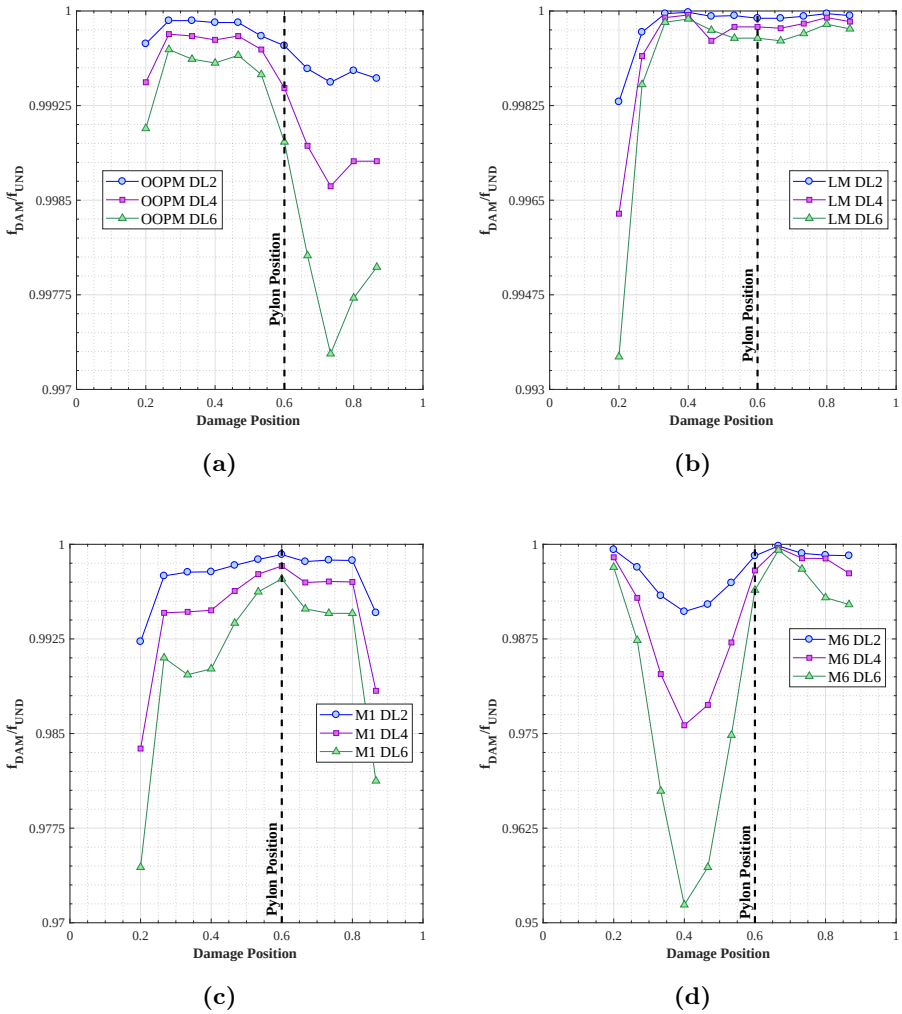

Fig. 6.15: Damage effects on the natural frequencies of the cable-stayed footbridge: frequency ratios of the first out of plane mode of the pylon (a), longitudinal mode (b) and the first and second vertical vibration modes (c and d, respectively) as a function of the damage position for DL2, DL4 and DL6 affecting 4 consecutive cables.

considered mode shapes present variations in the range of 10 - 25 % for all the damage level corresponding to a stiffness reduction higher than 30%.

The comparison between temperature and damage effects on natural frequencies highlights that small variations in the operating conditions produces apparent changes in eigenfrequencies that can be likely more significant than those produced by small damage. However, when damage severity and extension increase, changes in natural frequencies are sig-

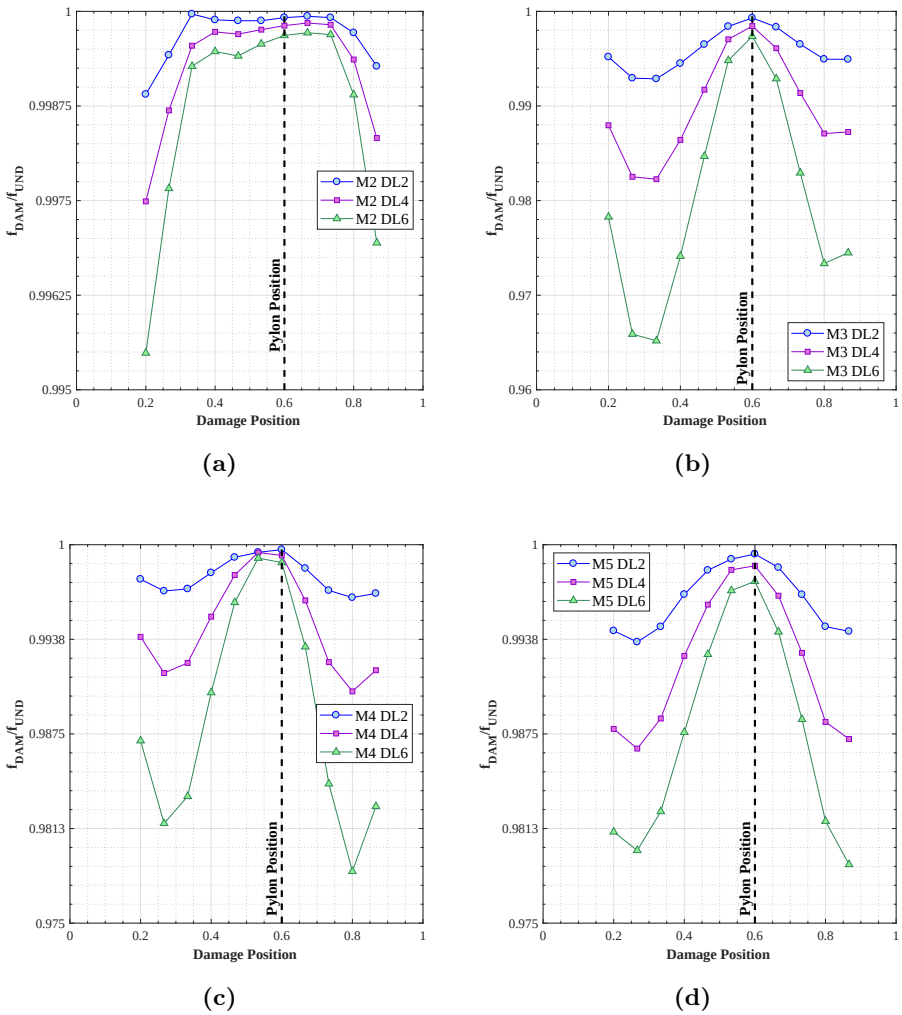

Fig. 6.16: Damage effects on the natural frequencies of the cable-stayed footbridge: frequency ratios of the first out of plane mode of the pylon (a), longitudinal mode (b) and the first and second vertical vibration modes (c and d, respectively) as a function of the damage position for DL2, DL4 and DL6 affecting 4 consecutive cables.

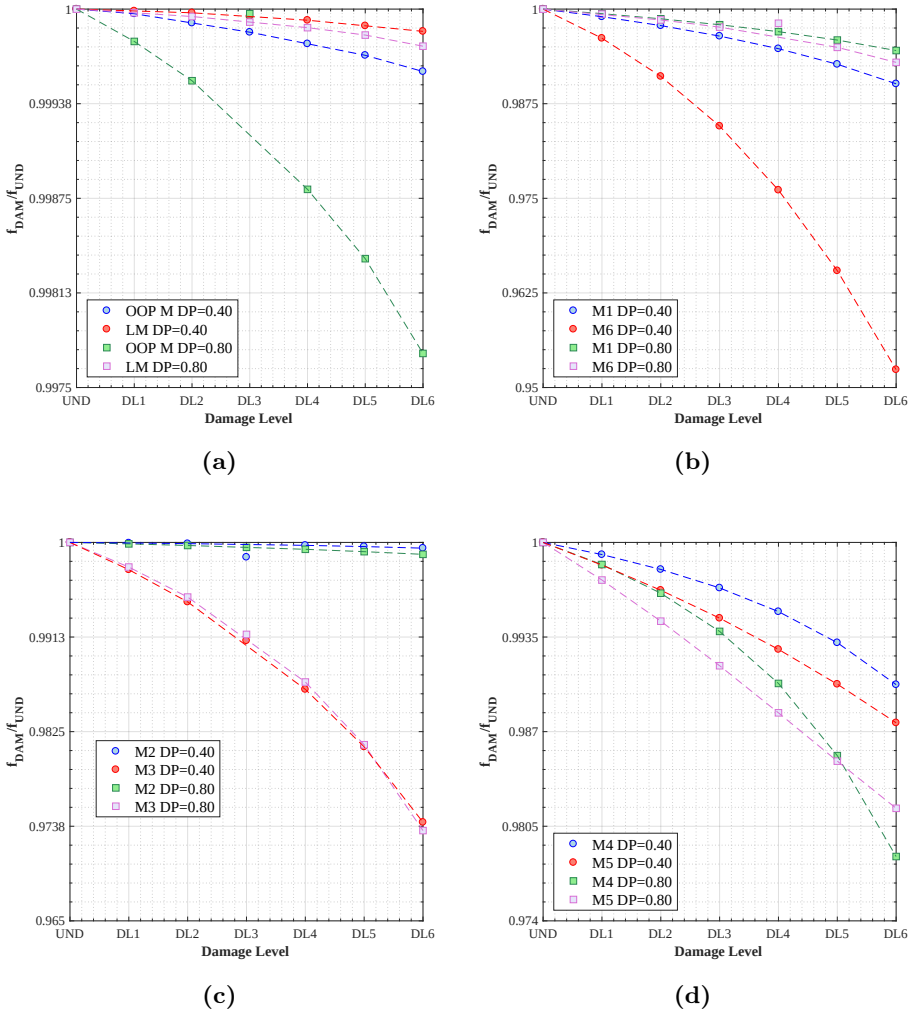

Fig. 6.17: Damage effects on the natural frequencies of the cable-stayed footbridge: frequency ratios of the out of plane mode of the pylon and the longitudinal modes (a), the first and the second vertical modes (b), the lateral and the torsional modes (c) and the two mixed vibration modes (d) as a function of the damage levels for two fixed positions DP=0.40 and DP=0.80 with damage affecting four consecutive cables.

nificantly higher than those produced by daily and seasonal fluctuations of temperature. Furthermore, variations of natural frequencies with temperature are linear and therefore temperature effect can be easily removed from the identified natural frequency time histories when a lot of observations are available.

Analysis results also show that frequencies are affected by damage position, damage ex-

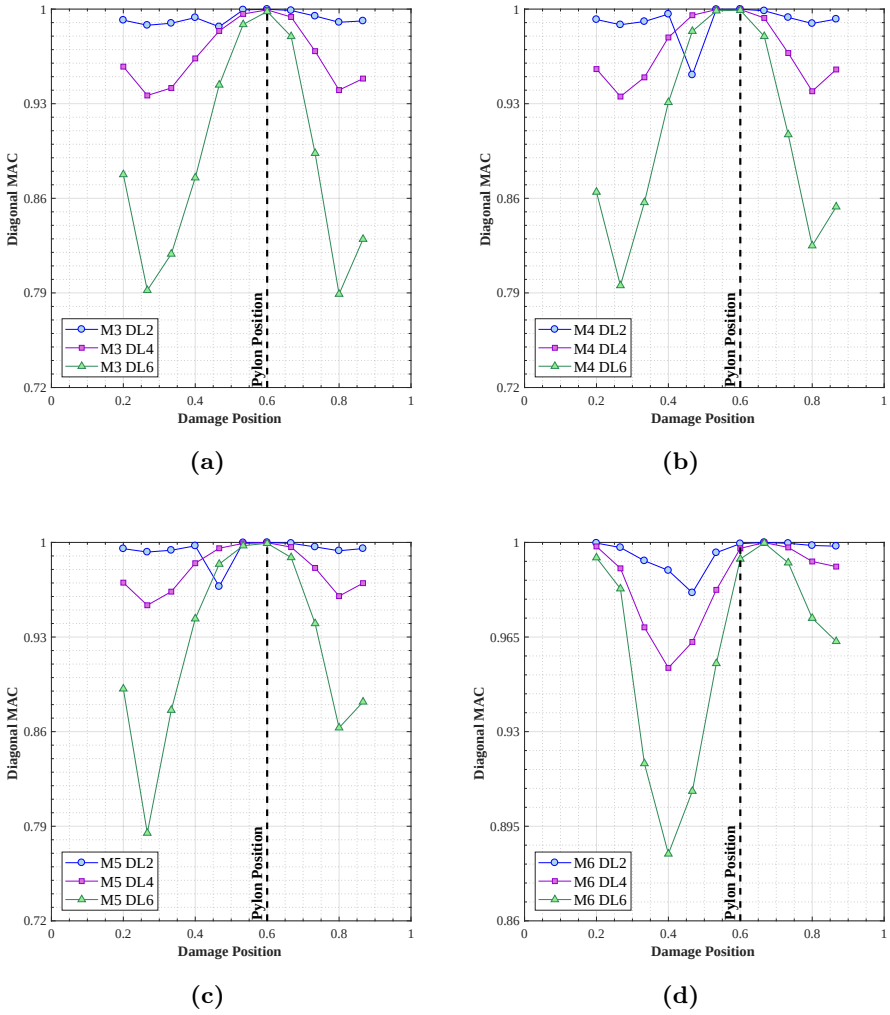

Fig. 6.18: Damage effects on the vibration modes of the cable-stayed footbridge: diagonal MAC coefficients of the torsional (a), the two mixed (b and c, respectively) and the second vertical vibration modes as a function of the damage position for DL2, DL4 and DL6 when damage affect four consecutive cables .

tension and level in quantitatively similar ways and therefore the damage quantification is not possible using natural frequencies as damage indicator. In fact, when small damage occurs (e.g single cable is subjected to maximum level of damage or consecutive cables affected by minimum level of damage) the frequency shifts are almost negligible or however smaller than the variations in the operating conditions (base excitation amplitude) and signal processing parameters. It is also difficult to detect the damage position using nat-

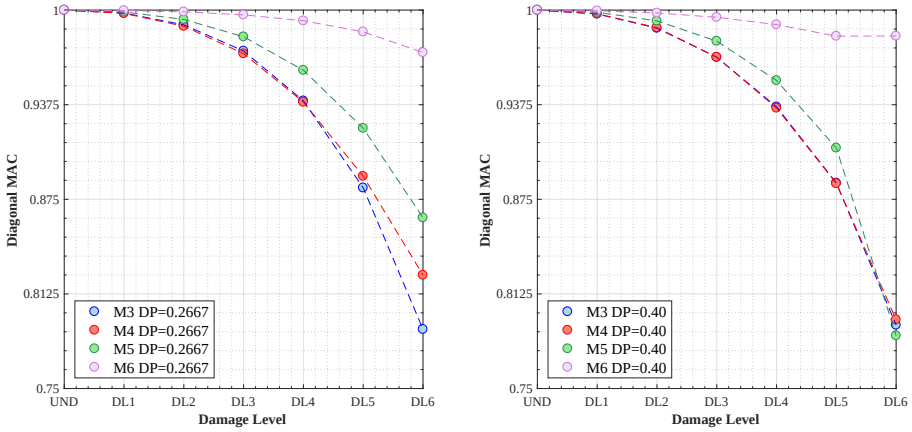

(a) **(b)**

Figure 6.19: Damage effects on the vibration modes of the cable-stayed footbridge: diagonal MAC of the torsional, the two mixed and the second vertical vibration mode shapes as a function of the damage levels for two fixed positions DP=0.2667 (a) and DP=0.40 (b) with damage affecting four consecutive cables.

ural frequencies since the same eigenfrequency shifts occur for different damage positions, level and extensions.

The diagonal MAC appears to be potentially a most powerful damage sensitive feature. The comparison between the temperature and the damage effects on the eigenvector highlights that small variations in temperature do not produce changes in the diagonal MAC. On the contrary, when significant damage extension is considered, even for low level of damage, changes in the diagonal MAC are significant. However, the eigenvectors are very sensitive to the operating conditions (amplitude of excitation) and signal processing parameters. Moreover, results show that the damage, the operating conditions and the signal processing parameters effects on the diagonal MAC shifts are comparatively similar making damage identification using MAC as damage indicator actually a challenge.

6.5 Effect of uncertainties on damage detection

After the preliminary results concerning the evaluation of the effects induced on modal frequencies and modal vectors by temperature, damage, base amplitude of excitation and signal processing parameters, the continuous dynamic responses is simulated.

Some details on the response simulation are produced first focusing the attention on the

main results obtained from the parametric analysis carried out in order to understand the effect induced on the eigenproperties by the base level of excitation, the signal processing parameters and the temperature.
First, the effect of amplitude base excitation plays a crucial role. The parametric analysis carried out in order to quantify the measurement uncertainty has shown that the variability of the identified modal frequencies and modal vectors is almost negligible when low level of excitation occur (A1 and A2 with reference to the nomenclature used in Section 6.2). Furthermore when the structural system is excited by low amplitude excitation the signal processing parameters (e.g. length of the signal, frequency resolution in the output PSDs) do not have a significant influence on natural frequencies and vibration modes; on the contrary, the accuracy of the experimental results depends strictly on the frequency resolution and on the time length of the signals when high base excitation is used. For this reason it has been chosen to simulate the continuous response using base excitation having white noise characteristics and a standard deviation equal to $0.03g$ (A1) and $0.06g$ (A2), where g is the acceleration of gravity.
The results of the parametric deterministic analysis carried out in order to quantify the accuracy of the experimental results when different time length of the signals are used has shown that a time length of half an hour can be considered as a sort of "optimal time length" for the dynamic response time histories to be used in the EFDD method. For this reason both modal frequencies and modal vectors are identified from continuous response simulated time histories lasting 30 minutes, 40 minutes and 1 hour. Finally, it has been shown that the frequency resolution does not have a crucial role in the estimation of the eigenfrequencies and eigenvectors, therefore a number of frequency lines in the output PSDs spectrum equal to 1024, 2048 and 4096 is used in the EFDD method.
The deterministic parametric analysis carried out in order to evaluate the effect of temperature on both eigenvectors and eigenfrequencies has shown that temperature induced eigenvector variations are negligible and that eigenfrequencies variations and changes in temperature are characterized by a linear relation. In literature there are well established methods for removing successfully the effect of temperature on natural frequency time histories when the natural frequency and temperature variations are linearly dependent. For this reason the simulation of continuous response is carried out neglecting the temperature effects.
Finally the parametric deterministic sensitivity analysis carried out for the evaluation of the damage induced effects on the system modal properties has been used in order to choose the damage scenario (DS) to be reproduced using continuous response simulation.

1. DS - 1:$\{DE = 0.0667, DP = 0.0667, DL6\}$
   This damage scenario is characterized by a damage diffused in the 1^{st} cable (with reference to Figure 6.10) corresponding to a damage position DP=0.0667 with maximum level of damage DL6 (i.e. reduction in cable stiffness of 60%). According to the results of the parametric analysis the maximum eigenfrequency variations are expected at the first and second vertical mode shapes (M1 and M6).

2. DS - 2:$\{DE = 0.20, DP = 0.80, DL6\}$
   This damage scenario is characterized by a damage diffused in the 10^{th},11^{th},12^{th},13^{th} cable (with reference to Figure 6.10) corresponding to a damage position DP=0.80 and to a damage extension of DE=0.20 with maximum level of damage DL6; according to the results of the parametric analysis the maximum eigenfrequency variations are expected at the torsional and the two mixed mode shapes (M3, M4 and M5).

3. DS - 3:$\{DE = 0.20, DP = 0.2667, DL6\}$
   This damage scenario is characterized by a damage diffused in the 2^{nd},3^{rd},4^{th},5^{th} cable (with reference to Figure 6.10) corresponding to a damage position DP=0.2667 and to a damage extension of DE=0.20 with maximum level of damage DL6; according to the results of the parametric analysis the maximum eigenvectors variations are expected at the torsional and the two mixed mode shapes (M3, M4 and M5).

The combinations of the damage position, level and extension have been selected in order to represent the artificial damage that provides the maximum variations in terms of natural frequencies and diagonal MAC basing on the results of the numerical parametric analysis shown in previous section. It is important to point out that the three defined damage scenarios allow to discuss the capability of the procedure to detect damage using the natural frequencies and the diagonal MAC as damage sensitive features when small, moderate or severe damage occur.
The continuum response simulation is therefore performed for each damage scenario using base excitation time histories A1 and A2 lasting two hours. Since three different time lengths of the virtual signals (30 minutes, 40 minutes and 1 hours) are used as input in the EFDD method and three different numbers of frequency lines (1024, 2048 and 4096) are used for the estimation of the output PSDs spectrum, for each damage scenario a set of 54 values of eigenfrequencies and diagonal MAC values are obtained.
Once that the variability of the modal parameters has been assessed in each damage scenario by varying the considered input factors, the capability to detect the artificial damage is discussed by comparing directly the set of eigenproperties obtained from the continuous

response of the structure in its damaged and undamaged state.
The artificial damage in DS-1 cannot be detected using the natural frequencies and the diagonal MAC coefficient as damage sensitive features. In fact, the set of the natural frequencies and the diagonal MAC coefficients identified in all the virtual data sets obtained from continuous response of the structure in its damaged state is not so different from the corresponding quantities obtained in case of undamaged state. Therefore it is impossible to distinguish if the variations in the natural frequencies and the diagonal MAC are due to the measurement uncertainty or to the presence of a severe local damage.
The effect of the artificial damage in DS-2 on both natural frequencies and diagonal MAC is instead evident in some mode shapes. Figure 6.20 shows the 54 values of natural frequencies identified from the virtual measurements obtained from the continuous response of the structure in its undamaged state (green empty circles). The variability of the natural frequencies related to the level of input base excitation is highlighted. The red filled area shows the total variability of the 54 natural frequencies identified from the different virtual data sets obtained from the continuous response of the structure in its damaged state.

The deterministic numerical analysis has shown that the the maximum variations in the natural frequency with respect to the undamaged state occur for the torsional mode shape (M3) and the two mixed mode shapes (M4 and M5). This result is only partially confirmed by the simulated response based dynamic identification procedure. In fact, the two sets of natural frequencies corresponding to a damaged and an undamaged state are characterized by two very well different trends only at the torsional mode shape (M3 in Figure 6.20a) and the first mixed mode shape (M4 in Figure6.20b). The results are completely different for the second mixed mode shape (M5 in Figure 6.20c). In this case it is clearly not possible to distinguish the effects on eigenfrequencies induced by a severe damage from the measurement variability. Confirming the results of the deterministic numerical analysis, all the other mode shapes are characterized by damage induced natural frequency variations almost negligible with reference to the undamaged state showing a behavior similar to the second vertical mode shape (M6 in Figure 6.20d).
It is noteworthy that even if the continuous response of the damaged structure is simulated using low levels of excitation and the dynamic identification is carried using virtual signals lasting more that 30 minutes, the variability of the eigenfrequencies remains significantly high in the mode shapes most sensitive to the considered damage scenario.
The same kind of analysis is carried out in order to assess if the diagonal MAC coefficients can be considered an effective damage sensitive feature. According to the results of the deterministic numerical analysis, the most significant damaged induced diagonal

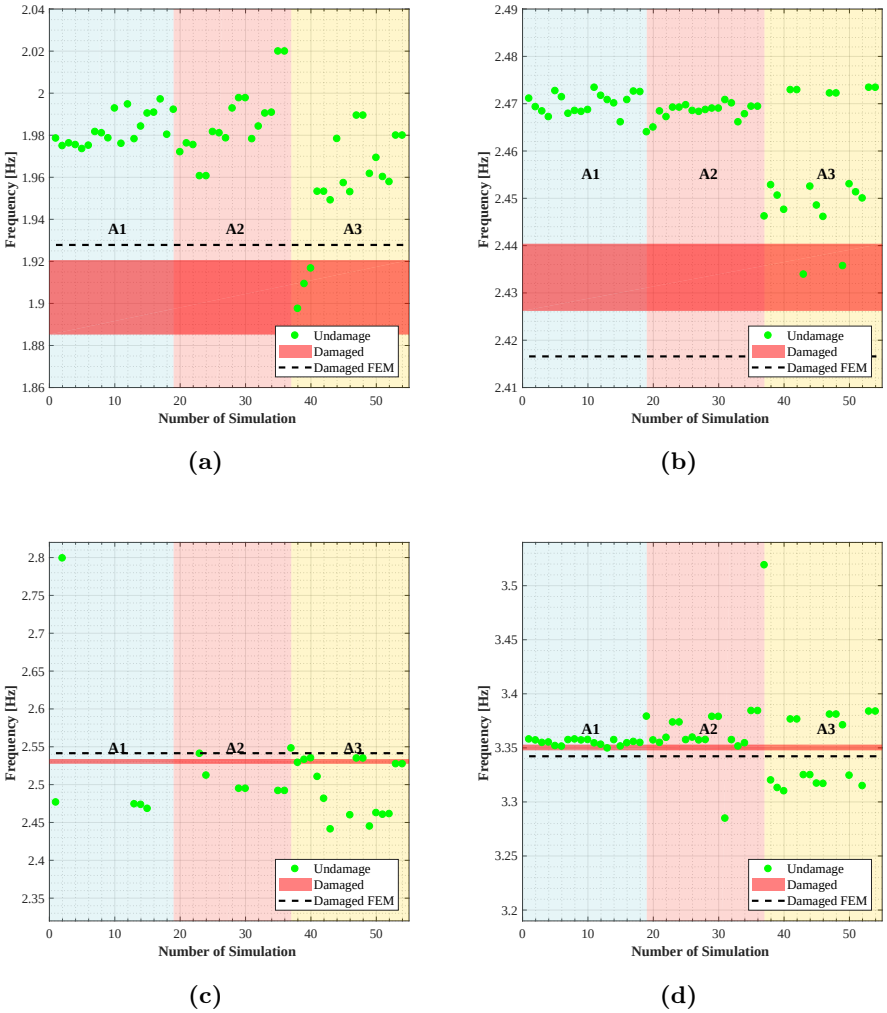

Fig. 6.20: Comparison between the distribution of eigenfrequencies identified from the virtual continuous simulation response of the structure it its damaged and undamaged state for the torsional mode shape M3 (a), the two mixed mode shapes M4 and M5 (b and c) and the second vertical mode shape M6 (d) in damage scenario DS-2.

MAC variations are expected at the torsional (M3) and the two mixed mode shapes (M4 and M5). Also in this case this result is confirmed only partially. In fact, the two sets of diagonal MAC coefficients obtained from the virtual continuous dynamic response of the structure in its damaged and undamaged state follow two very well separated trends only when the first mixed mode shape (M4 in Figure 6.21c) is considered. The torsional and the second mixed mode shapes (M3 and M5, respectively) present an opposite behavior: the

variability of the diagonal MAC coefficients related to the undamaged state is so high that damage induced diagonal MAC variations cannot be distinguished from the uncertainty due to the operating conditions (Figures 6.21b and 6.21d).
It is important to note that even if the deterministic parametric analysis has not shown significant variations in the diagonal MAC coefficient related to the first vertical mode shape (M1 in Figure 6.21a) the two sets of diagonal MAC coefficients obtained from the virtual continuous dynamic response of the structure in its damaged and undamaged state follow two very well separated trends.

The effect of the artificial damage in DS-3 is again analyzed in terms of variations of natural frequencies and diagonal MAC coefficients between the damaged and the undamaged state.
Figure 6.22 shows the comparison between the two sets of natural frequencies obtained from continuous structural responses of the structure in damaged and undamaged state for the torsional and the two mixed modes (M3, M4 and M5). It is important to observe that in this damage scenario the results of the parametric deterministic analysis have shown that the most significant damage induced variations in the eigenfrequencies with reference to the undamaged state occur for the torsional and the mixed mode shapes (M3, M4 and M5 in Figures 6.22a 6.22b and 6.22c). Also in this case results are only partially confirmed by the continuous response simulation of the damaged structure. The two sets of eigenfrequencies follow two very well separated trends only for the torsional and the first mixed mode shape (M3 and M4).

The same kind of analysis is carried out for analyzing the damage induced eigenvector variations in terms of diagonal MAC coefficients. According to the results of the deterministic numerical analysis the most significant damaged induced diagonal MAC variations are expected for the torsional (M3) and the two mixed mode shapes (M4 and M5). As in previous damage scenario this result is confirmed only partially. In fact, the two sets of diagonal MAC coefficients obtained from the virtual continuous dynamic response of the structure in its damaged and undamaged state follow two very well separated trends only in correspondence of the first mixed mode shape (M4 in figure 6.23c). The variability of the diagonal MAC coefficient in the torsional (M3 in figure 6.23b) and the second mixed mode shape (M5 in Figure 6.23d) related to the undamaged state is so high that damage induced diagonal MAC variations cannot be distinguished from the uncertainty due to the operating conditions.
Furthermore - as in previous damage scenario analysis - the two sets of diagonal MAC coefficients related to the first vertical mode shape (M1 in Figure 6.23a) in a damaged and

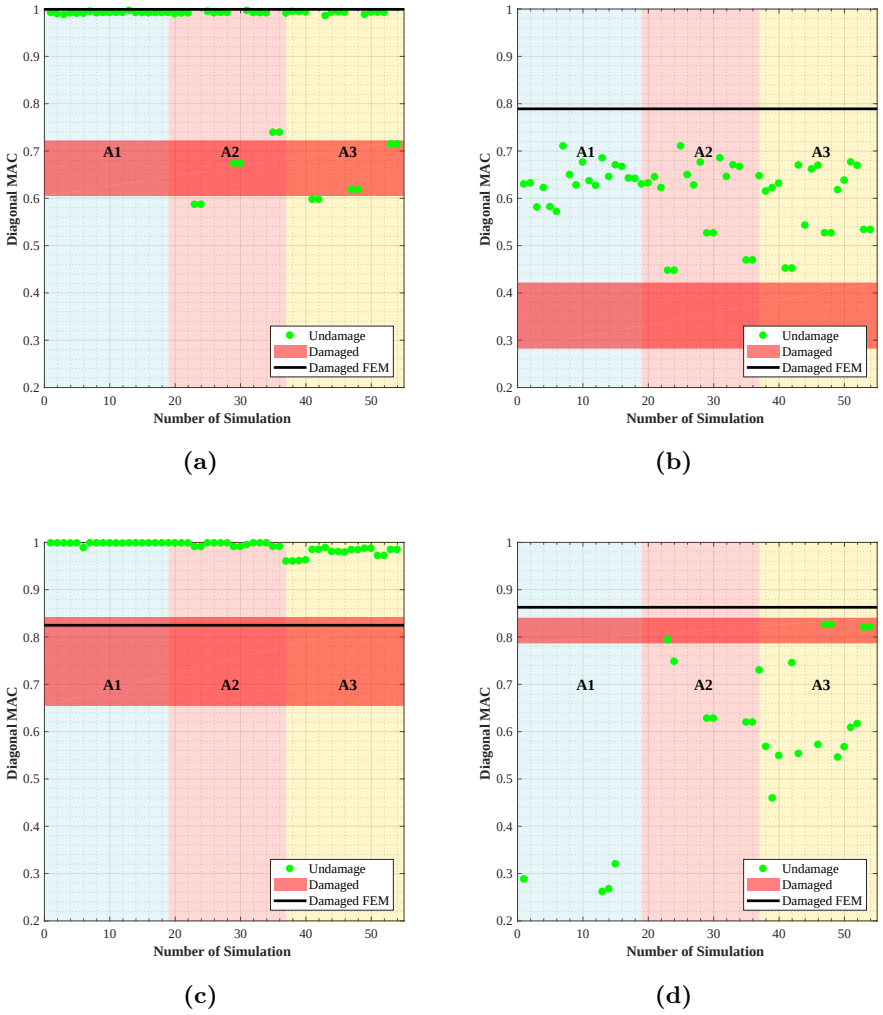

Fig. 6.21: Comparison between the distribution of diagonal MAC identified from the virtual continuous simulation response of the structure it its damaged and undamaged state for the first vertical mode M1(a) torsional mode shape M3 (b) and the two mixed mode shapes M4 and M5 (b and c) in damage scenario DS-2 .

undamaged state follow very well separated trends, even though the parametric deterministic analysis has shown that the first vertical mode shape is not one of the most sensitive to damage induced variations.

Summarizing, the eigenproperties variations between the damaged and the undamaged state cannot be recognized using continuous response simulation when a localized severe damage occur as in damage scenario DS-1. On the contrary, eigenfrequencies and eigen-

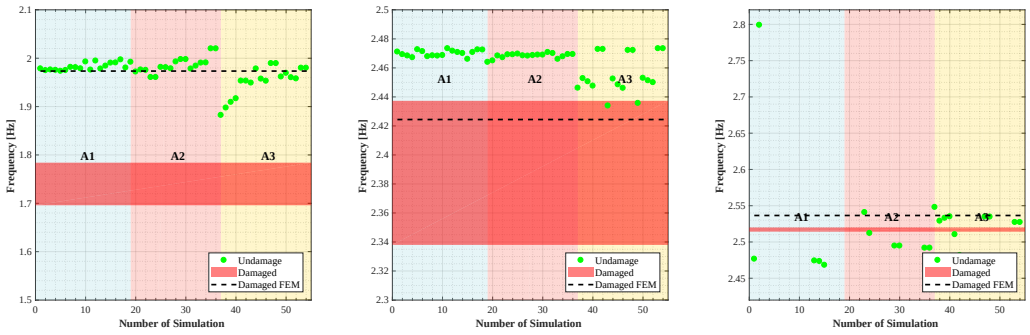

(a) **(b)** **(c)**

Fig. 6.22: Comparison between the distribution of eigenfrequencies identified from the virtual continuous simulation response of the structure it its damaged and undamaged state for the torsional mode shape M3 (a) and the two mixed mode shapes M4 and M5 (c and d) in damage scenario DS-3.

vectors variations between the damaged and the undamaged state can be recognized using continuous response simulation when damage is severe in terms of both damage position and damage extension.

Usually in literature the damage identification is performed by considering just the natural frequencies as suitable damage indicator. In this application, the diagonal MAC appears to be a powerful damage detection feature. This is due to the fact that the cable stayed footbridge is an high redundant structure and the eigenvectors, that reflects the distribution of the mass, the stiffness and the boundary conditions of the model, are most influenced by damage occurring on the cables. Furthermore even if the MAC matrix is a global quantity able to estimate the correlation between two different modal vectors, it is very sensitive also to small variations in single modal components.

Finally, as discussed in the previous section, the damage localization and quantification remains still a challenge since the effect of damage position, extension and severity provide comparable variations in both natural frequencies and MAC coefficients.

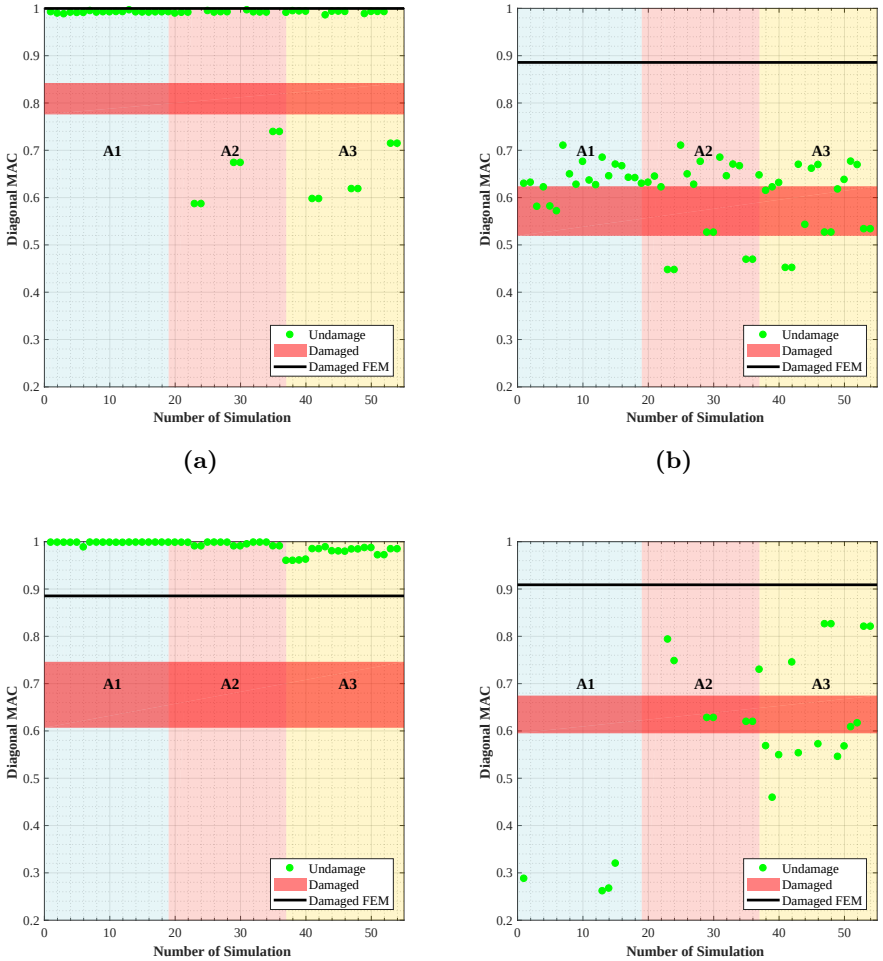

Fig. 6.23: Comparison between the distribution of diagonal MAC identified from the virtual continuous simulation response of the structure it its damaged and undamaged state for the first vertical mode M1(a) torsional mode shape M3 (b) and the two mixed mode shapes M4 and M5 (b and c) in damage scenario DS-3 .

Chapter 7

Conclusions

The present dissertation has dealt with the role of uncertainties in structural dynamic identification and damage detection. This chapter summarizes the most important conclusions of the thesis responding appropriately to the three research questions stated in Chapter 1:

(a) *Is it possible to reduce the uncertainties related to the modal parameter estimates due to different operating conditions occurring during the tests and signal sampling parameters?*

(b) *Is it possible to identify the existence, the localization and the severity of damage by means of global quantities such as the modal parameters? Which are the most suitable damage indicators to be used?*

(c) *Is it possible to overcome the limitations of the Bayesian updating framework speeding up the posterior evaluation by means of suitable and reliable procedures?*

First, the issue of reducing the computational costs related to the posterior evaluation in structural identification of complex structure such as cable stayed footbridge when real experimental modal data are used as target has been addressed.

The first stage of this work involved full scale ambient vibration tests to estimate the modal parameters of the structural system: natural frequencies, vibration modes and damping ratios. In particular, damping ratio estimates have been evaluated by varying the sampling parameters in order to assess the reliability of the obtained results. On the other side, the initial three-dimensional finite element numerical model of the footbridge has been developed taking into account the significance of non linear behavior of this class of bridge that is mainly due to cable sag and large deflection. An in depth sensitivity analysis is carried out from a deterministic and a probabilistic point of view for selecting the updated parameters in an efficient manner determining all the physical parameters having effects on the measured natural frequencies and mode shapes used as reference in the updating framework.

The finite element model response has been approximated by surrogate models in order to reduce significantly the computational burden using Polynomial Chaos representation method. The use of this kind of surrogate models in finite element analysis is well known in literature for representing the model predicted natural frequencies. In the proposed framework the polynomial chaos expansion based surrogate models have been extended and used for approximating both natural frequencies and eigenvector components, allowing to explicitly treat the experimental modal vector components as target in the Bayesian updating framework. Furthermore, the deterministic coefficients have been estimated combining least square minimization method and Gaussian quadrature rule making the whole procedure easy to be implemented from a computational point of view and particularly suitable to be used in continuous real time monitoring applications.

The posterior distribution has been evaluated using classical Markov Chain Monte Carlo - Metropolis Hastings procedure replacing the solution of the deterministic numerical model with the surrogate solution at each step of the chain. The importance of using an informative data set in the whole updating procedure has been demonstrated by a quantitative assessment of the remaining model uncertainties when different reference data sets are used.

Two main intermediate contributions are introduced to overcome the main limitations about the use of real experimental modal data: the first one regards the capability to take into account the correlation of model prediction errors during the procedure for the evaluation of the posterior distribution; the second one regards the formulation of the likelihood function rewritten in terms of modal assurance criterion when modal vectors are included in the reference data set. The modal vector prediction error is considered as the distance between perfect correlation and actual correlation for pair of experimental and numerical

eigenvectors.
Since it has been proven that the least square minimization is a suitable computational method for tuning the surrogate models and that the spectral expansion method can be used for the evaluation of the posterior distributions, the proposed procedure lends itself to be used in real time Structural Health Monitoring applications for assessing the performance of structures.
Therefore, a natural future development of this research work is to assess the effectiveness of the Bayesian updating to identify damage in terms of stiffness loss when small variations in the modal properties occur.

Second, the issue of analyzing the measurement uncertainties has been faced. The Enhanced Frequency Domain Decomposition method has been selected for extracting the modal parameters of the cable stayed footbridge in order to assess the capability of this method to be used in real time Structural Health Monitoring applications. Usually different methods (e.g. Stochastic Subspace Identification) easier to be automatized are used. Actually the Enhanced Frequency Domain Decomposition is a user friendly output only dynamic identification technique and therefore particularly suitable to be used by different kind of users with different level of details. In fact, the main scope of Structural Health Monitoring is to continuously monitor the evolution in time of the main modal parameters in order to detect damage when some change occur. This could be particularly useful for public administrations in maintenance programs, for Civil Defense in post emergency state management or for engineerings and practitioners in structural design and verification.
The main hypotheses at the base of Enhanced Frequency Domain Decomposition is that the structure is subjected to some kind of load excitation having white noise characteristics and that the structure is lightly damped. For this reason the measurement uncertainty analysis has been carried out when these two main assumptions are complied. The footbridge updated numerical model has been dynamically loaded by white noise base excitations with different amplitude in order to assess the effectiveness of the considered dynamic identification technique to provide natural frequencies, vibration modes and damping ratio when high excitation levels occur, e.g tremors or micro tremors. Then, the system identification has been performed using pseudo experimental response time histories by varying the signal sampling parameters (time length of the signals and frequency resolution of the output Power Spectral Density spectrum).
It has been shown that the variability of the natural frequencies and the vibration modes is related mainly to the base excitation amplitude and that the Enhanced Frequency Domain

Decomposition can provide misleading results when high excitation levels occur. Furthermore, an optimal time length of the signal has been obtained providing a useful recommendation for data processing in both single ambient vibration measurement campaign and continuous monitoring. Completely different results have been obtained for damping ratios: on one side, the considered sources of uncertainty has significant influence on the results and the frequency resolution of the output Power Spectral Density spectrum can be properly chosen for minimizing the leakage bias errors; on the other side, the obtained damping ratio estimates are not so accurate. Therefore the damping ratio estimation using output only dynamic identification technique in frequency domain remains a challenge.
For all these reasons the Enhanced Frequency Domain Decomposition method can be considered a reliable dynamic identification technique for natural frequencies and vibration modes. The natural future development for this research work is to quantify the uncertainties of the modal properties when different kind and a vast amount of real data are used.

The third issue concerning the damage detection - in terms of damage existence, location and quantification - has been finally addressed taking into account the measurement uncertainties.
Despite the vast amount of literature works, a lack of knowledge on the actual effectiveness of vibration based damage detection can be recognized. Trying to bridging this gap the last part of the thesis is focused on closing the procedure - which goes from modal properties extraction and structural parameters identification - by discussing the capability to detect a damage in complex redundant structure such as cable stayed footbridges by global quantity (mainly natural frequencies and vibration modes) variations used as damage sensitive features.
The updated footbridge numerical model is employed for comparing damage induced variations of natural frequencies and modal assurance criterion diagonal matrix with those induced by temperature variations and those produced by all the uncertainty related to system identification. The analytical model in different damaged state has been also used for generating pseudo experimental random response when different kind of dynamic base excitation occur. The modal parameters have been extracted from such experimental data and have been used for revealing the presence of a damage through direct comparison with the set of modal parameters identified from pseudo experimental data obtained in case of undamaged structure and accounting for measurement uncertainties.
Usually in literature the damage identification is performed by considering just the natural frequencies as suitable damage indicator. In this application, the diagonal modal assurance

criterion matrix appears to be a powerful damage detection feature, since it is the only global quantity able to provide information about local damage phenomena being strongly dependent to the spatial sensors location.
The damage presence can be identified only when severe damage occurs while the damage localization and quantification remains a challenge since the effect of the damage position and extension provides comparable variations in both natural frequencies and modal assurance criterion matrix.
The presented results have been entirely based on simulated data under the main hypotheses of output only dynamic identification techniques validity. In this sense, a natural future development of this work is to extend the obtained results accounting for different external factors such as wind and measurement noise.

Bibliography

[1] A.M. Ghaffar and M.A. Khalifa. "Importance of Cable Vibration in Dynamics of Cable Stayed Bridges". In: *Journal of Engineering Mechanics* 117.11 (1991), pp. 2571–2589. DOI: 10.1061/(ASCE)0733-9399(1991)117:11(2571).

[2] J.M.W. Brownjohn and P. Q. Xia. "Dynamic Assessment of Curved Cable-Stayed Bridge by Model Updating". In: *Journal of Structural Engineering* 126.2 (2000), pp. 252–260. DOI: 10.1061/(ASCE)0733-9445(2000)126:2(252).

[3] Ministero delle Infrastrutture e dei Trasporti. *Relazione Commissione Ispettiva*. 25 / 09/ 2018, pp. 37 –38.

[4] E. Simoen, G. De Roeck, and G. Lombaert. "Dealing with uncertainty in model updating for damage assessment: A review". In: *Mechanical Systems and Signal Processing* 56-57 (2015), pp. 123 –149. DOI: https://doi.org/10.1016/j.ymssp.2014.11.001.

[5] T. Marwala. *Finite-element-model Updating Using Computational Intelligence Techniques*. Springer-Verlag,London, UK, 2010.

[6] A. Tarantola. *Inverse Problem Theory and Methods for Model Parameter Estimation*. Society for Industrial and Applied Mathematics, 2005. DOI: 10.1137/1.9780898717921.

[7] T. Bayes. "An essay towards solving a problem in the doctrine of chances". In: *Philosophical Transactions of the Royal Society* 53 (1763), pp. 370 –418.

[8] J. L. Beck and L. S. Katafygiotis. "Updating Models and Their Uncertainties. I: Bayesian Statistical Framework". In: *Journal of Engineering Mechanics* 124.4 (1998), pp. 455–461. DOI: 10.1061/(ASCE)0733-9399(1998)124:4(455).

[9] M. W. Vanik, J. L. Beck, and S. K. Au. "Bayesian Probabilistic Approach to Structural Health Monitoring". In: *Journal of Engineering Mechanics* 126.7 (2000), pp. 738–745. DOI: 10.1061/(ASCE)0733-9399(2000)126:7(738).

[10] K.V. Yuen. *Bayesian methods for structural dynamics and civil engineering. First edition.* John Wiley and Sons, Singapore, 2010.

[11] S. Lambros et al. "A probabilistic approach to structural model updating". In: *Soil Dynamics and Earthquake Engineering* 17.7 (1998), pp. 495 –507. DOI: https://doi.org/10.1016/S0267-7261(98)00008-6.

[12] J. L. Beck. "Bayesian system identification based on probability logic". In: *Structural Control and Health Monitoring* 17.7 (2010), pp. 825–847. DOI: 10.1002/stc.424.

[13] G.E.P. Box and G.C. Tiao. *Bayesian Inference in Statistical Analysis.* Wiley, New York, 1992.

[14] D.J. Ewins. *Modal testing: theory and practice.* Mechanical engineering research studies: Engineering dynamics series. Research Studies Press, 1984.

[15] F. Magalhães and A. Cunha. "Explaining operational modal analysis with data from an arch bridge". In: *Mechanical Systems and Signal Processing* 25.5 (2011), pp. 1431 –1450. DOI: https://doi.org/10.1016/j.ymssp.2010.08.001.

[16] J.M.W. Brownjohn et al. "Ambient vibration re-testing and operational modal analysis of the Humber Bridge". In: *Engineering Structures* 32.8 (2010), pp. 2003 –2018. DOI: https://doi.org/10.1016/j.engstruct.2010.02.034.

[17] E. Reynders et al. "Combined Experimental-Operational Modal Testing of Footbridges". In: *Journal of Engineering Mechanics* 136.6 (2010), pp. 687–696. DOI: 10.1061/(ASCE)EM.1943-7889.0000119.

[18] L.F. Ramos et al. "Monitoring historical masonry structures with operational modal analysis: Two case studies". In: *Mechanical Systems and Signal Processing* 24.5 (2010). Special Issue: Operational Modal Analysis, pp. 1291 –1305. DOI: https://doi.org/10.1016/j.ymssp.2010.01.011.

[19] C. Gentile and C. Saisi. "Operational modal testing of historic structures at different levels of excitation". In: *Construction and Building Materials* 48 (2013), pp. 1273 –1285. DOI: https://doi.org/10.1016/j.conbuildmat.2013.01.013.

[20] C. Ruzzo et al. "Operational Modal Analysis of a Spar-Type Floating Platform Using Frequency Domain Decomposition Method". In: *Energies* 9 (Oct. 2016), p. 870.

[21] S. Chauhan et al. "Operational Modal Analysis of Operating Wind Turbines: Application to Measured Data". In: *Conference Proceedings of the Society for Experimental Mechanics Series* 5 (Mar. 2011), pp. 65–81.

[22] G. Oliveira et al. "Modal Identification of a Wind Turbine Before and After the Extension of the Blades". In: *IABSE Symposium Report* 105 (Sept. 2015), pp. 1–10.

[23] G. James, T. Carne, and J. Laufer. "The natural excitation technique (NExT) for modal parameter extraction from operating structures". In: *Journal of Analytical and Experimental Modal Analysis* 10 (Jan. 1995).

[24] B. Peeters and G. De Roeck. *Reference-Based Stochastic Subspace Identification for Output-Only Modal Analysis*. Vol. 13. Nov. 1999, pp. 855–878.

[25] T. P. Van Overschee McKelvey and B. De Moor. "Book review: Subspace Identification for Linear Systems: Theory, Implementation, Applications". In: *International Journal of Adaptive Control and Signal Processing* 12.6 (1998), pp. 540–541. DOI: 10.1002/(SICI)1099-1115(199809)12:6<540::AID-ACS505>3.0.CO;2-L.

[26] R. Brincker, L. Zhang, and P. Andersen. "Modal identification from ambient responses using frequency domain decomposition". In: *Proceedings of the International Modal Analysis Conference - IMAC* 1 (Jan. 2000).

[27] R. Brincker, C. Ventura, and P Andersen. *Damping estimation by Frequency Domain Decomposition*. Jan. 2001.

[28] C. Farrar and K. Worden. *Structural Health Monitoring A Machine Learning Perspective*. Jan. 2013. ISBN: 978-1-119-99433-6.

[29] W.H. Hu et al. "Comparison of different statistical approaches for removing environmental/operational effects for massive data continuously collected from footbridges: statistical approaches for removing environmental/operational effects". In: (Oct. 2016).

[30] G. Comanducci et al. "Environmental effects on natural frequencies of the San Pietro bell tower in Perugia, Italy, and their removal for structural performance assessment". In: *Mechanical Systems and Signal Processing* 82 (May 2016).

[31] J. S. Bendat and A. G. Piersol. *Random Data: Analysis and Measurement Procedures*. New York, NY, USA: John Wiley & Sons, Inc., 2000. ISBN: 0471317330.

[32] H. Cramer and M. R. Leadbetter. *Stationary and related stochastic processes : sample functions properties and their applications*. English. Wiley New York, 1967.

[33] W. Heylen, S. Lammens, and P. Sas. *Modal Analysis Theory and Testing*. Katholieke Universiteit Leuven, Faculty of Engineering, Department of Mechanical Engineering, Division of Production Engineering, Machine Design and Automation, 1998. ISBN: 9789073802612.

[34] L. Brincker R.and Zhang and P. Andersen. "Modal identification of output only systems using Frequency Domain Decomposition". In: *Smart Materials and Structures* 10 (June 2001), p. 441.

[35] R. Brincker and L. Zhang. "Frequency domain decomposition revisited". In: *IOMAC 2009 - 3rd International Operational Modal Analysis Conference* (Jan. 2009), pp. 615–626.

[36] R. Brincker. *Introduction to Operational Modal Analysis*. Wiley-Blackwell, 2015, pp. 1–16. ISBN: 9781118535141. DOI: 10.1002/9781118535141.ch1.

[37] A.J. Allemang. "The Modal Assurance Criterion (MAC): Twenty Years of Use and Abuse". In: *Journal of Sound and Vibrations* (2003), pp. 14–21.

[38] A. Brandt. *Noise and Vibration Analysis: Signal Analysis and Experimental Procedures*. Wiley, 2011. ISBN: 9780470978115.

[39] S.W. Doebling, C.R. Farrar, and M.B. Prime. "A Summary Review of Vibration-Based Damage Identification Methods". In: *Identification Methods," The Shock and Vibration Digest* 30 (1998), pp. 91–105.

[40] C. R. Farrar and K. Worden. "An Introduction to Structural Health Monitoring". In: *New Trends in Vibration Based Structural Health Monitoring*. Ed. by Arnaud Deraemaeker and Keith Worden. Vienna: Springer Vienna, 2010, pp. 1–17. DOI: 10.1007/978-3-7091-0399-9_1.

[41] J. Moughty and J. Casas. *A State of the Art Review of Modal-Based Damage Detection in Bridges: Development, Challenges, and Solutions*. Vol. 7. May 2017, p. 510.

[42] Anders Rytter. "Vibrational Based Inspection of Civil Engineering Structures". Ph.D.-Thesis defended publicly at the University of Aalborg, April 20, 1993 PDF for print: 206 pp. PhD thesis. Denmark, 1993.

[43] Jeong-Tae Kim et al. "Damage identification in beam-type structures: frequency-based method vs mode-shape-based method". In: *Engineering Structures* 25.1 (2003), pp. 57 –67. DOI: https://doi.org/10.1016/S0141-0296(02)00118-9.

[44] J.M. Ndambi, J. Vantomme, and K. Harri. "Damage assessment in reinforced concrete beams using eigenfrequencies and mode shape derivatives". In: *Engineering Structures* 24.4 (2002), pp. 501 –515. DOI: https://doi.org/10.1016/S0141-0296(01)00117-1.

[45] Y. Yamaguchi H. andMatsumoto et al. "Damage detection based on modal damping change in bridges". In: *In Proceedings of the 15th InternationalModal Analysis Conference,* (1997), 1531–1536.

[46] P. Moser and B. Moaveni. "Environmental effects on the identified natural frequencies of the Dowling Hall Footbridge". In: *Mechanical Systems and Signal Processing* 25 (Oct. 2011), pp. 2336–2357. DOI: 10.1016/j.ymssp.2011.03.005.

[47] B. Peeters and G. De Roeck. "One-year monitoring of the Z24-Bridge: environmental effects versus damage events". In: *Earthquake Engineering and Structural Dynamics* 30.2 (2000), pp. 149–171. DOI: 10.1002/1096-9845(200102)30:2<149::AID-EQE1>3.0.CO;2-Z.

[48] P. Cornwell et al. "Environmental variability on modal properties". In: *Experimental Techniques* 23.6 (1999), pp. 45–48. DOI: 10.1111/j.1747-1567.1999.tb01320.x.

[49] P. Peeters, J. Maeck, and G. De Roeck. "Vibration-based damage detection in civil engineering: excitation sources and temperature effects". In: *Smart Materials and Structures* 10.3 (2001), p. 518. DOI: 10.1088/0964-1726/10/3/314.

[50] A. Cabboi, C. Gentile, and A. Saisi. "From continuous vibration monitoring to FEM-based damage assessment: Application on a stone-masonry tower". In: *Construction and Building Materials* 156 (2017), pp. 252 –265. DOI: https://doi.org/10.1016/j.conbuildmat.2017.08.160.

[51] F. Ubertini et al. "Estimating aeroelastic effects from full bridge responses by operational modal analysis". In: *Journal of Wind Engineering and Industrial Aerodynamics* 99.6 (2011), pp. 786 –797. DOI: https://doi.org/10.1016/j.jweia.2011.03.016.

[52] F. Ubertini, A. L. Materazzi, and G. Comanducci. "Eigenfrequencies of damaged suspension bridges under wind". In: *IN VENTO* (Aug. 2012).

[53] C.W. Kim, M. Kawatani, and J. Hao. "Modal parameter identification of short span bridges under a moving vehicle by means of multivariate AR model". In: *Structure and Infrastructure Engineering* 8.5 (2012), pp. 459–472. DOI: 10.1080/15732479.2010.539061.

[54] E. Lai, C. Gentile, and M.G. Mulas. "Experimental and numerical serviceability assessment of a steel suspension footbridge". In: *Journal of Constructional Steel Research* 132 (2017), pp. 16 –28. DOI: https://doi.org/10.1016/j.jcsr.2017.01.005.

[55] P. Mohanty and D.J. Rixen. "Operational modal analysis in the presence of harmonic excitation". In: *Journal of Sound and Vibration* 270.1 (2004), pp. 93 –109. DOI: https://doi.org/10.1016/S0022-460X(03)00485-1.

[56] C. Devriendt et al. "Operational modal analysis in the presence of harmonic excitations by the use of transmissibility measurements". In: *Mechanical Systems and Signal Processing* 23.3 (2009), pp. 621 –635. DOI: https://doi.org/10.1016/j.ymssp.2008.07.009.

[57] B.M. Ayyub and G.J. Klir. " Uncertainty Modeling and Analysis in Engineering and the Sciences". In: *Chapman and Hall/CRC* (2006).

[58] H. G. Matthies. "Uncertainty Quantification with Stochastic Finite Elements". In: *Encyclopedia of Computational Mechanics* (2007). DOI: 10.1002/0470091355.ecm071.

[59] G.I. Schueller. "A state-of-the-art report on computational stochastic mechanics". In: *Probabilistic Engineering Mechanics* 12.4 (1997), pp. 197 –321. DOI: https://doi.org/10.1016/S0266-8920(97)00003-9.

[60] M. Grigoriu. *Stochastic Calculus: Applications in Science and Engineering*. Springer Science and Business Media, 2002.

[61] R. G. Ghanem and P. D. Spanos. *Stochastic Finite Elements: A Spectral Approach*. Berlin, Heidelberg: Springer-Verlag, 1991.

[62] R.E. Caflisch. "Monte Carlo and quasi-Monte Carlo methods". In: *Acta Numerica* 7 (1998), pp. 1–49. DOI: 10.1017/S0962492900002804.

[63] G.I. Schueller and P.D. Spanos. *Monte Carlo Simulation*. Taylor & Francis, 2001.

[64] R. L. Iman. *Latin Hypercube Sampling*. American Cancer Society, 2014. DOI: 10.1002/9781118445112.stat03803.

[65] S.A. Smolyak. "Quadrature and interpolation formulas for tensor products of certain classes of functions". In: *Dokl. Akad. Nauk SSSR* 148.5 (1963), pp. 1042 –1045.

[66] K. Konakli and B. Sudret. "Polynomial meta-models with canonical low-rank approximations: Numerical insights and comparison to sparse polynomial chaos expansions". In: *Journal of Computational Physics* 321 (2016), pp. 1144 –1169. DOI: https://doi.org/10.1016/j.jcp.2016.06.005.

[67] G.E.P. Box and N.R. Draper. *Response Surfaces for Mixture Ingredients*. Wiley-Blackwell, 2006. Chap. 16, pp. 509–533. DOI: 10.1002/9780470072769.ch16.

[68] W.J. Hill and W.G. Hunter. "A Review of Response Surface Methodology: A Literature Survey". In: *Technometrics* 8.4 (1966), pp. 571–590. DOI: 10.1080/00401706.1966.10490404.

[69] D. Xiu and G. E. Karniadakis. "The Wiener-Askey Polynomial Chaos for Stochastic Differential Equations". In: *SIAM J. Sci. Comput.* 24.2 (Feb. 2002), pp. 619–644.

[70] B. Sudret, S. Marelli, and J. Wiart. "Surrogate models for uncertainty quantification: An overview". In: *2017 11th European Conference on Antennas and Propagation (EUCAP)* (2017), pp. 793–797.

[71] R. Sharif. "A polynomial dimensional decomposition for stochastic computing". In: *International Journal for Numerical Methods in Engineering* 76.13 (2008), pp. 2091–2116. DOI: 10.1002/nme.2394.

[72] J. Rhim and S. W. Lee. "A neural network approach for damage detection and identification of structures". In: *Computational Mechanics* 16.6 (1995), pp. 437–443. DOI: 10.1007/BF00370565.

[73] E. Bernardini et al. "Aerodynamic shape optimization of civil structures: A CFD-enabled Kriging-based approach". In: *Journal of Wind Engineering and Industrial Aerodynamics* 144 (2015), pp. 154 –164. DOI: https://doi.org/10.1016/j.jweia.2015.03.011.

[74] C.E. Rasmussen and C.K.I. Williams. *Gaussian Processes for Machine Learning*. MIT Press, Jan. 2006, p. 248.

[75] Wiener N. "The Homogeneous chaos". In: *Am. J. Math* 60 (1938), pp. 897–936.

[76] B. Sudret. "Global sensitivity analysis using polynomial chaos expansions". In: *Reliability Engineering and System Safety* 93.7 (2008), pp. 964 –979. DOI: https://doi.org/10.1016/j.ress.2007.04.002.

[77] A. Kaintura, T. Dhaene, and D. Spina. "Review of Polynomial Chaos-Based Methods for Uncertainty Quantification in Modern Integrated Circuits". In: *Electronics* 7.3 (2018). DOI: 10.3390/electronics7030030.

[78] H. G. Matthies and C. Bucher. "Finite elements for stochastic media problems". In: *Computer Methods in Applied Mechanics and Engineering* 168.1 (1999), pp. 3 –17. DOI: https://doi.org/10.1016/S0045-7825(98)00100-5.

[79] H.G. Matthies et al. "Uncertainties in probabilistic numerical analysis of structures and solids-stochastic finite elements". In: *Structural Safety* 19.3 (1997), pp. 283 –336. DOI: https://doi.org/10.1016/S0167-4730(97)00013-1.

[80] R.H. Cameron and W. T. Martin. "The Orthogonal Development of Non-Linear Functionals in Series of Fourier-Hermite Functionals". In: *Annals of Mathematics* 48.2 (1947), pp. 385–392.

[81] C. Soize and R. Ghanem. In: *SIAM Journal on Scientific Computing* 26.2 (2004), pp. 395–410. DOI: 10.1137/S1064827503424505.

[82] R. V. Field and M. Grigoriu. "Convergence properties of polynomial chaos approximations for L2 random variables." In: *Technical Report SAND 2007 - 1262* (Mar. 2007). DOI: 10.2172/903430.

[83] O.P. Le Maitre et al. "Uncertainty propagation using Wiener–Haar expansions". In: *Journal of Computational Physics* 197.1 (2004), pp. 28 –57. DOI: https://doi.org/10.1016/j.jcp.2003.11.033.

[84] D. M. Ghiocel and R. G. Ghanem. "Stochastic Finite-Element Analysis of Seismic Soil–Structure Interaction". In: *Journal of Engineering Mechanics* 128.1 (2002), pp. 66–77. DOI: 10.1061/(ASCE)0733-9399(2002)128:1(66).

[85] O. P. Le Maitre et al. "A Stochastic Projection Method for Fluid Flow: II. Random Process". In: *Journal of Computational Physics* 181.1 (2002), pp. 9 –44. DOI: https://doi.org/10.1006/jcph.2002.7104.

[86] S.-K. Choi et al. "Polynomial Chaos Expansion with Latin Hypercube Sampling for Estimating Response Variability". In: *AIAA Journal* 42 (June 2004), pp. 1191–1198. DOI: 10.2514/1.2220.

[87] A. C. Atkinson. "Optimum Experimental Design". In: *International Encyclopedia of Statistical Science*. Ed. by Miodrag Lovric. Berlin, Heidelberg: Springer Berlin Heidelberg, 2011, pp. 1037–1039. DOI: 10.1007/978-3-642-04898-2_434.

[88] Z. Samih, B. Colson, and F. Glineur. "An Efficient Sampling Method for Regression-Based Polynomial Chaos Expansion". In: *Communications in Computational Physics* 13.4 (2013), 1173?1188. DOI: 10.4208/cicp.020911.200412a.

[89] S. Hosder, R. Walters, and M. Balch. "Efficient Sampling for Non-Intrusive Polynomial Chaos Applications with Multiple Uncertain Input Variables". In: *48th AIAA/ASME/ASCE/AHS/ASC Structures, Structural Dynamics, and Materials Conference* (2007). DOI: doi:10.2514/6.2007-1939.

[90] G. Blatman and B. Sudret. "Sparse polynomial chaos expansions and adaptive stochastic finite elements using a regression approach". In: *Comptes Rendus Mecanique* 336.6 (2008), pp. 518 –523. DOI: https://doi.org/10.1016/j.crme.2008.02.013.

[91] A. Saltelli and K. Chan. *Sensitivity Analysis*. Wiley New York, 2000.

[92] I.M. Sobol. "Sensitivity estimates for non linear mathematical model". In: *Mathematics and Computers in Simulation* 1 (1993), pp. 56–61.

[93] I.M. Sobol. "Global sensitivity indices for nonlinear mathematical models and their Monte Carlo estimates". In: *Mathematics and Computers in Simulation* 55.1 (2001), pp. 271 –280. DOI: https://doi.org/10.1016/S0378-4754(00)00270-6.

[94] L.A. Zadeh. "Fuzzy sets". In: *Information and Control* 8.3 (1965), pp. 338 –353. DOI: https://doi.org/10.1016/S0019-9958(65)90241-X.

[95] J.E. Hurtado, D.A. Alvarez, and J. Ramirez. "Fuzzy structural analysis based on fundamental reliability concepts". In: *Computers and Structures* 112-113 (2012), pp. 183 –192. DOI: https://doi.org/10.1016/j.compstruc.2012.08.004.

[96] T Haag, J. Herrmann, and M. Hanss. "Identification procedure for epistemic uncertainties using inverse fuzzy arithmetic". In: *Mechanical Systems and Signal Processing* 24.7 (2010), pp. 2021 –2034. DOI: https://doi.org/10.1016/j.ymssp.2010.05.010.

[97] Laplace P. *Memoire sur la probabilite des causes par les evenemens*. 1774.

[98] S.H. Cheung and J.L. Beck. "Bayesian Model Updating Using Hybrid Monte Carlo Simulation with Application to Structural Dynamic Models with Many Uncertain Parameters". In: *Journal of Engineering Mechanics* 135.4 (2009), pp. 243–255. DOI: 10.1061/(ASCE)0733-9399(2009)135:4(243).

[99] S.K. Au and Ni Y.C. Zhang F.L. "Bayesian operational modal analysis: Theory, computation, practice". In: *Computers and Structures* 126 (2013). Uncertainty Quantification in structural analysis and design: To commemorate Professor Gerhart I. Schueller for his life-time contribution in the area of computational stochastic mechanics, pp. 3 –14. DOI: https://doi.org/10.1016/j.compstruc.2012.12.015.

[100] J.L. Beck and K.V. Yuen. "Model Selection Using Response Measurements: Bayesian Probabilistic Approach". In: *Journal of Engineering Mechanics* 130.2 (2004), pp. 192–203. DOI: 10.1061/(ASCE)0733-9399(2004)130:2(192).

[101] L.S. Katafygiotis and J.L. Beck. "Updating Models and Their Uncertainties: Part II". In: *Journal of Engineering Mechanics* 124.4 (1998), pp. 463–467. DOI: 10.1061/(ASCE)0733-9399(1998)124:4(463).

[102] G. Bartoli et al. "Bayesian model updating of historic masonry towers through dynamic experimental data". In: *Procedia Engineering* 199 (2017). X International Conference on Structural Dynamics, EURODYN 2017, pp. 1258 –1263. DOI: https://doi.org/10.1016/j.proeng.2017.09.267.

[103] E. T. Jaynes. "Information Theory and Statistical Mechanics". In: *Phys. Rev.* 106 (1957), pp. 620–630. DOI: 10.1103/PhysRev.106.620.

[104] E. T. Jaynes. "Information Theory and Statistical Mechanics. II". In: *Phys. Rev.* 108 (2 1957), pp. 171–190. DOI: 10.1103/PhysRev.108.171.

[105] H. Jeffreys. *An invariant form for the prior probability in estimation problems*. Vol. 186. 1007. The Royal Society, 1946, pp. 453–461. DOI: 10.1098/rspa.1946.0056.

[106] J.M. Bernardo. *Reference Posterior Distributions for Bayesian Inference*. Vol. 41. 2. Royal Statistical Society, Wiley, 1979, pp. 113–147.

[107] J.O. Berger, J.M Bernardo, and D. Sun. "The Formal Definition of Reference Priors". In: *The Annals of Statistics* 37.2 (2009), pp. 905–938.

[108] Raiffah H. and Schlaifer R. " Applied Statistical Decision Theory." In: *Graduate School of Business Administration* (1961).

[109] D.V. Lindley. *Bayesian Statistics, A Review*. CBMS-NSF Regional Conference Series in Applied Mathematics. Society for Industrial and Applied Mathematics, 1972.

[110] E. Gutierrez-Pena and A.F.M. Smith. " Exponential and bayesian conjugate families: Review and extensions." In: *Test* (1997).

[111] E. Reynders, A. Teughels, and G De Roeck. "Finite element model updating and structural damage identification using OMAX data". In: *Mechanical Systems and Signal Processing* 24.5 (2010). Special Issue: Operational Modal Analysis, pp. 1306 –1323. DOI: https://doi.org/10.1016/j.ymssp.2010.03.014.

[112] J. Jang and A. Smyth. "Bayesian model updating of a full-scale finite element model with sensitivity-based clustering". In: *Structural Control and Health Monitoring* 24.11 (2017), e2004. DOI: 10.1002/stc.2004.

[113] S.K. Au. *Operational Modal Analysis*. Springer, 2017. DOI: 10.1007/978-981-10-4118-1.

[114] E. Simoen, C. Papadimitriou, and G. Lombaert. "On prediction error correlation in Bayesian model updating". In: *Journal of Sound and Vibration* 332.18 (2013), pp. 4136 –4152. DOI: https://doi.org/10.1016/j.jsv.2013.03.019.

[115] I. Behmanesh et al. "Hierarchical Bayesian Model Updating for Structural Identification". In: *Mechanical Systems and Signal Processing* 64-65.3849 (2015), pp. 360–376. DOI: 10.1016/j.ymssp.2015.03.026.

[116] E.L. Zhang, P. Feissel, and J. Antoni. "A comprehensive Bayesian approach for model updating and quantification of modeling errors". In: *Probabilistic Engineering Mechanics* 26.4 (2011), pp. 550 –560. DOI: https://doi.org/10.1016/j.probengmech.2011.07.001.

[117] P. Gardoni, A. Der Kiureghian, and K.M. Mosalam. "Probabilistic Capacity Models and Fragility Estimates for Reinforced Concrete Columns based on Experimental Observations". In: *Journal of Engineering Mechanics* 128.10 (2002), pp. 1024–1038. DOI: 10.1061/(ASCE)0733-9399(2002)128:10(1024).

[118] P. Gardoni. *Probabilistic models and fragility estimates for structural components and systems.* PhD dissertation, Univ. of California, Berkeley, Berkeley, California, 2002.

[119] A. Kucerova, B. Rosic, and Matthies H.G. "Comparison of Numerical Approaches to Bayesian Updating". In: *Informatik-Berichte der Technischen Universitat Braunschweig* 2014-10 (2014).

[120] D. Gamerman and H.F. Lopes. *Markov Chain Monte Carlo: Stochastic simulation for bayesian inference*. Chapmann & Hall, CRC2006, 2015.

[121] W.K. Hastings. *Monte Carlo Sampling Methods Using Markov Chains and Their Applications*. Vol. 57. 1. Oxford University Press, Biometrika Trust, 1970, pp. 97–109.

[122] S. Geman and D. geman. *Stochastic Relaxation, Gibbs Distributions, and the Bayesian Restoration of Images*. Ed. by M.A. Fischler and O. Firschein. San Francisco (CA), 1987. DOI: https://doi.org/10.1016/B978-0-08-051581-6.50057-X.

[123] A.E. Gelfand et al. "Illustration of Bayesian Inference in Normal Data Models Using Gibbs Sampling". In: *Journal of the American Statistical Association* 85.412 (1990), pp. 972–985. DOI: 10.1080/01621459.1990.10474968.

[124] J.L. Beck and S.K. Au. "Bayesian Updating of Structural Models and Reliability using Markov Chain Monte Carlo Simulation". In: *Journal of Engineering Mechanics* 128 (2002), pp. 380–391. DOI: https://doi.org/10.1061/(ASCE)0733-9399(2002)128:4(380).

[125] J. Ching, M. Muto, and J.L. Beck. "Structural Model Updating and Health Monitoring with Incomplete Modal Data Using Gibbs Sampler". In: *Computer Aided Civil and Infrastructure Engineering* 21.4 (2006), pp. 242–257. DOI: 10.1111/j.1467-8667.2006.00432.x.

[126] H. Haario, E. Saksman, and J. Tamminen. "An Adaptive Metropolis Algorithm". In: *Bernoulli* 7.2 (2001), pp. 223–242.

[127] Radford M. Neal. "MCMC using Hamiltonian dynamics". In: *Handbook of Markov Chain Monte Carlo* (2011).

[128] J. Ching and Yi-Chu Chen. "Transitional Markov Chain Monte Carlo Method for Bayesian Model Updating, Model Class Selection, and Model Averaging". In: *Journal of Engineering Mechanics* 133.7 (2007), pp. 816–832. DOI: 10.1061/(ASCE)0733-9399(2007)133:7(816).

[129] S. K. Au H.F. Lam J. Yang. "Bayesian model updating of a coupled-slab system using field test data utilizing an enhanced Markov Chain Monte Carlo simulation algorithm". In: *Engineering Structures* 102 (2015), pp. 144–155. DOI: 10.1016/j.engstruct.2015.08.005.

[130] A. Kucerova, B. Rosic, and H.G. Matthies. "Acceleration of uncertainty updating in the description of transport processes in heterogeneous materials". In: *Journal of Computational and Applied Mathematics* 236.18 (2012), pp. 4862 –4872. DOI: https://doi.org/10.1016/j.cam.2012.02.003.

[131] Litvinenko A. Rosic B. and H.G. Matthies. "Sampling free linear Bayesian update of polynomial chaos representations". In: *Journal of Computational Physics* 231.17 (2012), pp. 5761 –5787. DOI: https://doi.org/10.1016/j.jcp.2012.04.044.

[132] Studio Tecnico Marco Peroni. "Structural Project". In: ().

[133] "SAP2000. Static and dynamic finite element of structures." In: *Computers and structures, Inc Berkeley CA USA* (2009).

[134] Wei-Xin Ren, Xue-Lin Peng, and You-Qin Lin. "Experimental and analytical studies on dynamic characteristics of a large span cable-stayed bridge". In: *Engineering Structures* 27.4 (2005), pp. 535 –548. DOI: https://doi.org/10.1016/j.engstruct.2004.11.013.

[135] J. F. Fleming and E. A. Egeseli. "Dynamic behaviour of a cable-stayed bridge". In: *Earthquake Engineering & Structural Dynamics* 8.1 (), pp. 1–16. DOI: 10.1002/eqe.4290080102.

[136] D. Fotsch and D.J. Ewins. "Application of MAC in the Frequency Domain". In: *Proceedings of the International Modal Analysis Conference - IMAC* 2 (2000).

[137] W. E. Daniell and J.H.G. Macdonald. "Improved finite element modelling of a cable-stayed bridge through systematic manual tuning". In: *Engineering Structures* 29.3 (2007), pp. 358 –371. DOI: https://doi.org/10.1016/j.engstruct.2006.05.003.

[138] C. Pepi et al. "Dynamic characterization of a severely damaged historic masonry bridge". In: *Procedia Engineering* 199 (2017), pp. 3398 –3403. DOI: https://doi.org/10.1016/j.proeng.2017.09.579.

[139] M. Gioffré et al. "Laser doppler and radar interferometer for contactless measurements on unaccessible tie-rods on monumental buildings: Santa Maria della Consolazione Temple in Todi". In: *Journal of Physics: Conference Series* 778.1 (2017), p. 012008.

[140] F. Ubertini. "Effects of cables damage on vertical and torsional eigenproperties of suspension bridges". In: *Journal of Sound and Vibration* 333.11 (2014), pp. 2404 –2421. DOI: https://doi.org/10.1016/j.jsv.2014.01.027.